KINDER- UND JUGENDKLINIK
DER UNIVERSITÄTSMEDIZIN ROSTOCK
Arbeitsgruppe: Hirntumorforschung
Direktor: Prof. Dr. med. Manfred Ballmann

Bedeutung der Cyclin-abhängigen Kinasen als Zielstrukturen bei der Therapie von Glioblastoma multiforme und Kopf-Hals-Tumoren
- eine 2D- und 3D-Modell-Analyse -

kumulative Inauguraldissertation
zur Erlangung des akademischen Grades
Doktor der Medizinwissenschaften
***Doctor rerum humanarum* (Dr. rer. hum.)**
an der Universitätsmedizin Rostock

vorgelegt von
M.Sc. Christin Rieß, geb. Matzack am 02.01.1991 in Schwerin
aus Rostock

Rostock, 2022

https://doi.org/10.18453/rosdok_id00004366

Gutachter

Erstgutachter:	Prof. Dr. med. Carl-Friedrich Classen Universitätsmedizin Rostock, Kinder- und Jugendklinik, AG Onkologie/ Palliativmedizin
Zweitgutachter:	Prof. Dr. med. Holger Lode Universitätsmedizin Greifswald, Klinik und Poliklinik für Kinder und Jugendmedizin
Drittgutachter:	Prof. Dr. med. Friedrich Prall Universitätsmedizin Rostock, Institut für Pathologie

Datum der Verteidigung

17.05.2023

1. Einleitung

1.1 Glioblastoma multiforme

Das Glioblastoma multiforme (GBM) ist der häufigste, bösartigste Hirntumor astrozytärer Herkunft, definiert sich über ein aggressiv-diffuses Wachstum und wird nach WHO-Klassifikation als Gliom des Grades 4 bezeichnet [1,2]. GBMs umfassen über die Hälfte (≈ 57 %) aller Gliome und sind am häufigsten in den Frontal- und Temporallappen lokalisiert [3,4]. Dabei können sie *de novo* entstehen (primär) oder sich aus einem Astrozytom niedrigeren Grades entwickeln (sekundär) [5,6]. Mit einer Inzidenz von ≈ 3/100.000 Einwohner pro Jahr (USA) wird das GBM typischerweise im höheren Alter (Durchschnittsalter: 65 Jahre) und häufiger bei Männern diagnostiziert [7–9]. Zu den prognostischen Faktoren gehören neben dem Alter, dem Allgemein- und dem neurologischen Zustand spezifische molekulare Alterationen. Diese schließen u.a. den Promotormethylierungsstatus des DNA-Reparaturenzyms O^6-Methylguanin-DNA-Methyltransferase (MGMT), Mutationen in den Genen Isocitratdehydrogenase*, v-Raf murine sarcoma viral oncogene homolog B,* das Tumorsuppressor Retinoblastom-Protein1 (*Rb1)*, *telomerase reverse transcriptase*-Promotor, Deletionen im Chromosom 10 (*phosphatase and tensin homolog* (*PTEN)*, *epidermal growth factor receptor* (*EGFR)*-Alteration und *platelet-derived growth factor receptor A)*, CDK4/6 Amplifikationen, sowie homozygote *cyclin-dependent kinase inhibitor2A/B* (*CDKN2A/B)*-Deletionen ein [7,10–14]. Als Konsequenz dieser unterschiedlichen genetischen Aberrationen und oftmals variablen phänotypischen und epigenetischen Zuständen weisen GBMs eine erhebliche inter- und intratumorale Heterogenität auf [15,16]. Während Tumorsuppressor53 (*TP53)*-Mutationen sowie eine EGFR-Überexpression oftmals bei primären und sekundären GBMs nachweisbar sind [17], ist ein Verlust von *PTEN* typischerweise mit primären GBMs und das Fehlen von Chromosom 19q zusammen mit *TP53*-Mutationen mit sekundären GBMs assoziiert [18,19]. Prognostisch und therapeutisch relevant für das Ansprechen auf das Alkylanz Temozolomid (TMZ) ist der MGMT-Promotorstatus. MGMT entfernt Alkylgruppen von der O^6 Position des Guanins und konterkariert die Wirkung von Alkylanzien wie TMZ [20]. Epigenetische Modifikation mittels (Hyper-) Methylierung des MGMT-Promotors führen zu einem Verlust bzw. einer geringen Menge an funktionellem MGMT-Protein und damit zu einer unzureichenden Reparatur der DNA-Alkylierung [21].

Die Standardtherapie des GBM untergliedert sich in mehrere Säulen [11,22–24]. Zu den Grundpfeilern gehört die möglichst vollständige Resektion (Gesamtüberlebensvorteil: 3-6 Monate) [14,15], gefolgt von einer Radiotherapie (RT) (entsprechend ≈ 12 Monate), die mit TMZ begleitet wird (≈ 15 Monate; 5-Jahresüberlebensrate: 5-7 %) [5,7,8,10,25–28]. Eine zusätzliche, seit März 2020 zugelassene, Behandlung basiert auf elektrischen Wechselfeldern (t*umor treating fields* (TTF)) mit dem Ziel, einen Arrest der Tumorzellproliferation zu induzieren. Diese Therapie kann unabhängig vom MGMT Promotormethylierungsstatus erwogen werden [3,29,30]. Bei neu diagnostizierten GBM wurde

mit TTF plus TMZ-Erhaltungstherapie das mediane Überleben signifikant verlängert (~ 21 Monate) [29]. Die Prognose bleibt trotz multimodaler Behandlungsansätze und dem fortschreitenden Verständnis der zugrunde liegenden molekularen Veränderungen ungünstig. Zudem tritt in nahezu allen Fällen ein Rezidiv mit schlechterer Prognose und verändertem molekularen Muster auf (medianes Gesamtüberleben: 2-9 Monate) [31–34]. Eine ineffiziente Verabreichung von Medikamenten über die Blut-Hirn-(Tumor)-Schranke, eine immunsuppressive Tumor-Mikroumgebung (iTM), die Entwicklung von Resistenzen und die Heterogenität stellen wesentliche Ursachen für ein Therapieversagen dar [35–37]. Zahlreiche Studien haben zudem das Vorhandensein pluripotenter stammzell-ähnlicher GBM-Zellen (*glioma stem-like cells* (GSCs)) nachgewiesen, die für die Bildung, die Invasivität und das Wiederauftreten von GBM mitverantwortlich sind [38]. Auch neuronale Stammzellen tragen ursächlich zur GBM-Entwicklung in der subventrikulären Zone durch somatische *Driver* Mutationen bei [39,40]. Viele molekulare Mechanismen wurden mit der Resistenz von GSCs/neuronalen Stammzellen gegenüber zytotoxischen Therapien in Verbindung gebracht, darunter Mechanismen, die den G_2-M-DNA-Schadens-Checkpoint und verschiedene Signalwege (Notch, *kappa-light-chain-enhancer of activated B-cells*, *enhancer of zeste homolog 2* und Poly(ADP-ribose)-Polymerasen), sowie die WNT/β-Catenin-Signalkaskade einschließen [38,41–44]. In aktuellen Studien werden vermehrt Therapiekonzepte evaluiert, die auf spezifischer Inhibition von Signalwegen basieren, um die Prognose der betroffenen PatientInnen bei gleichzeitiger Reduktion therapie-assoziierter Nebenwirkungen und Prävention von Resistenzen zu verbessern [33,35,45–47].

1.2 Kopf-Hals-Tumoren

Kopf-Hals-Tumoren stehen paradigmatisch für die Heterogenität von Tumoren und repräsentieren weltweit die sechsthäufigste Tumorentität [48–50]. Diese entspringen dem mukosalen Epithel der Mundhöhle, des Naso-, Oro- und Hypopharynx, des Larynx, sowie der Speicheldrüsen [49,51]. Der vorherrschende histologische Typ von Kopf-Hals-Tumoren sind Plattenepithelkarzinome (*head and neck squamous cancer carcinoma* (HNSCC)) [51]. Die Prävalenz variiert regional und wird im Allgemeinen mit der Exposition gegenüber Karzinogenen, beispielsweise dem Tabakkonsum und dem übermäßigen Alkoholabusus in Verbindung gebracht. Zunehmend werden Tumoren, die im Oropharynx mit ausgeprägten klinischen, histopathologischen und molekularen Merkmalen entstehen, mit einer früheren Infektion onkogener *high-risk* Stämme des humanen Papillomavirus (HPV), wie etwa HPV-16 und -18, in Verbindung gebracht [52–54]. Im Allgemeinen haben Männer ein höheres Erkrankungsrisiko mit einem medianen Diagnosealter für nicht viral-assoziierte HNSCC von 66 Jahren und für HPV-assoziierte Oropharynxkarzinome bzw. Epstein-Barr-Virus-assoziierte Nasopharynxkarzinome von ~ 50 Jahren [55,56]. Therapeutisch betrachtet haben HPV-positive HNSCC eine bessere Prognose, da sie empfindlich gegenüber Radiochemotherapie (RCT) sind [57]. Obwohl ein Teil der prämalignen oralen Läsionen, die sich als Leukoplakie oder Erythroplakie präsentieren, zu invasivem Krebs fortschreiten,

stellt sich die Mehrheit (≈ 58 %) der PatientInnen im lokal-regional fortgeschrittenen Stadium vor, ohne dass eine klinische Vorgeschichte einer Prämalignität vorliegt [49,51]. Dies geht mit einer schlechten Prognose (5-Jahres-Überlebensrate ≤ 50 %) bei fortgeschrittenen HPV-negativen HNSCC-PatientInnen einher [58]. Darüber hinaus wurden zwar verschiedene Tumorsuppressor-Mutationen wie *TP53, CDKN2A* und *Notch* festgestellt, jedoch keine spezifischen *Driver* Mutationen [59–61]. Der Behandlungsansatz richtet sich nach anatomischer Lokalisation, dem Stadium, pathologischen Merkmalen, funktionellen Überlegungen und den Wünschen der PatientInnen. In der Regel erfolgt eine chirurgische Resektion, ggf. mit einer adjuvanten hypofraktionierten RT oder einer RCT [49]. In erster Linie werden die Wirkstoffe Cisplatin, Carboplatin, 5-Fluorouracil (5-FU) und/oder Taxane eingesetzt, aber auch Gemcitabin, Vinorelbin und Methotrexat kommen zur Anwendung [62]. Mit Ausnahme der Tumorerkrankung der Mundhöhle im Frühstadium oder des Larynx erfordert die Behandlung dieser Tumoren einen multimodalen Ansatz mit multidisziplinärer Betreuung [49]. HNSCC weisen eine hohe Tumormutationslast und Immunzellinfiltration auf, weshalb sie für Immuntherapien prädestiniert sind [63]. Daher sind Immuncheckpoint Inhibitoren, wie Pembrolizumab und Nivolumab, die auf das *programmed cell death protein 1* (PD-1) abzielen, für rezidivierende und metastasierte HNSCC in der Erst- und Zweitlinienbehandlung zugelassen [64,65]. Eine weitere Behandlungsoption bieten die zielgerichteten Therapieansätze. Zu diesen zählt u.a. der monoklonale Antikörper Cetuximab, welcher sich gegen EGFR richtet und von der *Food and Drug Administration* als Strahlensensibilisator oder in Kombination mit Chemotherapie für die Behandlung eines rezidivierten Tumors zugelassen ist [66]. Neben diesem existieren noch weitere EGFR-gerichtete monoklonale Antikörper, aber auch weitere Wachstumsfaktorrezeptor-Inhibitoren [67]. Die Implementierung zusätzlicher zielgerichteter Therapien zur Verbesserung der Prognose wird dringend benötigt. 2019 berichtete eine Phase-2-Studie über vielversprechende Ergebnisse bei Platin-resistentem bzw. Cetuximab-resistentem HPV-negativen HNSCC, die Palbociclib und Cetuximab erhielten [68].

1.3 Immun-*Escape*-Mechanismen

Maligne Gliome, wie GBMs, aber auch HNSCC, sind durch eine lokale und systemische Immunsuppression gekennzeichnet, die die Wirksamkeit von diversen, insbesondere immuntherapeutischen Behandlungsansätzen beeinträchtigt [69–71]. Tryptophan (Trp), eine essentielle Aminosäure, wird über den Kynurenin-Signalweg (KS) verstoffwechselt, wodurch eine Vielzahl von Metaboliten mit entscheidenden Funktionen bei der Neurotransmission und der Regulierung von Immunreaktionen entstehen [72]. Eine Überaktivierung des KS, vornehmlich durch die Indolamin 2,3-dioxygenase (IDO1) und Tryptophan 2,3-dioxygenase (TDO2) Überexpression sowie nachgeschalteter Effektormechanismen, einschließlich der Aryl-Hydrocarbon (AHR)-vermittelten Transkription, führt zu einer iTM und ist mit einer schlechten Prognose bei diversen Tumorentitäten assoziiert [71,73–77]. Die lokale Immuntoleranz wird durch Anergie und

Apoptose von CD8⁺ T-Zellen, Aktivierung von regulatorischen T-Zellen (Treg), sowie durch Akkumulation von immunsuppressivem Kynurenin (KYN), welches u.a. von dendritischen Zellen und myeloiden Suppressorzellen sezerniert wird, gefördert [78–81] (Abb. 1). Niedermolekulare Inhibitoren, die auf den Trp-Abbau abzielen, werden derzeit in klinischen Studien getestet, jedoch hat ein Großteil bisher lediglich heterogene Ergebnisse in der Immuntherapie erzielt [72,77]. Dies verdeutlicht, dass die Überwindung der iTM u.a. bei GBM und HNSCC eine besondere therapeutische Herausforderung darstellt, die es mit vielversprechenden Ansätzen zu überwinden gilt.

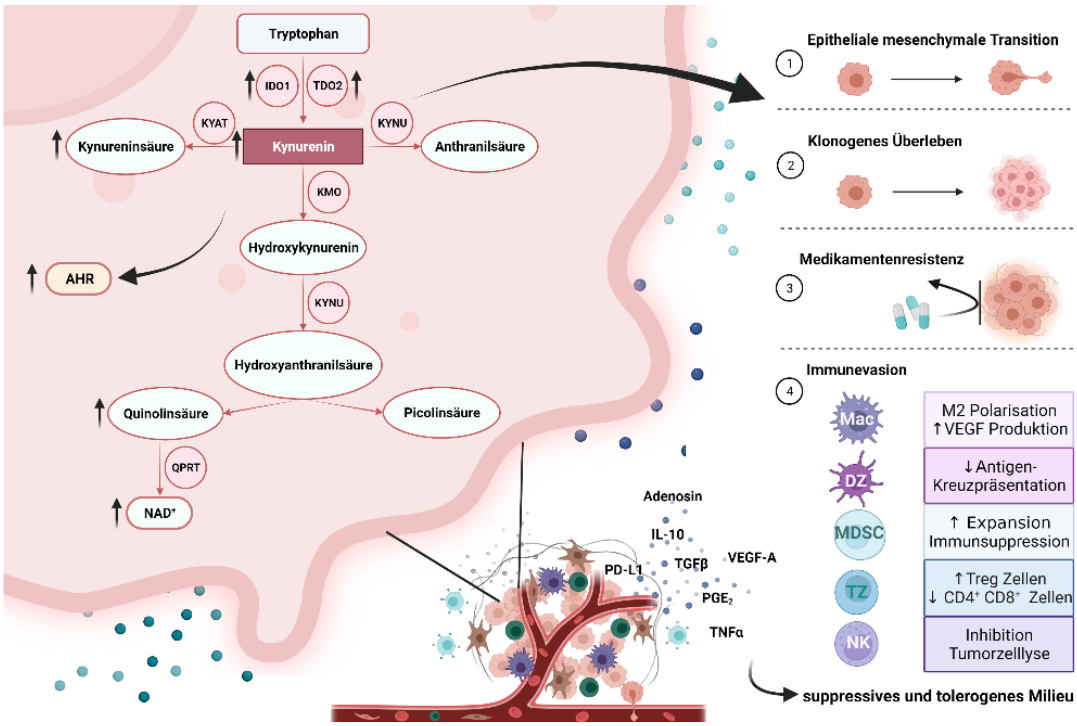

Abbildung 1: Wirkung des Trp-Abbaus auf Zellen in der Tumormikroumgebung. Die Auswirkungen des Trp-Katabolismus (Indolamin 2,3-dioxygenase, IDO1; Tryptophan 2,3-dioxygenase, TDO2; Kynurenin Oxoglutarattransaminase, KAT; Kynureninase, KYNU; Kynurenine 3-monooxygenase, KMO; Chinolinat-Phosphoribosyltransferase, QPRT; Anryl-Hydrocarbonrezeptor, AHR) sowie immunsuppressiver Metaboliten (Adenosin, IL-10, TGFβ, PGE2, TNFα, VEGF-A) und der Trp-Metaboliten auf Mac (Makrophagen), DZ (dendritische Zellen), MDSC (Myeloide Suppressorzellen), TZ (T Lymphozyten; T-Helfer-Zellen (TH1), regulatorische (Tregs) und cytotoxische T-Zellen (CD4⁺, CD8⁺)) und NK (Natürliche Killerzellen) (→ Immunevasion) sowie auf die Tumorzellen (→ EMT, klonogenes Überleben, Medikamentenresistenz) sind dargestellt [72,77,81]. Grafik wurde mit Biorender erstellt.

1.4 Replikative Immortalität durch konstitutive CDK-Aktivierung

Die meisten Tumoren, einschließlich GBM und HNSCC, weisen Genomveränderungen auf, die zur konstitutiven Aktivierung von Cyclin-abhängigen Kinasen (CDKs) führen [82,83]. Das wiederum mündet in eine unkontrollierte Zellproliferation, bei der viele Schutzmechanismen außer Kraft gesetzt werden und eine Deaktivierung von Zellzykluskontrollpunkten erfolgt [84–87]. CDKs gehören zur Familie der konservierten Serin/Threonin-Proteinkinasen. Unter physiologischen Bedingungen spielen sie in Verbindung mit ihren zugeordneten regulatorischen Untereinheiten, den Cyclinen, eine wichtige Rolle bei der Kontrolle der

Zellzyklusprogression (CDK 1-4, 6, 7, 11), der Transkriptionsregulation und mRNA-Prozessierung sowie der DNA-Reparatur (CDK 5, 7-11) [88,89] (Abb. 2).

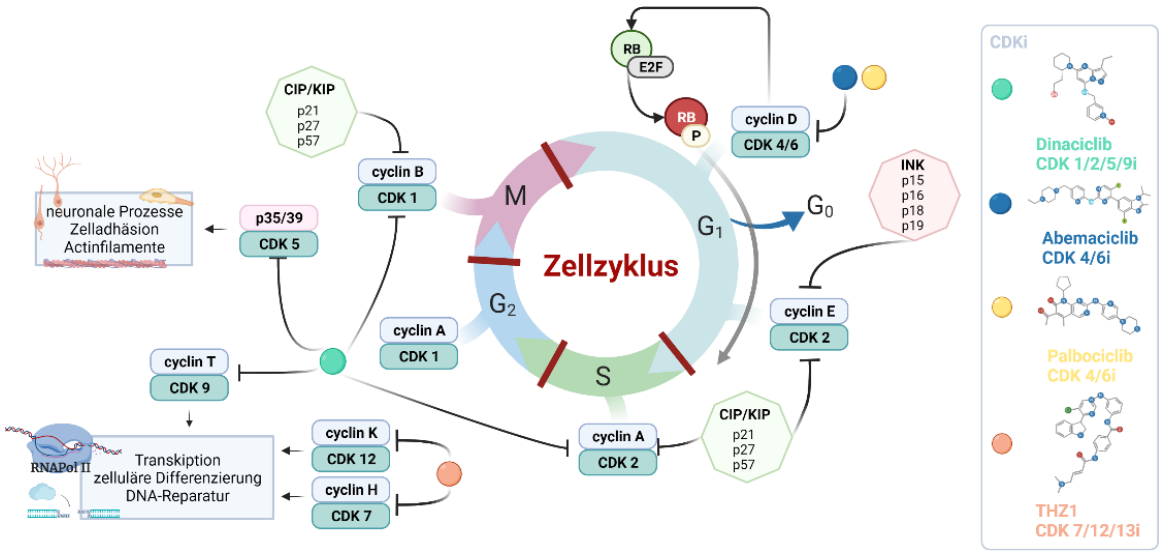

Abbildung 2: Die Zellzyklusphasen, die damit verbundenen CDK/Cyclin-Komplexe und die CDK-Inhibitoren. An der Progression sind mehrere CDK-Cyclin-Komplexe beteiligt, darunter CDK1/2/4/6 und verschiedene Cyclin-Klassen (Typ A, B, D, E). In der G1-Phase ist die Synthese von Cyclin D erhöht, dort arbeitet es mit CDK4/6 zusammen, um den Eintritt und das Fortschreiten durch G1 bzw. G1/S-Übergang zu fördern. Während in der S-Phase und den letzten Stadien von G2 Cyclin A stark exprimiert, kontrolliert CDK2-Cyclin A die Phosphorylierung von Proteinen, die an der DNA-Replikation beteiligt sind. In der G2-Phase ist der Hauptregulator CDK1. Die gebildeten Komplexe vermitteln auch die Transkriptionsregulation, die mRNA-Verarbeitung und die zelluläre Differenzierung. Grafik erstellt mit Biorender.

Weiterhin steuern die CDKs verschiedene Prozesse der Zellteilung, einschließlich der mitotischen Progression, epigenetischen Regulation und Selbsterneuerung von Nervenzellen (CDK 5, 12-20) [87,90–95]. Die Kinaseaktivität von CDK-Cyclin-Komplexen wird durch verschiedene körpereigene CDK-Inhibitoren (CDKi) kontrolliert [96]. An der CDK 4/6 Regulation sind die Mitglieder der Ink4-Familie (u.a. $p16^{INK4a}$) beteiligt [97] und an der Regulation der Aktivitäten der Cyclin D-, E-, A- und B-abhängigen Kinase-Komplexe (CDK 2, 4 und 6) partizipieren die Cip/Kip Mitglieder (u.a. $p21^{Cip1}$) [98,99]. Im Zentrum dieses Signalweges steht das Rb1, welches den Übergang von der G1 zur S-Phase mit Hilfe des Transkriptionsfaktors E2F kontrolliert [100] (Abb. 2). Das Ungleichgewicht zwischen CDKs und CDKi führt zu einer abnormalen Zellproliferation und fördert die Tumorprogression [93,101]. So weisen etwa 24 % aller malignen Erkrankungen genomische Veränderungen in Cyclin-sensibilisierenden Genen bzw. CDK-Signalwegen auf [85]. CDK5 fördert die Invasion und Migration durch Herunterregulation des Aktin-regulierenden Proteins Caldesmon [102,103]. CDK8 wurde als Koaktivator des β-Catenin-Signalwegs bei kolorektalen Karzinomen identifiziert [104] und CDK10 verursacht eine Resistenz gegen eine endokrine Therapie beim Mammakarzinom [105]. Aufgrund ihrer wesentlichen Rolle zum Erhalt der zellulären Homöostase [88] und des Befundes, dass die Cyclin D1 (CCND1)/CDK4/6–CDKN2A ($p16^{INK4A}$)–Rb-Achse in mehr als der Hälfte der GBM- und HNSCC-Fälle verändert ist, eignen sich CDKs hervorragend als therapeutische Angriffspunkte [106–109]. CDK4/6i binden

an den ATP-Spalt der Ziel-CDK, greifen in die Phosphorylierung des Rb-Proteins ein und führen so zu einem G1-Zellzyklusarrest. Drei oral verfügbare CDK4/6i (Palbociclib, Ribociclib, Abemaciclib) sind für die Behandlung von HR^+ $HER2^-$ Mammakarzinomen zugelassen [110–115]. Zu den prädiktiven Biomarkern für das Ansprechen von CDK4/6i gehören *CCND1*-Veränderungen und die Inaktivierung von CDKN2A/B [48]. Dabei ist Palbociclib durch größere Substituenten gekennzeichnet. Diese sterischen Eigenschaften sind für die höhere Selektivität gegenüber CDK4/D1/D3 und CDK6/D6 verantwortlich [116]. Im Gegensatz dazu weist Abemaciclib einen kleineren Substituenten auf, weswegen es sich leichter in die inaktive ATP-Tasche einbettet und andere Kinasen, einschließlich GSK3α/β und CaMKII α/β/γ, beeinflusst. Die Blockierung des G1-Zellzyklus, die Hemmung der DNA-Synthese und der pRb in verschiedenen Zellmodellen untermauern den Wirkmechanismus der CDK4/6i [106,117–122]. Jüngste Studien haben gezeigt, dass CDK4/6i das Tumorwachstum auch durch andere Mechanismen unterdrücken, einschließlich der Induktion von Seneszenz, durch Zellstoffwechselregulation und durch die Verstärkung der antitumoralen Immunantwort [123,124]. Neben der CDKi-Behandlung Rb-positiver Mammakarzinom-Modelle erwies sich diese Therapieform bei einer Vielzahl weiterer humaner Xenograft-Modelle, unter anderem GBM und HNSCC, als wirksam [73,119–122,125–131]. Aktuell laufen eine Phase-I-Studie mit einem ERK-Inhibitor in Kombination mit Abemaciclib (*NCT04391595*) und eine Phase-II-Studie mit Abemaciclib bei rezidivierten GBM (*NCT02981940*). In einer Studie mit HPV-negativen HNSCC-PatientInnen wird die Immunmodulation durch Abemaciclib evaluiert (*NCT04169074*). Im Gegensatz zu den selektiven CDK4/6i haben multi-CDKi bisher keine klinische Zulassung erhalten [124,132]. Ihre Fähigkeit, gleichzeitig auf CDKs einzuwirken, die am Zellzyklus und an der Transkription beteiligt sind, lässt vermuten, dass sie vielseitiger und wirksamer sein könnten, als die selektiven CDK4/6i [133]. Der multi-CDK7/12/13i THZ1 ist in der Lage, Apoptose zu induzieren, das Tumorwachstum zu hemmen und Resistenzen in murinen Xenograft-Modellen zu verhindern [134,135]. In Nasopharynx-Ca und GBM-Zellen zeigt THZ1 eine ausgeprägte antineoplastische Aktivität durch Modulation von *Super Enhancern* [135,136]. Der multi-CDK1/2/5/9i Dinaciclib hemmt bereits im nanomolaren Konzentrationsbereich das Zellwachstum [137]. Es ist gegen ein breites Spektrum solider und hämatopoetischer Tumormodelle wirksam und weist ein günstiges Sicherheits- und pharmakokinetisches Profil bei Mäusen auf [137,138]. Die Induktion von Apoptose konnte für mehrere Zelllinien, darunter Melanom-, Osteosarkom-, feline orale SCC- und GBM-Zellen beschrieben werden und hat sich bei refraktärer chronisch lymphatischer Leukämie als klinisch wirksam erwiesen [138–144]. Aktuell wird Dinaciclib in klinischen Phase-I/II-Studien eingesetzt; eine Phase-III-Studie wurde bereits abgeschlossen [143,145–149]. Eine synergistische Wirksamkeit wurde in Kombination mit Bcl-2/Bcl-xL-Inhibitoren nachgewiesen [142]. Dies belegt die grundsätzliche Wirksamkeit von CDKi und zeigt das Potential von CDKi-basierten Kombinationstherapien, die an unterschiedlichen molekularen Zielstrukturen ansetzen.

2. Zielstellung

Eine umfassende genomische Charakterisierung verschiedener Tumorentitäten hat wichtige tumorrelevante Signalwege aufgedeckt, die nahezu universell auf genetische oder epigenetische Veränderungen abzielen, die die Aktivität dieser Signalwege regulieren. Zu den häufigsten Veränderungen in GBM und HNSCC zählt die die CDKN2A ($p16^{INK4A}$)–Rb-Achse. Folglich wurden CDKs als therapeutische Zielstrukturen für die präklinische Anwendung interessant. Gleichzeitig stellt das immunsuppressive Tumormikromilieu eine besondere Herausforderung für die Therapie dar. Um das Tumorwachstum effektiv kontrollieren zu können, müssen verschiedene Faktoren berücksichtigt werden. Diese wurden im Rahmen der vorliegenden Arbeit adressiert.

Das Ziel dieser Promotionsarbeit war zunächst eine umfassende *in vitro*-Analyse zur Relevanz des Kynurenin-Stoffwechselweges in Patienten-abgeleiteten GBM-Zelllinien. Im zweiten Teil der Arbeit erfolgte die Untersuchung eines zielgerichteten CDK-Inhibierungsansatzes an GBM-Zellen im 2D- bzw. 3D-Modell und im dritten Teil fand eine Evaluierung einer kombinierten CDKi-Chemotherapie-basierten Behandlung an HNSCC *in vitro* und *in vivo* statt, um schließlich einen Beitrag zum besseren Verständnis der zugrunde liegenden Mechanismen zu leisten.

Folgende Ansätze wurden dabei verfolgt:

I. Untersuchung des Expressionsstatus von Schlüsselgenen und Metaboliten im Trp-Katabolismus basal und unter Einfluss von TMZ, Dinaciclib und dem IDO-Induktor Interferon-γ (IFN-γ).
II. Evaluierung der antitumoralen Wirkung von Abemaciclib, Palbociclib und Dinaciclib. Hierbei wurden sowohl Mono- als auch Kombinationsansätze getestet und die zugrunde liegenden funktionellen und molekularen Mechanismen im 2D- und 3D-Modell identifiziert.
III. Detaillierte Charakterisierung der Wirksamkeit eines kombinierten CDKi-Chemotherapie-Ansatzes an HNSCC-Zelllinien unter Berücksichtigung der Relevanz der zeitlichen Applikation und Aufklärung der funktionellen Veränderungen *in vitro* und *in vivo*.

3. Methoden

Detaillierte Informationen zum methodischen Ablauf können den zitierten Literaturstellen sowie den angefügten Originalpublikationen entnommen werden.

3.1 Zelllinien, Inhibitions- und *in vivo*-Versuche

In der vorliegenden Dissertation wurden, je nach Versuch und Publikation, bis zu 13 Patienten-abgeleitete GBM-Zelllinien (HROG02, -04, -05, -06, -10, -15, -24, -36, -38, -52, -63, -73, -75) sowie HNSCC-Zelllinien UT-SCC-14 (primärer Zungentumor) und UT-SCC-15 (Rezidiv, Lymphknotenmetastase) verwendet. 2D-Kulturen wurden in Vollmedium (DMEM/F12 + FCS, Glutamin, Pen/Strep.) bei 37 °C, befeuchteter Atmosphäre und 5 % CO_2 kultiviert. 3D-GBM-Sphäroide (GBS) und GSC wurden, wie in [150] beschrieben, kultiviert. Folgende CDKi wurden genutzt: Abemaciclib (10 µM), Palbociclib (1 oder 10 µM), THZ1 (5 oder 20 nM), Dinaciclib (5, 10 oder 100 nM). Die HNSCC-Zelllinien wurden mit folgenden Chemotherapeutika (CT) behandelt: 5-FU (0,32 µg/ml), Cisplatin (0,05/ 0,5 µg/ml), Cetuximab (0,5 µg/ml). IFN-γ (50 ng/ml) diente der IDO-1 Stimulation. Bei GBM war TMZ (10 µM) die Referenz. Alle Substanzen wurden 1x oder 2x 72h (Dosis: $<IC_{50}$) verwendet. Die Experimente wurden mindestens in drei biologischen Replikaten durchgeführt. Alle Tierversuche wurden vor Beginn durch das Landesamt für Landwirtschaft, Lebensmittelsicherheit und Fischerei Mecklenburg-Vorpommern gemäß dem deutschen Tierschutzgesetz und der EU-Richtlinie 2010/63/EU genehmigt (Aktenzeichen: 7221.3-1-066/18). Die Mäuse wurden in der zentralen Versuchstierhaltung der Universitätsmedizin Rostock gezüchtet und erhielten *Enrichment*. Während des Versuchs wurden die Mäuse in Käfigen des Typs III mit Futter-Pellets und Leitungswasser *ad libitum* gehalten. HNSCC-Xenotransplantate wurden durch subkutane Flankeninjektion in NMRI Foxn1^{nu}-Mäuse erzeugt, nach Tumorbildung (~50 mm^3) den Behandlungsgruppen zugeordnet und regelmäßig das Tumorvolumen (Tv) bestimmt. Die Tötung der Tiere erfolgte anhand definierter Abbruchkriterien. Anschließend wurden die Tumoren eingebettet und mit HE gefärbt.

3.2 Funktionelle Analyse zellbiologischer Parameter

Die Zellviabilität wurde im 2D-Modell mit dem fluorometrischen Calcein-(AM)-Farbstoff bzw. mit der Kristallviolettfärbung zur Biomassebestimmung und in den 3D-Kulturen luminometrisch mit dem CellTiter-Glo® 3D bewertet. Mittels Immunfluoreszenzfärbung (IF) wurden diverse Proteine bzw. Strukturen intra- und extrazellulär durch spezifische Antikörper/Substanzen markiert und angefärbt. Zu diesen zählten u.a.:

- IDO1: Enzym des Trp-Abbaus; Calretikulin (CalR): Nachweis immunogener Zelltod (ICD)
- p53, p21 Waf1/Cip1, p16 bzw. β-Galaktosidase-Aktivität: Seneszenz
- H2A.XPhospho (Ser139): DNA-Schäden und -Reparatur
- HLA-ABC, CD279 (PD-1), Phalloidin green (Aktinfilament)
- MitoTracker: Polarisation mitochondriale Membran, LysoTracker: saure Organellen

- ERTracker: ER, ImageIT Hypoxia: Hypoxie

  Analyse: inverses Licht-/Fluoreszenzmikroskop (Leica DMI 4000B) oder konfokales Lasermikroskop (Zeiss Elyra 7). Quantifizierung: Software ZEN (Zeiss) bzw. FIJI-ImageJ. Durchflusszytometrische Analysen umfassten:
- YO-PRO1/PI-Färbung: Apoptose und Nekrose, CalR-Translokation als Nachweis für ICD
- MitoSOX Red: reaktive mitochondriale O_2-Spezies
- CD107a/b (LAMP1/2) und Rab7a: spät-endosomale Marker

  Die durchflusszytometrischen Messungen und Auswertungen erfolgten am FACSCalibur™ bzw. FACSVerse™ mittels FACSuite™/ Cell-Quest-Pro-Software.

  Zur Beurteilung der Zellmotilität, Migration und Invasion wurden im 2D-Modell ein *wound healing* Assay und ein modifiziertes Boyden-Chamber-Assay durchgeführt. Die 3D-Invasionsfähigkeit wurde anhand des Eindringvermögens der Zellen aus ihren Sphäroiden in eine Matrigel-Matrix beurteilt. Zellkulturüberstände (un-/behandelt) wurden gesammelt und die KS-Metaboliten (Trp, KYN, Kynureninsäure (KYNA)) mit Hilfe eines LC/MS (AB Sciex 5500 QTrap™, in Kooperation am Institut für Immunologie und Transfusionsmedizin, Greifswald) gemessen. Die Impedanz wurde mit einem ECIS Z0, ausgestattet mit einer 96-Well-Array-Station mit interdigitalen Elektroden, gemessen (in Kooperation mit PD Dr. rer. nat. Nadja Engel, Klinik und Poliklinik für Mund-, Kiefer- und Plastische Gesichtschirurgie, Rostock).

3.3 RNA-Isolation, cDNA-Synthese, quantitative RT-PCR und Microarray-Analyse

Die Gesamt-RNA (un-/behandelt) wurde isoliert, in cDNA umgeschrieben und die Targets mittels quantitativer real-time PCR unter Verwendung von Taqman-Genexpressionsassays (*IDO1, TDO2, KMO, HAAO, KAT1/2/3/4, KYNU, QPRT* und Housekeeping Gen: *GAPDH/β-Aktin*) an einem Light Cycler Viia7 analysiert. Die Zielgen-mRNA wurde auf *GAPDH/β-Aktin* normalisiert und das Expressionslevel kalkuliert: $2^{-\Delta CT}$ ($\Delta Ct = Ct_{Zielgen} - Ct_{Housekeeping\ Gen}$). Zur genauen Erfassung der molekularen Veränderungen wurde die RNA von HROG63-Zellen (unbehandelt, Dinaciclib) extrahiert, quantifiziert und die Expressionsprofilierung (Affymetrix Human Clariom S Array) durchgeführt (in Kooperation mit Herrn Dr. Dirk Koczan, Core Facility Micro-Array-Technologie, Rostock). Die primäre Datenanalyse, einschließlich der SST-RMA Normalisierung, wurde mit der Affymetrix TAC-Software vorgenommen.

3.4 Statistik

Alle Werte sind als Mittelwert (MW) ± SD/SEM angegeben. Die Unterschiede zwischen un-/behandelten Zellen wurden mittels One- oder Two-way ANOVA nach Überprüfung der Normalitätsannahme (Shapiro-Wilk-Test) ermittelt. Wenn die Normalität nicht gegeben war, wurde der Kruskal-Wallis-Test angewendet. Die Kaplan-Meier-Überlebensanalyse wurde unter Anwendung des Log-Rank-Tests (Mantel-Cox-Test) durchgeführt. Die statistische Auswertung erfolgte mit GraphPad PRISM Software, Version 8.0.2. Als Signifikanzkriterium wurde $p < 0,05$ angenommen.

4. Ergebnisse

Die Resultate der Promotionsarbeit sind in drei Originalpublikationen mit Impact Factor veröffentlicht:

Riess C, Schneider B, Kehnscherper H, Gesche J, Irmscher N, Shokraie F, Classen CF, Wirthgen E, Domanska G, Zimpfer A, Strüder D, Junghanss C, Maletzki C. Activation of the Kynurenine Pathway in Human Malignancies Can Be Suppressed by the Cyclin-Dependent Kinase Inhibitor Dinaciclib. *Front Immunol*. 2020 Feb 14;11:55.
https://doi.org/10.3389/fimmu.2020.00055

Impact Factor 2022: 7.561

Riess C, Koczan D, Schneider B, Linke C, Del Moral K, Classen CF, Maletzki C. Cyclin-dependent kinase inhibitors exert distinct effects on patient-derived 2D and 3D glioblastoma cell culture models. *Cell Death Discov.* 2021 Mar 15;7(1):54 https://doi.org/10.1038/s41420-021-00423-1

Impact Factor 2022: 7.109

Schoenwaelder N, Salewski I, Engel N, Krause M, Schneider B, Müller M, **Riess C**, Lemcke H, Skorska A, Grosse-Thie C, Junghanss C, Maletzki C. The Individual Effects of Cyclin-Dependent Kinase Inhibitors on Head and Neck Cancer Cells - A Systematic Analysis. Cancers (Basel). 2021 May 15;13(10):2396.
doi: 10.3390/cancers13102396

Impact Factor 2022: 6.639

Im Folgenden werden die wesentlichen Ergebnisse zusammengefasst. Neben den Illustrationen im Text sind weitere Abbildungen den Veröffentlichungen im Anhang (Abschnitt 8.4) zu entnehmen.

4.1 Dinaciclib hemmt die IFN-γ induzierte KS-Aktivität

Der basale Expressionsstatus verschiedener KS-verwandter Gene wurde in 13 verschiedenen GBM-Zelllinien untersucht (Abb. 3A). *IDO1* war schwach exprimiert und wurde in 11/13 GBM-Proben nachgewiesen. *TDO2* und *KYNU* waren in allen GBM-Proben konstitutiv höher exprimiert als *IDO1*. In 1/3 klinischen GBM-Resektaten war IDO1 auch immunhistochemisch nachweisbar. Während die IDO1-Genexpression in 5/5 untersuchten GBM-Zelllinien durch IFN-γ induziert und der KS damit aktiviert wurde, war die Genexpression von *TDO2* und *KAT3* reduziert (Abb. 3B). Auf Proteinebene war ebenso in HROG05 eine starke IDO1 Hochregulation zu beobachten sowie eine marginale in HROG63 Zellen (Abb. 3D).

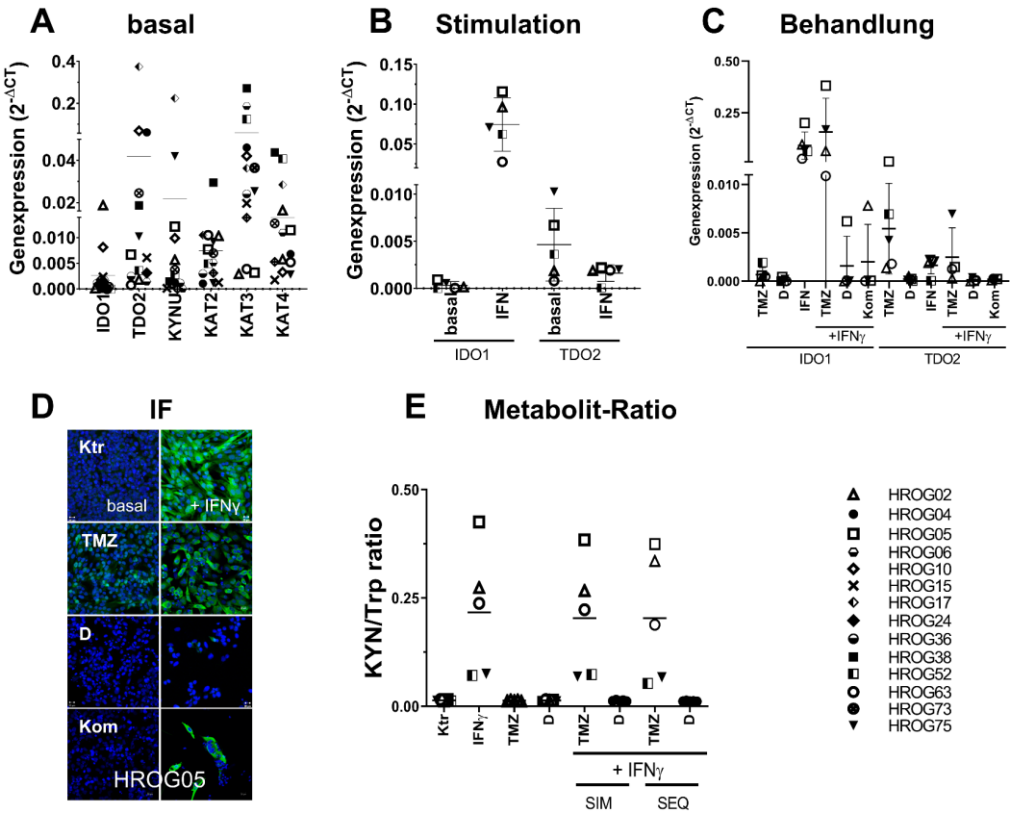

Abbildung 3: Spezifische Analyse des KS in GBM-Zellen auf Gen-, Protein- und Metabolitebene; basal, unter Stimulation und unter Behandlung. A basale relative mRNA-Expression ($2^{-\Delta CT}$) von *IDO1, TDO2, KYNU, KAT2, KAT3* und *KAT4* normalisiert auf *GAPDH* in 13 GBM-Zelllinien. **B** relative mRNA-Expression ($2^{-\Delta CT}$) von *IDO1* und *TDO2* unter IFN-γ Stimulation normalisiert auf *GAPDH* in fünf GBM-Zelllinien. **C** relative mRNA-Expression ($2^{-\Delta CT}$) von *IDO1* und *TDO2* unter dem Einfluss von TMZ, D und IFN-γ und der SIM-Gabe der Substanzen mit IFN-γ normalisiert auf *GAPDH* in fünf GBM-Zelllinien. **D** Immunfluoreszenz (IF) zum Nachweis von IDO1 an einer ausgewählten GBM-Zelllinie einzeln unter dem Einfluss von TMZ, D und IFN-γ sowie unter SIM-Gabe der Substanzen mit IFN-γ (Maßstab: 20 µm). **E** Metabolitenspiegel in GBM-Zellen einzeln, unter Therapie oder in SIM- oder SEQ-Gabe. Das KYN/Trp-Verhältnis in GBM-Zellen wurde durch Division der KYN-Werte durch die Trp-Werte ermittelt. Ktr – Kontrolle, TMZ – Temozolomid, D – Dinaciclib, Kom – Kombination, SIM – simultan, SEQ – sequentiell.

In weiterführenden Analysen wurde überprüft, ob TMZ und Dinaciclib, auch in Kombination mit IFN-γ, einen Einfluss auf die KS-vermittelte Gen-, Protein- und Metabolitebene ausüben

(Abb. 3C). Hierbei zeigte sich, dass TMZ in 3/5 Fällen *IDO1* herunterregulierte. Die Genexpression von *KAT2, KAT4* und *KMO* war zelllinien-spezifisch heterogen. Die TMZ/IFN-γ-Kombination, eine Nachahmung der *in vivo*-Situation, führte in 2/4 GBM-Proben zu einer stärkeren Hochregulation. Die Zugabe von Dinaciclib entweder zu IFN-γ oder TMZ reduzierte die mRNA-Expression von *IDO1* deutlich. Andere KP-verwandte Gene wie *TDO2* und *KAT1-4* wurden in ähnlicher Weise herunterreguliert. Dies konnte auch auf Proteinebene bestätigt werden, indem Dinaciclib das IFN-γ-induzierte IDO1 effektiv blockierte, während TMZ allein sowie in Kombination mit IFN-γ den Proteinspiegel stark erhöhte (Abb. 3D). Der IFN-γ-induzierende Stimulus konnte in einer Dreier-Kombination nicht weiter unterdrückt werden. Die KS-bezogenen Metabolite Trp, KYN und KYNA waren unter Zugabe von TMZ oder Dinaciclib nur geringfügig beeinflusst (Abb. 3E). Wie erwartet waren der Trp-Abbau und der KYN-Spiegel unter IFN-γ oder in Kombination mit TMZ stark erhöht. Im Gegensatz dazu blieb dies unter Dinaciclib im Vergleich zur Kontrolle unverändert. Somit ist Dinaciclib in der Lage, die IFN-γ-vermittelte und damit höchstwahrscheinlich auch die Chemotherapie-induzierte IDO1-Hochregulierung in GBM-Zellen zu blockieren.

4.2 Selektive CDKi weisen ein großes therapeutisches Potential im 2D- und 3D-GBM-Modell auf

In weiterführenden Untersuchungen wurden neben Dinaciclib auch die selektiven CDK4/6i Abemaciclib und Palbociclib und das Standardtherapeutikum TMZ in Mono- und Kombinationstherapie eingesetzt. Neben verschiedenen morphologischen Veränderungen, wie der Bildung kleiner Vakuolen und Zellschrumpfung bei Dinaciclib und einem multivakuolären Phänotyp bei Abemaciclib, führte die Monotherapie der beiden CDKi Dinaciclib und Abemaciclib zu einer stark verminderten Viabilität in den fünf getesteten Zelllinien (Abb. 4A). Anschließend wurde eine simultane (SIM) und eine sequentielle (SEQ) Kombinationsbehandlung durchgeführt. Dabei ließ sich feststellen, dass der Zeitpunkt des Einsatzes der einzelnen Kombinationspartner die Wirksamkeit beeinflusst: In 3/5 Fällen potenzierte (Synergismus) die SIM-Behandlung von Dinaciclib und Abemaciclib die antitumorale Wirkung der Monotherapie. Bei der SEQ-Behandlung von Dinaciclib und TMZ war ebenfalls ein synergistischer Effekt in 4/5 Fällen nachweisbar, wohingegen sich die anderen Behandlungsschemata meist antagonistisch auswirkten (Abb. 4A). In den 3D-Kulturen blieben die zytotoxischen Auswirkungen weitestgehend erhalten, wobei die GSCs deutlich empfindlicher gegenüber den CDKi waren als die GBSs. Die Behandlung mit Palbociclib und TMZ hatte in beiden Modellen einen geringen bzw. keinen Einfluss auf Viabilität und Morphologie. Aus diesem Grund wurde der Fokus in den weiteren Analysen auf die Behandlung mit den CDKi Abemaciclib und Dinaciclib und als Referenz TMZ gelegt. In funktionellen Analysen wurde überprüft, welchen Einfluss die CDK-Inhibition auf verschiedene zelluläre Parameter hat. Anhand einer Apoptose/Nekrose-Analyse konnte exemplarisch an HROG63 gezeigt werden, dass die Nekrose der dominierende Zelltod bei

Dinaciclib war, wohingegen Abemaciclib eher eine frühe Apoptose auslöste. Die duale CDK-Inhibition von Abemaciclib und Dinaciclib induzierte eine Mischform aus Apoptose und Nekrose (Abb. 4B). Der immunogene Zelltod, u.a. charakterisiert durch die Translokation von Calretikulin (CalR), war durch keine der Behandlungsschemata induzierbar und spielte daher eine untergeordnete Rolle (Pub. II Abb. 2C). Im Anschluss wurde die Ursache der zytoplasmatischen Vakuolbildung und der Einfluss der CDKi auf die Mitochondrien untersucht. Eine CDKi-induzierte lysosomale Aktivierung ließ sich vor allem unter Abemaciclib in den Zelllinien HROG05 und HROG63 erkennen. Darüber hinaus war eine mitochondriale Dysfunktion unter CDKi-Therapie nachweisbar, die sich durch Hyperpolarisation der mitochondrialen Membran (MMP) und mitochondrialen oxidativen Stress (Mito-ROS) in HROG05 auszeichnete (Abb. 4C, linke Bildreihen und unten rechts). Auch in den 3D-Modellen zeigten sich erhöhte MMP unter Dinaciclib (Pub. II, Abb. 3G).

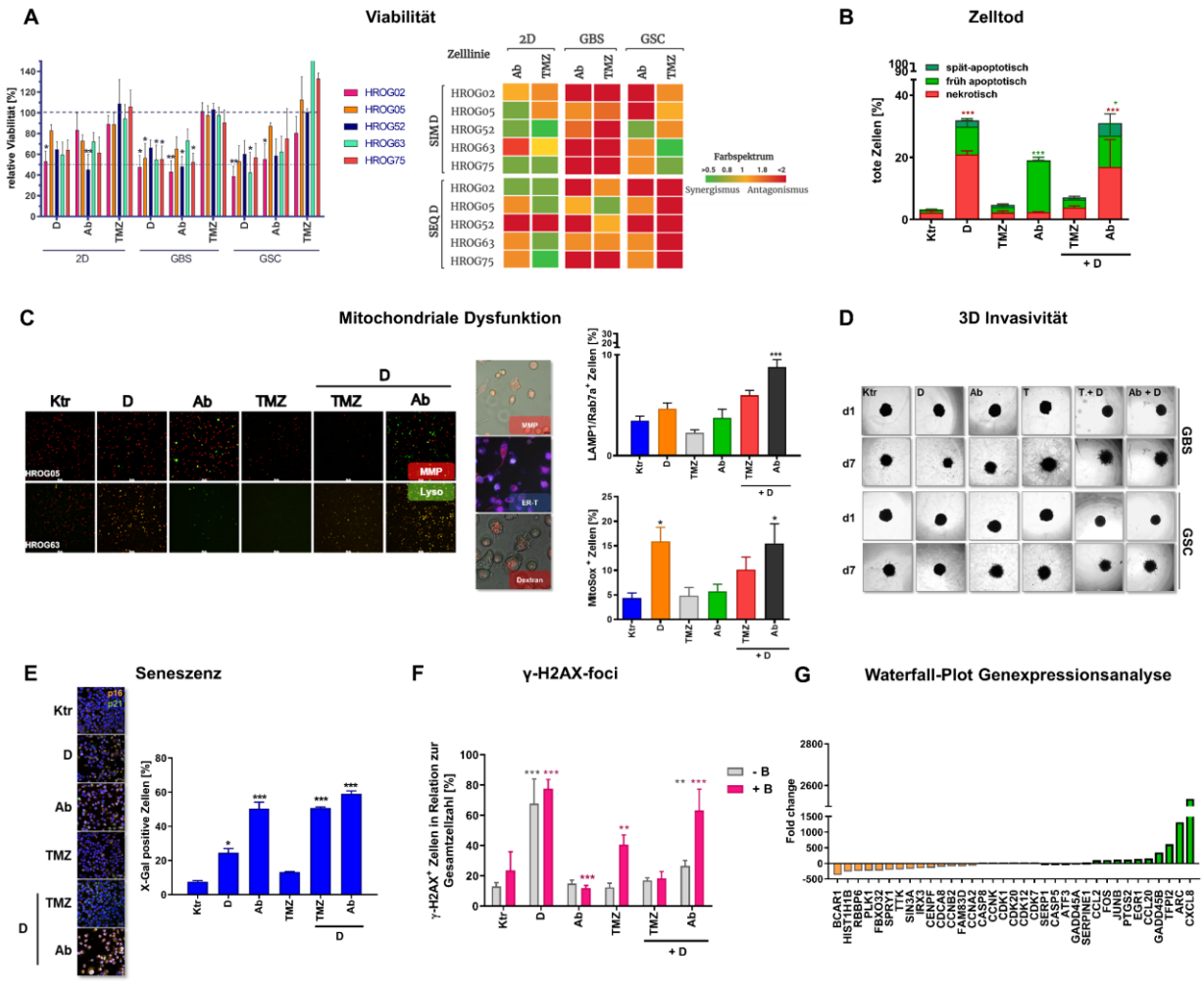

Abbildung 4: Viabilität, Invasivität und mitochondriale Funktionalität in GBM-Zellen nach CDKi- und TMZ-Behandlung. A links: Quantitative Analyse der Zellvitalität (% vs. Ktr = 100 %). n = 5; MW ± SEM, $^{**}p < 0{,}01$; $^{*}p < 0{,}05$ vs. Ktr (One-way-ANOVA). rechts: Bliss-Unabhängigkeitsmodell – SIM/SEQ-Behandlung mit Dinaciclib sowie Abemaciclib oder TMZ aller getesteten Zelllinien im 2D- und 3D Modell. Wenn Δ<1 wirkten Substanzen synergistisch (grünes Muster); bei Δ=1 wirkten Substanzen additiv (gelbes Muster); bei Δ>1 wirkten

die Substanzen antagonistisch (oranges und rotes Muster); Grafik wurde mit Biorender erstellt. **B** Durchflusszytometrische Analyse des Zelltods (in %): früh apoptotisch (YO-PRO-1$^+$), spät apoptotisch (YO-PRO-1$^+$/PI$^+$), nekrotisch (PI$^+$). n = 3, MW ± SEM, ***p < 0,001; *p < 0,05 vs. Ktr (Two-way ANOVA). **C** Vakuolisierung unter CDKi-Therapie. linke Bildreihen: Repräsentative Darstellung aus n = 3 von HROG05 und HROG63. grün (Lyso) = saure Komponenten, rot (MitoT) = MMP, mittige Bildreihe: rot (MitoT) = MMP (mitochondrialer Ursprung), blau (ERT) = endoplasmatischer Ursprung, rot (Dextran) = Macropinocytose-Ursprung (Maßstab: 50 µm). rechts oben: Quantitative durchflusszytometrische Analyse der LAMP1/Rab7a$^+$-Zellen in %. n = 3, MW± SEM, ***p < 0,001; **p < 0,01 vs. Kontrolle. (One-way-ANOVA). rechts unten: Quantitative durchflusszytometrische Analyse der Mito-ROS. Anteil MitoSox$^+$-Zellen in %. n = 3, MW ± SEM, *p < 0,05 vs. Ktr (One-way-ANOVA). **D** Einfluss auf 3D-Invasivität. Repräsentative Darstellung aus n = 3, HROG05, d1 und d7, (Maßstab: 250 µm). **E** Seneszenzinduktion durch Aktivierung von p16/p21 und ß-Galactosidase. links: Repräsentative Darstellung aus n = 3, HROG05. blau = Dapi, orange = p16, grün = p21, (Maßstab: 50 µm). rechts: Quantitative Analyse der X-Gal-positiven Zellen im Verhältnis zur Gesamtzellzahl, HROG05, n = 3, MW± SEM, ***p < 0,001; *p < 0,05 vs. Ktr., (Two-way-ANOVA). **F** Quantitative Analyse der γ-H2AX-Foci-Anzahl im Verhältnis zur Gesamtzellzahl mit Bestrahlung (+ B) und ohne Bestrahlung (- B). Zellkerne wurden als positiv deklariert, wenn mehr als 20 Foci/Kern sichtbar waren, HROG05, n = 3, MW ± SEM, ***p < 0,001; **p < 0,01 vs. Ktr. (Two-way-ANOVA). **G** Waterfall-Plot des RNA-Expressionsniveaus (Fold-Change) von HROG63, ausgewählte Gene: p < 0,001. Limma wurde hier zur Berechnung des P-Wertes verwendet, n = 3. Ktr – Kontrolle, TMZ – Temozolomid, D – Dinaciclib, Ab – Abemaciclib, SIM – simultan, SEQ – sequentiell.

Einige große CDKi-induzierte Vakuolen in HROG05 waren weder positiv für MMP noch für eine lysosomale Aktivität, den ER-Tracker oder 10 kDa Dextran (Abb. 4C, Mitte). In diesen Behandlungsschemata wurde die Vakuolisierung von einer höheren Abundanz der spät-endosomalen Marker LAMP1 und Rab7a in HROG05 begleitet (Abb. 4C, rechts oben). Der Einfluss auf die Migration und Invasion im 2D-System ließ sich zwar nicht durch Dinaciclib verändern, allerdings konnte die GBM-Motilität in beiden Zelllinien vollständig verhindert werden (Pub. II, Abb. 5). Beide CDKi unterdrückten die Invasivität von GB- und GSC-Sphäroiden über einen Zeitraum von 7d in beiden Zelllinien effektiv, wohingegen TMZ diese gleichermaßen verstärkte (Abb. 4D). Zusätzlich zu den beschriebenen Effekten induzierten die CDKi Abemaciclib und Dinaciclib Seneszenz über die Aktivierung von p16/p21 (Abb. 4E). Lediglich Dinaciclib induzierte γ-H2AX-Foci, ein Nachweis für DNA-Doppelstrangbrüche, die nach einer kombinierten CDKi-Strahlentherapie verstärkt auftraten (Abb. 4F). Schließlich wurde die starke globale zytotoxische Wirkung von Dinaciclib in HROG63 durch eine Genexpressionsanalyse bestätigt. Hierbei wurden u.a. Gene, die an der Regulierung und Progression des Zellzyklus, der Transkriptionsregulation und der Zellmigration beteiligt sind, stark herunterreguliert, während das Expressionsniveau von Chemotaxis-vermittelnden Genen und DNA-Stress- und Schädigungsgenen signifikant hochreguliert wurde (Abb. 4G). Erstaunlicherweise beeinträchtigte Abemaciclib die Koloniebildung in einer Langzeitbehandlung besser als Dinaciclib. Die kombinierte Gabe beider CDKi war aber im Stande, einer intrinsischen/erworbenen Resistenz in HROG05 effektiv entgegenzuwirken (Pub. II, Abb. 8).

4.3 Implementierung eines kombinierten CDKi/Chemotherapeutika-Ansatzes bei HNSCC-Modellen

An den HNSCC-Zelllinien UT-SCC-14 und UT-SCC-15 wurde schließlich das therapeutische Potential eines kombinierten Behandlungsansatzes basierend auf den CDKi Dinaciclib, Palbociclib und THZ1 sowie den HNSCC-Standardtherapeutika 5-FU, Cisplatin und Cetuximab evaluiert.

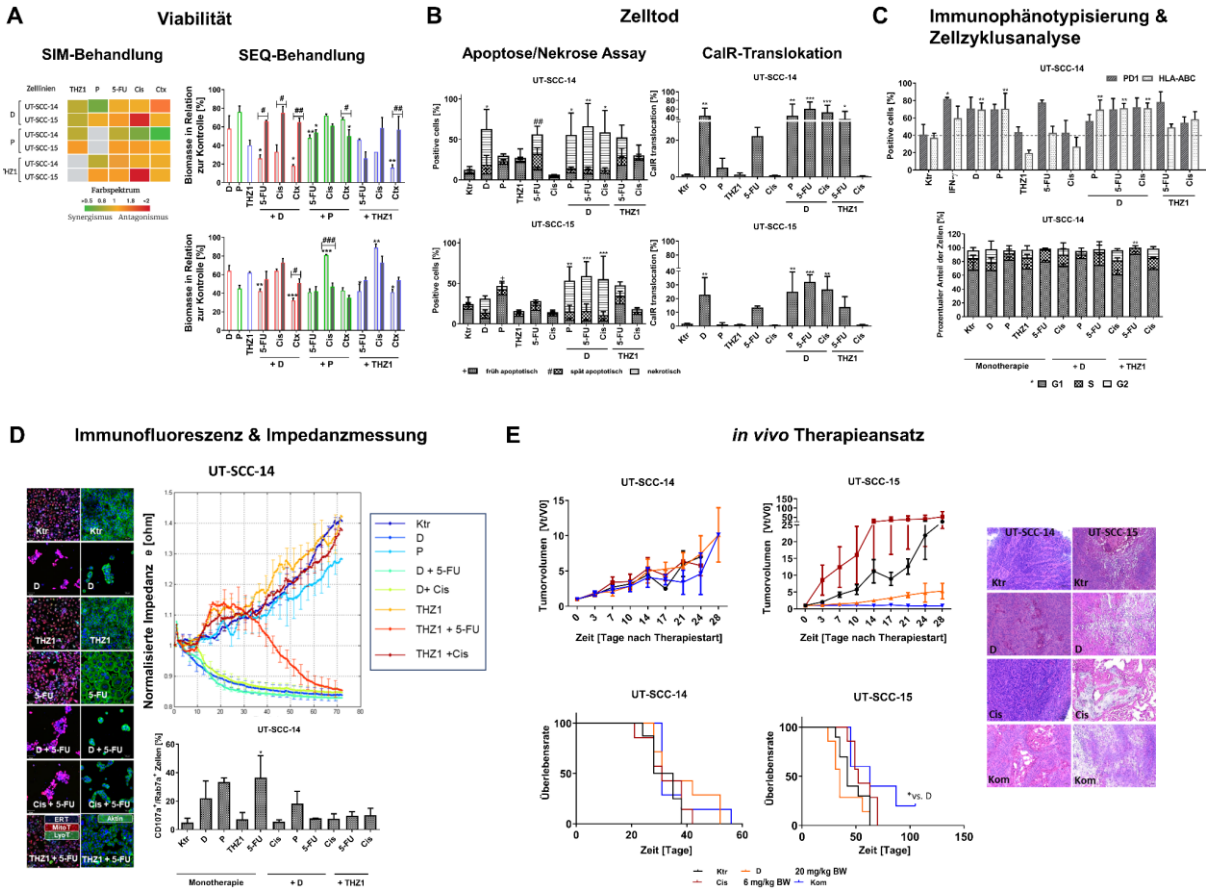

Abbildung 5: CDKi/CT-Kombination erhöht anti-tumorale Effekte in HNSCC über verschiedene Mechanismen *in vitro* und *in vivo*. A Quantitative Viabilitätsanalyse der UT-SCC-14 (oben) und UT-SCC-15 (unten) im SIM- und SEQ-Schema. links: Bliss-Unabhängigkeitsmodell – SIM-Behandlung der Zelllinien UT-SCC-14 und UT-SCC-15 mit jeweiligen Subtanzen. Grün indiziert synergistische Wirkung, gelb weist auf additiven Effekt hin und orange/rot deutet jeweils eine antagonistische Wirkung an. Grafik wurde mit Biorender erstellt. rechts: Relative Biomasse (% vs. Ktr). n=3-4; MW±SD, ***p<0,0002; **p<0,002; *p<0,05 vs. Ktr. (Mann-Whitney U-Test); ##p<0,002; #p<0,05 vs. CDKi (Kruskal-Wallis-Test). **B** Durchflusszytometrische Analyse des Zelltods (in %); links: Apoptose-Nekrose-Assay von UT-SCC-14 (oben) und UT-SCC-15 (unten): früh apoptotisch (YO-PRO-1$^+$), spät apoptotisch (YO-PRO-1$^+$/PI$^+$) oder nekrotisch (PI$^+$); n = 4-5, MW ± SD, Kruskal-Wallis-Test; spät apoptotisch # p < 0,05 vs. Ktr; nekrotisch * p < 0,05, ** p < 0,01 vs. Ktr; rechts: immunogener Zelltod (CalR$^+$) von UT-SCC-14 (oben) und UT-SCC-15 (unten), MW ± SD, One-way-ANOVA, n = 3-4, * p < 0,05, ** p < 0,01, *** p < 0,001 vs. Ktr. **C** Phänotypisierung und Zellzyklusanalyse von UT-SCC-14. oben: Quantitative durchflusszytometrische Analyse des Phänotyps (PD-1 und HLA-ABC in %), n > 3; MW ± SD, * p < 0,05, ** p < 0,01, vs. Ktr, One-way-ANOVA. unten: Quantitative durchflusszytometrische Analyse des Zellzyklus mit Angabe der Zellen in der G1-, S- und G2-Phase (in %), n > 3; MW ± SD, * p < 0,05, ** p < 0,01 vs. Ktr. **D** Impedanzmessung und Immunfluoreszenzfärbung des Zytoskeletts und weiterer Kompartimente. links: Repräsentative Darstellung verschiedener Kompartimente unter Behandlung von UT-SCC-14 (Maßstab: 50 µm): erste Bildreihe: rot (MitoT) = mitochondriale Aktivität, grün (Lyso) = saure Komponenten, blau = endoplasmatischer Ursprung; zweite Bildreihe: grün (Phalloidin green) = Aktinfilament, blau (DAPI) = Zellkern;

rechts oben: Realzeit Impedanzmessung von (un-) behandelten UT-SCC-14; rechts unten: Quantitative durchflusszytometrische Analyse der Vakuolbildung von UT-SCC-14, dargestellt ist der prozentuale Anteil ($LAMP1^+/Rab7a^+$), n > 3, MW ± SD, * p < 0,05 vs. Ktr. **E** *in vivo* Therapieansatz. links: Tumorwachstumskurve und Kaplan-Meier-Überlebenskurve: Berechnung Tumorvolumen (Tv): Tv des jeweiligen Tages x (Vt)/ Tv zu Beginn des Experimentes; Log-Rank-Test (Mantel-Cox), UT-SCC-14: Ktr (n = 8 Mäuse); Cis/D/Kombination (n = 7 Mäuse/Gruppe); UT-SCC-15: Ktr (n = 10 Mäuse); Cis/D (n = 7 Mäuse/Gruppe); Kombination (n = 5 Mäuse); MW±SEM, * p < 0,05 vs. Dinaciclib. rechts: Repräsentative Darstellung der HE-gefärbten Tumorproben der einzelnen Behandlungsgruppen. Maßstab: 20x. Ktr – Kontrolle, D – Dinaciclib, P – Palbociclib, Cis – Cisplatin, 5-FU – 5-Fluorouracil, Ctx – Cetuximab, Kom – Kombination, SEQ – sequentiell, CalR - Calretikulin.

Beide Zelllinien waren empfindlich gegenüber der Monoapplikation der CDKi. Die dualen SIM-CDKi-Behandlungen führten bei den UT-SCC-14 überwiegend zu additiven bzw. synergistischen Effekten, welche zum Teil auch bei den UT-SCC-15 erzielt wurden. Die SIM-CDKi/CT-Kombinationen waren dagegen hauptsächlich antagonistisch. Eine Ausnahme bildeten Cisplatin in Verbindung mit Dinaciclib (UT-SCC-14) sowie Cetuximab mit Dinaciclib oder THZ1 (UT-SCC-15). Im SEQ-Ansatz wurden die CDKi entweder vor oder nach den CT verabreicht. Eine stärkere Biomassereduktion ergab sich, mit Ausnahme der SEQ-Palbociclib/Cisplatin bzw. Cetuximab-Gabe, wenn zunächst die CT und im Anschluss Dinaciclib verabreicht wurde (Abb. 5A, Pub. III, Abb.1). In weiterführenden funktionellen Analysen wurde gezeigt, dass Dinaciclib und deren Kombinationen Nekrosen auslösten, wohingegen THZ1 und deren Kombinationen Apoptose und eine Mischform hervorriefen (Abb. 5B, links). Die CalR-Translokation, die anhand CalR-positiver Zellen und des mittleren Fluoreszenzsignals erfasst wurde, wurde hier durch Dinaciclib, dessen Kombinationen sowie durch die THZ1/5-FU Applikation hervorgerufen (Abb. 5B, rechts). Auch die immunologisch relevanten Marker HLA-ABC und PD-1 waren nach Dinaciclib-, dessen Kombinationen und Palbociclib-Behandlung speziell bei den UT-SCC-14 erhöht (Abb. 5C, oben). Zusätzlich zeigte sich eine mäßige Seneszenzinduktion nach CDKi-Therapie (Pub. III, *Supplement*). Ein signifikanter G1-Arrest ließ sich nach kombinierter THZ1/5-FU-Therapie (UT-SCC-14) beobachten, während dies bei den UT-SCC-15 nur nach Palbociclib und 5-FU-Monotherapie der Fall war (Abb. 5C, unten). Die Zellimpedanz, welche Aufschluss über Zellschichtveränderungen, Adhäsionseigenschaften und die Membranintegrität gibt, wurde massiv durch Dinaciclib und die Kombinationen verringert, hauptsächlich bedingt durch Zellablösung (Abb. 5D, rechts oben). Bestätigt wurden die Daten der Zellimpedanzmessung durch das Anfärben des Aktinfilaments (Abb. 5D, zweite Bildreihe). Bei THZ1 konnte ein leichter Impedanzanstieg verzeichnet werden, der sich auch in verstärkten Stressfasern widerspiegelte. Im Gegensatz dazu verstärkten Cisplatin und 5-FU die Aktinausbreitung. Der Kombinationsansatz aus THZ1/5-FU führte zu einem verzögerten Impedanzabfall ebenfalls einhergehend mit einem Ablösen der Zellen (Abb. 5D, rechts oben). Durch die Behandlung induzierte Doppelstrangbrüche wurden anhand von γ-H2AX-Foci bestimmt und konnten lediglich bei Palbociclib sowie den THZ1/5-FU basierten Therapien verzeichnet werden (Pub. III, Abb. 4). In Kongruenz mit den zuvor erhobenen Daten (Pub. II, hier 4.3) konnte bestätigt werden, dass Dinaciclib und die Kombinationen einen Einfluss auf die MMP in beiden Zelllinien ausübten. Palbociclib, THZ1

oder Cisplatin induzierten die Bildung von Lysosomen in UT-SCC-14-Zellen (Abb. 5D, erste Bildreihe). Eine höhere Abundanz der spät-endosomalen Marker LAMP1 und Rab7a wurde Zelllinien- und therapiespezifisch nachgewiesen. Hier konnte ein Anstieg nach Dinaciclib, Palbociclib und 5-FU bei den UT-SCC-14 und nach SIM-Palbociclib/Dinaciclib-Gabe bei den UT-SCC-15 festgestellt werden (Abb. 5D, rechts unten). Die Zellmotilität war, wie in Pub. II beschrieben, auch hier durch Dinaciclib und in Verbindung mit THZ1 bei den UT-SCC-14 stark beeinträchtigt. Diese Effekte wirkten sich auch auf die Invasivität der UT-SCC-14-Zellen aus (Pub. III, *Supplement*). Abschließend wurden die *in vitro*-Daten von Dinaciclib und Cisplatin im *in vivo*-Modell validiert. UT-SCC-14 Xenografts zeigten ein schlechtes Therapieansprechen, da lediglich ein geringer Einfluss auf das Tumorwachstum zu verzeichnen war. Im Gegensatz dazu wurde das Tumorwachstum bei den UT-SCC-15 Xenotransplantaten deutlich reduziert, am ausgeprägtesten bei der Kombination. Die Immunhistologie bestätigte dabei die beobachteten Ergebnisse. Während bei den UT-SCC-14 Transplantaten eine anfängliche Nekrose bei Dinaciclib und Cisplatin Monotherapie zu sehen war, ließ sich bei den UT-SCC-15 Transplantaten eine deutliche Nekrose in allen Behandlungsmodalitäten erkennen (Abb. 5E).

5. Diskussion

Das häufige Auftreten von Rezidiven und die Resistenz gegenüber der konventionellen Therapie stellen sowohl beim GBM als auch bei HNSCC eine große Herausforderung dar. Bisherige Bestrebungen, die Prognose der betroffenen GBM-PatientInnen zu verbessern, haben in den letzten 50 Jahren nur zu einer marginalen Verbesserung geführt [45,151,152]. Auch die Überlebensrate bei HNSCC hat sich in den letzten drei Jahrzehnten nur moderat gebessert [153]. Genomische Alterationen in den CDKs und die Generierung eines immunsuppressiven Mikromilieus sind dabei entscheidende Faktoren [154–157]. Therapeutische Ansätze basierend auf der Inhibition der CDKs werden aktuell in präklinischen und klinischen Studien evaluiert [45,154,157–162]. Zur Steigerung der therapeutischen Effektivität werden zunehmend multimodale Behandlungsprotokolle mit klassischen Chemotherapeutika, Biologika wie beispielsweise monoklonalen Antikörpern und immuntherapeutischen Ansätzen, aber auch zielgerichteten Therapien eingesetzt [45,106,160,163–166]. CDK-Inhibitoren gehören zur Klasse der zielgerichteten Substanzen und wurden in der vorliegenden Dissertationsschrift als Therapeutika verwendet.

Der Fokus der vorliegenden Arbeit lag neben der grundsätzlichen Relevanz des KS beim GBM vor allem auf der detaillierten Charakterisierung der zellbiologischen Effekte nach CDKi Mono- sowie Kombinationstherapie mit Chemotherapeutika bei GBM und HNSCC. Hierzu wurden die CDKi sowohl simultan als auch sequentiell an Patienten-abgeleiteten GBM-Zelllinien im 2D- und 3D-Modell *in vitro* und an HNSCC im 2D- und am Xenotransplantatmodell eingesetzt. Diese Behandlungsansätze besitzen einen innovativen Charakter und stellen eine vielversprechende Strategie dar.

5.1 Analyse IDO1-assoziierter Gene und Metaboliten und Suppression des KS durch Dinaciclib

IDO1, aber auch *TDO2,* sind in verschiedenen Entitäten, wie etwa malignen Gliomen und HNSCC, konstitutiv überexprimiert und durch eine lokale und systemische Immunsuppression gekennzeichnet. Dies korreliert mit der Aggressivität und dem Tumorgrad [73,167–170]. In dieser Arbeit konnte gezeigt werden, dass der KS in den untersuchten GBM-Zelllinien bzw. primären Geweben aktiv ist und zu einem iTM beiträgt. Dies ist charakterisiert durch eine geringe basale *IDO1*- und eine konstitutiv hohe *TDO2*-Expression. Obwohl *IDO1* normalerweise nicht oder nur in sehr geringen Mengen im Gehirn exprimiert wird, steigt es bei entzündlichen Prozessen rasch an. Dabei wird IDO1 in 96 % der malignen Gliome exprimiert [171,172]. Auch *TDO2* mRNA war bereits in einer Reihe von menschlichen Tumorproben detektierbar, darunter auch beim GBM [173,174]. Um die immunvermittelte entzündliche TM nachzuahmen, wurde das Zytokin IFN-γ verwendet. IFN-γ induziert IDO1, wodurch der Trp-Serumspiegel sinkt und der KYN-Metabolit ansteigt [175]. So wurde unter IFN-γ-Stimulation die Expression von *IDO1* sowohl auf Gen- als auch

Proteinebene hochreguliert. Dahingegen verhielt sich die Genexpression von *TDO2* und *KAT3* unter Stimulation invers. Während TMZ *IDO1* auf der mRNA-Expressionsebene negativ beeinflusste, stieg die Menge des resultierenden Proteins an. Dieses könnte entweder auf eine verlängerte Halbwertzeit des Proteins aufgrund einer verringerten Abbaugeschwindigkeit oder auf eine bevorzugte Translation während des zellulären Stresses zurückzuführen sein. Die IFN-γ-Stimulation in Kombination mit TMZ war hingegen von einer erhöhten *IDO1*-Expression und einer vermehrten KYN- und KYNA-Produktion begleitet. Der Anstieg des Trp-Katabolismus und der KYN-Produktion (KYN/Trp-Verhältnis) werden häufig als indirekter Indikator für die kumulativen Aktivitäten von TDO2, IDO1 und IDO2 verwendet [176,177]. Einige Tumoren, wie GBM, können *IDO1* als adaptiven Resistenzmechanismus exprimieren, wobei IDO1 über IFN-γ von Tumor-infiltrierenden T-Zellen induziert wird [178]. Darüber hinaus weisen Gliome und glioneuronale Tumoren eine erhöhte Trp-Aufnahme und einen erhöhten Trp-Abbau *in vivo* auf [179]. Angesichts dieser Beobachtung könnte dies eine Erklärung für die (erworbene) Arzneimittelresistenz und das Rezidiv-Verhalten bei GBM liefern. Aus diesem Grunde sollten IDO1 Inhibitoren auf TMZ basierte Therapieansätze untersucht werden. In dieser Studie war lediglich Dinaciclib in der Lage, den KS unabhängig vom Kombinationspartner zu beeinträchtigen, da es die IFN-γ-induzierte IDO1-Hochregulation nach gleichzeitiger Behandlung wirksam unterdrückte. Es ist allerdings davon auszugehen, dass es sich eher um eine indirekte Beeinflussung handelt, da GBM-Zellen mit einer starken IDO-Expression nach Dinaciclib-Behandlung nur eine geringfügig veränderte IDO-Proteinabundanz aufwiesen. Nach längeren oder wiederholten Behandlungszyklen könnte sich dieser beobachtete Effekt noch verstärken lassen. So wurde bereits von mehreren präklinischen Studien in Erwägung gezogen, (nicht) selektive IDO-Inhibitoren in Verbindung mit Chemo- und/oder Strahlentherapie zu verabreichen, um synergistische Effekte zu erzielen [180]. Schließlich könnte dieses Phänomen Auswirkungen auf weitere immuntherapeutische Ansätze haben und der zu diesem Zeitpunkt ermittelte KYN/Trp-Index dabei ein relevanter klinischer Maßstab als prognostischer Wert für GBM-PatientInnen sein [181].

5.2 Mechanistische Erkenntnisse zu CDKs auf Viabilität, Invasion, Vakuolisierung und mitochondriale Beeinträchtigung in GBM-Zellen

Alle getesteten GBM-Zelllinien waren sowohl im 2D- als auch im 3D-Modell empfindlich gegenüber Abemaciclib und Dinaciclib. Demgegenüber wurden nur marginale zytotoxische Effekte durch Palbociclib erzielt. Abemaciclib und Palbociclib werden als selektive CDK4/6i beschrieben. Abemaciclib unterscheidet sich jedoch strukturell von Palbociclib. In der Konsequenz weist Abemaciclib eine andere Selektivität für CDK4/6 und andere Kinasen auf [182]. Dieser Umstand könnte eine Erklärung für die hier beobachtete unterschiedliche Zytotoxizität liefern. Damit sprechen die Daten für eine zukünftige Anwendung von Abemaciclib und Dinaciclib anstelle von Palbociclib bei der Behandlung von GBM-

PatientInnen, auch unter der Berücksichtigung der Permeabilität von Abemaciclib über die Blut-Hirn-Schranke. Sowohl Abemaciclib als auch Dinaciclib führten zur Bildung saurer Kompartimente mit unterschiedlicher Intensität. Abemaciclib induzierte eine frühe Apoptose, während Dinaciclib primär Nekrose hervorrief. CDKi-vermittelte Apoptose ist in verschiedenen Tumormodellen beschrieben worden [126,141,154,183–189]. Im Gegensatz dazu wurde die Autophagie erst kürzlich für Abemaciclib beschrieben [190,191] und nur eine Veröffentlichung deskribierte die zytoprotektive Rolle der Autophagie unter Dinaciclib-Therapie [192]. Wie bereits für einen anderen pan-CDKi (Flavopiridol) gezeigt, sind Veränderungen der LC3B-II-Aggregation und die verringerte Expression von p62/Sequestosome1 mögliche Ursachen [193]. Die GBM-Motilität war durch beide CDKi stark beeinträchtigt, wohingegen die Migration und Invasion im 2D-System stärker durch Abemaciclib beeinflusst wurde. Beide CDKi waren jedoch im Stande, die Invasivität von GBS und GSC erheblich zu inhibieren. In anderen Studien wurde bereits eine verringerte Motilität unter CDKi-Behandlung beschrieben: Die Hemmung von CDK4 konnte die Invasion, metastatische Ausbreitung und das Fortschreiten eines duktalen Adenokarzinom-Modelles verringern [194]. In anderen Berichten wurde sogar die Beteiligung von CDK5, CDK2, CDK9, Cyclin-B/CDK1, Vimentin, Snail, COX-2 und PGE2 an der metastatischen Ausbreitung vermutet [195–197]. Auffallend war, dass TMZ das invasive Wachstum in beiden 3D-Modellen gleichermaßen verstärkte. Übereinstimmend mit diesen Ergebnissen beobachteten Kochanowski *et al*. eine gesteigerte Invasivität in $MGMT^{high}$-GBM-Zellen unter langfristiger TMZ-Belastung [198]. Durch die CDK-Inhibition waren die behandelten Zellen metabolischem Stress ausgesetzt. Dieser ist durch eine übermäßige Aktivität der Mitochondrien sowie eine eminente ROS-Produktion gekennzeichnet [199]. Dementsprechend konnte eine CDKi-induzierte mitochondriale Dysfunktion festgestellt werden, charakterisiert durch MMP sowie Mito-ROS. Auch in einer anderen Studie induzierte eine CDK4/6i Applikation ROS-Bildung und eine gesteigerte Mito-Aktivität [200]. Zusätzlich zu den bisher beschriebenen Effekten war die Behandlung mit Abemaciclib ebenso durch die Bildung eines multivakuolären Phänotyps charakterisiert. Dies wird auch in anderen Publikationen übereinstimmend beschrieben [201–203]. Einige große CDKi-induzierte Vakuolen waren dabei für die verschiedenen Tracker unempfindlich. Das lässt darauf schließen, dass die Vakuolen nicht aus den Mitochondrien oder dem ER entstammen. In diesem Fall wurde die Vakuolisierung von einer höheren Abundanz der spät-endosomalen Marker LAMP1/2 und Rab7a begleitet. Der beobachtete Phänotyp ähnelt oberflächlich einer speziellen Form des Zelltods, der Methuosis. Diese ist durch die Bildung multipler zytoplasmatischer Vakuolen gekennzeichnet, die von Endosomen durch Förderung der Makropinozytose stammen [204–206].

GBM-Zellen können eine intrinsische und/oder erworbene Strahlenresistenz aufweisen [207,208]. Unter den hier verwendeten Substanzen war nur Dinaciclib in der Lage, diese Resistenz umzukehren, indem es γ-H2AX-Foci, einen DSB-Biomarker, induzierte. Ein kombinierter CDKi-Strahlentherapieansatz verstärkte diesen Effekt. Dieser Vorgang ging

mit einer Herunterregulierung von *CDK1* und der strahlenresistenz-vermittelten *SIRT3* mRNA-Expression einher (Pub. II, Abb. 7). Auf dieser Grundlage lässt sich die Hypothese aufstellen, dass die CDKi-Behandlung den oxidativen Stress der Zellen erhöht, DSB induziert und die Seneszenz potenziert, um den Zelltod auszulösen. Dinaciclib ist im direkten Vergleich mit anderen getesteten CDKi zytotoxischer. Dies lässt sich wahrscheinlich auf die globale Aktivität bei der Beeinflussung mehrerer CDKs zurückführen. Bestätigt durch die Microarray-Daten ließ sich vergegenwärtigen, dass die Wirkungsweise von Dinaciclib noch komplexer ist als bislang angenommen. Dazu gehört nicht nur die Unterbrechung des Zellzyklus, sondern auch der induzierte Zelltod über zahlreiche Mechanismen, wie etwa die gestörte DNA-Schadensreparatur, genomische Instabilität, gestörte Transkriptions-regulierung, Induktion von dysregulierten Mitochondrien, Seneszenz und Autophagie.

5.3 Bedeutung der CDKi-Therapie bei HNSCC *in vitro* und *in vivo*

Um die Effekte der zielgerichteten CDK-Inhibition einzeln und in Kombination mit Chemotherapeutika genauer zu charakterisieren und die Wirkmechanismen zu identifizieren, wurden funktionelle zellbiologische Parameter *in vitro* ermittelt und *in vivo* validiert. Hierbei spielte der Kombinationspartner zusammen mit der zeitlichen Reihenfolge der einzelnen Substanzen eine entscheidende Rolle. So wirkte die SIM CDKi-Gabe, nicht aber die duale Applikation mit CT, synergistisch. Die SEQ Anwendung führte zu heterogenen Ergebnissen. Theoretisch sollten CT von einer vorherigen CDKi-Behandlung profitieren. Dies war jedoch nur bei Palbociclib-Vorbehandlung der Fall und bestätigt die Ergebnisse einer kürzlich durchgeführten Studie, in der über eine intrinsische Resistenz in Form einer *c-Myc* und *Cyclin E* Hochregulation bei einer SEQ-Cisplatin/Palbociclib Gabe berichtet wurde [209]. Ein weiteres Argument für eine CDKi-Erstlinientherapie liefert der Schutz normaler hämatopoetischer Stamm- und Vorläuferzellen durch einen G1-Arrest sowie die Aufrechterhaltung der Antitumorimmunität [210]. Dies konnte kürzlich in einer Phase-II-Studie von SCLC unter Trilaciclib-Therapie beobachtet werden [210,211]. Bei den beiden multi-CDKi war die SEQ Anwendung der Erstlinien-CT der Zweitlinien-CT überlegen. Mechanistisch betrachtet war die Zytotoxität auf eine frühe Apoptose mit einem anschließenden Übergang zur Nekrose zurückzuführen. Auch Hossain *et al.* konnten eine Apoptoseinduktion unter Dinaciclib beobachten [212]. Ganz im Einklang damit verringerte sich die Impedanz unter Dinaciclib Mono- und Kombinationstherapie massiv, welches mit Veränderungen der Zellform und der Organisation des Zytoskeletts einherging. Dies wiederum kann die Zell-Zell-Kontakte über Adhäsionsmoleküle, die elektrische Kopplung und die Passage durch *Gap Junctions* beeinträchtigen [213]. Bei der THZ1/5-FU-Kombination konnte ein verzögerter Impedanzabbau beobachtet werden, vermutlich hervorgerufen durch 5-FU. Umgekehrt bewirkte die THZ1-Therapie einen geringfügigen Impedanzanstieg, begleitet von einer Aktinumstrukturierung der Stressfasern. Stressfasern erhöhen die zelluläre Steifigkeit und verringern die Motilität [214–216]. Die Verschiebung der

Aktinorganisation und Beeinflussung der Impedanz könnte damit eine der wichtigsten Reaktionen auf die CDKi-Behandlung sein. Außerdem ist davon auszugehen, dass der Aktinfilamentumbau und der Impedanzabfall auch Einfluss auf die Suszeptibilität gegenüber immunvermittelter Zytolyse haben könnte und die Wirksamkeit immuntherapeutischer (Kombinations-)strategien beeinflusst [217,218]. Im Rahmen dieser Arbeit ließ sich eine erhöhte CalR-Translokation bei der SEQ THZ1/5-FU- und bei der Dinaciclib- Applikation gegenüber HNSCC-Zellen erkennen. Neben dieser war ebenso eine Hochregulation von MHC I und PD-1 ersichtlich. Auch Hossain *et al.* stellten einen Dinaciclib-vermittelten ICD bei Kolonkarzinomzellen fest [212]. Wie bereits in Publikation II beschrieben, konnte auch bei dem HNSCC-Modell eine MMP nach CDKi-Behandlung verzeichnet werden. In einem finalen *in vivo*-Experiment wurden schließlich Dinaciclib und Cisplatin aufgrund der vorherigen komplexen *in vitro* Wirkmechanismen ausgewählt. Während die Therapien bei den UT-SCC-14-Modell kaum einen Effekt erzielten, war eine ausgeprägte Inhibition der Proliferation speziell unter der Kombination bei den UT-SCC-15-abgeleiteten Xenografts zu verzeichnen. Die Diskrepanz des Ansprechens könnte in dem *Staging* der Tumoren begründet liegen, so dass fortgeschrittene Tumoren sogar eher von der Therapie profitieren als niedrig-gradige. Dies sollte prospektiv an einem größeren PatientInnen-Kollektiv evaluiert werden.

Zusammenfassend konnte in dieser Dissertation gezeigt werden, dass die CDKs wesentlich an der Proliferation, Invasivität und Malignität von Tumorzellen beteiligt sind. Eine Inhibition der CDK führte einerseits zu einer indirekten Hemmung des IFN-γ-induzierten-KS, andererseits zu einer Beeinträchtigung der Viabilität, bedingt durch eine mitochondriale Dysfunktion und ausgeprägte Vakuolisierung bei GBM-Zellen. Auch das HNSCC-Modell lieferte weitere Beweise für die komplexe Wirkungsweise und therapeutische Aktivität der CDKi. Für die Zukunft gilt es, die Wirkung der Substanzen weiter zu charakterisieren und mit weiteren zielgerichteten bzw. immunverstärkenden Ansätzen zu kombinieren, um die daraus resultierenden Ergebnisse *in vivo*- bzw. am *Organ-on a Chip*-Modell zu validieren und so zur Verbesserung der bestehenden Therapiestrategien beizutragen.

6. Zusammenfassung und Ausblick

Aufgrund des aggressiven Charakters stellen die Behandlungen des Glioblastoma multiforme (GBM) und der Kopf-Hals-Tumoren (HNSCC) eine besondere Herausforderung dar. Zusätzlich können genomische Veränderungen, die zur konstitutiven Aktivierung bzw. Überexpression von Cyclin-abhängigen Kinasen (CDK) führen und damit zu einem immunsuppressiven Tumormikromilieu beitragen, entscheidend den Tumorprogress begünstigen. Die noch immer infauste Prognose von GBM-PatientInnen sowie die nach wie vor hohe HNSCC-Morbiditäts- und Mortalitätsrate unterstreicht die Notwendigkeit, neue und wirksamere Behandlungsoptionen zu entwickeln.

Im ersten Teil der Arbeit wurde das Expressionsmuster von Schlüsselgenen und Metaboliten des Tryptophan-Katabolismus basal und unter Einfluss des Zytokins IFN-γ, des Standardtherapeutikums Temozolomid (TMZ) und des multi-CDK Inhibitors (CDKi) Dinaciclib an Patienten-abgeleiteten GBM-Zelllinien untersucht. Dabei konnte gezeigt werden, dass der Kynurenin-Signalweg (KS) in den untersuchten GBM-Zelllinien und Geweben aktiv ist. Dies ist durch eine heterogene basale Indolamin 2,3-dioxygenase-Expression (*IDO1)* und konstitutiv exprimiertes Tryptophan 2,3-dioxygenase *(TDO2)* charakterisiert. Unter IFN-γ-Stimulation wurde IDO1 auf Gen- und Proteinebene induziert, wohingegen TMZ die *IDO1* mRNA-Menge negativ beeinflusste. Im Gegensatz dazu war die IFN-γ-Stimulation in Kombination mit TMZ von einer erhöhten *IDO1*-Expression und einer vermehrten Kynurenin- und Kynureninsäure-Produktion begleitet. Lediglich Dinaciclib war nach gleichzeitiger Gabe der Kombinationspartner in der Lage, die IFN-γ-induzierte IDO1-Hochregulierung wirksam zu unterdrückten und damit den KS wahrscheinlich indirekt zu beeinträchtigen.

Im zweiten Teil der Dissertation wurde das antitumorale Potential der selektiven CDK4/6i Abemaciclib und Palbociclib, sowie des multi-CDKi Dinaciclib im 2D- und 3D-GBM-Modell analysiert. Abemaciclib und Dinaciclib beeinträchtigten die Viabilität in beiden Modellen signifikant, einhergehend mit deutlichen morphologischen Veränderungen sowie verminderter Motilität und Invasion. Zusätzlich induzierten beide CDKis Seneszenz, eine mitochondriale Dysfunktion und eine Hyperpolarisation der mitochondrialen Membran. Während nach der Behandlung mit Abemaciclib vor allem eine Zunahme von sauren Kompartimenten zu beobachten war, löste Dinaciclib DNA-Doppelstrangbrüche aus, die durch Radiatio noch verstärkt wurden. Die Gabe beider CDKi wirkte synergistisch, die Kombination mit TMZ antagonistisch. Eine Genexpressionsanalyse bestätigte die globale Wirkung von Dinaciclib durch stark signifikant veränderte Gene – u.a. des Zellzyklus, der Transkriptionsregulation, der *DNA-damage response* und des Stress-Segments. In einem Langzeitversuch wurde in einem der mit Dinaciclib behandelten Fälle eine Resistenzentwicklung beobachtet, die jedoch durch Abemaciclib verhindert werden konnte. Die Wirksamkeit von Palbociclib war insgesamt schwächer und zelllinienspezifisch, TMZ hatte kaum messbare antineoplastische Effekte auf das GBM-Wachstum.

Auf Basis dieser Befunde wurde im dritten Teil der Arbeit die therapeutische Wirksamkeit verschiedener CDKi (Palbociclib, Dinaciclib und THZ1) einzeln und in Kombination mit Chemotherapeutika (5-FU, Cetuximab, Cisplatin) in HNSCC-Modellen genauer charakterisiert und die Wirkmechanismen identifiziert. Dabei ergaben sich individuelle Effekte, die in der Heterogenität dieser Tumorentität begründet liegen. Die simultane duale CDKi-Applikation und die sequentielle Therapie, bei denen zunächst die Chemotherapeutika und im Anschluss die CDKi gegeben wurden, waren hier am effektivsten. Wie zuvor bereits im zweiten Teil beobachtet, löste Dinaciclib auch bei den HNSCC hauptsächlich Nekrose aus, wobei ein Part des immunogenen Zelltods, die CalR-Translokation, bei dieser Tumorentität eine größere Rolle zu spielen schien. Auch die immunologisch relevanten Marker HLA-ABC und PD-1 wurden nach Dinaciclib- und Palbociclib-Behandlung vermehrt nachgewiesen. Weiterhin konnte gezeigt werden, dass die Zellimpedanz unter Dinaciclib deutlich beeinträchtigt war, was ebenfalls mit einer eingeschränkten Invasivität einherging. Das *in vivo*-Modell zeigte eine zelllinienspezifische Suszeptibilität mit dem besten Therapieansprechen bei der Kombinationsapplikation aus Dinaciclib und Cisplatin.

Zusammenfassend belegen die Ergebnisse dieser Promotionsarbeit die hohe Wirksamkeit der CDKi allein und in Kombination. Besonders das gezeigte breite Wirkspektrum deutet auf ein großes therapeutisches Potential beim GBM und HNSCC hin. Hierbei wurden neuartige Wirkmechanismen identifiziert, die eine ideale Ausgangsbasis für die künftige Nutzung dieser Substanzen als innovative Therapiestrategie für GBM- und HNSCC-PatientInnen sowohl in der Primär- als auch in der Rezidivsituation darstellen.

7. Literaturverzeichnis

1 Louis DN, Perry A, Reifenberger G, von Deimling A, Figarella-Branger D, Cavenee WK *et al.* The 2016 World Health Organization Classification of Tumors of the Central Nervous System: a summary. *Acta Neuropathol 2016 1316* 2016; **131**: 803–820.

2 Louis DN, Perry A, Wesseling P, Brat DJ, Cree IA, Figarella-Branger D *et al.* The 2021 WHO Classification of Tumors of the Central Nervous System: a summary. *Neuro Oncol* 2021; **23**: 1231–1251.

3 Davis ME. Glioblastoma: Overview of Disease and Treatment. *Clin J Oncol Nurs* 2016; **20**: S2.

4 Phillips HS, Kharbanda S, Chen R, Forrest WF, Soriano RH, Wu TD *et al.* Molecular subclasses of high-grade glioma predict prognosis, delineate a pattern of disease progression, and resemble stages in neurogenesis. *Cancer Cell* 2006; **9**: 157–173.

5 Agnihotri S, Burrell KE, Wolf A, Jalali S, Hawkins C, Rutka JT *et al.* Glioblastoma, a Brief Review of History, Molecular Genetics, Animal Models and Novel Therapeutic Strategies. *Arch Immunol Ther Exp 2012 611* 2012; **61**: 25–41.

6 Ohgaki H, Kleihues P. The Definition of Primary and Secondary Glioblastoma. *Clin Cancer Res* 2013; **19**: 764–772.

7 Tamimi AF, Juweid M. Epidemiology and Outcome of Glioblastoma. *Glioblastoma* 2017; : 143–153.

8 Ostrom QT, Cioffi G, Gittleman H, Patil N, Waite K, Kruchko C *et al.* CBTRUS Statistical Report: Primary Brain and Other Central Nervous System Tumors Diagnosed in the United States in 2012–2016. *Neuro Oncol* 2019; **21**: v1–v100.

9 Leece R, Xu J, Ostrom QT, Chen Y, Kruchko C, Barnholtz-Sloan JS. Global incidence of malignant brain and other central nervous system tumors by histology, 2003–2007. *Neuro Oncol* 2017; **19**: 1553–1564.

10 Gliome im Erwachsenenalter. 2021.https://www.onkopedia.com/de/onkopedia/guidelines/gliome-im-erwachsenenalter/@@guideline/html/index.html.

11 Weller M, van den Bent M, Preusser M, Le Rhun E, Tonn JC, Minniti G *et al.* EANO guidelines on the diagnosis and treatment of diffuse gliomas of adulthood. *Nat Rev Clin Oncol 2020 183* 2020; **18**: 170–186.

12 Cheng CK, Gustafson WC, Charron E, Houseman BT, Zunder E, Goga A *et al.* Dual blockade of lipid and cyclin-dependent kinases induces synthetic lethality in malignant glioma. *Proc Natl Acad Sci U S A* 2012; **109**: 12722–12727.

13 Golebiewska A, Hau A-C, Oudin A, Stieber D, Yabo YA, Baus V *et al.* Patient-derived organoids and orthotopic xenografts of primary and recurrent gliomas represent relevant patient avatars for precision oncology. *Acta Neuropathol 2020 1406* 2020; **140**: 919–949.

14 McLendon R, Friedman A, Bigner D, Van Meir EG, Brat DJ, Mastrogianakis GM *et al.* Comprehensive genomic characterization defines human glioblastoma genes and core pathways. *Nat 2008 4557216* 2008; **455**: 1061–1068.

15 Brennan CW, Verhaak RGW, McKenna A, Campos B, Noushmehr H, Salama SR *et al.* The somatic genomic landscape of glioblastoma. *Cell* 2013; **155**: 462.

16 Marusyk A, Polyak K. Tumor heterogeneity: Causes and consequences. *Biochim Biophys Acta - Rev Cancer* 2010; **1805**: 105–117.

17 Li R, Li H, Yan W, Yang P, Bao Z, Zhang C *et al.* Genetic and clinical characteristics of primary and secondary glioblastoma is associated with differential molecular subtype distribution. *Oncotarget* 2015; **6**: 7318–7324.

18 Morokoff A, Ng W, Gogos A, Kaye AH. Molecular subtypes, stem cells and heterogeneity: Implications for personalised therapy in glioma. *J Clin Neurosci* 2015; **22**: 1219–1226.

19 Korshunov A, Sycheva R, Golanov A. Genetically distinct and clinically relevant subtypes of glioblastoma defined by array-based comparative genomic hybridization (array-CGH). *Acta Neuropathol 2006 1115* 2006; **111**: 465–474.

20 Gerson SL. MGMT: its role in cancer aetiology and cancer therapeutics. *Nat Rev Cancer 2004 44* 2004; **4**: 296–307.

21 Mansouri A, Hachem LD, Mansouri S, Nassiri F, Laperriere NJ, Xia D *et al.* MGMT promoter

methylation status testing to guide therapy for glioblastoma: refining the approach based on emerging evidence and current challenges. *Neuro Oncol* 2019; **21**: 167–178.
22 NCCN Guidelines for Patients Brain Cancer Gliomas. 2021.https://www.nccn.org/patients/guidelines/content/PDF/brain-gliomas-patient.pdf.
23 Wen PY, Weller M, Lee EQ, Alexander BM, Barnholtz-Sloan JS, Barthel FP *et al.* Glioblastoma in adults: a Society for Neuro-Oncology (SNO) and European Society of Neuro-Oncology (EANO) consensus review on current management and future directions. *Neuro Oncol* 2020; **22**: 1073–1113.
24 Malmström A, Grønberg BH, Marosi C, Stupp R, Frappaz D, Schultz H *et al.* Temozolomide versus standard 6-week radiotherapy versus hypofractionated radiotherapy in patients older than 60 years with glioblastoma: the Nordic randomised, phase 3 trial. *Lancet Oncol* 2012; **13**: 916–926.
25 McNeill KA. Epidemiology of Brain Tumors. *Neurol Clin* 2016; **34**: 981–998.
26 Ostrom QT, Truitt G, Gittleman H, Brat DJ, Kruchko C, Wilson R *et al.* Relative survival after diagnosis with a primary brain or other central nervous system tumor in the National Program of Cancer Registries, 2004 to 2014. *Neuro-Oncology Pract* 2020; **7**: 306–312.
27 Stupp R, Mason WP, van den Bent MJ, Weller M, Fisher B, Taphoorn MJB *et al.* Radiotherapy plus Concomitant and Adjuvant Temozolomide for Glioblastoma. *http://dx.doi.org/101056/NEJMoa043330* 2009; **352**: 987–996.
28 Stupp R, Hegi ME, Mason WP, Bent MJ van den, Taphoorn MJ, Janzer RC *et al.* Effects of radiotherapy with concomitant and adjuvant temozolomide versus radiotherapy alone on survival in glioblastoma in a randomised phase III study: 5-year analysis of the EORTC-NCIC trial. *Lancet Oncol* 2009; **10**: 459–466.
29 Stupp R, Taillibert S, Kanner A, Read W, Steinberg DM, Lhermitte B *et al.* Effect of Tumor-Treating Fields Plus Maintenance Temozolomide vs Maintenance Temozolomide Alone on Survival in Patients With Glioblastoma: A Randomized Clinical Trial. *JAMA* 2017; **318**: 2306–2316.
30 Guzauskas GF, Salzberg M, Wang BC. Estimated lifetime survival benefit of tumor treating fields and temozolomide for newly diagnosed glioblastoma patients. *CNS Oncol* 2018; **7**: CNS23.
31 Weller M, Cloughesy T, Perry JR, Wick W. Standards of care for treatment of recurrent glioblastoma—are we there yet? *Neuro Oncol* 2013; **15**: 4–27.
32 Audureau E, Chivet A, Ursu R, Corns R, Metellus P, Noel G *et al.* Prognostic factors for survival in adult patients with recurrent glioblastoma: a decision-tree-based model. *J Neuro-Oncology 2017 1363* 2017; **136**: 565–576.
33 Chen W, Wang Y, Zhao B, Liu P, Liu L, Wang Y *et al.* Optimal Therapies for Recurrent Glioblastoma: A Bayesian Network Meta-Analysis. *Front Oncol* 2021; **0**: 952.
34 Schäfer N, Gielen GH, Rauschenbach L, Kebir S, Till A, Reinartz R *et al.* Longitudinal heterogeneity in glioblastoma: moving targets in recurrent versus primary tumors. *J Transl Med 2019 171* 2019; **17**: 1–9.
35 Banerjee K, Núñez FJ, Haase S, McClellan BL, Faisal SM, Carney S V. *et al.* Current Approaches for Glioma Gene Therapy and Virotherapy. *Front Mol Neurosci* 2021; **14**. doi:10.3389/FNMOL.2021.621831.
36 Galstyan A, Markman JL, Shatalova ES, Chiechi A, Korman AJ, Patil R *et al.* Blood–brain barrier permeable nano immunoconjugates induce local immune responses for glioma therapy. *Nat Commun 2019 101* 2019; **10**: 1–13.
37 Dymova MA, Kuligina E V., Richter VA. Molecular Mechanisms of Drug Resistance in Glioblastoma. *Int J Mol Sci 2021, Vol 22, Page 6385* 2021; **22**: 6385.
38 Bao S, Wu Q, McLendon RE, Hao Y, Shi Q, Hjelmeland AB *et al.* Glioma stem cells promote radioresistance by preferential activation of the DNA damage response. *Nat 2006 4447120* 2006; **444**: 756–760.
39 Tomasetti C, Li L, Vogelstein B. Stem cell divisions, somatic mutations, cancer etiology, and cancer prevention. *Science (80-)* 2017; **355**: 1330–1334.
40 Lee JH, Lee JE, Kahng JY, Kim SH, Park JS, Yoon SJ *et al.* Human glioblastoma arises from subventricular zone cells with low-level driver mutations. *Nat 2018 5607717* 2018; **560**: 243–247.
41 Marzagalli M, Fontana F, Raimondi M, Limonta P. Cancer Stem Cells—Key Players in Tumor Relapse. *Cancers 2021, Vol 13, Page 376* 2021; **13**: 376.
42 Bazzoni R, Bentivegna A. Role of Notch Signaling Pathway in Glioblastoma Pathogenesis.

Cancers 2019, Vol 11, Page 292 2019; **11**: 292.
43 Shevchenko V, Arnotskaya N, Korneyko M, Zaytsev S, Khotimchenko Y, Sharma H *et al.* Proteins of the Wnt signaling pathway as targets for the regulation of CD133+ cancer stem cells in glioblastoma. *Oncol Rep* 2019; **41**: 3080–3088.
44 Bhuvanalakshmi G, Gamit N, Patil M, Arfuso F, Sethi G, Dharmarajan A *et al.* Stemness, Pluripotentiality, and Wnt Antagonism: sFRP4, a Wnt antagonist Mediates Pluripotency and Stemness in Glioblastoma. *Cancers 2019, Vol 11, Page 25* 2018; **11**: 25.
45 Stylli SS. Novel Treatment Strategies for Glioblastoma. *Cancers 2020, Vol 12, Page 2883* 2020; **12**: 2883.
46 Wang X, Lu J, Guo G, Yu J. Immunotherapy for recurrent glioblastoma: practical insights and challenging prospects. *Cell Death Dis 2021 124* 2021; **12**: 1–15.
47 Jin L, Guo S, Zhang X, Mo Y, Ke S, Duan C. Optimal treatment strategy for adult patients with newly diagnosed glioblastoma: a systematic review and network meta-analysis. *Neurosurg Rev 2020 444* 2020; **44**: 1943–1955.
48 Schoenwaelder N, Salewski I, Engel N, Krause M, Schneider B, Müller M *et al.* The individual effects of cyclin-dependent kinase inhibitors on head and neck cancer cells—a systematic analysis. *Cancers (Basel)* 2021; **13**. doi:10.3390/cancers13102396.
49 Johnson DE, Burtness B, Leemans CR, Lui VWY, Bauman JE, Grandis JR. Head and neck squamous cell carcinoma. *Nat Rev Dis Prim 2020 61* 2020; **6**: 1–22.
50 Ortiz-Cuaran S, Bouaoud J, Karabajakian A, Fayette J, Saintigny P. Precision Medicine Approaches to Overcome Resistance to Therapy in Head and Neck Cancers. *Front Oncol* 2021; **11**: 104.
51 Grünwald V, Chirovsky D, Cheung WY, Bertolini F, Ahn MJ, Yang MH *et al.* Global treatment patterns and outcomes among patients with recurrent and/or metastatic head and neck squamous cell carcinoma: Results of the GLANCE H&N study. *Oral Oncol* 2020; **102**: 104526.
52 Isayeva T, Li Y, Maswahu D, Brandwein-Gensler M. Human Papillomavirus in Non-Oropharyngeal Head and Neck Cancers: A Systematic Literature Review. *Head Neck Pathol 2012 61* 2012; **6**: 104–120.
53 Stein AP, Saha S, Kraninger JL, Swick AD, Yu M, Lambert PF *et al.* Prevalence of human papillomavirus in oropharyngeal cancer: a systematic review. *Cancer J* 2015; **21**: 138.
54 Michaud DS, Langevin SM, Eliot M, Nelson HH, Pawlita M, McClean MD *et al.* High-risk HPV types and head and neck cancer. *Int J Cancer* 2014; **135**: 1653.
55 Windon MJ, D'Souza G, Rettig EM, Westra WH, van Zante A, Wang SJ *et al.* Increasing prevalence of human papillomavirus-positive oropharyngeal cancers among older adults. *Cancer* 2018; **124**: 2993–2999.
56 Fung SYH, Lam JWK, Chan KCA. Clinical utility of circulating Epstein-Barr virus DNA analysis for the management of nasopharyngeal carcinoma. *Chinese Clin Oncol* 2016; **5**: 6–6.
57 Huang SH, Xu W, Waldron J, Siu L, Shen X, Tong L *et al.* Refining American joint committee on cancer/union for international cancer control TNM stage and prognostic groups for human papillomavirus-related oropharyngeal carcinomas. *J Clin Oncol* 2015; **33**: 836–845.
58 Pignon JP, Maître A le, Maillard E, Bourhis J. Meta-analysis of chemotherapy in head and neck cancer (MACH-NC): An update on 93 randomised trials and 17,346 patients. *Radiother Oncol* 2009; **92**: 4–14.
59 Loganathan SK, Schleicher K, Malik A, Quevedo R, Langille E, Teng K *et al.* Rare driver mutations in head and neck squamous cell carcinomas converge on NOTCH signaling. *Science* 2020; **367**: 1264–1269.
60 Lawrence MS, Sougnez C, Lichtenstein L, Cibulskis K, Lander E, Gabriel SB *et al.* Comprehensive genomic characterization of head and neck squamous cell carcinomas. *Nat 2015 5177536* 2015; **517**: 576–582.
61 Stransky N, Egloff AM, Tward AD, Kostic AD, Cibulskis K, Sivachenko A *et al.* The mutational landscape of head and neck squamous cell carcinoma. *Science (80-)* 2011; **333**: 1157–1160.
62 Hoffmann TK. Systemic therapy strategies for head-neck carcinomas: Current status. *GMS Curr Top Otorhinolaryngol Head Neck Surg* 2012; **11**: Doc03.
63 Shibata H, Saito S, Uppaluri R. Immunotherapy for Head and Neck Cancer: A Paradigm Shift From Induction Chemotherapy to Neoadjuvant Immunotherapy. *Front Oncol* 2021; **11**: 3533.
64 Ferris RL, Blumenschein G, Fayette J, Guigay J, Colevas AD, Licitra L *et al.* Nivolumab for Recurrent Squamous-Cell Carcinoma of the Head and Neck. *N Engl J Med* 2016; **375**: 1856–1867.
65 Cohen EEW, Soulières D, Le Tourneau C, Dinis J, Licitra L, Ahn MJ *et al.* Pembrolizumab

versus methotrexate, docetaxel, or cetuximab for recurrent or metastatic head-and-neck squamous cell carcinoma (KEYNOTE-040): a randomised, open-label, phase 3 study. *Lancet* 2019; **393**: 156–167.

66 Bonner JA, Harari PM, Giralt J, Azarnia N, Shin DM, Cohen RB *et al.* Radiotherapy plus Cetuximab for Squamous-Cell Carcinoma of the Head and Neck. *http://dx.doi.org/101056/NEJMoa053422* 2009; **354**: 567–578.

67 Kozakiewicz P, Grzybowska-Szatkowska L. Application of molecular targeted therapies in the treatment of head and neck squamous cell carcinoma. *Oncol Lett* 2018; **15**: 7497.

68 Adkins D, Ley J, Neupane P, Worden F, Sacco AG, Palka K *et al.* Palbociclib and cetuximab in platinum-resistant and in cetuximab-resistant human papillomavirus-unrelated head and neck cancer: a multicentre, multigroup, phase 2 trial. *Lancet Oncol* 2019; **20**: 1295–1305.

69 Platten M, Ochs K, Lemke D, Opitz C, Wick W. Microenvironmental Clues for Glioma Immunotherapy. *Curr Neurol Neurosci Reports 2014 144* 2014; **14**: 1–10.

70 Platten M, Reardon DA. Concepts for Immunotherapies in Gliomas. *Semin Neurol* 2018; **38**: 062–072.

71 Chen SMY, Krinsky AL, Woolaver RA, Wang X, Chen Z, Wang JH. Tumor immune microenvironment in head and neck cancers. *Mol Carcinog* 2020; **59**: 766–774.

72 Opitz CA, Somarribas Patterson LF, Mohapatra SR, Dewi DL, Sadik A, Platten M *et al.* The therapeutic potential of targeting tryptophan catabolism in cancer. *Br J Cancer 2019 1221* 2019; **122**: 30–44.

73 Pham QT, Taniyama D, Akabane S, Harada K, Babasaki T, Sekino Y *et al.* TDO2 overexpression correlates with poor prognosis, cancer stemness, and resistance to cetuximab in bladder cancer. *Cancer Rep* 2021; : e1417.

74 Liu M, Wang X, Wang L, Ma X, Gong Z, Zhang S *et al.* Targeting the IDO1 pathway in cancer: from bench to bedside. *J Hematol Oncol 2018 111* 2018; **11**: 1–12.

75 PP S, LA S, L H. The Kynurenine Pathway: A Primary Resistance Mechanism in Patients with Glioblastoma. *Anticancer Res* 2017; **37**: 2159–2171.

76 Ala M. The footprint of kynurenine pathway in every cancer: a new target for chemotherapy. *Eur J Pharmacol* 2021; **896**: 173921.

77 Platten M, Friedrich M, Wainwright DA, Panitz V, Opitz CA. Tryptophan metabolism in brain tumors — IDO and beyond. *Curr Opin Immunol* 2021; **70**: 57–66.

78 Triplett TA, Garrison KC, Marshall N, Donkor M, Blazeck J, Lamb C *et al.* Reversal of indoleamine 2,3-dioxygenase–mediated cancer immune suppression by systemic kynurenine depletion with a therapeutic enzyme. *Nat Biotechnol 2018 368* 2018; **36**: 758–764.

79 Cervenka I, Agudelo LZ, Ruas JL. Kynurenines: Tryptophan's metabolites in exercise, inflammation, and mental health. *Science (80-)* 2017; **357**. doi:10.1126/SCIENCE.AAF9794.

80 Munn DH, Sharma MD, Hou D, Baban B, Lee JR, Antonia SJ *et al.* Expression of indoleamine 2,3-dioxygenase by plasmacytoid dendritic cells in tumor-draining lymph nodes. *J Clin Invest* 2004; **114**: 280–290.

81 Routy JP, Routy B, Graziani GM, Mehraj V. The Kynurenine Pathway Is a Double-Edged Sword in Immune-Privileged Sites and in Cancer: Implications for Immunotherapy. *Int J Tryptophan Res* 2016; **9**: 67.

82 Peyressatre M, Prével C, Pellerano M, Morris MC. Targeting Cyclin-Dependent Kinases in Human Cancers: From Small Molecules to Peptide Inhibitors. *Cancers (Basel)* 2015; **7**: 179.

83 Riess C, Irmscher N, Salewski I, Strüder D, Classen C-F, Große-Thie C *et al.* Cyclin-dependent kinase inhibitors in head and neck cancer and glioblastoma—backbone or add-on in immune-oncology? *Cancer Metastasis Rev 2020 401* 2020; **40**: 153–171.

84 Martin CA, Cullinane C, Kirby L, Abuhammad S, Lelliott EJ, Waldeck K *et al.* Palbociclib synergizes with BRAF and MEK inhibitors in treatment naïve melanoma but not after the development of BRAF inhibitor resistance. *Int J Cancer* 2018; **142**: 2139–2152.

85 Jardim DL, Millis SZ, Ross JS, Woo MS-A, Ali SM, Kurzrock R. Cyclin Pathway Genomic Alterations Across 190,247 Solid Tumors: Leveraging Large-Scale Data to Inform Therapeutic Directions. *Oncologist* 2021; **26**: e78–e89.

86 Crespo I, Vital AL, Gonzalez-Tablas M, Patino MDC, Otero A, Lopes MC *et al.* Molecular and Genomic Alterations in Glioblastoma Multiforme. Am. J. Pathol. 2015; **185**: 1820–1833.

87 Ding L, Cao J, Lin W, Chen H, Xiong X, Ao H *et al.* The Roles of Cyclin-Dependent Kinases in Cell-Cycle Progression and Therapeutic Strategies in Human Breast Cancer. *Int J Mol Sci* 2020; **21**. doi:10.3390/IJMS21061960.

88 Asghar U, Witkiewicz AK, Turner NC, Knudsen ES. The history and future of targeting cyclin-

dependent kinases in cancer therapy. Nat. Rev. Drug Discov. 2015; **14**: 130–146.
89 Cicenas J, Valius M. The CDK inhibitors in cancer research and therapy. *J Cancer Res Clin Oncol 2011 13710* 2011; **137**: 1409–1418.
90 Baker SJ, Reddy EP. CDK4: A Key Player in the Cell Cycle, Development, and Cancer. *Genes Cancer* 2012; **3**: 658.
91 Roskoski R. Cyclin-dependent protein serine/threonine kinase inhibitors as anticancer drugs. Pharmacol. Res. 2019; **139**: 471–488.
92 Whittaker SR, Mallinger A, Workman P, Clarke PA. Inhibitors of cyclin-dependent kinases as cancer therapeutics. Pharmacol. Ther. 2017; **173**: 83–105.
93 Malumbres M, Barbacid M. Is Cyclin D1-CDK4 kinase a bona fide cancer target? Cancer Cell. 2006; **9**: 2–4.
94 Malumbres M. Cyclin-dependent kinases. *Genome Biol 2014 156* 2014; **15**: 1–10.
95 Lim S, Kaldis P. Cdks, cyclins and CKIs: roles beyond cell cycle regulation. *Development* 2013; **140**: 3079–3093.
96 Boyer MJ, Cheng T. The CDK inhibitors: potential targets for therapeutic stem cell manipulations? *Gene Ther 2008 152* 2007; **15**: 117–125.
97 Roussel MF. The INK4 family of cell cycle inhibitors in cancer. *Oncogene 1999 1838* 1999; **18**: 5311–5317.
98 Marqués-Torrejón MÁ, Porlan E, Banito A, Gómez-Ibarlucea E, Lopez-Contreras AJ, Fernández-Capetillo Ó *et al.* Cyclin-Dependent Kinase Inhibitor p21 Controls Adult Neural Stem Cell Expansion by Regulating Sox2 Gene Expression. *Cell Stem Cell* 2013; **12**: 88–100.
99 Li H, Collado M, Villasante A, Matheu A, Lynch CJ, Cañamero M *et al.* p27Kip1 Directly Represses Sox2 during Embryonic Stem Cell Differentiation. *Cell Stem Cell* 2012; **11**: 845–852.
100 Zhang HS, Postigo AA, Dean DC. Active Transcriptional Repression by the Rb–E2F Complex Mediates G1 Arrest Triggered by p16INK4a, TGFβ, and Contact Inhibition. *Cell* 1999; **97**: 53–61.
101 Malumbres M, Barbacid M. To cycle or not to cycle: a critical decision in cancer. *Nat Rev Cancer 2001 13* 2001; **1**: 222–231.
102 Wang F, Zhao W, Gao Y, Zhou J, Li H, Zhang G *et al.* CDK5-mediated phosphorylation and stabilization of TPX2 promotes hepatocellular tumorigenesis. *J Exp Clin Cancer Res 2019 381* 2019; **38**: 1–15.
103 Sharma S, Sicinski P. A kinase of many talents: non-neuronal functions of CDK5 in development and disease. *Open Biol* 2020; **10**. doi:10.1098/RSOB.190287.
104 Firestein R, Hahn WC. Revving the throttle on an oncogene: CDK8 takes the driver seat. *Cancer Res* 2009; **69**: 7899.
105 Iorns E, Turner NC, Elliott R, Syed N, Garrone O, Gasco M *et al.* Identification of CDK10 as an Important Determinant of Resistance to Endocrine Therapy for Breast Cancer. *Cancer Cell* 2008; **13**: 91–104.
106 Ettl T, Schulz D, Bauer RJ. The Renaissance of Cyclin Dependent Kinase Inhibitors. *Cancers 2022, Vol 14, Page 293* 2022; **14**: 293.
107 Cemeli T, Guasch-Vallés M, Nàger M, Felip I, Cambray S, Santacana M *et al.* Cytoplasmic cyclin D1 regulates glioblastoma dissemination. *J Pathol* 2019; **248**: 501–513.
108 Wiedemeyer WR, Dunn IF, Quayle SN, Zhang J, Chheda MG, Dunn GP *et al.* Pattern of retinoblastoma pathway inactivation dictates response to CDK4/6 inhibition in GBM. *Proc Natl Acad Sci U S A* 2010; **107**: 11501–11506.
109 Cen L, Carlson BL, Schroeder MA, Ostrem JL, Kitange GJ, Mladek AC *et al.* P16-Cdk4-Rb axis controls sensitivity to a cyclin-dependent kinase inhibitor PD0332991 in glioblastoma xenograft cells. *Neuro Oncol* 2012; **14**: 870–881.
110 Palbociclib (IBRANCE) | FDA. https://www.fda.gov/drugs/resources-information-approved-drugs/palbociclib-ibrance (accessed 15 Sep2021).
111 Ribociclib (Kisqali) | FDA. https://www.fda.gov/drugs/resources-information-approved-drugs/ribociclib-kisqali (accessed 15 Sep2021).
112 FDA approves abemaciclib as initial therapy for HR-positive, HER2-negative metastatic breast cancer | FDA. https://www.fda.gov/drugs/resources-information-approved-drugs/fda-approves-abemaciclib-initial-therapy-hr-positive-her2-negative-metastatic-breast-cancer (accessed 15 Sep2021).
113 Ibrance | European Medicines Agency.

https://www.ema.europa.eu/en/medicines/human/EPAR/ibrance (accessed 15 Sep2021).
114 Verzenios | European Medicines Agency. https://www.ema.europa.eu/en/medicines/human/EPAR/verzenios (accessed 15 Sep2021).
115 Kisqali | European Medicines Agency. https://www.ema.europa.eu/en/medicines/human/EPAR/kisqali (accessed 15 Sep2021).
116 Poratti M, Marzaro G. Third-generation CDK inhibitors: A review on the synthesis and binding modes of Palbociclib, Ribociclib and Abemaciclib. *Eur J Med Chem* 2019; **172**: 143–153.
117 Ingham M, Schwartz GK. Cell-Cycle Therapeutics Come of Age. *https://doi.org/101200/JCO2016690032* 2017; **35**: 2949–2959.
118 Patnaik A, Rosen LS, Tolaney SM, Tolcher AW, Goldman JW, Gandhi L *et al.* Efficacy and safety of Abemaciclib, an inhibitor of CDK4 and CDK6, for patients with breast cancer, non–small cell lung cancer, and other solid tumors. *Cancer Discov* 2016; **6**: 740–753.
119 Raub TJ, Wishart GN, Kulanthaivel P, Staton BA, Ajamie RT, Sawada GA *et al.* Brain exposure of two selective dual CDK4 and CDK6 inhibitors and the antitumor activity of CDK4 and CDK6 inhibition in combination with temozolomide in an intracranial glioblastoma xenograft. *Drug Metab Dispos* 2015; **43**: 1360–1371.
120 Yin L, Yao Z, Wang Y, Huang Y-H, Mazuranic M, Yin A. EXTH-14. PRECLINICAL EVALUATION OF NOVEL CDK4/6 INHIBITOR GLR2007 IN GLIOBLASTOMA MODELS. *Neuro Oncol* 2021; **23**: vi166–vi166.
121 Ku BM, Yi SY, Koh J, Bae Y-H, Sun J-M, Lee S *et al.* The CDK4/6 inhibitor LY2835219 has potent activity in combination with mTOR inhibitor in head and neck squamous cell carcinoma. *Oncotarget* 2016; **7**: 14803–14813.
122 van Caloen G, Schmitz S, Baroudi M El, Caignet X, Pyr dit Ruys S, Roger PP *et al.* Preclinical Activity of Ribociclib in Squamous Cell Carcinoma of the Head and Neck. *Mol Cancer Ther* 2020; **19**: 777–789.
123 Klein ME, Kovatcheva M, Davis LE, Tap WD, Koff A. CDK4/6 inhibitors: The mechanism of action may not be as simple as once thought. *Cancer Cell* 2018; **34**: 9.
124 Zhang M, Zhang L, Hei R, Li X, Cai H, Wu X *et al.* CDK inhibitors in cancer therapy, an overview of recent development. *Am J Cancer Res* 2021; **11**: 1913.
125 Long F, He Y, Fu H, Li Y, Bao X, Wang Q *et al.* Preclinical characterization of SHR6390, a novel CDK 4/6 inhibitor, in vitro and in human tumor xenograft models. *Cancer Sci* 2019; **110**: 1420–1430.
126 Thangavel C, Boopathi E, Liu Y, Mcnair C, Haber A, Perepelyuk M *et al.* Cancer Therapy: Preclinical Therapeutic Challenge with a CDK 4/6 Inhibitor Induces an RB-Dependent SMAC-Mediated Apoptotic Response in Non-Small Cell Lung Cancer. 2018. doi:10.1158/1078-0432.CCR-17-2074.
127 Finn RS, Dering J, Conklin D, Kalous O, Cohen DJ, Desai AJ *et al.* PD 0332991, a selective cyclin D kinase 4/6 inhibitor, preferentially inhibits proliferation of luminal estrogen receptor-positive human breast cancer cell lines in vitro. *Breast Cancer Res 2009 115* 2009; **11**: 1–13.
128 Hortobagyi GN, Stemmer SM, Burris HA, Yap Y-S, Sonke GS, Paluch-Shimon S *et al.* Ribociclib as First-Line Therapy for HR-Positive, Advanced Breast Cancer. *https://doi.org/101056/NEJMoa1609709* 2016; **375**: 1738–1748.
129 Goetz MP, Toi M, Campone M, Trédan O, Bourayou N, Sohn J *et al.* MONARCH 3: Abemaciclib as initial therapy for advanced breast cancer. *J Clin Oncol* 2017; **35**: 3638–3646.
130 Liao X, Hong Y, Mao Y, Chen N, Wang Q, Wang Z *et al.* SPH3643: A novel CDK4/6 inhibitor with good anti-cancer efficacy and strong blood-brain barrier permeability. *Cancer Sci* 2020; : cas.14367.
131 Francis AM, Alexander A, Liu Y, Vijayaraghavan S, Low KH, Yang D *et al.* CDK4/6 inhibitors sensitize Rb-positive sarcoma cells to Wee1 kinase inhibition through reversible cell cycle arrest. *Mol Cancer Ther* 2017; **16**: 1751.
132 Asghar U, Witkiewicz AK, Turner NC, Knudsen ES. The history and future of targeting cyclin-dependent kinases in cancer therapy. *Nat Rev Drug Discov* 2015; **14**: 130–146.
133 Howard D, James D, Murphy K, Garcia-Parra J, Pan-Castillo B, Rex S *et al.* Dinaciclib, a Bimodal Agent Effective against Endometrial Cancer. *Cancers (Basel)* 2021; **13**: 1–17.
134 Hu S, Marineau JJ, Rajagopal N, Hamman KB, Choi YJ, Schmidt DR *et al.* Discovery and Characterization of SY-1365, a Selective, Covalent Inhibitor of CDK7. *Cancer Res* 2019; **79**: 3479–3491.
135 Yuan J, Jiang YY, Mayakonda A, Huang M, Ding LW, Lin H *et al.* Super-Enhancers Promote Transcriptional Dysregulation in Nasopharyngeal Carcinoma. *Cancer Res* 2017; **77**: 6614–

6626.
136 Meng W, Wang J, Wang B, Liu F, Li M, Zhao Y *et al.* CDK7 inhibition is a novel therapeutic strategy against GBM both in vitro and in vivo. *Cancer Manag Res* 2018; **10**: 5747–5758.
137 Parry D, Guzi T, Shanahan F, Davis N, Prabhavalkar D, Wiswell D *et al.* Dinaciclib (SCH 727965), a novel and potent cyclin-dependent kinase inhibitor. *Mol Cancer Ther* 2010; **9**: 2344–2353.
138 Saqub H, Proetsch-Gugerbauer H, Bezrookove V, Nosrati M, Vaquero EM, de Semir D *et al.* Dinaciclib, a cyclin-dependent kinase inhibitor, suppresses cholangiocarcinoma growth by targeting CDK2/5/9. *Sci Reports 2020 101* 2020; **10**: 1–13.
139 Piegols HJ, Takada M, Parys M, Dexheimer T, Yuzbasiyan-Gurkan V, Piegols HJ *et al.* Investigation of novel chemotherapeutics for feline oral squamous cell carcinoma. *Oncotarget* 2018; **9**: 33098–33109.
140 Abdullah C, Wang X, Becker D. Expression analysis and molecular targeting of cyclin-dependent kinases in advanced melanoma. *http://dx.doi.org/104161/cc10615079* 2011; **10**: 977–988.
141 Fu W, Ma L, Chu B, Wang X, Bui MM, Gemmer J *et al.* The Cyclin-Dependent Kinase Inhibitor SCH 727965 (Dinacliclib) Induces the Apoptosis of Osteosarcoma Cells. *Mol Cancer Ther* 2011; **10**: 1018–1027.
142 Jane EP, Premkumar DR, Cavaleri JM, Sutera PA, Rajasekar T, Pollack IF. Dinaciclib, a cyclin-dependent kinase inhibitor promotes proteasomal degradation of Mcl-1 and enhances ABT-737-mediated cell death in malignant human glioma cell liness. *J Pharmacol Exp Ther* 2016; **356**: 354–365.
143 Ghia P, Scarfò L, Perez S, Pathiraja K, Derosier M, Small K *et al.* Efficacy and safety of dinaciclib vs ofatumumab in patients with relapsed/refractory chronic lymphocytic leukemia. Blood. 2017; **129**: 1876–1878.
144 Premkumar DR, Jane EP, Thambireddy S, Sutera PA, Cavaleri JM, Pollack IF. Mitochondrial dysfunction RAD51, and Ku80 proteolysis promote apoptotic effects of Dinaciclib in Bcl-xL silenced cells. *Mol Carcinog* 2018; **57**: 469–482.
145 Kumar SK, LaPlant B, Chng WJ, Zonder J, Callander N, Fonseca R *et al.* Dinaciclib, a novel CDK inhibitor, demonstrates encouraging single-agent activity in patients with relapsed multiple myeloma. *Blood* 2015; **125**: 443–448.
146 Nemunaitis JJ, Small KA, Kirschmeier P, Zhang D, Zhu Y, Jou YM *et al.* A first-in-human, phase 1, dose-escalation study of dinaciclib, a novel cyclin-dependent kinase inhibitor, administered weekly in subjects with advanced malignancies. *J Transl Med* 2013; **11**. doi:10.1186/1479-5876-11-259.
147 Mita MM, Joy AA, Mita A, Sankhala K, Jou YM, Zhang D *et al.* Randomized phase II trial of the cyclin-dependent kinase inhibitor Dinaciclib (MK-7965) versus capecitabine in patients with advanced breast cancer. *Clin Breast Cancer* 2014; **14**: 169–176.
148 Flynn J, Jones J, Johnson AJ, Andritsos L, Maddocks K, Jaglowski S *et al.* Dinaciclib is a novel cyclin-dependent kinase inhibitor with significant clinical activity in relapsed and refractory chronic lymphocytic leukemia. *Leukemia* 2015; **29**: 1524–1529.
149 Murphy AG, Zahurak M, Shah M, Weekes CD, Hansen A, Siu LL *et al.* A Phase I Study of Dinaciclib in Combination With MK-2206 in Patients With Advanced Pancreatic Cancer. *Clin Transl Sci* 2020; **13**: 1178–1188.
150 Riess C, Koczan D, Schneider B, Linke C, del Moral K, Classen CF *et al.* Cyclin-dependent kinase inhibitors exert distinct effects on patient-derived 2D and 3D glioblastoma cell culture models. *Cell Death Discov* 2021; **7**: 54.
151 Stupp R, Hegi ME, Mason WP, Bent MJ van den, Taphoorn MJ, Janzer RC *et al.* Effects of radiotherapy with concomitant and adjuvant temozolomide versus radiotherapy alone on survival in glioblastoma in a randomised phase III study: 5-year analysis of the EORTC-NCIC trial. *Lancet Oncol* 2009; **10**: 459–466.
152 Birzu C, French P, Caccese M, Cerretti G, Idbaih A, Zagonel V *et al.* Recurrent Glioblastoma: From Molecular Landscape to New Treatment Perspectives. *Cancers (Basel)* 2021; **13**: 1–29.
153 Pulte D, Brenner H. Changes in Survival in Head and Neck Cancers in the Late 20th and Early 21st Century: A Period Analysis. *Oncologist* 2010; **15**: 994–1001.
154 Juric V, Hudson L, Fay J, Richards CE, Jahns H, Verreault M *et al.* Transcriptional CDK inhibitors, CYC065 and THZ1 promote Bim-dependent apoptosis in primary and recurrent GBM through cell cycle arrest and Mcl-1 downregulation. *Cell Death Dis 2021 128* 2021; **12**:

1–12.
155 Wei Z, Liu X, Cheng C, Yu W, Yi P. Metabolism of Amino Acids in Cancer. *Front Cell Dev Biol* 2021; **0**: 1628.
156 Tormoen GW, Crittenden MR, Gough MJ. Role of the immunosuppressive microenvironment in immunotherapy. *Adv Radiat Oncol* 2018; **3**: 520–526.
157 Juric V, Murphy B. Cyclin-dependent kinase inhibitors in brain cancer: current state and future directions. *Cancer Drug Resist* 2020; **3**: 48–62.
158 Przystal JM, Hajji N, Khozoie C, Renziehausen A, Zeng Q, Abaitua F *et al.* Efficacy of arginine depletion by ADI-PEG20 in an intracranial model of GBM. *Cell Death Dis 2018 912* 2018; **9**: 1–10.
159 Mörén L, Perryman R, Crook T, Langer JK, Oneill K, Syed N *et al.* Metabolomic profiling identifies distinct phenotypes for ASS1 positive and negative GBM. *BMC Cancer 2018 181* 2018; **18**: 1–16.
160 Lubanska D, Porter L. Revisiting CDK Inhibitors for Treatment of Glioblastoma Multiforme. Drugs R D. 2017; **17**: 255–263.
161 Pilot Study of Abemaciclib With Bevacizumab in Recurrent Glioblastoma Patients With Loss of CDKN2A/B or Gain or Amplification of CDK4/6 - Full Text View - ClinicalTrials.gov. https://clinicaltrials.gov/ct2/show/NCT04074785?term=cdk&cond=gbm&draw=2&rank=2 (accessed 5 Oct2021).
162 LY3214996 Plus Abemaciclib in Recurrent Glioblastoma Patients - Full Text View - ClinicalTrials.gov. https://clinicaltrials.gov/ct2/show/NCT04391595?term=cdk&cond=gbm&draw=2&rank=3 (accessed 5 Oct2021).
163 Riess C, Irmscher N, Salewski I, Strüder D, Classen CF, Große-Thie C *et al.* Cyclin-dependent kinase inhibitors in head and neck cancer and glioblastoma—backbone or add-on in immune-oncology? *Cancer Metastasis Rev 2020 401* 2020; **40**: 153–171.
164 ADI-PEG 20 Plus Radiotherapy and Temozolomide in Subjects With Glioblastoma Multiforme - Full Text View - ClinicalTrials.gov. https://clinicaltrials.gov/ct2/show/NCT04587830 (accessed 5 Oct2021).
165 Ruiz-Garcia H, Ramirez-Loera C, Malouff TD, Seneviratne DS, Palmer JD, Trifiletti DM. Novel Strategies for Nanoparticle-Based Radiosensitization in Glioblastoma. *Int J Mol Sci 2021, Vol 22, Page 9673* 2021; **22**: 9673.
166 Dapash M, Hou D, Castro B, Lee-Chang C, Lesniak MS. The Interplay between Glioblastoma and Its Microenvironment. *Cells 2021, Vol 10, Page 2257* 2021; **10**: 2257.
167 Krishna S, Ulrich P, Wilson E, Parikh F, Narang P, Yang S *et al.* Human Papilloma Virus Specific Immunogenicity and Dysfunction of CD8+ T Cells in Head and Neck Cancer. *Cancer Res* 2018; **78**: 6159–6170.
168 Foy JP, Bertolus C, Michallet MC, Deneuve S, Incitti R, Bendriss-Vermare N *et al.* The immune microenvironment of HPV-negative oral squamous cell carcinoma from never-smokers and never-drinkers patients suggests higher clinical benefit of IDO1 and PD1/PD-L1 blockade. *Ann Oncol* 2017; **28**: 1934–1941.
169 Zhai L, Ladomersky E, Lauing K, Wu M, Genet M, Gritsina G *et al.* Infiltrating T cells increase IDO1 expression in glioblastoma and contribute to decreased patient survival. *Clin Cancer Res* 2017; **23**: 6650.
170 Uyttenhove C, Pilotte L, Théate I, Stroobant V, Colau D, Parmentier N *et al.* Evidence for a tumoral immune resistance mechanism based on tryptophan degradation by indoleamine 2,3-dioxygenase. *Nat Med 2003 910* 2003; **9**: 1269–1274.
171 Wainwright DA, Balyasnikova I V., Chang AL, Ahmed AU, Moon K-S, Auffinger B *et al.* IDO Expression in Brain Tumors Increases the Recruitment of Regulatory T Cells and Negatively Impacts Survival. *Clin Cancer Res* 2012; **18**: 6110–6121.
172 Mitsuka K, Kawataki T, Satoh E, Asahara T, Horikoshi T, Kinouchi H. Expression of Indoleamine 2,3-Dioxygenase and Correlation With Pathological Malignancy in Gliomas. *Neurosurgery* 2013; **72**: 1031–1039.
173 Pilotte L, Larrieu P, Stroobant V, Colau D, Dolušić E, Frédérick R *et al.* Reversal of tumoral immune resistance by inhibition of tryptophan 2,3-dioxygenase. *Proc Natl Acad Sci* 2012; **109**: 2497–2502.
174 Opitz CA, Litzenburger UM, Sahm F, Ott M, Tritschler I, Trump S *et al.* An endogenous tumour-promoting ligand of the human aryl hydrocarbon receptor. *Nat 2011 4787368* 2011; **478**: 197–203.

175 Badawy AA-B, Guillemin G. The Plasma [Kynurenine]/[Tryptophan] Ratio and Indoleamine 2,3-Dioxygenase: Time for Appraisal. *Int J Tryptophan Res* 2019; **12**. doi:10.1177/1178646919868978.

176 Adam I, Dewi DL, Mooiweer J, Sadik A, Mohapatra SR, Berdel B *et al.* Upregulation of tryptophanyl-tRNA synthethase adapts human cancer cells to nutritional stress caused by tryptophan degradation. *https://doi.org/101080/2162402X20181486353* 2018; **7**. doi:10.1080/2162402X.2018.1486353.

177 Suzuki Y, Suda T, Asada K, Miwa S, Suzuki M, Fujie M *et al.* Serum indoleamine 2,3-dioxygenase activity predicts prognosis of pulmonary tuberculosis. *Clin Vaccine Immunol* 2012; **19**: 436–442.

178 Spranger S, Spaapen RM, Zha Y, Williams J, Meng Y, Ha TT *et al.* Up-regulation of PD-L1, IDO, and Tregs in the melanoma tumor microenvironment is driven by CD8+ T cells. *Sci Transl Med* 2013; **5**. doi:10.1126/SCITRANSLMED.3006504.

179 Juhász C, Chugani DC, Muzik O, Wu D, Sloan AE, Barger G *et al.* In Vivo Uptake and Metabolism of α-[11C]Methyl-l-Tryptophan in Human Brain Tumors: *http://dx.doi.org/101038/sj.jcbfm9600199* 2005; **26**: 345–357.

180 Muller AJ, DuHadaway JB, Donover PS, Sutanto-Ward E, Prendergast GC. Inhibition of indoleamine 2,3-dioxygenase, an immunoregulatory target of the cancer suppression gene Bin1, potentiates cancer chemotherapy. *Nat Med 2005 113* 2005; **11**: 312–319.

181 Zhai L, Dey M, Lauing KL, Gritsina G, Kaur R, Lukas R V. *et al.* The kynurenine to tryptophan ratio as a prognostic tool for glioblastoma patients enrolling in immunotherapy. *J Clin Neurosci* 2015; **22**: 1964–1968.

182 Poratti M, Marzaro G. Third-generation CDK inhibitors: A review on the synthesis and binding modes of Palbociclib, Ribociclib and Abemaciclib. Eur. J. Med. Chem. 2019; **172**: 143–153.

183 Bhattacharya S, Ray RM, Johnson LR. Cyclin-dependent kinases regulate apoptosis of intestinal epithelial cells. *Apoptosis* 2014; **19**: 451.

184 Paiva C, Godbersen JC, Soderquist RS, Rowland T, Kilmarx S, Spurgeon SE *et al.* Cyclin-dependent kinase inhibitor P1446A induces apoptosis in a JNK/p38 MAPK-dependent manner in chronic lymphocytic leukemia B-cells. *PLoS One* 2015; **10**: e0143685.

185 Parker BW, Kaur G, Nieves-Neira W, Taimi M, Kohlhagen G, Shimizu T *et al.* Early Induction of Apoptosis in Hematopoietic Cell Lines After Exposure to Flavopiridol. *Blood* 1998; **91**: 458–465.

186 Ringer L. Role of p53 in cdk Inhibitor VMY-1-103-Induced Apoptosis in Prostate Cancer. 2012.https://apps.dtic.mil/sti/citations/ADA567635 (accessed 15 Oct2021).

187 Noonan JJ, Jarzabek M, Lincoln FA, Cavanagh BL, Pariag AR, Juric V *et al.* Implementing Patient-Derived Xenografts to Assess the Effectiveness of Cyclin-Dependent Kinase Inhibitors in Glioblastoma. *Cancers (Basel)* 2019; **11**: 2005.

188 Mandal R, Becker S, Strebhardt K. Targeting CDK9 for Anti-Cancer Therapeutics. *Cancers (Basel)* 2021; **13**: 2181.

189 Danilov A V., Hu S, Orr B, Godek K, Mustachio LM, Sekula D *et al.* Dinaciclib induces anaphase catastrophe in lung cancer cells via inhibition of cyclin-dependent kinases 1 and 2. *Mol Cancer Ther* 2016; **15**: 2758–2766.

190 Iriyama N, Hino H, Moriya S, Hiramoto M, Hatta Y, Takei M *et al.* The cyclin-dependent kinase 4/6 inhibitor, abemaciclib, exerts dose-dependent cytostatic and cytocidal effects and induces autophagy in multiple myeloma cells. *https://doi.org/101080/10428194201713767 41* 2017; **59**: 1439–1450.

191 Small J, Washburn E, Millington K, Zhu J, Holder SL. The addition of abemaciclib to sunitinib induces regression of renal cell carcinoma xenograft tumors. *Oncotarget* 2017; **8**: 95116.

192 Jeong EH, Lee TG, Ko YJ, Kim SY, Kim HR, Kim H *et al.* Anti-tumor effect of CDK inhibitors on CDKN2A-defective squamous cell lung cancer cells. *Cell Oncol* 2018; **41**: 663–675.

193 Wang S, Wang K, Wang H, Han J, Sun H. Autophagy is essential for flavopiridol-induced cytotoxicity against MCF-7 breast cancer cells. *Mol Med Rep* 2017; **16**: 9715–9720.

194 Chou A, Froio D, Nagrial AM, Parkin A, Murphy KJ, Chin VT *et al.* Tailored first-line and second-line CDK4-targeting treatment combinations in mouse models of pancreatic cancer. *Gut* 2018; **67**: 2142–2155.

195 Feldmann G, Mishra A, Bisht S, Karikari C, Garrido-Laguna I, Rasheed Z *et al.* Cyclin-dependent kinase inhibitor dinaciclib (SCH727965) inhibits pancreatic cancer growth and progression in murine xenograft models. *Cancer Biol Ther* 2011; **12**: 598–609.

196 Bisht S, Nolting J, Schütte U, Haarmann J, Jain P, Shah D *et al.* Cyclin-dependent kinase 5

(CDK5) controls melanoma cell motility, invasiveness, and metastatic spread—identification of a promising novel therapeutic target. *Transl Oncol* 2015; **8**: 295–307.

197 Qin G, Xu F, Qin T, Zheng Q, Shi D, Xia W *et al.* Palbociclib inhibits epithelial-mesenchymal transition and metastasis in breast cancer via c-Jun/COX-2 signaling pathway. *Oncotarget* 2015; **6**: 41794–41808.

198 Kochanowski P, Catapano J, Pudełek M, Wróbel T, Madeja Z, Ryszawy D *et al.* Temozolomide Induces the Acquisition of Invasive Phenotype by O6-Methylguanine-DNA Methyltransferase (MGMT)+ Glioblastoma Cells in a Snail-1/Cx43-Dependent Manner. *Int J Mol Sci* 2021; **22**. doi:10.3390/IJMS22084150.

199 Scialò F, Fernández-Ayala DJ, Sanz A. Role of Mitochondrial Reverse Electron Transport in ROS Signaling: Potential Roles in Health and Disease. *Front Physiol* 2017; **0**: 428.

200 Uzhachenko R V, Bharti V, Ouyang Z, Arteaga C, Richmond A, Vilgelm Correspondence AE *et al.* Metabolic modulation by CDK4/6 inhibitor promotes chemokine-mediated recruitment of T cells into mammary tumors. *CellReports* 2021; **35**: 108944.

201 Hino H, Iriyama N, Kokuba H, Kazama H, Moriya S, Takano N *et al.* Abemaciclib induces atypical cell death in cancer cells characterized by formation of cytoplasmic vacuoles derived from lysosomes. *Cancer Sci* 2020; **n/a**. doi:10.1111/cas.14419.

202 Knudsen ES, Hutcheson J, Vail P, Witkiewicz AK, Knudsen ES, Hutcheson J *et al.* Biological specificity of CDK4/6 inhibitors: dose response relationship, in vivo signaling, and composite response signature. *Oncotarget* 2017; **8**: 43678–43691.

203 Liang M-L, Chen C-H, Liu Y-R, Huang M-H, Lin Y-C, Wong T-T *et al.* Abemaciclib, A Selective CDK4/6 Inhibitor, Restricts the Growth of Pediatric Ependymomas. *Cancers (Basel)* 2020; **12**: 1–17.

204 Maltese WA, Overmeyer JH. Methuosis: Nonapoptotic cell death associated with vacuolization of macropinosome and endosome compartments. Am. J. Pathol. 2014; **184**: 1630–1642.

205 Overmeyer JH, Young AM, Bhanot H, Maltese WA. A chalcone-related small molecule that induces methuosis, a novel form of non-apoptotic cell death, in glioblastoma cells. *Mol Cancer* 2011; **10**. doi:10.1186/1476-4598-10-69.

206 Maltese WA, Overmeyer JH. Non-apoptotic cell death associated with perturbations of macropinocytosis. *Front Physiol* 2015; **0**: 38.

207 Shu H-KG, Kim MM, Chen P, Furman F, Julin CM, Israel MA. The intrinsic radioresistance of glioblastoma-derived cell lines is associated with a failure of p53 to induce p21BAX expression. *Proc Natl Acad Sci* 1998; **95**: 14453–14458.

208 Ali MY, Oliva CR, Noman ASM, Allen BG, Goswami PC, Zakharia Y *et al.* Radioresistance in Glioblastoma and the Development of Radiosensitizers. *Cancers 2020, Vol 12, Page 2511* 2020; **12**: 2511.

209 Robinson AM, Rathore R, Redlich NJ, Adkins DR, VanArsdale T, Van Tine BA *et al.* Cisplatin exposure causes c-Myc-dependent resistance to CDK4/6 inhibition in HPV-negative head and neck squamous cell carcinoma. *Cell Death Dis 2019 1011* 2019; **10**: 1–13.

210 Weiss JM, Csoszi T, Maglakelidze M, Hoyer RJ, Beck JT, Domine Gomez M *et al.* Myelopreservation with the CDK4/6 inhibitor trilaciclib in patients with small-cell lung cancer receiving first-line chemotherapy: a phase Ib/randomized phase II trial. *Ann Oncol* 2019; **30**: 1613–1621.

211 Hart LL, Ferrarotto R, Andric ZG, Beck JT, Subramanian J, Radosavljevic DZ *et al.* Myelopreservation with Trilaciclib in Patients Receiving Topotecan for Small Cell Lung Cancer: Results from a Randomized, Double-Blind, Placebo-Controlled Phase II Study. *Adv Ther* 2021; **38**: 350–365.

212 Hossain DMS, Javaid S, Cai M, Zhang C, Sawant A, Hinton M *et al.* Dinaciclib induces immunogenic cell death and enhances anti-PD1–mediated tumor suppression. *J Clin Invest* 2018; **128**: 644–654.

213 Dominiak A, Chełstowska B, Olejarz W, Nowicka G. Communication in the Cancer Microenvironment as a Target for Therapeutic Interventions. *Cancers 2020, Vol 12, Page 1232* 2020; **12**: 1232.

214 Northcott JM, Dean IS, Mouw JK, Weaver VM. Feeling stress: The mechanics of cancer progression and aggression. *Front Cell Dev Biol* 2018; **6**: 17.

215 Brückner BR, Nöding H, Skamrahl M, Janshoff A. Mechanical and morphological response of confluent epithelial cell layers to reinforcement and dissolution of the F-actin cytoskeleton. *Prog Biophys Mol Biol* 2019; **144**: 77–90.

216 Shannon S, Jia D, Entersz I, Beelen P, Yu M, Carcione C *et al.* Inhibition of glioblastoma dispersal by the MEK inhibitor PD0325901. *BMC Cancer* 2017; **17**: 1–11.
217 Cerignoli F, Abassi YA, Lamarche BJ, Guenther G, Ana DS, Guimet D *et al.* In vitro immunotherapy potency assays using real-time cell analysis. *PLoS One* 2018; **13**. doi:10.1371/JOURNAL.PONE.0193498.
218 Trono P, Tocci A, Musella M, Sistigu A, Nisticò P. Actin Cytoskeleton Dynamics and Type I IFN-Mediated Immune Response: A Dangerous Liaison in Cancer? *Biol 2021, Vol 10, Page 913* 2021; **10**: 913.

8. Anhang

8.1 Abkürzungsverzeichnis

Bcl ..... B-cell lymphoma 2
BRAF ..... v-Raf murine sarcoma viral oncogene homolog B
CaMKII ..... Calcium/calmodulin-dependent protein kinase
CCND1 ..... G1/S-specific cyclin-D1
CDK ..... Cyclin-abhängige Kinasen
CDKi ..... CDK-Inhibitor
CDKN2A/B ..... cyclin-dependent kinase inhibitor2A/B
Cip ..... CDK-interagierenden Proteine
COX-2 ..... Cyclooxygenase-2
DMEM ..... Dulbecco's Modified Eagle Medium
DNA ..... deoxyribonucleic acid
DSB ..... *Doublestrandbreak*
EGFR ..... Epidermal Growth Factor Receptor
ER ..... Endoplasmatisches Retikulum
FCS ..... Fetal calf serum
GAPDH ..... Glyceraldehyde-3-phosphate dehydrogenase
GBM ..... Glioblastoma multiforme
GBS ..... GBM-Sphäroide
GSC ..... *stammzellähnliche GBM-Zellen*
GSK ..... Glycogen synthase kinase
H2A. X ..... *Histon H2AX*
HAAO 3-hydroxyanthranilate 3,4-dioxygenase
HR^+-$HER2^-$ ..... *Hormonrezeptor positiv, human epidermal growth factor receptor 2 negativ*
IF ..... Immunfluoreszenzfärbung
IFN-γ ..... *Interferon gamma*
Kip ..... Kinase-Inhibitor Proteine
KMO ..... Kynurenine 3-monooxygenase
KAT ..... Kynurenine--oxoglutarate transaminase 3
KYN ..... Kynurenin
KYNA ..... Kynureninsäure
KYNU ..... Kynureninase
LAMP ..... Lysosome-associated membrane glycoprotein
MGMT ..... O^6-Methylguanin-DNA-Methyltransferase
Mito-ROS ..... mitochondriale Sauerstoffspezies
MMP ..... Hyperpolarisation der mitochondrialen Membran
mRNA ..... *messanger RNA*
PDGFRA ..... platelet-derived growth factor receptor A
Pen/Strep ..... *Penicillin/Streptomycin*
PGE2 ..... *Prostaglandin E2*
PI ..... Propidiumiodid
PTEN ..... Phosphatase and Tensin homolog
QPRT ..... Nicotinate-nucleotide pyrophosphorylase [carboxylating]
Rab ..... Ras-related protein
Rb1 ..... Retinoblastom-Protein1
RNA ..... ribonucleic acid
RT ..... *Radiotherapie*
SD/SEM ..... *Standardabweichung/-fehler*
SEQ ..... sequentiell
SIM ..... simultan
SIRT3 ..... NAD-dependent protein deacetylase sirtuin-3, mitochondrial
TERT ..... telomerase reverse transcriptase
TM ..... *Tumor-Mikroumgebung*
TMZ ..... *Temozolomid*
TP53 ..... *Tumorsuppressorprotein53*
Treg ..... *regulatorische T-Zellen*
TTF ..... *Tumor Treating Fields*
Wnt ..... *Wingless Int-1*

8.2 Abbildungsverzeichnis

8.3 Vollständiges Publikationsverzeichnis

1. **Riess, C**., del Moral, K., Fiebig, A. et al. Implementation of a combined CDK inhibition and arginine-deprivation approach to target arginine-auxotrophic glioblastoma multiforme cells. Cell Death Dis 13, 555 (2022). https://doi.org/10.1038/s41419-022-05006-1
2. Schoenwaelder N, Salewski I, Engel N, Krause M, Schneider B, Müller M, **Riess C**, Lemcke H, Skorska A, Grosse-Thie C, Junghanss C, Maletzki C. The Individual Effects of Cyclin-Dependent Kinase Inhibitors on Head and Neck Cancer Cells - A Systematic Analysis. Cancers (Basel). 2021 May 15;13(10):2396.
3. **Riess C**, Koczan D, Schneider B, Linke C, del Moral K, Classen CF, Maletzki C. Cyclin-dependent kinase inhibitors exert distinct effects on patient-derived 2D and 3D glioblastoma cell culture models. Cell Death Discov. 2021 Mar 15;7(1):54.
4. **Riess C**, Irmscher N, Salewski I, Strüder D, Classen CF, Große-Thie C, Junghanss C, Maletzki C. Cyclin-dependent kinase inhibitors in head and neck cancer and glioblastoma-backbone or add-on in immune-oncology? Cancer Metastasis Rev. 2021 Mar;40(1):153-171.
5. **Riess C**, Schneider B, Kehnscherper H, Gesche J, Irmscher N, Shokraie F, Classen CF, Wirthgen E, Domanska G, Zimpfer A, Strüder D, Junghanss C, Maletzki C. Activation of the Kynurenine Pathway in Human Malignancies Can Be Suppressed by the Cyclin-Dependent Kinase Inhibitor Dinaciclib. Front Immunol. 2020 Feb 14;11:55.
6. **Riess C**, Shokraie F, Classen CF, Kreikemeyer B, Fiedler T, Junghanss C, Maletzki C. Arginine-Depleting Enzymes - An Increasingly Recognized Treatment Strategy for Therapy-Refractory Malignancies. Cell Physiol Biochem. 2018;51(2):854-870.
7. Maletzki C, Rosche Y, **Riess C**, Scholz A, William D, Classen CF, Kreikemeyer B, Linnebacher M, Fiedler T. Deciphering molecular mechanisms of arginine deiminase-based therapy - Comparative response analysis in paired human primary and recurrent glioblastomas. Chem Biol Interact. 2017 Dec 25;278:179-188.

8.4 Tagungsbeiträge

8.4.1 Vorträge

"*S. pyogenes* ADI-based therapies for treatment of arginine-auxotrophic glioblastoma multiforme". Christin Riess, Tomas Fiedler, Bernd Kreikemeyer, Carl Friedrich Classen und Claudia Maletzki. 12th Rostock Symposion for Tumor Immunology and Brain Tumor Research in Pediatrics. Februar 2018 in Rostock.

"CDKs as target structures for cancer therapy – an *in vitro* analysis on patient-derived glioblastoma cell lines –". Christin Riess, Dirk Koczan, Carl Friedrich Classen und Claudia Maletzki. 28th Symposium Experimental Neurooncology. April 2019 in Minden

"Cyclin-dependent kinase inhibitors exert distinct effects on patient-derived 2D and 3D glioblastoma cell culture". Christin Riess, Charlotte Linke, Katharina del Moral, Claudia Maletzki, Carl Friedrich Classen. 15th Rostock Symposion for Tumor Immunology and Brain Tumor Research in Pediatrics. Februar 2021 in Rostock (virtuell).

8.4.2 Poster

S. pyogenes ADI zur Behandlung Arginin-auxotropher Patienten-abgeleiteter Glioblastomzellen. Christin Rieß, Dirk Koczan, Carl Friedrich Classen, Tomas Fiedler, Christian Junghanß, Claudia Maletzki. DGHO Jahrestagung 2019. Oktober 2019 in Berlin.

Cyclin-abhängige Kinasen als therapeutische Zielstrukturen - eine komparative *in vitro*-Analyse an Patienten-abgeleiteten Glioblastomzellen. Christin Rieß, Dirk Koczan, Katharina del Moral, Carl Friedrich Classen, Christian Junghanß, Claudia Maletzki. DGHO Jahrestagung 2020. Oktober 2020 (virtuell).

Cyclin-dependent kinases as therapeutic targets – a comparative *in vitro* analysis on patient-derived glioblastoma cell models. Christin Rieß, Dirk Koczan, Carl Friedrich Classen, Claudia Maletzki. 19th ISPNO 2020. Dezember 2020 (virtuell).

Combined CDK inhibition and arginine-deprivation boosts antitumoral effects against arginine-auxotrophic glioblastoma multiforme cells. Katharina del Moral, Christin Riess, Adina Fiebig, Charlotte Linke, Marcus Frank, Tomas Fiedler, Christian Junghanss, Carl Friedrich Classen, Claudia Maletzki. DGHO Jahrestagung 2021. Oktober 2021 (virtuell).

Targeting arginine deprivation in dinaciclib-resistant glioblastoma multiforme cells. Katharina del Moral, Christin Riess, Carl Friedrich Classen, Claudia Maletzki. ESMO Congress 2021. September 2021 (virtuell).

8.5 Eigenanteil an dem im Promotionszeitraum eingereichten Originalpublikationen

Activation of the Kynurenine Pathway in Human Malignancies Can Be Suppressed by the Cyclin-Dependent Kinase Inhibitor Dinaciclib.

Christin Riess, Björn Schneider, Hanna Kehnscherper, Julia Gesche, Nina Irmscher, Fatemeh Shokraie, Carl Friedrich Classen, Elisa Wirthgen, Grazyna Domanska, Annette Zimpfer, Daniel Strüder, Christian Junghanss, Claudia Maletzki.

Front. Immunol., 14 February 2020 | https://doi.org/10.3389/fimmu.2020.00055

Impact Factor 2022: 7.561

- Verfassung des Manuskripts zusammen mit PD Dr. rer. nat. Claudia Maletzki
- Beteiligung an der Durchführung der experimentellen Arbeiten (Zellkultur und Behandlung, RT-qPCR, Immunfluoreszenzfärbung, statistische Auswertung)
- Bearbeitung der Kommentare von Gutachtern und Überarbeitung des Manuskripts nach Revision gemeinsam mit PD Dr. rer. nat. Claudia Maletzki

Cyclin-dependent kinase inhibitors exert distinct effects on patient-derived 2D and 3D glioblastoma cell culture models.

Christin Riess, Dirk Koczan, Björn Schneider, Charlotte Linke, Katharina del Moral, Carl Friedrich Classen and Claudia Maletzki.

Riess et al. Cell Death Discovery (2021) 7:54 I https://doi.org/10.1038/s41420-021-00423-1

Impact Factor 2022: 7.109

- Verfassung des Manuskripts
- Maßgebliche Beteiligung an der Studienplanung
- Maßgebliche Durchführung der experimentellen Arbeiten (Zellkultur im 2D- und 3D-Modell und Behandlung, Probenvorbereitung für Microarray, Immunfluoreszenz- und weitere Färbungen, durchflusszytometrische Messungen, Analyse der Vakuolen, Invasionsanalysen, statistische Auswertung)
- Mitbetreuung von medizinischen Doktoranden
- Bearbeitung der Kommentare von Gutachtern und Überarbeitung des Manuskripts nach Revision gemeinsam mit PD Dr. rer. nat. Claudia Maletzki

The Individual Effects of Cyclin-Dependent Kinase Inhibitors on Head and Neck Cancer Cells - A Systematic Analysis. Cancers.

Nina Schoenwaelder, Inken Salewski, Nadja Engel, Mareike Krause, Björn Schneider, Michael Müller, Christin Riess, Heiko Lemcke, Anna Skorska, Christina Grosse-Thie, Christian Junghanss, Claudia Maletzki

Impact Factor 2022: 6.639

Eigenanteil:

- Verfassen von Textbausteinen, Hauptarbeit galt Nina Schönwälder zusammen mit PD Dr. rer. nat. Claudia Maletzki
- Beteiligung an der Durchführung der experimentellen Arbeiten (Immunfluoreszenzfärbung)
- Validierung der Ergebnisse

8.5.1 Activation of the Kynurenine Pathway in Human Malignancies Can Be Suppressed by the Cyclin-Dependent Kinase Inhibitor Dinaciclib.

frontiers in Immunology

ORIGINAL RESEARCH
published: 14 February 2020
doi: 10.3389/fimmu.2020.00055

Activation of the Kynurenine Pathway in Human Malignancies Can Be Suppressed by the Cyclin-Dependent Kinase Inhibitor Dinaciclib

*Christin Riess[1,2,3], Björn Schneider[4], Hanna Kehnscherper[3], Julia Gesche[3], Nina Irmscher[3], Fatemeh Shokraie[1], Carl Friedrich Classen[1], Elisa Wirthgen[1], Grazyna Domanska[5], Annette Zimpfer[4], Daniel Strüder[6], Christian Junghanss[3] and Claudia Maletzki[3]**

[1] University Children's Hospital, Rostock University Medical Centre, Rostock, Germany, [2] Institute for Medical Microbiology, Virology, and Hygiene, Rostock University Medical Centre, Rostock, Germany, [3] Medical Clinic III - Hematology, Oncology, Palliative Care, Department of Internal Medicine, Rostock University Medical Center, Rostock, Germany, [4] Institute of Pathology, Rostock University Medical Center, University of Rostock, Rostock, Germany, [5] Institute of Immunology and Transfusion Medicine, University of Greifswald, Greifswald, Germany, [6] Department of Otorhinolaryngology, Head and Neck Surgery "Otto Koerner", Rostock University Medical Center, Rostock, Germany

OPEN ACCESS

Edited by:
Ignacio Melero,
University of Navarra, Spain

Reviewed by:
Benjamin Heng,
Macquarie University, Australia
Michael Platten,
German Cancer Research Center (DKFZ), Germany

***Correspondence:**
Claudia Maletzki
claudia.maletzki@med.uni-rostock.de

Specialty section:
This article was submitted to Cancer Immunity and Immunotherapy, a section of the journal Frontiers in Immunology

Received: 16 September 2019
Accepted: 09 January 2020
Published: 14 February 2020

Citation:
Riess C, Schneider B, Kehnscherper H, Gesche J, Irmscher N, Shokraie F, Classen CF, Wirthgen E, Domanska G, Zimpfer A, Strüder D, Junghanss C and Maletzki C (2020) Activation of the Kynurenine Pathway in Human Malignancies Can Be Suppressed by the Cyclin-Dependent Kinase Inhibitor Dinaciclib. Front. Immunol. 11:55. doi: 10.3389/fimmu.2020.00055

Indoleamine 2,3-dioxygenase (IDO) and tryptophan 2,3-dioxygenase (TDO2) are the key enzymes of tryptophan (TRP) metabolism in the kynurenine pathway (KP). Both enzymes function as indicators of immunosuppression and poor survival in cancer patients. Direct or indirect targeting of either of these substances seems thus reasonable to improve therapy options for patients. In this study, glioblastoma multiforme (GBM) as well as head and neck squamous cell carcinomas (HNSCC) were examined because of their different mechanisms of spontaneous and treatment-induced immune escape. Effects on gene expression and protein levels were examined. Accompanying assessment of TRP metabolites from treated GBM cell culture supernatants was conducted. Our results show a heterogeneous and inversely correlated expression profile of TRP-metabolizing genes among GBM and HNSCC cells, with low, but inducible *IDO1* expression upon IFNγ treatment. *TDO2* expression was higher in GBM cells, while genes encoding kynurenine aminotransferases were mainly confined to HNSCC cells. These data indicate that the KP is active in both entities, with however different enzymes involved in TRP catabolism. Upon treatment with Temozolomide, the standard of care for GBM patients, *IDO1* was upregulated. Comparable, although less pronounced effects were seen in HNSCC upon Cetuximab and conventional drugs (i.e., 5-fluorouracil, Gemcitabine). Here, *IDO1* and additional genes of the KP (*KYAT1*, *KYAT2*, and *KMO*) were induced. Vice versa, the novel yet experimental cyclin-dependent kinase inhibitor Dinaciclib suppressed KP in both entities. Our comprehensive data imply inhibition of the TRP catabolism by Dinaciclib, while conventional chemotherapeutics tend to activate this pathway. These data point to limitations of conventional therapy and highlight the potential of targeted therapies to interfere with the cells' metabolism more than anticipated.

Keywords: targeted therapy, solid tumor models, tryptophan metabolites, IDO1, chemotherapy

INTRODUCTION

Tumor cells release immunosuppressive factors that shape a tolerogenic environment and enable progression and invasion. Indoleamine 2,3-dioxygenase (IDO1) is an intracellular monomeric, immune-checkpoint molecule that degrades the essential amino acid l-tryptophan along the kynurenine pathway (KP) (1, 2). Like other immune checkpoints, including programmed cell death protein 1 and cytotoxic T-lymphocyte-associated protein 4, IDO suppresses the hosts' antitumor immunity by inducing apoptosis in T- and natural killer cells (3). As a direct consequence of this, many cancer and cancer-associated cells express *IDO1* (mesenchymal stromal cells, myeloid-derived suppressor cells, dendritic cells, endothelial cells, tumor-associated macrophages, and fibroblasts) (3–6). *IDO1* is influenced by interferon-γ (IFNγ) (7–9), nitric oxide (10), pro- [interleukin (IL)-1β, tumor necrosis factor α] and anti-inflammatory (IL4, IL10, transforming growth factor β) cytokines. *IDO1* activity inhibits T-cell activation and proliferation and even mediates regulatory T-cell recruitment to the tumor microenvironment, provoking local immune tolerance. In head and neck squamous cell carcinomas (HNSCCs), *IDO1* inversely correlates with programmed cell death protein ligand 1, which constitutes an important prognostic biomarker for immune-checkpoint inhibition (11). The increased IDO1 activation decreases intratumoral TRP levels, resulting in tumor starvation and increase in kynurenine (KYN) metabolites (which are toxic to lymphocytes) (12). This immune exhaustion may be further boosted by conventional chemotherapeutics, leading to decreased efficacy. Therefore, *IDO1* overexpression in the tumor microenvironment intimately impairs patients' outcome and may serve as a future prognostic predictor and drug target (13–18).

In the KP, most studies focused on IDO1 because this molecule is amenable to pharmacological intervention (19–22), and a couple of specific and global IDO inhibitors [including natural compounds (17, 23, 24)] already entered clinical trials, mostly reporting safe application and efficacy (stable disease at best outcome) (25). Current trials are evaluating the efficacy of IDO1 inhibitors in combination with chemotherapy, radiotherapy, and other immunotherapies including cytotoxic T-lymphocyte-associated protein 4 blockade (11, 22). The latter is based on the observation of an enhanced lytic ability of tumor-antigen-specific T cells upon IDO1 inhibition and decreased numbers of local immunosuppressive cells such as regulatory T cells and myeloid-derived suppressor cells (20, 26). The efficacy and toxicity data from recent clinical trials with IDO1 inhibitors is reviewed in Yentz and Smith (27). In most cases, however, overall survival was not significantly improved, leaving the future role for this combination therapy in question (28). More key enzymes are involved in TRP metabolism: tryptophan 2.3-dioxygenase (TDO2), a member of the oxidoreductases family, catalyzes the same initial step of the KP as IDO1 (2). Thus, TDO2 has been shown to be constitutively and highly expressed in various cancer cells such as malignant glioma and HNSCC (29, 30). More importantly, TDO2 also has immunomodulatory functions by promoting immune tolerance. This, in turn, promotes survival, growth, invasion, and metastasis and decreases patients' survival (just like *IDO1*) (13, 22, 31, 32).

In this study, we performed a comprehensive analysis on the expression status of genes belonging to the KP. HNSCC and glioblastoma multiforme (GBM) were picked as prime examples for different spontaneous and treatment-induced immune escape mechanisms. Therefore, expression changes were determined under standard and targeted therapy, and results were compared among each other.

Abbreviations: CDKi, cyclin-dependent kinase inhibitor; GBM, glioblastoma multiforme; HNSCC, head and neck squamous cell carcinoma; IDO1, indoleamine 2,3-dioxygenase; IFN, interferon; KYAT, kynurenine aminotransferase; KP, kynurenine pathway; PBMC, peripheral blood mononuclear cells; SCC, squamous cell carcinoma; TDO2, tryptophan 2,3-dioxygenase.

MATERIALS AND METHODS

Tumor Cell Lines and Culture Conditions

Patient-derived GBM cell lines ($N = 13$; HROG02, HROG04, HROG05, HROG06, HROG10, HROG15, HROG24, HROG36, HROG38, HROG52, HROG63, HROG73, HROG75) and HNSCC cell lines ($N = 6$; FADU, Detroit-562, Cal-33, PE/CA/PJ-15, UT-SCC-14, UT-SCC-15) were either established and basically characterized in our lab or originally obtained from the German collection of cell cultures (DSMZ; Braunschweig, Germany). UT-SCC14 and UT-SCC15 cells were kindly provided by Prof. R. Grenman [University of Turku, Finland (33)]. All cells were routinely cultured in our lab and maintained in full medium: Dulbecco's modified Eagle Medium/HamsF12 supplemented with 10% fetal calf serum, glutamine (2 mmol/L), and antibiotics (medium and supplements were purchased from PAA, Cölbe, Germany). For functional analysis, cell lines from each tumor entity were chosen, and all subsequent experiments were performed with these lines only.

IFNγ Stimulation

Cells were cultured in six-well plates or ibidi chamber slides, incubated overnight and treated with IFNγ (50 ng/ml, Immunotools, Friesoythe, Germany) for 24 and 72 h, respectively. Thereafter, cells were harvested and further processed.

Cytostatic Drugs and Targeted Substance

Cytostatics used in this study included 5-fluorouracil (5-FU) (2.5 μM), Cisplatin (0.2 μM), Gemcitabine (0.0002 μM), and Cetuximab (0.34 μM) for HNSCC, as well as Temozolomide (10 μM, TMZ) for GBM (pharmacy of the University Hospital Rostock). CDKi Dinaciclib (10 or 100 nM) was used as experimental targeted drug. All substances were used in doses below the IC_{50} as determined before.

Apoptosis/Necrosis Assay

A Yo-Pro-1/PI-based assay for discriminating early apoptotic, late apoptotic, and necrotic cells was applied as described before (34).

Hemolysis Assay

Hemolytic activity of Dinaciclib was determined by hemoglobin release from whole blood cells after 2 h of incubation. Briefly,

whole blood of healthy donors ($N = 5$) was seeded in 96-well plates and treated with increasing Dinaciclib doses (ranging from 1, 5, and 10 μM). Negative controls were left untreated, and positive controls (=maximum lysis) were treated with 1% sodium dodecyl sulfate. Following the incubation period, cell-free supernatants were transferred into a new 96-well plate, and absorption was measured on a plate reader at 560 nm (reference wave length, 750 nm). Hemolytic activity was quantified according to the following formula and corrected for spontaneous hemolysis (=untreated controls):

$$\%\text{Hemolysis} = ((OD_{560nm}\text{sample} - OD_{560nm}\text{buffer})/OD_{560nm}\text{max} - OD_{560nm}\text{buffer}) \times 100$$

In addition, peripheral blood mononuclear cells' (PBMC) viability ($N = 5$) were determined by Calcein AM staining. This was done upon 24 h incubation at the above-mentioned doses. Fluorescence measurement and quantification were done as described (34).

IDO1 Immunofluorescence

Tumor cells were treated with 50 ng/ml of IFNγ (Immunotools), TMZ, Cetuximab, or Dinaciclib for 24 h in chamber slides, respectively. Cells were washed with phosphate-buffered saline, fixed in 4% paraformaldehyde w/o methanol (Thermo Scientific, Darmstadt, Germany) for 20 min, washed again, followed by cell permeabilization in 0.3% Triton X−100/5% normal bovine serum in phosphate-buffered saline for 60 min. Cells were then incubated overnight at 4°C in monoclonal rabbit IDO1 primary antibody (1:100; Cell Signaling Technology, Frankfurt/Main, Germany). Cells were washed, labeled with fluorochrome-conjugated secondary antibody using goat antirabbit secondary antibody (1:250, Boster Biological Technology, Pleasanton CA, USA), and incubated in the dark for 2 h. Cell nuclei were stained with 4′,6-diamidino-2-phenylindole (DAPI), and cells were analyzed with a Zeiss LSM-780 Confocal Laser Microscope (Zeiss, Jena, Germany). Quantification of staining intensity was done using the ImageJ software. Therefore, channels were split into red, green, and blue. Subsequently, integrated density profiles of the same size were measured in the green channel.

IDO1 Immunohistochemistry on Patients' Tumor Samples

Primary antibody against IDO1 (rabbit IgG, clone D5J4E, Cell Signaling Technology, dilution 1:200) was used. All samples were pretreated for 20 min at 97°C and pH 6.9. Standard immunoperoxidase technique was applied using an automated immunostainer (DAKO link) with diaminobenzidine as chromogen. IDO1 expression was defined as cytoplasmatic and membranous staining in >1% inflammatory cells.

Quantification of Tryptophan, Kynurenine, and Kynurenic Acid in Cell Culture Supernatant by Liquid Chromatography Tandem Mass Spectrometry System

The basis for the measurement was the method of Fuertig et al. which was adapted to the system used here (35).

Sample Preparation

Cell culture supernatant was mixed 1:1 with internal standards [10 μM D5-kynurenic acid (Buchem BV, Apeldoorn, Netherlands), 10 μM D5-phenylalanine (Cambridge Isotope Laboratories, Inc. Andover, MA, United States), 5 μM D4-kynurenine (Cambridge Isotope Laboratories), 10 μM D5-tryptophan (Sigma Aldrich, Hamburg, Germany), 10 μM D3-quinolinic acid (Buchem BV), 5.5 nM 15N5-8-hydroxy-2-deoxyguanosine (Cambridge Isotope Laboratories)], and with 10 μl of mobile phase (0.4% formic acid, 1% acetonitrile in water). Reagents were gently shaken on a mixer, and 150 μl of ice-cold methanol was added. Samples were incubated overnight at −20°C to allow protein precipitation. On the following day, samples were centrifugated at 0°C and 18,000×*g* for 15 min. Supernatants were transferred to a new tube, and the liquid phase was removed by evaporation at 30°C among vacuum. Solid samples were stored until measurement at −20°C. Afterwards, dried extracts were reconstituted in 100 μl of acidified mobile phase. Samples were incubated at 40°C (1 h), centrifuged (4°C, 18,000×*g*, 5 min), and clear supernatant (100 μl) was transferred onto a 96-well plate.

Liquid Chromatography Tandem Mass Spectrometry

Measurements were performed on an AB Sciex 5500 QTrap™ mass spectrometer (AB SCIEX, Darmstadt, Germany) with electrospray ionization in positive mode combined with a high-performance liquid chromatography system (Agilent 1260 Infinity Binary LC, Santa Clara, United States) including a degasser unit, column oven, autosampler, and a binary pump. Twenty microliters of the supernatant was injected and separated using a VisionHT C18 column (100 × 2.1 mm; particle size, 3 μm; Grace, MD, United States). To prevent contamination, a precolumn (VisionHT C18, Guard 5 × 2 mm) was used additionally. The temperature of the column oven was set at 15°C. The flowrate was set to 0.4 ml/min, and the sample was separated in a total run time of 11 min using solution A (water + 0.1% formic acid + 0.01% trifluoroacetic acid) and solution B (MeOH + 0.1% formic acid + 0.01% trifluoroacetic acid) with the following gradient: 0–2.8 min, 97% A, 3% B; 2.8–3.3 min, 70% A, 30% B; 3.3–4.4, 40% A, 60% B; 4.5–5.0 min, 40% A, 60% B; 5.0–5.5, 5% A, 95% B; 5.5–6.9 min, 5% A, 95% B; 6.9–7.0 min, 97% A, 3% B; 7.0–11.0 min, 97% A, 3% B.

The eluate between 0.5 and 9 min was introduced into the mass spectrometer and analyzed in MRM mode. The ion spray voltage (IS) was 4,000 V, the curtain gas flow was 40.0 psi, and the ion source temperature were set at 550°C.

Internal standards were used for metabolite quantification (**Table 1**). Data analysis, including peak integration and concentration determination, was performed with Analyst software (Version 1.5.1, AB Sciex, Darmstadt, Germany).

RNA Isolation, cDNA Synthesis, and Quantitative Real-Time PCR

Total RNA was isolated with RNeasy Mini Kit (Qiagen, Hilden, Germany) according to the manufacturers' instructions. RNA was reverse transcribed into complementary DNA (cDNA) from

1 µg RNA using 1 µl dNTP mix (10 mM), oligo (dT)15 primer (50 ng/µl), 1 µl reverse transcriptase (100 U), and 4 µl 5× reverse transcription buffer complete (all purchased from Bioron GmbH, Ludwigshafen, Germany). Final reaction volume was 20 µl (filled with RNAse free water). cDNA synthesis conditions were as follows: 70°C for 10 min, 45°C for 120 min, and 70°C for 10 min. Target cDNA levels of human cell lines were analyzed by quantitative real-time PCR using TaqMan Universal PCR Master Mix and self-designed TaqMan gene expression assays either labeled with 6-FAM-3′ BHQ-1 or 5′ HEX−3′ BHQ-1 to be used as duplex: *IDO1*, *TDO2*, *KMO*, *HAAO*, *KYAT1/2/3/4*, *KYNU*, *QPRT*, and *GAPDH* or *ß-actin* were used as housekeeping genes. Reaction was performed in the light cycler Viia7 (Applied Biosystems, Foster City, USA) with the following PCR conditions: 95°C for 10 min, 40 cycles of 15 s at 95°C, and 1 min at 60°C. All reactions were run in triplicates. The messenger RNA (mRNA) levels of target genes were normalized to *GAPDH/β-actin*. Reactions were performed in triplicate wells and repeated four times. The general expression level of each sample was considered by calculating $2^{-\Delta CT}$ ($\Delta Ct = Ct_{target} - Ct_{Housekeeping\ genes}$).

TABLE 1 | Internal standards.

Analyte	Q1 mass (m/z)	Q3 mass (m/z)	CE (V)	DP (V)
Tryptophan	205.1	118.0	28.0	39.0
d5-Tryptophan	210.1	122.1	37.0	31.0
Kynurenine	209.1	94.1	19.6	41.0
d4-Kynurenine	213.1	140.1	21.0	39.0
Kynurenic acid	190.1	162.0	24.0	65.0
d5-Kynurenic acid	195.1	167.1	24.0	65.0

Statistical Analysis

All values are reported as mean ± SD. After proving the assumption of normality, differences between controls and treated cells were determined using the unpaired Student's *t*-test. If normality failed, the non-parametric Mann-Whitney *U*-test was applied. Statistical evaluation was performed using GraphPad PRISM software, version 5.02 (GraphPad Software, San Diego, CA, USA). In case of multiple comparisons, two- or one-way ANOVA on ranks (Bonferroni's multiple comparison test) was used. The criterion for significance was taken to be $p < 0.05$.

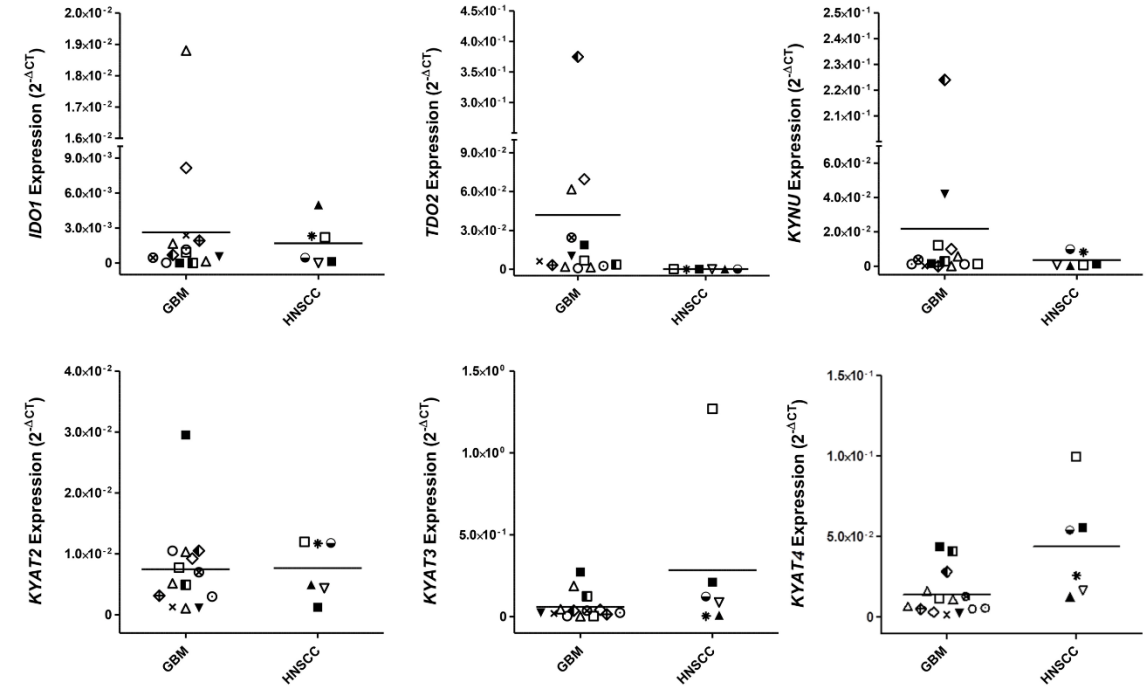

FIGURE 1 | Relative messenger RNA (mRNA) expression of IDO1, TDO2, KYNU, KYAT2, KYAT3, and KYAT4 in glioblastoma multiforme (GBM) and head and neck squamous cell carcinoma cells (HNSCC). The graphs indicate the mRNA expression normalized to the housekeeping genes ($2^{-\Delta}$CT). GBM ($N = 13$, HROG02, HROG04, HROG05, HROG06, HROG10, HROG15, HROG24, HROG36, HROG38, HROG52, HROG63, HROG73, HROG75) and HNSCC cell lines [$N = 6$; FADU, Detroit-562, Cal-33, PE/CA/PJ-15, UT-SCC14, UT-SCC-15 (33)].

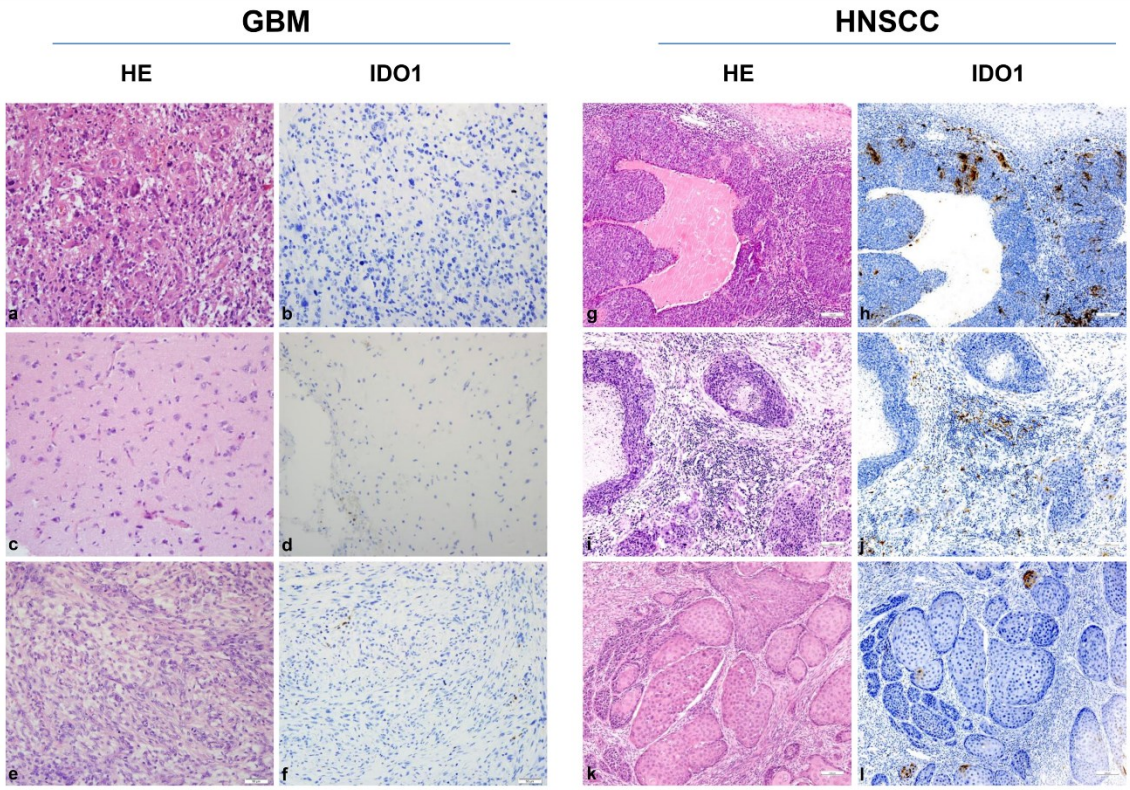

FIGURE 2 | IDO1 immunohistochemistry. Representative images of primary glioblastoma multiforme (GBM) [HROG36 **(a,b)**, HROG63 **(c,d)**, and HROG73 **(e,f)**] and head and neck squamous cell carcinoma (HNSCC) [HNSCC06 **(g,h)**, HNSCC02 **(i,j)**, HNSCC01 **(k,l)**] samples. Left panel: Routine HE staining. Right panel: Note the focal IDO1 expression on tumor-infiltrating lymphocytes exclusively in HNSCC cases. HNSCC case 1 **(g,h)**: tonsil ($HPV^{positive}$); case 2 **(i,j)**: mouth base ($HPV^{negative}$, relapse); case 3 **(k,l)**: larynx ($HPV^{negative}$). Pictures were taken at 20× and 10× magnification, respectively.

RESULTS

Basal IDO1 and Related Genes in GBM and HNSCC Cell Lines

While IDO1 itself is not the only mechanism by which tumors can resist immune-mediated killing, we studied the expression status of different KP-related genes on a panel of human GBM and HNSCC cell lines. These experiments revealed not only differences between both entities but also a heterogeneous profile of all tested genes among cell lines (**Figure 1**). *IDO1* was differently expressed by most glioma samples (11/13) analyzed. In general, *IDO1* was only detectable at very low levels (**Figure 1**). *TDO2*, the other rate-limiting enzyme of the KP (36), was constitutively expressed by all glioma samples, and expression was even higher in comparison to *IDO1*. Generally, expression status for *TDO2* and kynurenine hydrolase (*KYNU*) was higher in GBM, while HNSCC expressed more kynurenine aminotransferases (*KYAT*) (**Figure 1**). Hence, these data indicate that the KP is active in both entities, with however different enzymes being involved in TRP catabolism.

Still, tumor cell lines grown *in vitro* not necessarily represent the *in vivo* situation; we therefore analyzed the IDO1 abundance in clinical resection specimens (**Figure 2**). In GBM, IDO1 was detectable in one of three cases (representative images are shown in **Figure 2**). By contrast, HNSCC samples presented with IDO1 but only on a small fraction of tumor-infiltrating lymphocytes (**Figure 2**). Although not analyzed systematically, the only $HPV^{positive}$ case in this small cohort showed highest IDO1 abundance, nicely reflecting the tumors' immunogenicity (11, 37).

Gene Expression and Protein Changes Upon IFNγ Stimulation

IDO1 is an IFNγ-inducible enzyme. Upon stimulation, the KP is activated to induce immunosuppression. *In vitro* stimulation with IFNγ mimics the *in vivo* situation of an inflammatory microenvironment. Hence, upon immune-mediated inflammation, IDO1-negative tumor cells may upregulate *IDO1* as resistance mechanism.

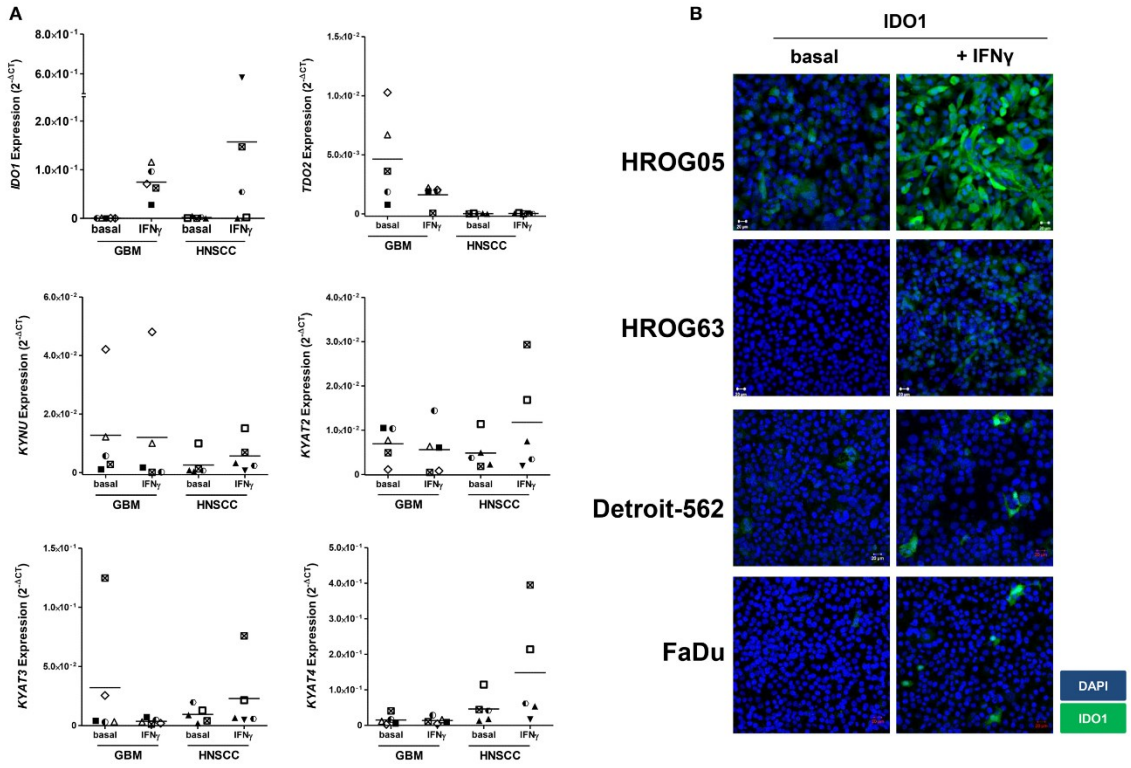

FIGURE 3 | Relative messenger RNA (mRNA) expression of *IDO1, TDO2, KYNU, KYAT2, KYAT3*, and *KYAT4* as well as IDO1 protein abundance following interferon-γ (IFNγ) stimulation in glioblastoma multiforme (GBM) and head and neck squamous cell carcinoma (HNSCC) cells. The cell cultures were either untreated or treated with IFNγ (50 ng/ml) for 24 h. **(A)** The graphs indicate the mRNA expression normalized to the housekeeping genes ($2^{-\Delta}$CT). GBM $N = 5$ cell lines (HROG02, HROG05, HROG52, HROG63, HROG75); HNSCC, $N = 4$ cell lines (FADU, Detroit-562, Cal-33, PE/CA/PJ-15). **(B)** IDO1 immunofluorescence in selected cell lines. Cell nuclei were stained with DAPI, and IDO1 was depicted by monoclonal rabbit IDO1 primary antibody (1:100; Cell Signaling Technology), followed by secondary antibody (1:250, Boster Biological Technology Pleasanton, CA, United States) labeling. Cells were analyzed with a Zeiss LSM-780 Confocal Laser Microscope. Original magnification 20×.

Using five individual GBM cell lines, *IDO1* expression was inducible in all cases (**Figure 3A**). Upregulation of *IDO1* was high on protein levels in HROG05 cells and marginal in HROG63 (**Figure 3B**). *TDO2* and *KYAT3* were suppressed upon IFNγ stimulation in three of five samples and hardly detectable in one cell line, supporting data from a recent publication (38). *KYNU* was not affected by IFNγ stimulation (**Figure 3A**).

Just as in GBM, *IDO1* was inducible in HNSCC cells (**Figure 3A**). Immunofluorescence revealed focal expression of singular cells with different intensity (**Figure 3B**). Of note, IFNγ stimulation even induced upregulation of *KYAT1*, *KYAT2*, *KYAT3*, and *KYAT4* (**Figure 3A** and data not shown), most likely constituting a compensatory mechanism as described before in experimental autochthonous tumor models (39).

Interference With the KP of Cytostatic and Targeted Therapies

Next, we examined whether cytostatic and targeted drugs have an influence on the KP. For GBM, TMZ was chosen, and for HNSCC, 5-FU, Cisplatin, Gemcitabine, as well as Cetuximab were used. As a targeted yet still experimental agent, the potent and specific CDKi Dinaciclib was applied to cells of both entities.

Before this experiment, drug doses were carefully tested in dose-response analyses (data not shown) along with discrimination of apoptosis and necrosis. Generally, drugs used in this study tended to induce necrosis, while apoptosis, if present, was only detectable at early time points. Exemplary results for the HNSCC cell line Detroit-562 are given in **Supplementary Figures 1A,B**. While cytostatics are well-known to affect normal cells' viability, the impact of the CDKi Dinaciclib on immune and red blood cells is less clear. We therefore performed a hemolysis and leukocyte viability assay. In this experiment, no toxicity was seen against normal cells (**Supplementary Figure 1C**). Even at high concentrations, Dinaciclib impaired cellular viability/integrity only marginally (**Supplementary Figure 1C**).

TMZ is an oral alkylating agent that methylates DNA at the O^6 position of guanine causing cell cycle arrest at G2/M. It is used as standard of care for GBM. However, acquired resistance, a process not fully understood, leads to

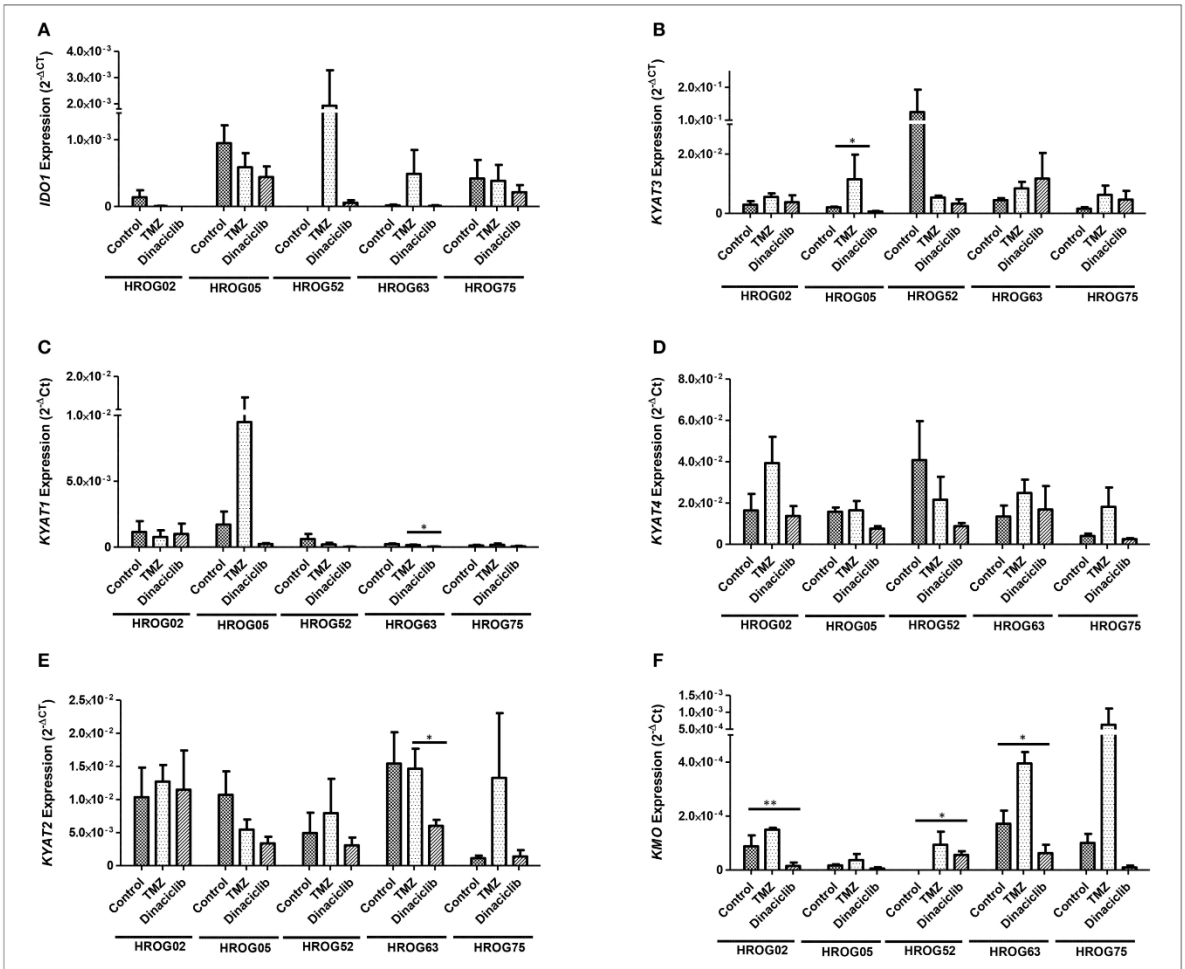

FIGURE 4 | Relative messenger RNA (mRNA) expression of *IDO1, KYAT1, KYAT2, KYAT3*, *KYAT4,* and KMO upon cytostatic drugs and targeted therapy in glioblastoma multiforme (GBM) cells. Graphs indicate the mRNA expression of selected kynurenine pathway (KP)-related genes normalized to the housekeeping genes ($2^{-\Delta}$CT). Results show data of three independent experiments. *$p < 0.05$; **$p < 0.01$ vs. control. Two-way ANOVA.

major limitations in treatment. Here, TMZ downregulated *IDO1* in three of five GBM cell lines but led to increased expression in HROG52 and HROG63—a paired GBM cell line established from the very same patient (primary lesion and upon relapse) (**Figure 4**). Gene expression of *KYAT2*, *KYAT4*, and *KMO* was heterogeneous. Generally, there was a trend toward higher expression of those genes but with cell-line-specific differences (e.g., *KYAT3*: $p < 0.05$ vs. control in HROG05 cells; **Figure 4**). *KYNU* expression was not affected by TMZ (data not shown). Interestingly, the combination of IFNγ and TMZ that mimics the *in vivo* situation led to similar or even stronger *IDO1* upregulation compared to IFNγ alone in two out of four glioma samples (**Figure 5**). Adding Dinaciclib to either IFNγ or TMZ lowered the mRNA expression of *IDO1* massively. Other KP-related genes like *TDO2* and *KYAT1-4* were similarly downregulated (**Figure 5**). **Supplementary Table for Figure 5** provides a detailed statistical analysis of each cell line in relation to the individual treatment regimens.

In HNSCC cells, Cetuximab was the only *IDO1*-inducing substance (exemplary results for Detroit-562 cells are given in **Figure 6**). Beyond that, the cytostatics as well as Cetuximab induced at least one of the KP-related genes ($p < 0.05$ vs. control), implicating activation of this pathway *via* different effectors. By adding Dinaciclib to cytostatic drugs, this effect was abrogated, even in the presence of IFNγ (**Figure 6** and data not shown). Of note, Dinaciclib alone as well as in combination with other substances effectively suppressed all KP-related genes, implying inhibition of the TRP catabolism by this CDKi.

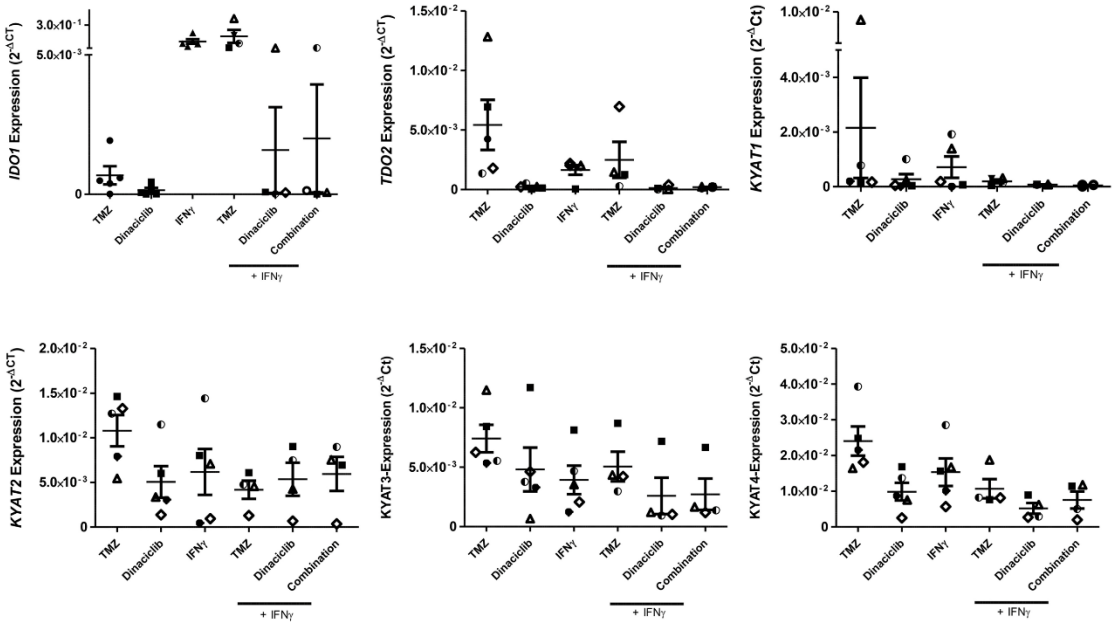

FIGURE 5 | Relative messenger RNA (mRNA) expression of *IDO1, TDO2, KYAT1, KYAT2, KYAT3*, and *KYAT4* upon concomitant treatment with interferon-γ (IFNγ) and cytostatic drugs in glioblastoma multiforme (GBM) cells. The cell cultures ($N = 5$, HROG02, HROG05, HROG52, HROG63, HROG75) were either left untreated or treated with IFNγ (50 ng/ml) for 24 h. Treatments were performed simultaneously, i.e., IFNγ ± TMZ, and/or Dinaciclib. Graphs indicate the mRNA expression of selected KP-related genes normalized to the housekeeping genes ($2^{-\Delta}$CT). Results show data of three independent experiments. A statistical report is given in **Supplementary Table for Figure 5**.

Dinaciclib Blocks IFNγ-Induced IDO1 Expression in GBM and HNSCC Cells

Considering the active downregulation of KP-related genes by Dinaciclib, we investigated whether this CDKi is able to inhibit or reverse IFNγ-induced IDO1 upregulation in GBM and HNSCC cells on a protein level. TMZ and Cetuximab were included as active inductors of *IDO1* and associated KP-related genes.

IFNγ and selected drugs were added simultaneously for 72 h. Dinaciclib effectively blocked IFNγ-induced IDO1 protein in both entities, while TMZ alone as well as the combination with IFNγ strongly enhanced IDO1 protein level (**Figure 7**). Hence, mRNA expression data were nicely confirmed.

When Dinaciclib was combined with IFNγ and TMZ, the IDO1-inducing stimulus of these latter substances was far too strong to be suppressed (**Figure 7**). However, the low number of residual cells in this combination hints toward additive or even synergistic effects independent from IDO1 (**Figures 7A,B**).

While IDO1 was highly inducible in GBM cells only, we then determined protein level upon IFNγ-prestimulation approaching the *in vivo* situation. The cytotoxic effect of Dinaciclib was preserved; however, levels of IDO1 enzyme were not significantly altered (**Supplementary Figures 2A,B**). Comparable results were obtained for TMZ. Virtually, all residual cells showed positive staining; still there was a trend toward lower intensity in monotherapy and in combination (**Supplementary Figure 2B**).

Taken together, the CDKi Dinaciclib is able to block IFNγ-mediated and thus most likely even chemotherapy-induced *IDO1* upregulation in GBM and HNSCC cells. However, blunt interference with this TRP-metabolizing enzyme is unlikely.

Treatment Induced Influence on KP-Related Metabolites

Our data revealed IDO1 induction by TMZ, which is reversible by Dinaciclib. Thus, we examined the influence on KP-related metabolites in GBM cell lines.

TRP, KYN, and the downstream metabolite kynurenic acid (KYNA) were quantified by MS using cell culture supernatants of GBM cell lines (**Figures 8A,B**). TRP was catabolized after 24 h from all cell lines among all treatment regimens. Adding TMZ or Dinaciclib in monotherapy marginally affected TRP consumption as well as KYN and KYNA production. Stimulation with either IFNγ or a combination of TMZ resulted in greatly enhanced TRP depletion and increased KYN levels, although to varying degrees in the different cell lines (**Figure 8A**). Small amounts of KYNA were produced constitutively and to a greater extent after IFNγ mono- and TMZ combination in all cell lines (**Figure 8A**). In contrast, KYNA level remained unchanged upon Dinaciclib in combination with IFNγ, confirming immunofluorescence results (please see **Figure 7** for details). The same was true for the KYN/TRP ratio, being only

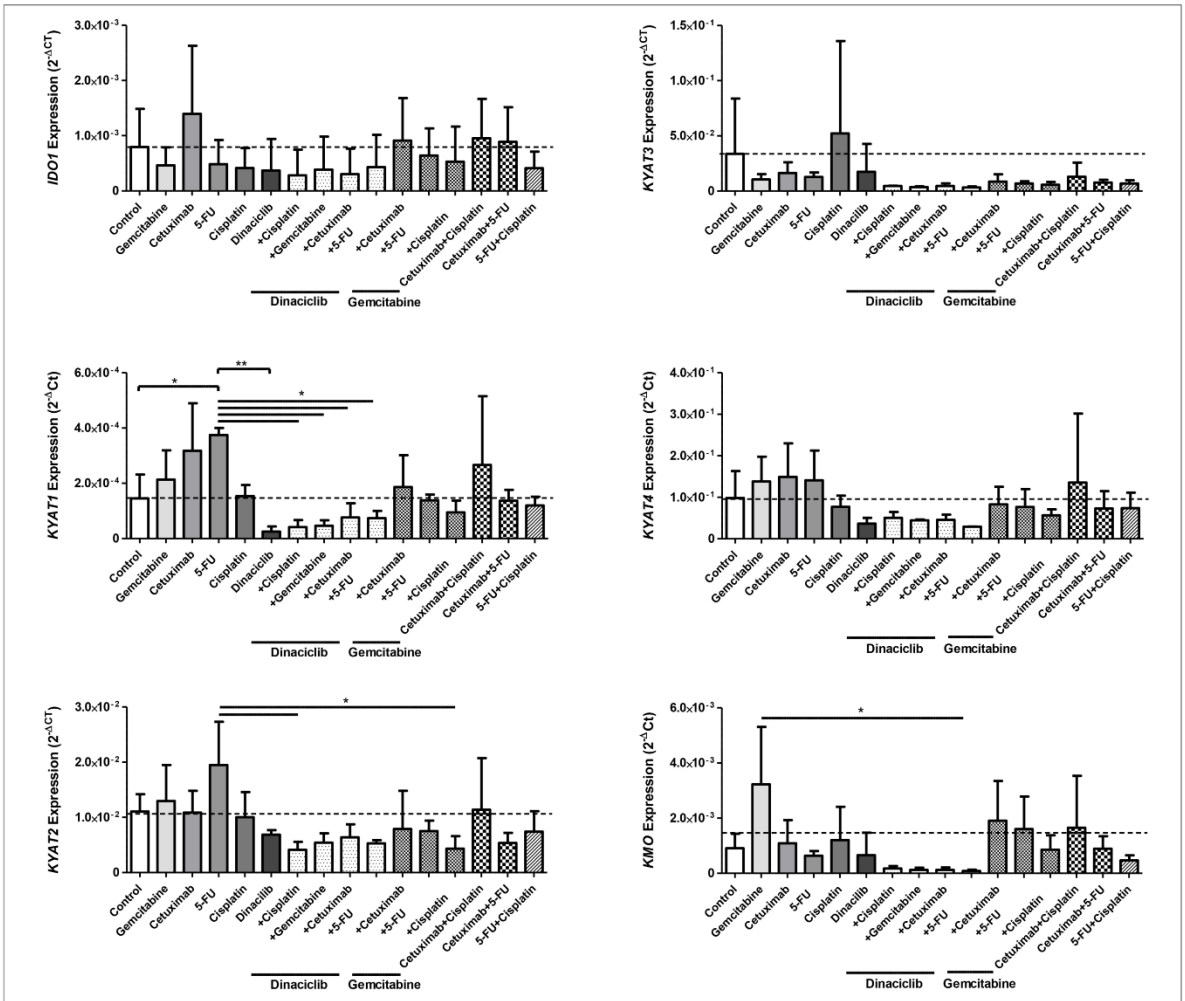

FIGURE 6 | Relative messenger RNA (mRNA) expression of *IDO1*, *KYAT1*, *KYAT2*, *KYAT3*, *KYAT4*, and KMO upon cytostatic drugs and targeted therapy in head and neck squamous cell carcinoma (HNSCC) cells. Graphs indicate the mRNA expression of selected KP-related genes normalized to the housekeeping genes ($2^{-\Delta}$CT). Results show data of three independent experiments using HNSCC cell line Detroit-562. $^{*}p < 0.05$; $^{**}p < 0.01$. One-way ANOVA (Bonferroni's multiple comparison test).

affected in samples treated with IFNγ as well as the combination of IFNγ and TMZ (**Figure 8B**).

These data underline our gene and protein expression data. The CDKi Dinaciclib is directly or indirectly capable of blocking the KP. TMZ particularly in combination with the proinflammatory cytokine IFNγ accelerates TRP consumption accompanied by KYN and KYNA production in GBM cells.

DISCUSSION

The finding that high *IDO1* expression is associated with shorter survival in cancer patients made IDO1 a promising target either by specific inhibitors or indirectly by immunomodulation. A recent study described dramatically suppressed tumor growth upon *IDO1* knockdown by increasing the number of $CD4^{+}$ and $CD8^{+}$ T cells in murine GBM models (9). However, the exact mechanisms underlying IDO1 and thus TRP metabolism along the KP remain unclear. Therefore, we focused on the expression of *IDO1* and *IDO*-related KP genes and their potential involvement in immune evasion in experimental models of HNSCC and GBM.

We were able to show that the KP is active in both entities, with different enzymes involved in TRP catabolism. Of note, basal *IDO1* expression was low and inversely correlated with *TDO2*. In the only prior study on primary GBM cultures, similar results were described with constitutive *TDO2* expression in

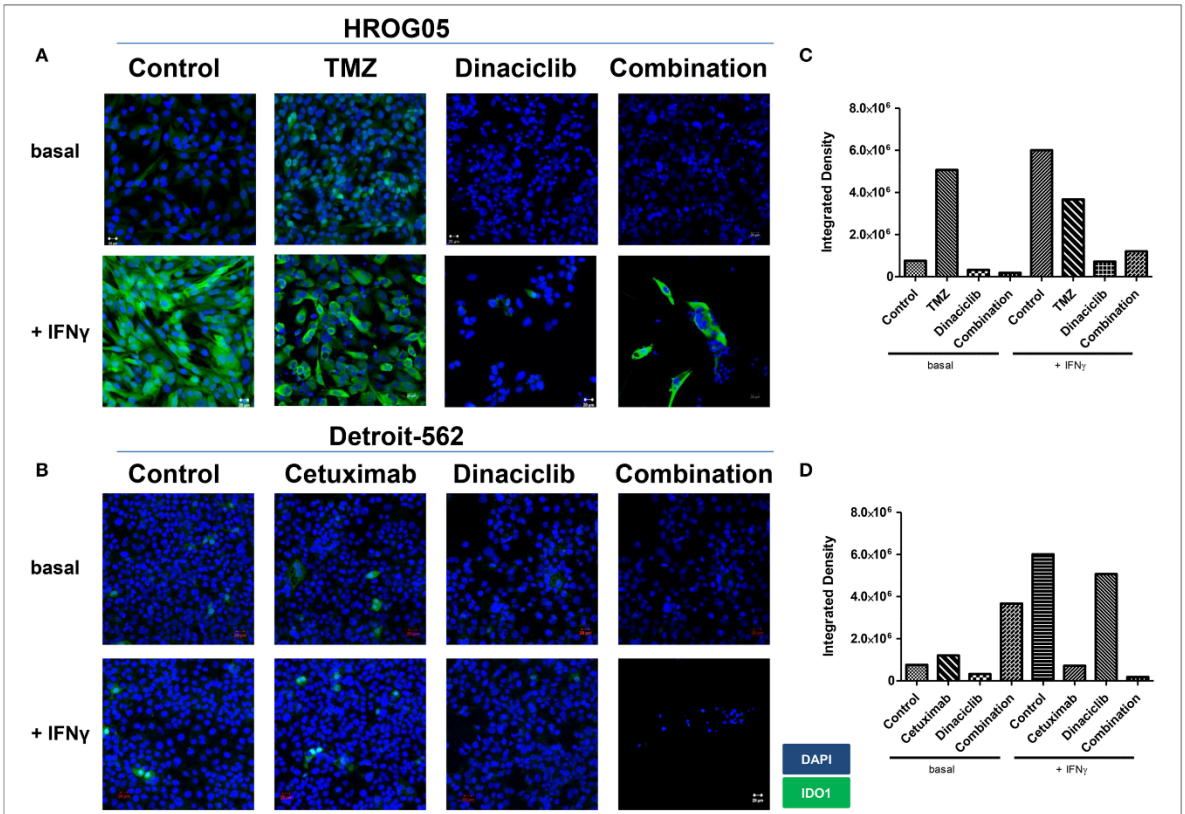

FIGURE 7 | Indoleamine 2,3-dioxygenase (IDO1) protein abundance in selected glioblastoma multiforme (GBM) and head and neck squamous cell carcinoma (HNSCC) cells upon cytostatic drugs and targeted therapy. The cell cultures [**(A)** GBM: HROG05; **(B)** HNSCC: Detroit-562] were either left untreated or treated with IFNγ (50 ng/ml) for 24 h. Treatments were performed simultaneously, i.e., IFNγ ± TMZ, Cetuximab, and/or Dinaciclib. Cell nuclei were stained with DAPI. Original magnification 20×. **(C,D)** Quantification was done to score staining intensity in untreated and treated HROG05 and Detroit-562 cells. This was carried out using ImageJ software as described in Material and Methods.

most GBM cell cultures (29). In here, TDO2 likely promotes tumor growth by suppressing antitumor immune responses (2, 31). KP products are considered as therapeutic targets because *IDO1* and other genes of the TRP metabolism are not expressed in healthy brain tissue, but gradually increase with GBM dedifferentiation (low vs. high grade GBM). In HNSCC, different results on *IDO1* are documented, and expression is heterogeneous among different HNSCC cell lines. Of note, IDO1 abundance of primary resection specimen and cultured cells seems to be independent from anatomical site and HPV status (40). Still, IDO1 is a useful marker for progression of in oral squamous cell carcinoma (41). In esophageal squamous cell carcinoma, progression and metastasis correlates with strong inflammation at the tumors' invasive front and disturbed TRP metabolism (42). These cumulative data highlight the biological relevance of the KP in malignancies and may explain why IDO1 is barely detectable upon long-term *in vitro* culture. By mimicking the inflamed microenvironment and thus taking a step closer to the *in vivo* situation, IFNγ was added as strong IDO1 inductor (43). While GBM cells responded with the expected *IDO1* upregulation on mRNA expression and protein level as well as accelerated TRP consumption, this molecule was barely inducible in HNSCC cells. It is conceivable that this is due to the duration of *in vitro* culture. GBM cells were established recently and thus used in defined low passages (<P40), whereas half of the HNSCC cell lines were long-term cultures with more or less unknown passage [Detroit-562 as well as UT-SCC14 and UT-SCC15 (44) are the only exceptions; <P40]. Cell lines may acquire additional mutations overtime changing their protein expression. Another *in vitro* limitation is that experiments were conducted without immunological pressure. *In vivo* studies are desirable to verify the results.

Indirect effects of TRP metabolism include interference with other biological functions like migration, angiogenesis, and cell growth regulation (18, 40). To investigate the influence of anticancer drugs on TRP catabolism, we performed a comprehensive analysis using conventional chemotherapy (TMZ, 5-FU, Cisplatin, Gemcitabine) and targeted drugs

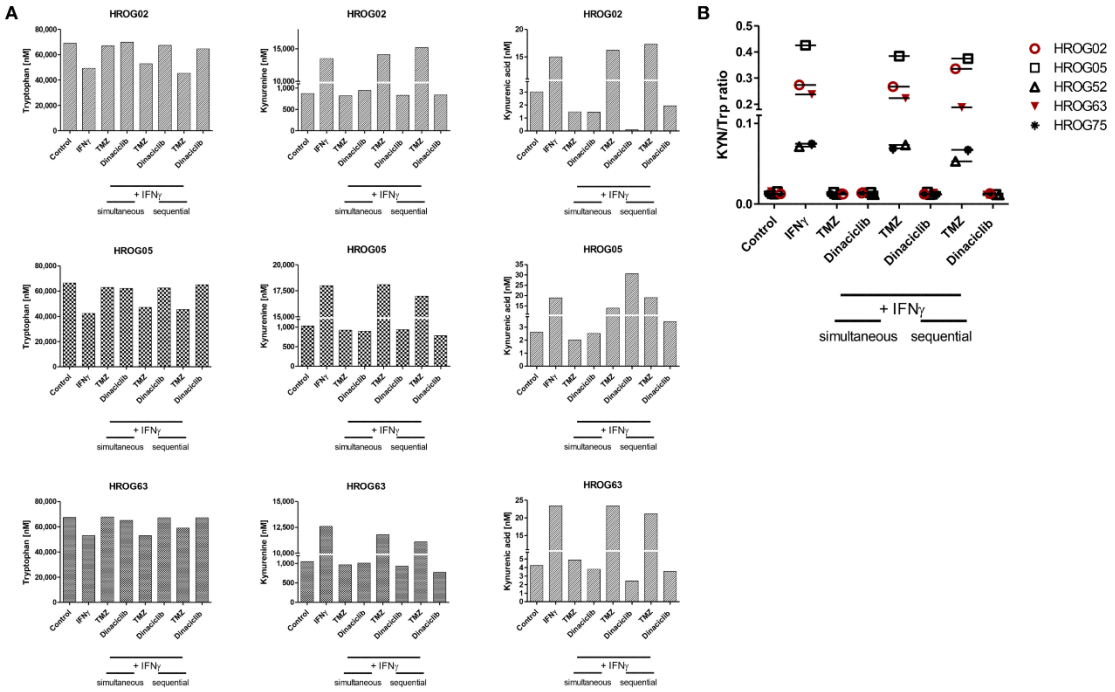

FIGURE 8 | Indoleamine 2,3-dioxygenase (IDO) protein abundance in glioblastoma multiforme (GBM) and head and neck squamous cell carcinoma (HNSCC) cells as well as kynurenine pathway (KP) metabolite levels in GBM cells upon cytostatic drugs and targeted therapy. Treatments were performed sequentially, i.e., interferon-γ (IFNγ) pretreatment for IDO1 induction, followed by Temozolomide (TMZ) and/or Dinaciclib. **(A)** KP metabolites changed upon TMZ but not Dinaciclib treatment. The combination of TMZ and IFNγ accelerates tryptophan (TRP) consumption accompanied by kynurenine (KYN) and kynurenic acid (KYNA) production **(B)**. KYN/TRP ratios in GBM cells were determined dividing KYN values by TRP values. Results show data of a single measurement.

(Cetuximab, Dinaciclib). The KP-related gene expression and metabolites were determined in residual cells. In GBM, the standard of care drug TMZ was applied either with or without IFNγ stimulation. While this substance affected *IDO1* on the expression level, the amount of the resulting protein increased. This may be explained by either increased protein's half-life due to a reduced rate of degradation or the preferential translation during cellular stress. In previous studies, exposure of several cultured human malignant glioma cell lines, primary neurons, and a neuroblastoma cell line to IFNγ reduced TRP levels in culture medium accompanied by increased *IDO1* expression and KYN production (29, 45). Our results confirm these data, and in addition, we were able to demonstrate that IFNγ stimulation in combination with TMZ stimulated KYN and KYNA production and TRP catabolism in GBM cell cultures. The increase in TRP catabolism and KYN production (KYN/TRP ratio) is widely used as indirect indicator of the cumulative activities of TDO2, IDO1, and IDO-2 (38, 46). The KP in brain tumors is likely triggered by IFNγ from immediate surrounding tissue (29, 47, 48). Thus, *IDO1* expression in brain tumor cells is likely to be triggered when IFNγ is produced from activated T cells and/or microglia and neurons. Furthermore, gliomas and glioneuronal tumors have an elevated tryptophan uptake and catabolism *in vivo* (49). Given our observation on a further enhanced KP activity upon TMZ treatment, this might provide an explanation of (acquired) drug resistance and final relapse. Hence, IDO1 blocking agents should be investigated in TMZ-tailored therapeutic approaches.

In HNSCC cells, KP activation was different. KP-related genes were exclusively induced by standard drugs, and only Cetuximab induced *IDO1*. Additional upregulated genes involved kynurenine aminotransferases, responsible for synthesizing a neuroprotectant, and KMO. While the specific biochemical activity of these molecules and biological relevance in cancer is barely examined, we interpret this result as one possible mechanism of resistance upon therapy—a finding quite common after conventional chemotherapy and usually also being associated with poor response toward neoadjuvant therapy in other entities (50).

Mechanistically, this can be attributed to the secretion of proinflammatory substances, such as prostaglandin E2 or high-mobility group protein B1 by dying tumor cells, secondary contributing to KP activation. By accumulating TRP, toxic metabolites of tumor cells actively shape an immunosuppressive microenvironment. Breaking down this shield is one of the main objectives in pharmacological inhibition of KP. Questions remain why most inhibitors failed in clinical trials, and mechanisms are

only just beginning to become clear. A fact worth mentioning is the functional redundancy of IDO1, IDO-2, and TDO2 (51), augmenting the risk of mechanistic bypass.

Dinaciclib is a potent and specific CDK inhibitor of CDK1, CDK2, CDK5, and CDK9. Preclinical studies showed that this inhibitor is capable of decelerating tumor growth in numerous cancer entities via cell cycle arrest and apoptosis induction (52, 53). In our study, Dinaciclib was the only KP-inhibiting substance tested here. Of note, impairment of the KP was independent from the combination partner, and this CDKi effectively suppressed IFNγ-induced *IDO1* upregulation after simultaneous treatment. While this result was completely unexpected and has—to the best of our knowledge—not been described previously, our data do not support the idea of blunt interference with the KP. GBM cells with strong *IDO1* expression showed only marginally reduced IDO1 protein level after Dinaciclib treatment. This effect might be boosted after long or repeated treatment cycles. In line with these findings, several preclinical studies already proposed synergistic effects of selective and unselective IDO1 inhibitors when administered in conjunction with chemo- and/or radiotherapy (4). This may finally have impact for second- or third-line immunotherapeutic approaches. Therefore, the late KYN/TRP index is indeed a relevant clinical benchmark providing prognostic value for GBM patients (54).

Summarizing our findings, we provide evidence for the relevance of TRP catabolism in malignancies especially in the context of standard therapy. The CDKi Dinaciclib was identified as indirect KP inhibitor. Lastly, specific KP inhibition may increase the efficacy of standard drugs by restoring immune function and thus improve patients' outcome.

DATA AVAILABILITY STATEMENT

The datasets generated for this study are available on request to the corresponding author.

AUTHOR CONTRIBUTIONS

CR performed experiments, analyzed data, and participated in manuscript writing. BS and AZ performed immunohistochemistry and analysis, and provided images. HK, JG, NI, and FS performed experiments and analyzed data. GD performed LC-MS analyses. CC and CJ participated in paper finalization and critically revised the manuscript. DS and EW critically revised the manuscript. CM designed study, the outline of the manuscript, performed data interpretation, and wrote the manuscript.

FUNDING

CM was supported by grants from the Deutsche Forschungsgemeinschaft (MA5799/2-1 and MA5799/2-2).

ACKNOWLEDGMENTS

The authors are also grateful to Susanne Neumeister and Dr. Ann-Kristin Henning from the Institute of Clinical Chemistry and Laboratory Medicine, University of Greifswald, for assisting with the quantification of TRP metabolites.

SUPPLEMENTARY MATERIAL

The Supplementary Material for this article can be found online at: https://www.frontiersin.org/articles/10.3389/fimmu.2020.00055/full#supplementary-material

Supplementary Figure 1 | Quantitative analysis of cell death in Detroit-562 HNSCC cells upon cytostatic drugs and targeted therapy. The cells were treated with the given substances for 24 and 72 h. Thereafter, cells were harvested and stained with Yo-Pro-1 to detect early and late apoptotic cells, as well as propidium iodide for necrosis determination. Apoptosis/necrosis discrimination was done on a flow cytometer (BD FACSVerse™) as described in material and methods. **(A)** Quantitative analysis of cell death after 24 and 72 h, respectively. $*p < 0.05$ vs. control; $**p < 0.01$ vs. control. *t*-test. **(B)** Representative dot plots showing elevated numbers of necrotic cells upon treatment. **(C)** Hemolysis and viability of PBMC upon treatment with Dinaciclib. Therefore, whole blood and PBMC were cultured in the presence of increasing Dinaciclib concentrations (1, 5, and 10 μM) for 2 and 24 h, respectively. Hemolytic activity was determined from cell-free supernatants (red blood cell lysis), Calcein AM was used for quantifying viability of PBMC. Mean + SD, $N = 5$ individual donors.

Supplementary Figure 2 | IDO1 protein abundance in HROG05 GBM cells upon cytostatic drugs and targeted therapy. The cells were pretreated with IFNγ (50 ng/ml) for 24 h. Thereafter TMZ, Dinaciclib and the combination of both substances was added to see whether IFNγ-induced upregulation of IDO1 is reversible. **(A)** None of these substances downregulated IDO1 in the sequential setting. Cell nuclei were stained with DAPI. Original magnification 20x. **(B)** Quantification was done to score staining intensity in untreated and treated HROG05 cells. This was carried out by using ImageJ software as described in material and methods.

Supplementary Table for Figure 5 | Statistical analysis of individual treatment regimens, depicted for each cell line, and genes analyzed.

REFERENCES

1. Liu M, Wang X, Wang L, Ma X, Gong Z, Zhang S, et al. Targeting the IDO1 pathway in cancer: from bench to bedside. *J Hematol Oncol.* (2018) 11:100. doi: 10.1186/s13045-018-0644-y
2. Platten M, Wick W, Van den Eynde BJ. Tryptophan catabolism in cancer: beyond IDO and tryptophan depletion. *Cancer Res.* (2012) 72:5435–40. doi: 10.1158/0008-5472.CAN-12-0569
3. Gajewski TF, Schreiber H, Fu Y-X. Innate and adaptive immune cells in the tumor microenvironment. *Nat Immunol.* (2013) 14:1014–22. doi: 10.1038/ni.2703
4. Muller AJ, DuHadaway JB, Donover PS, Sutanto-Ward E, Prendergast GC. Inhibition of indoleamine 2,3-dioxygenase, an immunoregulatory target of the cancer suppression gene Bin1, potentiates cancer chemotherapy. *Nat Med.* (2005) 11:312–9. doi: 10.1038/nm1196
5. Moon YW, Hajjar J, Hwu P, Naing A. Targeting the indoleamine 2,3-dioxygenase pathway in cancer. *J Immunother Cancer.* (2015) 3:51. doi: 10.1186/s40425-015-0094-9
6. Munn DH, Mellor AL. IDO in the tumor microenvironment: inflammation, counter-regulation, and tolerance. *Trends Immunol.* (2016) 37:193–207. doi: 10.1016/j.it.2016.01.002

7. Avril T, Saikali S, Vauleon E, Jary A, Hamlat A, De Tayrac M, et al. Distinct effects of human glioblastoma immunoregulatory molecules programmed cell death ligand-1 (PDL-1) and indoleamine 2,3-dioxygenase (IDO) on tumour-specific T cell functions. *J Neuroimmunol.* (2010) 225:22–33. doi: 10.1016/j.jneuroim.2010.04.003
8. Wainwright DA, Chang AL, Dey M, Balyasnikova IV, Kim CK, Tobias A, et al. Durable therapeutic efficacy utilizing combinatorial blockade against IDO, CTLA-4, and PD-L1 in mice with brain tumors. *Clin Cancer Res.* (2014) 20:5290–301. doi: 10.1158/1078-0432.CCR-14-0514
9. Hanihara M, Kawataki T, Oh-Oka K, Mitsuka K, Nakao A, Kinouchi H. Synergistic antitumor effect with indoleamine 2,3-dioxygenase inhibition and temozolomide in a murine glioma model. *J Neurosurg.* (2016) 124:1594–601. doi: 10.3171/2015.5.JNS141901
10. Badawy AAB. Kynurenine pathway of tryptophan metabolism: regulatory and functional aspects. *Int J Tryptophan Res.* (2017) 10:1178646917691938. doi: 10.1177/1178646917691938
11. Solomon B, Young RJ, Rischin D. Head and neck squamous cell carcinoma: genomics and emerging biomarkers for immunomodulatory cancer treatments. *Semin Cancer Biol.* (2018) 52:228–40. doi: 10.1016/j.semcancer.2018.01.008
12. Acovic A, Gazdic M, Jovicic N, Harrell CR, Fellabaum C, Arsenijevic N, et al. Role of indoleamine 2,3-dioxygenase in pathology of the gastrointestinal tract. *Therap Adv Gastroenterol.* (2018) 11:1756284818815334. doi: 10.1177/1756284818815334
13. Sordillo PP, Sordillo LA, Helson L. The kynurenine pathway: a primary resistance mechanism in patients with glioblastoma. *Anticancer Res.* (2017) 37:2159–71. doi: 10.21873/anticanres.11551
14. Zamanakou M, Germenis AE, Karanikas V. Tumor immune escape mediated by indoleamine 2,3-dioxygenase. *Immunol Lett.* (2007) 111:69–75. doi: 10.1016/j.imlet.2007.06.001
15. Ma W-J, Wang X, Yan W-T, Zhou Z-G, Pan Z-Z, Chen G, et al. Indoleamine-2,3-dioxygenase 1/cyclooxygenase 2 expression prediction for adverse prognosis in colorectal cancer. *World J Gastroenterol.* (2018) 24:2181–90. doi: 10.3748/wjg.v24.i20.2181
16. Brandacher G, Perathoner A, Ladurner R, Schneeberger S, Obrist P, Winkler C, et al. Prognostic value of indoleamine 2,3-dioxygenase expression in colorectal cancer: effect on tumor-infiltrating T cells. *Clin Cancer Res.* (2006) 12:1144–51. doi: 10.1158/1078-0432.CCR-05-1966
17. Jeong Y-I, Kim SW, Jung ID, Lee JS, Chang JH, Lee C-M, et al. Curcumin suppresses the induction of indoleamine 2,3-dioxygenase by blocking the Janus-activated kinase-protein kinase Cdelta-STAT1 signaling pathway in interferon-gamma-stimulated murine dendritic cells. *J Biol Chem.* (2009) 284:3700–8. doi: 10.1074/jbc.M807328200
18. Platten M, von Knebel Doeberitz N, Oezen I, Wick W, Ochs K. Cancer immunotherapy by targeting IDO1/TDO and their downstream effectors. *Front Immunol.* (2014) 5:673. doi: 10.3389/fimmu.2014.00673
19. Uyttenhove C, Pilotte L, Theate I, Stroobant V, Colau D, Parmentier N, et al. Evidence for a tumoral immune resistance mechanism based on tryptophan degradation by indoleamine 2,3-dioxygenase. *Nat Med.* (2003) 9:1269–74. doi: 10.1038/nm934
20. Fox E, Oliver T, Rowe M, Thomas S, Zakharia Y, Gilman PB, et al. Indoximod: an immunometabolic adjuvant that empowers T cell activity in cancer. *Front Oncol.* (2018) 8:370. doi: 10.3389/fonc.2018.00370
21. Beatty GL, O'Dwyer PJ, Clark J, Shi JG, Bowman KJ, Scherle PA, et al. First-in-human phase I study of the oral inhibitor of indoleamine 2,3-dioxygenase-1 epacadostat (INCB024360) in patients with advanced solid malignancies. *Clin Cancer Res.* (2017) 23:3269–76. doi: 10.1158/1078-0432.CCR-16-2272
22. Platten M, Nollen EAA, Röhrig UF, Fallarino F, Opitz CA. Tryptophan metabolism as a common therapeutic target in cancer, neurodegeneration and beyond. *Nat Rev Drug Discov.* (2019) 18:379–401. doi: 10.1038/s41573-019-0016-5
23. Kanai M, Yoshimura K, Asada M, Imaizumi A, Suzuki C, Matsumoto S, et al. A phase I/II study of gemcitabine-based chemotherapy plus curcumin for patients with gemcitabine-resistant pancreatic cancer. *Cancer Chemother Pharmacol.* (2011) 68:157–64. doi: 10.1007/s00280-010-1470-2
24. Maletzki C, Scheinpflug P, Witt A, Klar E, Linnebacher M. Targeting immune-related molecules in cancer therapy: a comprehensive *in vitro* analysis on patient-derived tumor models. *Biomed Res Int.* (2019) 2019:4938285. doi: 10.1155/2019/4938285
25. Vacchelli E, Aranda F, Eggermont A, Sautes-Fridman C, Tartour E, Kennedy EP, et al. Trial watch: IDO inhibitors in cancer therapy. *Oncoimmunology.* (2014) 3:e957994. doi: 10.4161/21624011.2014.957994
26. Schafer CC, Wang Y, Hough KP, Sawant A, Grant SC, Thannickal VJ, et al. Indoleamine 2,3-dioxygenase regulates anti-tumor immunity in lung cancer by metabolic reprogramming of immune cells in the tumor microenvironment. *Oncotarget.* (2016) 7:75407–24. doi: 10.18632/oncotarget.12249
27. Yentz S, Smith D. Indoleamine 2,3-dioxygenase (IDO) inhibition as a strategy to augment cancer immunotherapy. *BioDrugs.* (2018) 32:311–7. doi: 10.1007/s40259-018-0291-4
28. Long GV, Dummer R, Hamid O, Gajewski TF, Caglevic C, Dalle S, et al. Epacadostat plus pembrolizumab versus placebo plus pembrolizumab in patients with unresectable or metastatic melanoma (ECHO-301/KEYNOTE-252): a phase 3, randomised, double-blind study. *Lancet Oncol.* (2019) 20:1083–97. doi: 10.1016/S1470-2045(19)30274-8
29. Adams S, Teo C, McDonald KL, Zinger A, Bustamante S, Lim CK, et al. Involvement of the kynurenine pathway in human glioma pathophysiology. *PLoS ONE.* (2014) 9:e112945. doi: 10.1371/journal.pone.0112945
30. Ball HJ, Jusof FF, Bakmiwewa SM, Hunt NH, Yuasa HJ. Tryptophan-catabolizing enzymes—party of three. *Front Immunol.* (2014) 5:485. doi: 10.3389/fimmu.2014.00485
31. Pilotte L, Larrieu P, Stroobant V, Colau D, Dolusic E, Frederick R, et al. Reversal of tumoral immune resistance by inhibition of tryptophan 2,3-dioxygenase. *Proc Natl Acad Sci USA.* (2012) 109:2497–502. doi: 10.1073/pnas.1113873109
32. Abdel-Magid AF. Targeting the inhibition of tryptophan 2,3-dioxygenase (TDO-2) for cancer treatment. *ACS Med Chem Lett.* (2017) 8:11–3. doi: 10.1021/acsmedchemlett.6b00458
33. Jamieson SM, Tsai P, Kondratyev MK, Budhani P, Liu A, Senzer NN, et al. Evofosfamide for the treatment of human papillomavirus-negative head and neck squamous cell carcinoma. *JCI Insight.* (2018) 3:122204. doi: 10.1172/jci.insight.122204
34. Maletzki C, Klier U, Marinkovic S, Klar E, Andrä J, Linnebacher M. Host defense peptides for treatment of colorectal carcinoma-a comparative *in vitro* and *in vivo* analysis. *Oncotarget.* (2014) 5:4467–79. doi: 10.18632/oncotarget.2039
35. Fuertig R, Ceci A, Camus SM, Bezard E, Luippold AH, Hengerer B. LC-MS/MS-based quantification of kynurenine metabolites, tryptophan, monoamines and neopterin in plasma, cerebrospinal fluid, and brain. *Bioanalysis.* (2016) 8:1903–17. doi: 10.4155/bio-2016-0111
36. Opitz CA, Litzenburger UM, Sahm F, Ott M, Tritschler I, Trump S, et al. An endogenous tumour-promoting ligand of the human aryl hydrocarbon receptor. *Nature.* (2011) 478:197–203. doi: 10.1038/nature10491
37. Guo T, Califano JA. Molecular biology and immunology of head & neck cancer. *Surg Oncol Clin N Am.* (2015) 24:397–407. doi: 10.1016/j.soc.2015.03.002
38. Adam I, Dewi DL, Mooiweer J, Sadik A, Mohapatra SR, Berdel B, et al. Upregulation of tryptophanyl-tRNA synthethase adapts human cancer cells to nutritional stress caused by tryptophan degradation. *Oncoimmunology.* (2018) 7:e1486353. doi: 10.1080/2162402X.2018.1486353
39. Smith C, Chang MY, Parker KH, Beury DW, DuHadaway JB, Flick HE, et al. IDO is a nodal pathogenic driver of lung cancer and metastasis development. *Cancer Discov.* (2012) 2:722–35. doi: 10.1158/2159-8290.CD-12-0014
40. Bates AM, Gomez Hernandez MP, Lanzel EA, Qian F, Brogden KA. Matrix metalloproteinase (MMP) and immunosuppressive biomarker profiles of seven head and neck squamous cell carcinoma (HNSCC) cell lines. *Transl Cancer Res.* (2018) 7:533–42. doi: 10.21037/tcr.2018.05.09
41. Seppala M, Halme E, Tiilikainen L, Luukkainen A, Laranne J, Rautiainen M, et al. The expression and prognostic relevance of indoleamine 2,3-dioxygenase in tongue squamous cell carcinoma. *Acta Otolaryngol.* (2016) 136:729–35. doi: 10.3109/00016489.2016.1152631
42. Cheng J, Jin H, Hou X, Lv J, Gao X, Zheng G. Disturbed tryptophan metabolism correlating to progression and metastasis of esophageal squamous cell carcinoma. *Biochem Biophys Res Commun.* (2017) 486:781–7. doi: 10.1016/j.bbrc.2017.03.120

43. Grant RS, Naif H, Espinosa M, Kapoor V. IDO induction in IFN-gamma activated astroglia: a role in improving cell viability during oxidative stress. *Redox Rep*. (2000) 5:101–4. doi: 10.1179/135100000101535357
44. Tonlaar N, Galoforo S, Thibodeau BJ, Ahmed S, Wilson TG, Yumpo Cardenas P, et al. Antitumor activity of the dual PI3K/MTOR inhibitor, PF-04691502, in combination with radiation in head and neck cancer. *Radiother Oncol.* (2017) 124:504–12. doi: 10.1016/j.radonc.2017.08.001
45. Miyazaki T, Moritake K, Yamada K, Hara N, Osago H, Shibata T, et al. Indoleamine 2,3-dioxygenase as a new target for malignant glioma therapy. Laboratory investigation. *J Neurosurg.* (2009) 111:230–7. doi: 10.3171/2008.10.JNS081141
46. Suzuki Y, Suda T, Asada K, Miwa S, Suzuki M, Fujie M, et al. Serum indoleamine 2,3-dioxygenase activity predicts prognosis of pulmonary tuberculosis. *Clin Vaccine Immunol.* (2012) 19:436–42. doi: 10.1128/CVI.05402-11
47. Guillemin GJ, Smythe G, Takikawa O, Brew BJ. Expression of indoleamine 2,3-dioxygenase and production of quinolinic acid by human microglia, astrocytes, and neurons. *Glia.* (2005) 49:15–23. doi: 10.1002/glia.20090
48. Adams S, Braidy N, Bessede A, Brew BJ, Grant R, Teo C, et al. The kynurenine pathway in brain tumor pathogenesis. *Cancer Res.* (2012) 72:5649–57. doi: 10.1158/0008-5472.CAN-12-0549
49. Juhasz C, Chugani DC, Muzik O, Wu D, Sloan AE, Barger G, et al. *In vivo* uptake and metabolism of alpha-[11C]methyl-L-tryptophan in human brain tumors. *J Cereb Blood Flow Metab.* (2006) 26:345–57. doi: 10.1038/sj.jcbfm.9600199
50. Li F, Wei L, Li S, Liu J. Indoleamine-2,3-dioxygenase and Interleukin-6 associated with tumor response to neoadjuvant chemotherapy in breast cancer. *Oncotarget.* (2017) 8:107844–58. doi: 10.18632/oncotarget.22253
51. Muller AJ, Manfredi MG, Zakharia Y, Prendergast GC. Inhibiting IDO pathways to treat cancer: lessons from the ECHO-301 trial and beyond. *Semin Immunopathol.* (2019) 41:41–8. doi: 10.1007/s00281-018-0702-0
52. Parry D, Guzi T, Shanahan F, Davis N, Prabhavalkar D, Wiswell D, et al. Dinaciclib (SCH 727965), a novel and potent cyclin-dependent kinase inhibitor. *Mol Cancer Ther.* (2010) 9:2344–53. doi: 10.1158/1535-7163.MCT-10-0324
53. Lin SF, Lin JD, Hsueh C, Chou TC, Wong RJ. A cyclin-dependent kinase inhibitor, dinaciclib in preclinical treatment models of thyroid cancer. *PLoS ONE.* (2017) 12:e172315. doi: 10.1371/journal.pone.0172315
54. Zhai L, Dey M, Lauing KL, Gritsina G, Kaur R, Lukas RV, et al. The kynurenine to tryptophan ratio as a prognostic tool for glioblastoma patients enrolling in immunotherapy. *J Clin Neurosci.* (2015) 22:1964–8. doi: 10.1016/j.jocn.2015.06.018

Conflict of Interest: The authors declare that the research was conducted in the absence of any commercial or financial relationships that could be construed as a potential conflict of interest.

8.5.2 Cyclin-dependent kinase inhibitors exert distinct effects on patient-derived 2D and 3D glioblastoma cell culture models

Riess et al. *Cell Death Discovery* (2021)7:54
https://doi.org/10.1038/s41420-021-00423-1

Cell Death Discovery

ARTICLE Open Access

Cyclin-dependent kinase inhibitors exert distinct effects on patient-derived 2D and 3D glioblastoma cell culture models

Christin Riess[1,2], Dirk Koczan[3], Björn Schneider[4], Charlotte Linke[1], Katharina del Moral[1], Carl Friedrich Classen[1] and Claudia Maletzki[2]

Abstract

Current therapeutic approaches have met limited clinical success for glioblastoma multiforme (GBM). Since GBM harbors genomic alterations in cyclin-dependent kinases (CDKs), targeting these structures with specific inhibitors (CDKis) is promising. Here, we describe the antitumoral potential of selective CDKi on low-passage GBM 2D- and 3D models, cultured as neurospheres (NSCs) or glioma stem-like cells (GSCs). By applying selective CDK4/6i abemaciclib and palbociclib, and the more global CDK1/2/5/9-i dinaciclib, different effects were seen. Abemaciclib and dinaciclib significantly affected viability in 2D- and 3D models with clearly visible changes in morphology. Palbociclib had weaker and cell line-specific effects. Motility and invasion were highly affected. Abemaciclib and dinaciclib additionally induced senescence. Also, mitochondrial dysfunction and generation of mitochondrial reactive oxygen species (ROS) were seen. While autophagy was predominantly visible after abemaciclib treatment, dinaciclib evoked γ-H2AX-positive double-strand breaks that were boosted by radiation. Notably, dual administration of dinaciclib and abemaciclib yielded synergistic effects in most cases, but the simultaneous combination with standard chemotherapeutic agent temozolomide (TMZ) was antagonistic. RNA-based microarray analysis showed that gene expression was significantly altered by dinaciclib: genes involved in cell-cycle regulation (different CDKs and their cyclins, *SMC3*), mitosis (*PLK1, TTK*), transcription regulation (*IRX3, MEN1*), cell migration/division (*BCAR1*), and E3 ubiquitination ligases (*RBBP6, FBXO32*) were downregulated, whereas upregulation was seen in genes mediating chemotaxis (*CXCL8, IL6, CCL2*), and DNA-damage or stress (*EGR1, ARC, GADD45A/B*). In a long-term experiment, resistance development was seen in 1/5 cases treated with dinaciclib, but this could be prevented by abemaciclib. Vice versa, adding TMZ abrogated therapeutic effects of dinaciclib and growth was comparable to controls. With this comprehensive analysis, we confirm the therapeutic activity of selective CDKi in GBM. In addition to the careful selection of individual drugs, the timing of each combination partner needs to be considered to prevent resistance.

Introduction

Cyclin-dependent kinases (CDKs) play indispensable roles in a variety of biological processes, including cell-cycle control, oncogenic transcription, DNA-damage repair, and stem cell self-renewal[1,2]. In most cancers, genomic alterations in specific CDKs either result in constitutive activation or loss of endogenous modulators, including those of the p16/CDK4-Cyclin-D/pRb pathway[3]. This imbalance pushes cell-cycle progression and malignant transformation[2]. CDK inhibitors (CDKi's) specifically targeting these proteins are widely applied in (pre-)clinical oncological research[1,4–8]. CDKi has synergistic activity when applied in conjunction with other

Correspondence: Claudia Maletzki (claudia.maletzki@med.uni-rostock.de)
[1]University Children's Hospital, Rostock University Medical Centre, Ernst-Heydemann-Straße 8, 18057 Rostock, Germany
[2]Department of Medicine Clinic III - Hematology, Oncology, Palliative Medicine, Rostock University Medical Center, Rostock University Medical Centre, Ernst-Heydemann-Str. 6, 18057 Rostock, Germany
Full list of author information is available at the end of the article
Edited by Maria Victoria Niklison Chirou

targeted drugs, such as BRAF and MEK inhibitors for malignant melanomas[3]. Most clinical trials have confirmed manageable toxicity profiles, with clinical responses in many cases and even significantly prolonged overall survival in selected patients cohorts[9]. To date, the three FDA-approved CDK4/6i abemaciclib, palbociclib, and ribociclib are a front-line treatment in combination with hormonal therapy for metastatic HR^{+}-$HER2^{-}$ breast cancer (BC)[9,10]. Numerous ongoing clinical phase II and III studies evaluate the therapeutic potential in other entities. Functionally, CDK4/6 are cell-cycle-regulatory proteins that initiate the G_1–S-phase transition by interaction with D-type cyclins and regulating Rb phosphorylation to activate or repress gene transcription[2,11].

GBM is the most common and aggressive primary brain tumor[12]. Current therapeutic approaches using surgery and combined radio-/chemotherapy have met limited clinical success, contributing to the extremely poor 5-year survival rate of <3%[13,14]. Genomic analysis revealed alterations in the p16/CDK4-Cyclin-D/pRb pathway[13] as well as specific interphase CDKs, namely CDK1 and CDK5. The latter is strongly associated with tumor initiation[15]. As for GBM, a few studies have investigated the potential of CDKi's. Raub et al. described the antitumor activity of abemaciclib in an orthotopic glioblastoma rat model showing promising effects that were additive in combination with TMZ[16]. Another recent study even recommended nanoparticle encapsulated with dinaciclib in combination with radiation therapy for GBM via targeting tumor-associated macrophages[17].

Here, we report the successful elimination of GBM cells by CDKi application with several morphology changes, including cell differentiation and vacuolization. We show that abemaciclib and the more global acting CDKi dinaciclib have individual effects on patient-derived 2D- and 3D models that result in senescence, autophagy, and mitochondrial impairment. By performing long-term in vitro treatment, developing resistance against dinaciclib can be prevented by abemaciclib, but not chemotherapy. These results are highly encouraging to move forward with this strategy.

Results

CDKi treatment impairs viability in 2D- and 3D-cultured GBM cells

In a preliminary pilot experiment, we applied the three CDKi's dinaciclib, abemaciclib, and palbociclib in mono- and combination therapy with TMZ/radiation for 144 h using mostly clinically relevant doses. Abemaciclib is the only exception. Here, higher doses were applied.

As determined by light microscopy, several morphology changes were observed in GBM 2D cultures after dinaciclib and abemaciclib treatment. Exemplarily shown for HROG05 and HROG63, dinaciclib treatment-induced small vacuoles and cell shrinkage. Abemaciclib-treated cells were enlarged, accompanied by a flattened structure and a striking multivacuolar phenotype (Fig. 1A). Notably, such morphological changes were seen in all cell lines and resulted in reduced cell viability (Fig. 1D). Palbociclib was less effective and TMZ treatment had no impact on viability and morphology at the doses used.

Then, we performed simultaneous and sequential combination regimens (72 h each, dose: IC_{20}). The simultaneous treatment describes the concomitant administration of two substances, whereas the sequential regimen is characterized by consecutive administration of the respective drugs. In this comparative setting, only simultaneous, but not sequential treatment with dinaciclib and abemaciclib synergistically potentiated antitumor effects of the monotherapy in 3/5 cases (Supplementary Table 1). With regard to TMZ, a synergistic effect was observed when this drug was added after dinaciclib, while the simultaneous treatment was mostly antagonistic. Combination of abemaciclib and TMZ showed also no benefit (Supplementary Table 1). Dual CDK blockade with dinaciclib and palbociclib was again only antagonistic (Supplementary Table 1).

In the 3D spheroids, cytotoxic effects of CDKi's were preserved. Still, we observed differences between individual 3D cultures, in which GSCs were more susceptible toward CDKi's than NSCs (Fig. 1B, C). In detail, dinaciclib and abemaciclib impaired GSC and NSC morphology, contributing to a significantly reduced viability (Fig. 1D). Here again, palbociclib had cell line-specific and only minor impact on viability. TMZ did not have any effect on 3D cultures (Fig. 1B, C). With regard to the combination, we again identified striking differences between simultaneous and sequential regimens and also between individual 3D cultures (Fig. 1D).

To sum up these findings, the timing of each combination partner influences effectiveness. Our results favor the sequential instead of the simultaneous treatment in both 2D- and 3D-cultured GBM cell lines. Also, palbociclib had lower activity against GBM cells than the other CDKi's dinaciclib and abemaciclib. Consequently, we focused on the latter two agents in further experiments.

CDKi's induce apoptotic and necrotic cell death

To describe the effects of CDKi's in more detail, we then performed flow cytometric apoptosis/necrosis analysis and focused on drug monoapplication. Figure 2 shows HROG63 as an example. Dinaciclib evoked necrosis, abemaciclib triggered early apoptosis (Fig. 2A, B). Dual CDK inhibition induces a mixed response but was not able to enhance cytotoxic effects (Fig. 2A, B). Immunogenic cell death, a common result of CDKi therapy, was not inducible by either treatment (Fig. 2C).

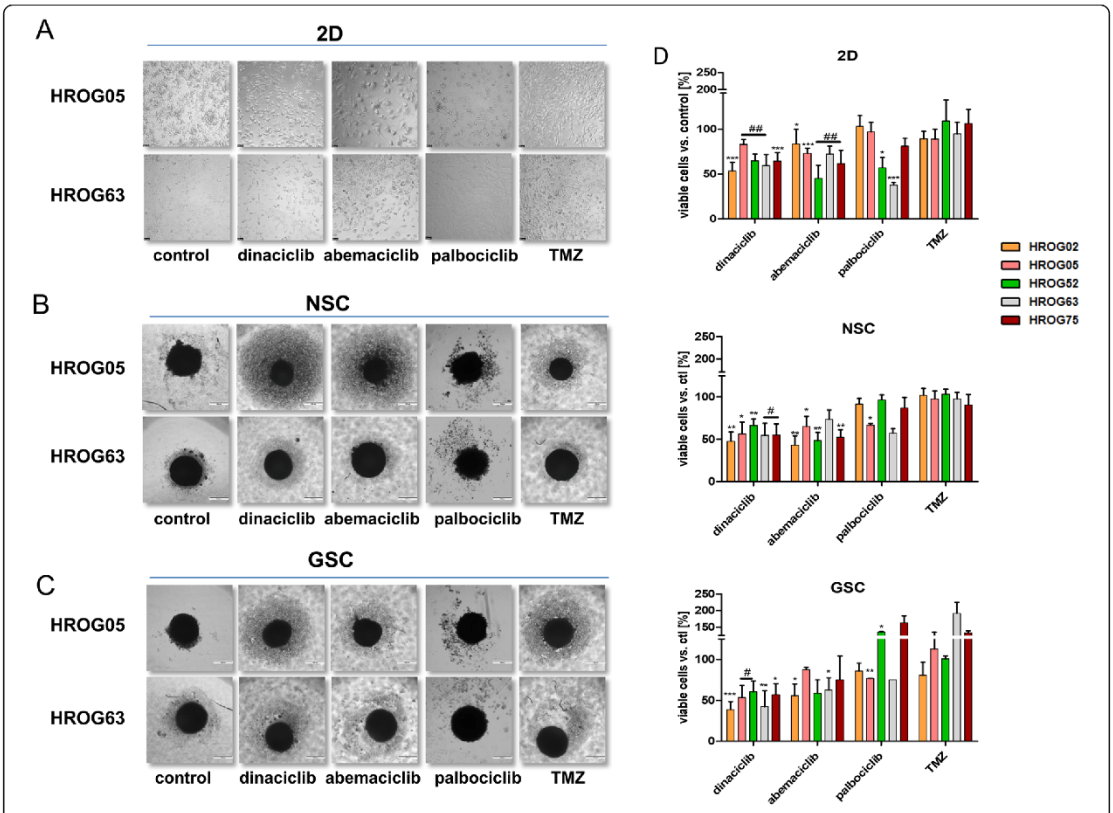

Fig. 1 CDKi impairs GBM cell proliferation. GBM cells were treated with the respective substances for 72 h or 2 × 72 h. **A**–**C** Images are representative for the different treatment regimens in HROG05 and HROG63 in 2D- and 3D models (scale bar **A**: 50 µm; **B** and **C**: 200 µm). **D** Quantitative analysis of cell vitality was done via calcein-AM in the 2D model and with 3D-Glo in our 3D systems. Viability reduction (%) after treatment was quantified by normalization to control values (untreated cells set to be 100%). $N = 5$ independent experiments; mean ± SEM, $^{***}P < 0.001$; $^{**}P < 0.01$; $^{*}P < 0.05$ vs. control; $^{\#\#}P < 0.01$; $^{\#}P < 0.05$ as indicated by line. Unpaired two-tailed Student's t test was used.

CDKi's impair mitochondrial function and evoke methuosis-like processes

Then, we analyzed the cause of cytoplasmic vacuole formation after CDKi treatment and screened the GBM cells for autophagy induction. Autophagy is responsible for maintaining cellular homeostasis, but promotes cell death after long-term stress. We indeed observed CDKi-induced lysosomal activation in HROG05 and HROG63, primarily in abemaciclib-treated cells (Fig. 3A). While this was hardly the only explanation for the observed morphology changes, we checked whether CDKi treatment causes mitochondrial damage. The mitochondrial membrane potential (MMP) increased in the 2D culture upon dinaciclib and abemaciclib, indicative of mitochondrial hyperpolarization (Fig. 3A). Such mitochondrial dysfunction may lead to oxidative stress and ROS production. Indeed, mono- and dual-CDKi administration additionally increased mitochondrial reactive oxygen species (mito-ROS) levels (Fig. 3B), which corresponds to an increased MMP. TMZ alone or in combination with dinaciclib did not boost MMP and mito-ROS levels (Fig. 3A, B). Intensified MMP signals were partially accompanied by a higher intensity of the acidic activity. In HROG63 cells, MMP signals and acidic compartments overlapped, while this was not the case in HROG05 (Fig. 4A). Also, CDKi-induced huge vacuoles in HROG05 cells were neither positive for MMP, lysosomal activity, ER-Tracker, nor Dextran (Fig. 3C–E). Hence, CDKi may block the lysosomal processing of these vesicles.

So, we next investigated the origin of vacuole formation. By measuring LAMP-1/-2 and Rab7a via flow cytometry, single- and dual-CDKi application increased the percentage of LAMP1/2-Rab7a-positive cells. The cell line HROG05 showed the most pronounced morphological changes with massive vacuolization and LAMP1/2-Rab7a abundance under CDKi therapy (Fig. 3C–F). These

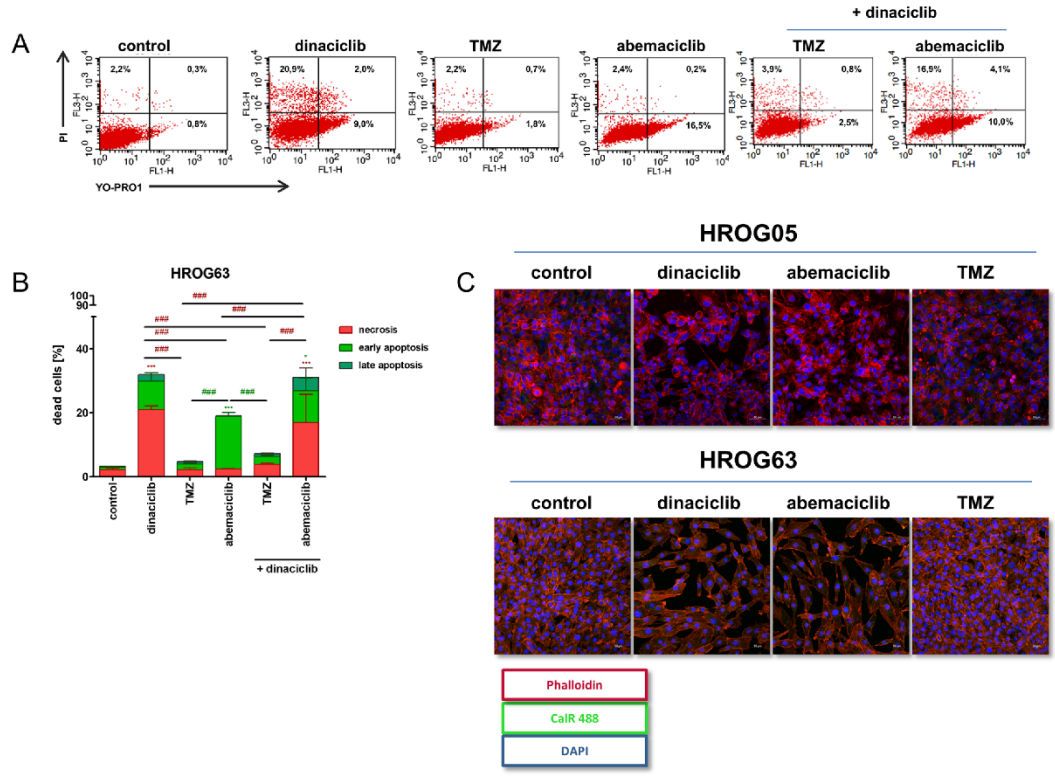

Fig. 2 Analysis of cell death induction by CDKi. A, **B** Quantitative analysis of cell death using flow cytometric YO-PRO-1/PI staining after incubation with test substances for 72 h in 2D culture. For each sample, 10,000 events were measured. Dead cells were defined as early apoptotic (YO-PRO-1$^+$), late apoptotic (YO-PRO-1+/PI$^+$), or necrotic (PI$^+$). Given are the % numbers of stained cells after treatment. $N = 3$ independent experiments, mean ± SEM, $^{***}P < 0.001$; $^{*}P < 0.05$ vs. control; $^{\#\#\#}P < 0.001$ as indicated by the line. Two-way ANOVA (Bonferroni's multiple-comparison test). **C** ICD was detected by using a LSM-780 confocal laser microscope. 2D-cultured cells were stained with anti-Calreticulin Rabbit mAb (Alexa Fluor® 488 Conjugate) and Flash Phalloidin™ Red 594 to visualize surface-exposed CalR and filamentous actin (scale bar **C**: 50 µm).

cumulative data are indicative of the induction of early methuosis-like processes.

To see whether similar mechanisms are present in 3D cultures, we next checked mitochondrial activity and hypoxia within NSC and GSC spheres (Fig. 3G). In both culture models, MMP was seen at the edge of the spheres. Mitochondrial hyperpolarization was especially seen after dinaciclib and abemaciclib treatment of NSC. Dual-CDKi treatment and dinaciclib in combination with TMZ accelerated the abundance of MMP signals, which were also visible in the inner sphere (Fig. 3G, upper part). Additional hypoxia analysis revealed that NSC had more hypoxic cores than GSC—irrespective of the applied treatment schedule (Fig. 3G, lower part). Mono- and dual-CDKi application increased hypoxia in these cells. In GSC, hypoxic cores increased after dinaciclib and abemaciclib monotherapy. The combination of CDKi's or with TMZ did not boost hypoxia significantly. Hence, hypoxia plays a minor role here.

Taken together, CDKi alone or in combination triggers a specific and uncommon mode of cell death that is characterized by a multivacuolar phenotype and signs of early methuosis.

CDKi's trigger senescence induction in 2D- and 3D-cultured GBM cell lines

Senescence can be triggered by different damaging stimuli, including telomere shortening (replicative senescence), oxidative DNA damage, and a persistent DNA damage response. Here, senescence is likely provoked by either ROS in hyperpolarized mitochondria (oxidative DNA damage) or accumulation of γH2AX foci that represent a subset of repair-proof lesions that seem to persist (DNA-damage response). Hence, we examined the activity of β-galactosidase, as well as activation of p16/p21 in selected 2D- and 3D models as markers of senescence (Fig. 4). Senescence induction was observed in HROG05 and

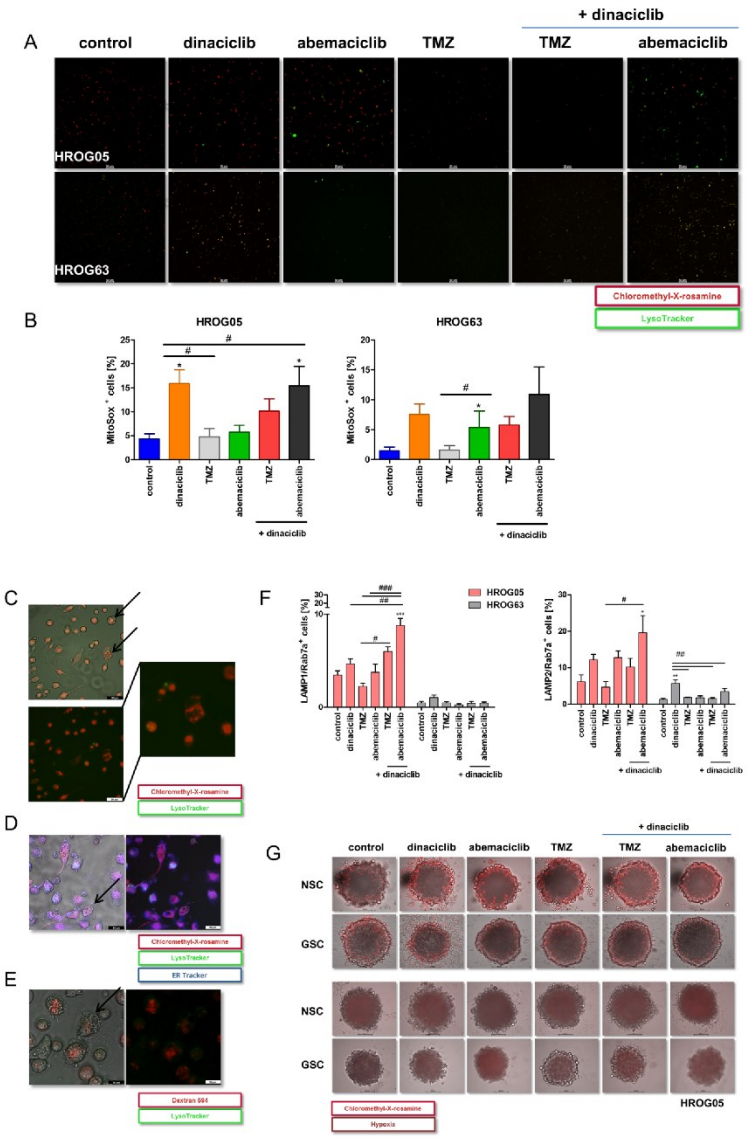

Fig. 3 Effects of CDK inhibition on mitochondrial membrane potential and mitochondrial ROS and analysis of vacuole formation by CDKi. **A** 2D-and 3D-cultured GBM cells were treated with CDKi for 72 h and subjected to immunofluorescence imaging as described in "Materials and Methods" (Mito- and Lyso-Tracker). Merged fluorescence is presented (scale bar **A**: 50 µm). **B** Quantitative analysis of mitochondrial ROS. 2D-cultured GBM cells were treated with respective substances for 72 h, stained with MitoSox Red for 30 min, and analyzed by flow cytometry. MitoSox$^+$ cells were presented as (%). $N = 3$ independent experiments, mean ± SEM, $^*P < 0.05$ vs. control. $^{\#}P < 0.05$ as indicated by line. One-way ANOVA (Bonferroni's multiple- comparison test) was indicated. **C**–**E** Analysis of vacuole formation. Merged and separated fluorescence/bright-field images are presented (Mito-, Lyso, and ER-Tracker or dextran and LysoTracker). Arrows indicate vacuoles not colocalizing with green (acidic components), blue, and red dots (ER and dextran = endoplasmic origin, MMP = mitochondrial origin) (scale bar **C**–**E**: 50 µm). A high-magnification image is indicated by the two lines. **F** GBM cells were treated as indicated, stained with CD107a/CD107b and Rab7a, and analyzed via flow cytometry. Presented are cells (HROG05, HROG63) positive for LAMP1/Rab7a and LAMP2/Rab7a in percentage. $N = 3$ independent experiments, mean ± SEM, $^{***}P < 0.001$; $^{**}P < 0.01$ vs. control. $^{\#\#\#}P < 0.001$; $^{\#\#}P < 0.01$; $^{\#}P < 0.05$ as indicated by line. One-way ANOVA (Bonferroni's multiple-comparison test) is indicated. **G** 3D-cultured GBM cells as stated in "Materials and Methods", treated for 72 h and stained with MitoTracker Red (30 min at 37 °C) or Hypoxia IT Image Red (hypoxia reagent was exposed for 3 h) (scale bar **G**: 200 µm).

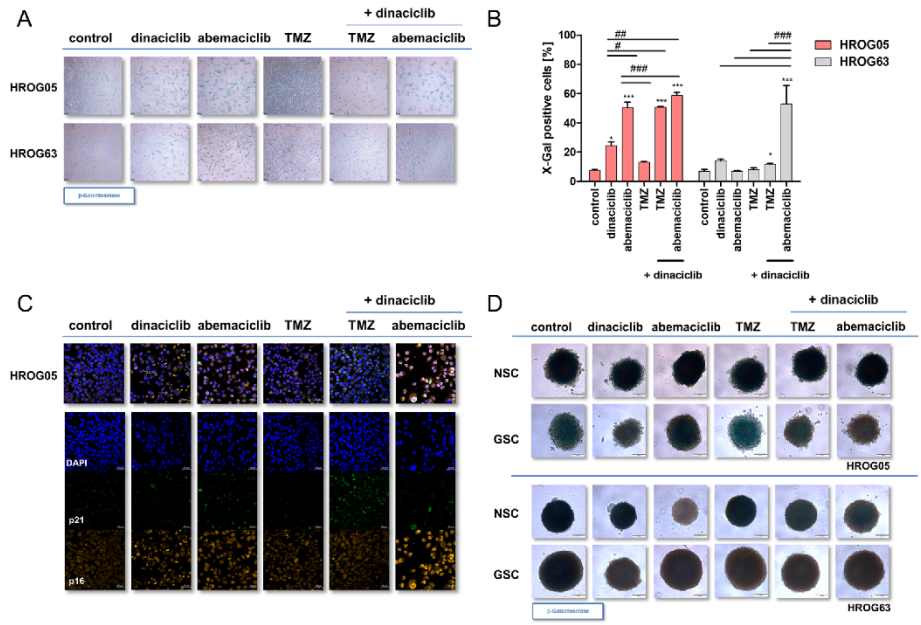

Fig. 4 CDK inhibition induces senescence via activation of p16/p21 and ß-galactosidase. 2D- and 3D-cultured GBM cells (**A**, **C**, **D**) were treated with test substances for 72 h, fixed, and stained with β-galactosidase staining solution overnight at 37 °C without CO_2. Blue: ß-galactosidase activity, indicative for senescence. Representative images are shown (scale bar: **A**: 50 µm; **C**: 200 µm). **B** Quantitative analyses of X-Gal-positive 2D-cultured cells in relation to the whole-cell number/image. **C** Representative images of GBM demonstrate an increase in p16 and p21 after CDK inhibition. The cell was treated as indicated, fixed, permeabilized, and stained with p21 Waf1/Cip1 (12D1) rabbit mAb (Alexa 488 conjugate) (green) and p16 antibody (JC8): sc-56330 Alexa 546 (orange) (scale bar: **D**: 20 µm). $N = 3$ independent experiments, mean ± SEM; $^{***}P < 0.001$; $^{*}P < 0.05$ vs. control; $^{\#\#\#}P < 0.001$ as indicated by the line. Two-way ANOVA (Bonferroni's multiple-comparison test).

HROG63 cells, with, however, interindividual differences (Fig. 4A, B). Mono- and dual application of dinaciclib and abemaciclib was most effective. TMZ induced senescence in HROG05 cells, the combination with dinaciclib boosted the effects (Fig. 4A, B). The expression of senescence markers p16 and p21 increased in HROG05 cells after CDKi treatment and underlines the results of the β-galactosidase staining. p16 was detected in the nucleus and cytoplasm of the cells, whereas p21 was only found in the nucleus. Dual application of both CDKi leads to strong nuclear induction of p16. p21 expression was strongly elevated after dinaciclib and TMZ treatment. In some cases, e.g., in the combination regimens, colocalization of both markers was seen (Fig. 4C). Comparable, though less pronounced effects of β-galactosidase staining were observed in 3D cultures and again mainly visible in HROG05 cells (Fig. 4D). To sum up, CDKi's trigger senescence via activation of p21 and p16.

CDKi's interfere with invasiveness and migratory potential of 2D- and 3D-cultured GBM cell lines

In subsequent experiments, the impact of CDKi's treatment on cell motility as prerequisites for invasiveness and metastasis was studied in 2D- and 3D cultures.

First, a wound-healing assay was done. Figure 5A, B shows representative images of 2D-cultured HROG05 cells along with quantified scratch areas. Control and TMZ-treated cells proliferated appeared normal and almost closed the wound within 3 days (scratch completion after 7 days). Dinaciclib completely prevented GBM cell proliferation, which was characterized by cell shrinkage and cell death, leading to scratch areas higher than at day zero (Fig. 5A, B). Abemaciclib treatment decelerated wound healing and scratches did not fully close within the specified time of seven days (Fig. 5A, B). Dual CDKi treatment had comparable effects as the monotherapy; the addition of TMZ had no influence.

In a subsequent Matrigel-based invasion–migration assay, the migration and invasiveness of GBM cells slightly increased under dinaciclib treatment, likely constituting to some kind of escape. Abemaciclib reduced migration/invasion in HROG05 cells and led to a significant 4-fold decrease in HROG63 cells (Fig. 5C, $P < 0.01$ vs. control).

To determine the effect of CDKi on GBM spheroids, we finally implanted defined individual NSC and GSC of cell line HROG05 in Matrigel and monitored sphere

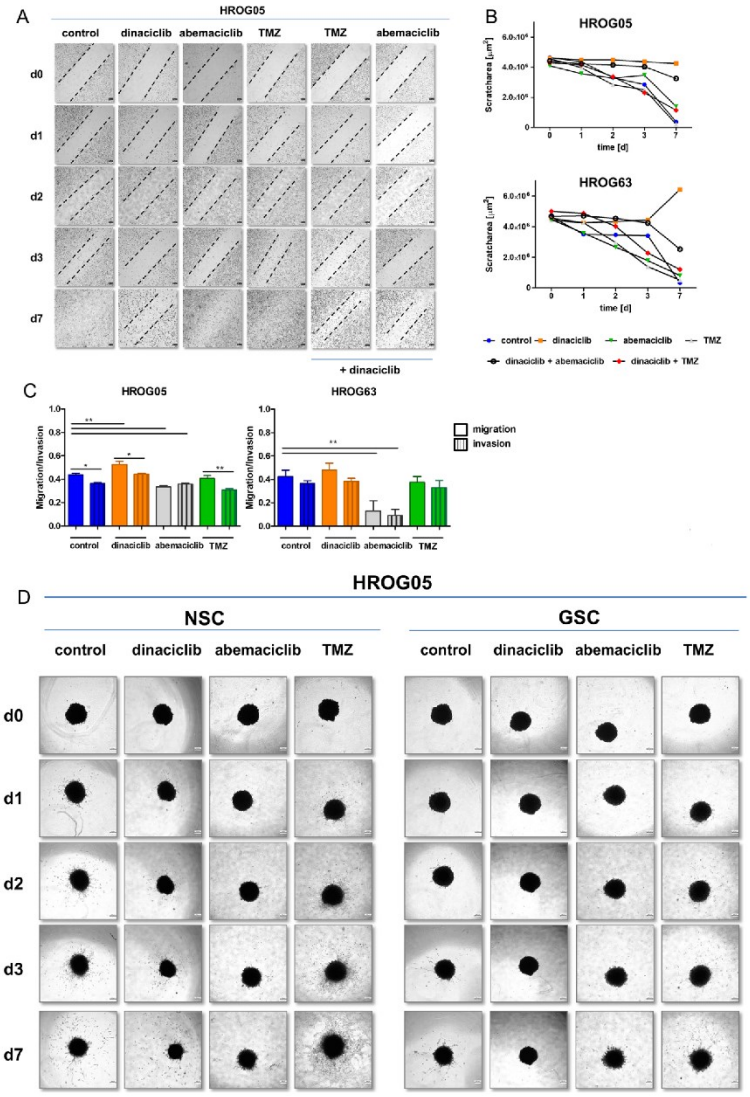

Fig. 5 The impact of CDKi on motility, migration, and invasion in 2D- and 3D models. A, **B** 2D-cultured GBM cells were seeded and grown to 90% confluency. A standard scratch was placed on the plate utilizing a 200-µl pipette tip. Detached cells were removed, and the above-mentioned substances were added. The scratch closure was monitored for 7 days using a Leica DMI 4000B microscope (scale bar **A**: 50 µm). For manual identification of scratch area (=open wound area), captured images were converted to grayscale. Finally, a threshold, a band-pass, and minimum filter were applied. Region of interest(s) (ROI) could then be set and scratch area analyzed. The scratch area (µm^2) was plotted over time for each substance. Data are presented as mean. **C** Effects of CDKi on cell invasion and migration assessed by a Boyden chamber assay. $N = 3$ independent experiments, mean ± SEM, $^{**}P < 0.01$; $^{*}P < 0.05$ as indicated by the line. One-way ANOVA (Bonferroni's multiple-comparison test). **D** Analysis of CDKi-treated 3D-cultured GBM cell invasion into a Matrigel matrix (scale bar **D**: 250 µm). GBM cells were monitored for a total of 7 days.

outgrowth (Fig. 5D). Control cells showed high basal invasiveness into the Matrigel in which NSCs were much more invasive than GSCs. CDKi treatment with dinaciclib or abemaciclib reduced their invasiveness, in some cases they did not even penetrate into the matrix (Fig. 5D). However, TMZ treatment was not able to prevent invasiveness of spheroids, which was even higher than in the control. The main body of the implanted spheroid (NSC) was partially disintegrated due to the massive penetration into the matrix.

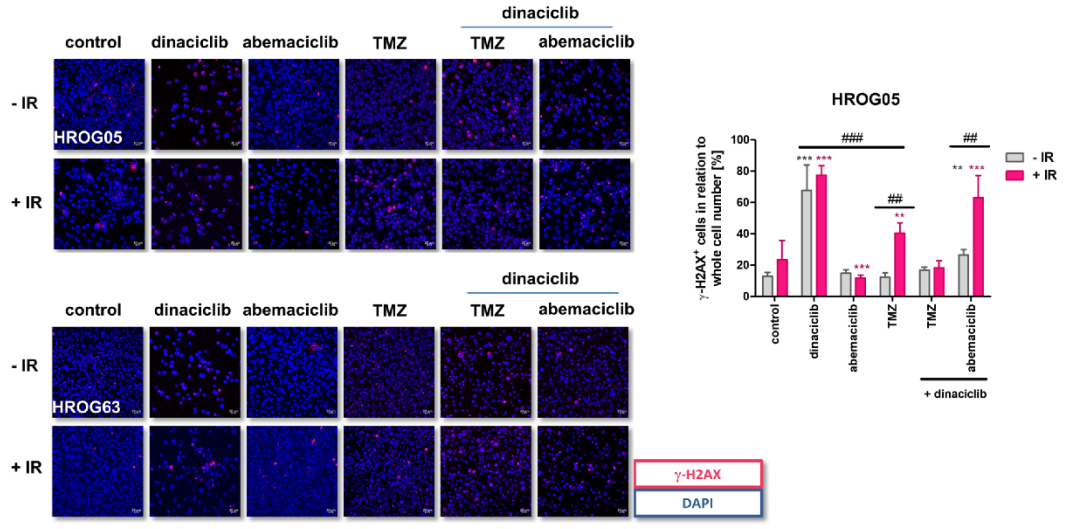

Fig. 6 Effect of CDKi on γ-H2AX foci formation in irradiated GBM cells. 2D-cultured cells were seeded on ibidi slides, treated, and irradiated (2 Gy) 24 h after treatment using an IBL 637, followed by 3-day incubation at 37 °C and 5% CO_2. Cells were incubated with Alexa Fluor® 594 anti-H2A. X Phospho (Ser139) antibody. Nuclei were counterstained with DAPI and analyzed on a confocal laser microscope (scale bar: 20 µm). In addition, nuclei were declaimed as positive if more than 20 foci/nuclei were visible. $N = 3$ independent experiments, mean ± SEM, $^{***}P < 0.001$; $^{**}P < 0.01$ vs. control; $^{###}P < 0.001$; $^{##}P < 0.01$ as indicated by line. Two-way ANOVA (Bonferroni's multiple- comparison test).

Hence, these findings nicely confirm the therapeutic potential of selective CDKi's to prevent invasion and migration. However, the addition of TMZ has a minor effect.

CDKi's have a minor impact on double-strand breaks and radiosensitivity

Thereafter, we evaluated the effects on signaling and DNA-damage repair. Double-strand breaks (DSB) were determined by γ-H2AX staining, which promotes chromatin remodeling and the assembly of repair proteins (Fig. 6). Monotherapy of 2D-cultured cells with dinaciclib, but not abemaciclib elevated γ-H2AX foci to a degree comparable to TMZ. Dual CDKi treatment or in combination with TMZ was not able to potentiate the effects of the monotherapy.

Then, we examined radiation-induced DSB. Radiation itself had little impact on γ-H2AX foci, but dinaciclib pretreatment boosted DSB. No such radiosensitizing effect was seen for abemaciclib. TMZ likewise induced radiation-induced DSB, but in combination with dinaciclib, this effect completely vanished in HROG05 cells whereas this was not the case in HROG63 cells.

Microarray analysis identifies molecular alterations upon dinaciclib and confirms the therapeutic activity

As a part of our study, we conducted microarray analyses of 2D-cultured HROG63 cells, either treated with dinaciclib or left untreated (Fig. 7 and Supplementary Table 2). Among the 8008 genes in this analysis having a fold change of 2 and a *P* value of <0.05, 4447 were up- and 3561 downregulated.

The most downregulated genes were *BCAR1*, *PLK1*, *TTK*, *SIN3A*, *CENPF*, and *SMC3*, all being involved in cell-cycle and mitosis inhibition. Genes mediating transcription regulation (*RBBP6*, *IRX3*, *RTF1*, and *MEN1*), chromosome remodeling (*HIST1H1B*), and those encoding for E3 ubiquitination ligases (*RBBP6*, *FBXO32*, *CUL1*) were also strongly downregulated. The expression levels of *CXCL8*, *ARC*, *EGR1*, *TFPI2*, *GADD45B*, *CCL20*, *EGR1*, *PTGS2*, *JUNB*, *FOS*, *CCL2*, *DUSP2*, *IER5*, and *IL6* mRNA significantly increased. CDKs that were downregulated involved the known targets CDK1 (*CCNA2*, *B1/2*) and CDK9 (*CCNK*, *T1*) as well as other CDKs, including CDK7 (*CCNA2*, *B1/2*, E1), CDK12 (*CCNK*), CDK17, and CDK20. While senescence was already confirmed by SA-β-Gal staining, senescence-associated genes (*SERPINB2/E1*, *BTG2*, and *NEK4*) were also elevated. The same applies to genes regulating autophagy and apoptosis. The former were upregulated (*ULK2*, *MAP1LC3A/B*, *BECN1*, *ATG12*, *DRAM2*, *SQSTM1*, and *EI24*), the latter (*CASP* genes) showed mostly downregulation. *CASP5* is the only exception.

Taken together, these molecular data nicely underpin our findings on the complex effects of the multi-CDKi dinaciclib on GBM cells.

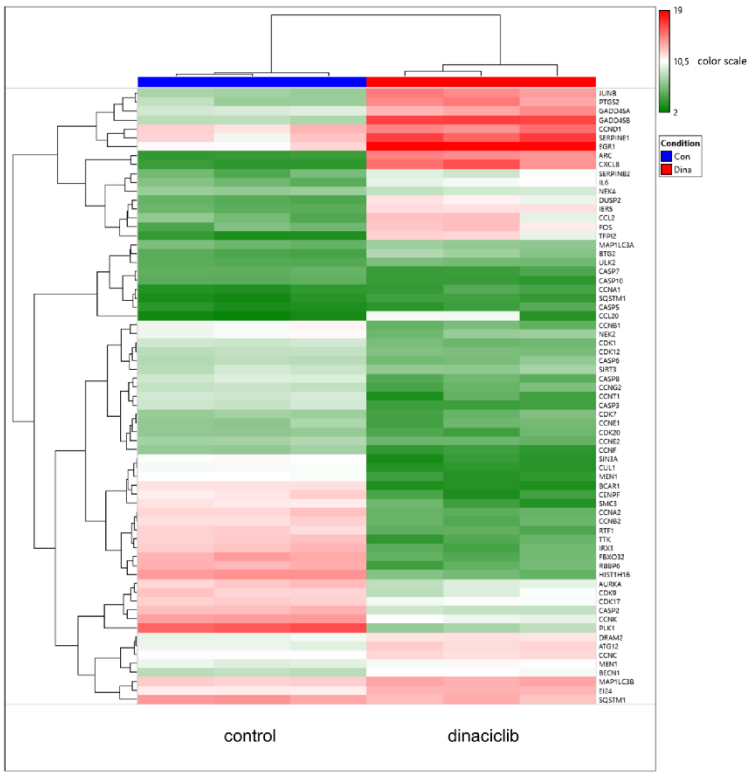

Fig. 7 Molecular alterations upon dinaciclib. Heatmap showing RNA expression level from 2D-cultured HROG63 cells assessed by Affymetrix Human Clariom S Array. Primary data analysis was performed with the Affymetrix TAC including the SST-RMA for normalization. Gene expression data were log-transformed. Limma was used here to calculate the p-value. A change was considered significant when the Limma eBayes *P* value met the criterion $P < 0.05$ at fold changes >|2|, i.e., expression increments or declines larger than two. $N = 3$ independent experiments.

Resistance development can be abrogated by combined CDK inhibition

Finally, we studied resistance development under ongoing treatment. A long-term treatment approach of ten repetitive weekly cycles was carried out on 2D-cultured cells. Crystal-violet and calcein-AM/Mito-Tracker staining were used to visualize effects (Fig. 8).

Dinaciclib long-term treatment completely inhibited colony formation in 3/5 cases. Interestingly, most colonies were seen in HROG05 cells that already displayed the weakest sensitivity toward dinaciclib in 2D short-term therapy. Hence, is it likely that a pre-existing resistant clone was responsible for outgrowth. The other cell line was HROG63, showing small colonies after dinaciclib long-term exposure. Notably, no colony formation was seen after repetitive abemaciclib treatment (Fig. 8). Hence, we formally confirm the therapeutic activity of this CDKi. As anticipated and in addition to the minor effects after short-term exposure, TMZ did not influence colony formation, with growth comparable to controls. Adding dinaciclib to TMZ prevented colony formation in one case (HROG52), but abrogated the therapeutic effect in the remaining cell lines (Fig. 8). The combination of both CDKi was effective in four cases; still, continued growth was seen in cell line HROG63. It is therefore tempting to speculate that the same clone seen with long-term dinaciclib monotherapy was responsible for colony formation in this setting.

Summing up, these data provide evidence that intrinsic rather than acquired resistance plays a role in CDKi treatment failure.

Discussion

In this study, we provide functional evidence for the antitumoral effects of mono- and dual treatment with CDKi on low-passage GBM models and identify mechanisms of response. Notably, all patient-derived GBM cell lines tested in this study were sensitive to abemaciclib and dinaciclib, while the overall response to palbociclib was weaker and additionally cell line-specific.

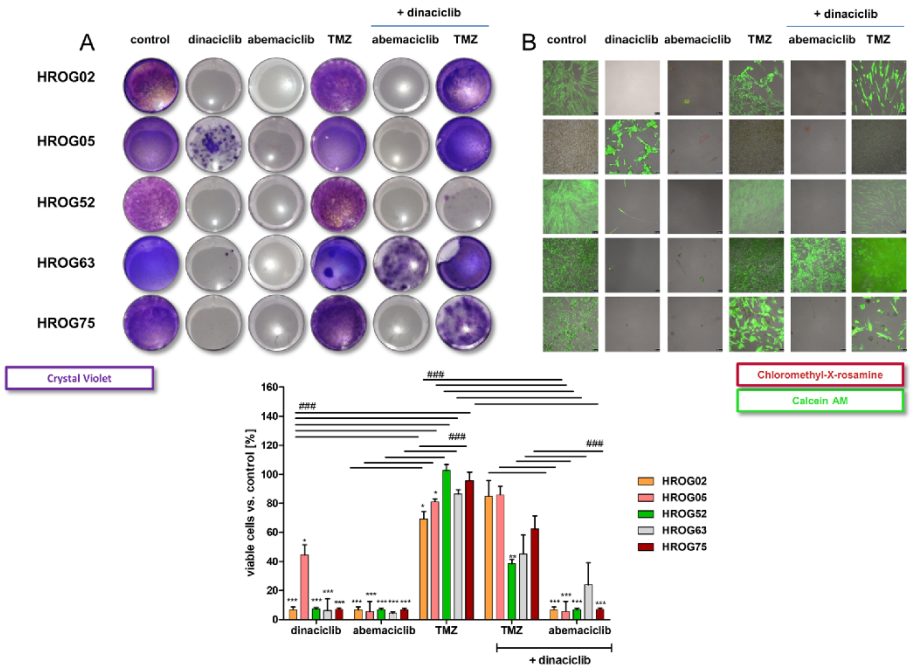

Fig. 8 Effects of long-term exposition to CDKi on 2D-cultured GBM cells. A, **B** Analysis of cell viability performed by Calcein AM/MitoTracker and crystal violet staining after long-term exposure of respective substances in a ×10 repetitive treatment cycle. Representative images are shown (scale bar **B**: 50 µm). Viability reduction (%) after treatment was quantified by normalization to control values (untreated cells, set to be 100%). $N = 4$ independent experiments, $^{***}P < 0.001$; $^{**}P < 0.01$ vs. control; $^{\#\#\#}P < 0.001$; as indicated by the line. Two-way ANOVA (Bonferroni's multiple-comparison test).

Abemaciclib is structurally distinct from palbociclib, with higher selectivity for CDK4 than CDK6 and targeting additional kinases, including GSK3α/β and CAMKII α/β/γ[18], which may explain the individual effects of the two CDK4/6i seen here. In support of this, we also observed different responses to the CDK4/6i in the 3D-spheroid system. By including two individual 3D-culture models (NSC, GSC) that closely resemble in vivo features, these data favor prospective abemaciclib and dinaciclib application instead of palbociclib in treating GBM patients—also due to the blood–brain-barrier permeability of abemaciclib. To underpin this, the mode of cell death was studied in more detail. Here, we focused on abemaciclib and dinaciclib. While both agents induced autophagy with different intensities, abemaciclib additionally increased early apoptotic cells, while dinaciclib predominantly evoked necrosis. CDKi-mediated apoptosis has been described in various tumor models[19–23]. By contrast, autophagy was only recently described for abemaciclib[24] and just one publication described the cytoprotective role of autophagy under dinaciclib therapy in NSCLC[25]. Though not analyzed in detail here, LC3B-II aggregation and decreased p62/sequestosome1 expression levels are likely alterations as earlier shown for flavopiridol, another pan-CDKi[26]. In addition to the effects described above, abemaciclib and dinaciclib induced senescence via activation of p16/p21 and likewise evoked DNA-damage response, also confirmed by changes in mRNA expression pattern.

Cell motility and invasion are prerequisites for tumor progression and metastasis. Here, abemaciclib decelerated motility and migration/invasion of GBM cells. Dinaciclib completely prevented GBM motility, but was unable to affect migration/invasion in the 2D system. Other studies already described reduced motility in solid tumors under CDKi treatment. CDK4 inhibition was shown to decrease invasion, metastatic spread, and tumor progression in a RB-high pancreatic ductal adenocarcinoma model[27]. One report even suggested the involvement of CDK5 in the metastatic spread; another trial proposed the contribution of vimentin, Snail, COX-2, and PGE2[27–30]. Strikingly, both CDKi prevented invasiveness of NSC and GSC spheroids. Although the natural invasive behavior was higher in NSC compared to GSC, TMZ equally enhanced invasive growth in both 3D models. In NSC, the main body of the implanted spheroid was partially disintegrated

into the matrix. In addition to CDK4 and CDK5, cyclin-B/CDK1 may play a role in tumor cell spreading, motility, and invasion[31,32]. Previous studies have also shown that inhibition of CDK2/9 in triple-negative BC cells and CDK9 inhibition in osteosarcoma cells decreased migration by preventing phosphorylation of CDK-mediated Smad3 and RNA POL-ll in triple-negative BC[33,34].

We further demonstrated mitochondrial dysfunction characterized by elevated MMP levels and overproduction of mito-ROS. The results from the 2D system were additionally confirmed in 3D models showing elevated MMP upon dinaciclib. While the inner sphere showed less MMP signals, they were visible on the edge of the sphere. Mono- and dual CDKi increased hypoxia in NSC, indicating loss of mitochondrial function mainly in the inner sphere[35,36].

We, therefore, hypothesize that mono- or dual CDKi treatment increases oxidative stress, induces DSB, and potentiates senescence to trigger cell death[37–42]. While MMP signals and acidic compartments overlapped in 2D-cultured HROG63 cells, this was not the case in cell line HROG05. Intriguingly, we also observed multiple huge vacuoles in CDKi-treated cells. CDKi seemed to trigger the uptake of 10-kDa dextrans and the acidotropic agent in small vacuoles, but rarely in the most enlarged ones. Also, huge vacuoles were insensitive for ER-Tracker and MMP, suggesting vacuoles also did not originate from the mitochondria or endoplasmic reticulum. Here, vacuolization was accompanied by a higher abundance of LAMP1/2 and Rab7a, which are late endosomal markers formed in the early stages of methuosis. Methuosis is a nonapoptotic cell death phenotype defined as the accumulation of large fluid-filled cytoplasmic vacuoles that originate from macropinosomes[43]. Here, these characteristics superficially may resemble methuosis(-like) processes in addition to the appearance of apoptosis[43]. Recent data from the literature support this mechanism, as some antineoplastic agents, including abemaciclib promote vacuolization, which may lead to methuosis[24,44,45].

GBM cells may have intrinsic and/or acquired radioresistance. Dinaciclib, but not abemaciclib induced γ-H2AX foci that were boosted after combined CDKi radiotherapy. The induction of DSBs was accompanied by downregulation of *CDK1* and *SIRT3*, the latter being known to mediate radioresistance[46]. Hence, dinaciclib reversed radioresistance.

By directly comparing the cytotoxic activity of abemaciclib and dinaciclib, the latter was more potent, likely due to the global activity in targeting multiple CDK. Finally, the strong cytotoxic effects of dinaciclib were confirmed in the microarray data of HROG63 cells. Genes involved in cell-cycle regulation/progression, mitosis, transcription regulation, cell migration/adhesion/division, and those encoding for E3 ubiquitination ligases were strongly downregulated, whereas the expression level of chemotaxis-mediating and DNA-damage or stress genes was significantly upregulated. The upregulation of DDR genes such as *GADD45A/B* which affects aurora-A and Nek2 and therefore promotes genomic instability and histone alterations[47,48] along with reduced *CDK1* and *SIRT3* expression may explain the treatment-induced accumulation of γ-H2AX. While CDKs are not only involved in cell-cycle progression, they play also crucial roles in neuronal differentiation, transcription regulation, and migration/invasion. Here, several CDKs and their corresponding cyclins are downregulated. Among them, *CDK1* is required for successful completion of M-phase but also contributes to DNA-damage repair, checkpoint activation, and the progression of senescence escape by modulating the survivin pathway in glioma cells[49,50]. Though dinaciclib is widely described as CDK1/2/5/9i, we also detected downregulation of genes encoding for *CDK9*, *CDK12*, and *CDK20* which may have an impact on the protein level. CDK20 promotes cell growth and facilitates radio-chemoresistance in lung cancer cells[51]. CDK12, a transcriptional regulator of homologous recombination that shares sequence homology with CDK9, was previously identified as a target of dinaciclib in BC cells. The therapeutic effect included resensitization to a PARP inhibitor yielding durable regression in a patient-derived xenograft model[52]. Dinaciclib has an even more complex mode of action than previously anticipated. This not only involves cell-cycle arrest, but also cell death via numerous mechanisms: impaired DNA-damage repair, genomic instability, disturbed transcription regulation, and induction of dysregulated mitochondria, senescence, and autophagy. Whether abemaciclib likewise alters gene expression on such a global level, is a matter of speculation and has to be addressed prospectively. Still, our complex set of data indicate that similar mechanisms are altered by abemaciclib. Quite in line, long-term treatment with abemaciclib prevented colony formation even better than dinaciclib. Small viable colonies in some cases might be best explained by single outgrowing clones either intrinsically resistant or rapidly acquiring resistance upon therapeutic pressure. Residual cells showed MMP signals, with reduced viability, indicative of nonintact or almost dying cells.

Summarizing our findings, we show that abemaciclib and dinaciclib, but not palbociclib, inhibited GBM viability/motility, and invasion through multiple mechanisms: senescence, autophagy, necrosis/apoptosis, and mitochondrial dysfunction. We additionally provide mechanistic insights regarding the single-agent activity of dinaciclib. Our data support the idea of using CDKs as therapeutic targets in GBM and suggest dual CDKi application as a new therapeutic approach in clinical trials.

Materials and methods

Patient-derived tumor cell lines and culture conditions

Patient-derived GBM cell lines ($N = 5$; HROG02, HROG05, HROG52, HROG63, HROG75) were established in our lab and basically characterized, including molecular analysis and MGMT promoter methylation status[53]. 2D cell cultures were cultured in full medium and incubated at 37 °C in a humidified atmosphere of 5% CO_2: Dulbecco's modified eagle medium: nutrient mixture F-12 supplemented with 10% FCS, L-glutamine (2mmol/l), and antibiotics (100 U/ml penicillin/100 µg/ml streptomycin) (all from Pan Biotech, Aidenbach, Germany). 3D GBM neurosphere cells (NSC) and glioma stem-like cells (GSC) were cultured in ultra-low-attachment (ULA) plates (Greiner Bio-One, Kremsmünster, Austria) in a defined medium. NSC was grown in serum-containing medium (=sphere medium), whereas GSC was cultivated in serum-free medium containing stem cell-inducing additives (=stem cell medium) (+ 1× B-27® supplement (50×) (Gibco™, Life Technologies™, Carlsbad, USA), + 20 ng/ml recombinant human epidermal growth factor (rhEGF), + 10 ng/ml bFGF (Immunotools, Friesoythe, Germany). Prior treatment, cells were incubated until spheroids form (~72–96 h). Using this methodology, a single well-defined spheroid with cell line-specific appearance of a particular size was generated.

Cytostatic drugs and targeted substance

The cytostatics included the CDKi's (all from Selleckchem, Munich, Germany) abemaciclib (10 µM), palbociclib (10 µM), and dinaciclib (10 or 100 nM). TMZ (10 µM) was obtained from MSD (Haar, Germany). All substances were used in doses below the IC_{50} as determined in the preliminary dose-finding study (range 10 nM –10 µM).

Viability and senescence assays

Cell viability was assessed by calcein-acetoxymethyl (AM) (Biomol GmbH, Hamburg, Germany) fluorometric assay in 2D culture as described in ref. [54]. 3D cultures were analyzed luminometric using the CellTiter-Glo® 3D cell viability assay (Promega, Walldorf, Germany) according to the manufacturer's instruction. CellTiter-Glo® 3D luminescence signal was read with a microplate reader (Infinite® M200, Tecan Group, Switzerland). In addition, ten cycles of single and combined therapy were done in long-term treatment. Readout was done by Calcein AM + MitoTracker Red (Cell Signaling Technology, Frankfurt/Main, Germany) and crystal violet staining (0.2%, Sigma-Aldrich, St. Louis, USA). Senescence-associated β-galactosidase (SA-β-gal, Cell Signaling Technology, Cambridge, UK), as well as apoptosis and necrosis using flow cytometry-based Yo-Pro1/propidium iodide staining, was measured as described in refs. [54,55]. For p16 and p21 detection, cells were fixed with 2% paraformaldehyde (PFA) w/o methanol (15 min, Thermo Fisher Scientific, Darmstadt, Germany), washed twice, permeabilized, and blocked with 2% BSA, 0.5% Triton X-100 in PBS for 60 min and stained with p21 Waf1/Cip1 (12D1) rabbit mAb (Alexa 488 Conjugate) (green) (1:300, Cell Signaling Technology) and p16 antibody (JC8): sc-56330 Alexa 546 (orange) (1:50, Santa Cruz Biotechnology, Dallas, TX) overnight at 4 °C. Nuclei were counterstained with DAPI and cells were analyzed on a Zeiss LSM-780 Confocal Laser Microscope (Zeiss, Jena, Germany).

Immunogenic cell death assays

GBM cells were treated for 72 h. Cells were fixed in 4% PFA w/o methanol (30 min)). Surface-exposed Calreticulin (CalR) was detected using an anti-Calreticulin Rabbit mAb (Alexa Fluor® 488 conjugate) (1:50; overnight, Cell Signaling Technology), followed by filamentous actin staining (Flash Phalloidin™ Red 594 (1:20, 20 min, Biolegend). Nuclei were counterstained with DAPI and cells analyzed on a Zeiss LSM-780 confocal laser microscope.

Cs-137 γ-irradiation

Cs-137 γ-irradiation (2Gy) was performed 24 h after treatment using an IBL 637 (CIS Bio-International, Codolet, France), followed by 3-day incubation at 37 °C and 5% CO_2. Double-strand breaks (DSB) were assessed with γ-H2AX staining. For the latter, cells were fixed with 4% PFA/PBS, washed twice, permeabilized (0.5% Triton X-100, 15 min), blocked in 1% BSA (45 min), and incubated with Alexa Fluor® 594 anti-H2A.X Phospho (Ser139) antibody (1:1000, overnight, 4 °C) (Biolegend). Nuclei were counterstained with DAPI and analyzed on a Zeiss LSM-780 confocal laser microscope.

In vitro wound-healing assay and 2D cellular migration/invasion assay

A wound-healing assay was done as described in ref. [56], data acquisition was made using a Leica DMI 4000B microscope (Leica, Heidelberg, Germany). Then, a modified Boyden chamber technique (ThinCerts, Greiner Bio-One) with and without Matrigel-coated membranes (Corning, Corning, USA) was applied according to Ramer et al.[57].

Tumor spheroid invasion assay

After sphere formation, 96-ULA well plates were placed on ice; half of the medium was removed, and reagents were added at a twofold final concentration (+ EGF = to stimulate invasion) into U-bottom wells containing ice-cold matrigel (Corning). Spheres were monitored for 7 days and images were taken at 24 h to 3-day intervals with a final record on day 7 (Leica DMI 4000B).

MitoTracker® Red CMXRos, MitoSOX™ Red, LysoTracker™ Green DND-26 ER Tracker ™ Blue-White DPX, and Dextran Alexa Fluor™ 594; 10,000 MW

MitoTracker CMXRos (8-(4'-chloromethyl) phenyl-2,3,5,6,11,12,14,15-octahydro-1 H,4 H,10 H,13 H-diquinolizino-8 H-xanthylium chloride), LysoTracker Green, ER-Tracker™ Blue-White (Dapoxyl) DPX and Molecular Probes™ Dextran, Alexa Fluor™ 594; 10,000 MW, anionic, fixable dyes were prepared according to the manufacturer's instructions (Cell Signaling Technology, Thermo Fisher Scientific). Mitochondria (MitoTracker Red CMXRos, 20 nM), ER (ER Tracker, 500 nM), and acidic components (LysoTracker, 50 nM) were stained (30 min, 37 °C) 72 h post treatment; Dextran (100 µg/ml) was given simultaneously with treatment and incubated 72 h. Images were taken on fluorescence microscopy (Leica DMI 4000B). MitoSOX™ Red (5 µM, 30 min, 37 °C, Thermo Fisher Scientific) was used as indicator of mitochondrial superoxide and analyzed via flow cytometry (FACS Verse, BD Bioscience, Franklin Lakes, USA).

LAMP1/2, Rab7a measurement

Vacuole formation was quantified on cells stained with CD107a, CD107b (lysosomal-associated membrane proteins 1 and 2, LAMP1, LAMP2), and GTPase Ras-related protein (Rab7a; 30 min, 4 °C, + intracellular staining) (all purchased from Biolegend). The analysis was done on a FACS Verse.

Image-iT hypoxia reagent

3D cultures were maintained, plated, and treated as described. Hypoxia reagent (Thermo Fisher Scientific) was added (10 µM, 3 h, 37 °C). The medium was replaced and cells kept in the incubator (24 h). Cells were imaged using a fluorescence microscope (Leica DMI 4000B).

Microarray analysis of RNA expression profiles

RNA of treated and control HROG63 cells (5×10^5 cells/treatment) were extracted employing RNeasy Plus Kit (Qiagen, Hilden, Germany) according to the manufacturer's protocol. The total RNA was quantified on a spectrophotometer (NanoDrop 1000, Thermo Fisher Scientific) and integrity confirmed using the Agilent Bioanalyzer 2100 with an RNA Nano chip kit (both from Agilent Technologies, Waldbronn, Germany). Expression profiling was performed by taking advantage of the Affymetrix Human Clariom S Array (Affymetrix/Thermo Fisher Scientific, Santa Clara, USA), which interrogates over 20,000 well-annotated genes. Therefore, the so-called Whole Transcriptome protocol was employed described in ref. [58]. Primary data analysis was performed with the Affymetrix Transcriptome Analysis Console (TAC) software, including the SST-RMA for normalization. Gene expression data were log-transformed. Limma was used here to calculate the P value. A change was considered significant when the Limma eBayes P value met the criterion $P < 0.05$ at fold changes $>|2|$, i.e., expression increments or declines larger than two.

Image processing

Quantification of the images was done by using the FIJI-ImageJ software as follows:

Staining intensity was determined by dividing the channels into red, green, and blue. Subsequently, integrated density profiles of the same size were measured in the respective channels.

For manual identification of scratch area (= open wound area), captured images were converted to grayscale. Finally, a threshold, a band-pass, and minimum filter were applied. Region of interest(s) (ROI) could then be set and scratch area analyzed. The scratch area [μm^2] was plotted over the time for each substance. Data are presented as mean.

Statistics

All values are given as mean ± SEM. After proving the assumption of normality, differences between controls and treated cells were determined by using the unpaired Student's t-test viability determination. In the case of multiple comparisons, one- or two-way *ANOVA* on ranks (Bonferroni's multiple-comparison test) was applied. Statistical evaluation was performed using GraphPad PRISM software, version 5.02 (GraphPad Software, San Diego, CA, USA). The criterion for significance was taken to be $P < 0.05$.

Acknowledgements

Open Access funding enabled and organized by Projekt DEAL.

Author details

[1]University Children's Hospital, Rostock University Medical Centre, Ernst-Heydemann-Straße 8, 18057 Rostock, Germany. [2]Department of Medicine Clinic III - Hematology, Oncology, Palliative Medicine, Rostock University Medical Center, Rostock University Medical Centre, Ernst-Heydemann-Str. 6, 18057 Rostock, Germany. [3]Core Facility for Microarray Analysis, Institute for Immunology, Rostock University Medical Centre, 18057 Rostock, Germany. [4]Institute of Pathology, Strempelstraße 14, 18055 Rostock, Rostock University Medical Centre, 18057 Rostock, Germany

Author contributions

C.R., D.K., and K.D.M. performed all experiments, D.K. performed the microarray, C.L. did the p21/p16 immunofluorescence staining, K.D.M. the Boyden-chamber assay, C.M. and C.R. designed the study, analyzed, and interpreted the data, prepared all figures, and performed statistical analysis; C.R. and C.M. wrote the paper, all authors participated in paper finalization and critically revised the paper.

Funding

This work was supported by a grant from the Lieselotte Beutel Stiftung to C. Riess and C. Maletzki.

Conflict of interest
The authors declare that the research was conducted in the absence of any commercial or financial relationships that could be construed as a potential conflict of interest.

Publisher's note
Springer Nature remains neutral with regard to jurisdictional claims in published maps and institutional affiliations.

Supplementary information The online version contains supplementary material available at https://doi.org/10.1038/s41420-021-00423-1.

Received: 29 September 2020 Revised: 23 November 2020 Accepted: 23 December 2020
Published online: 15 March 2021

References

1. Sherr, C. J., Beach, D. & Shapiro, G. I. Targeting CDK4 and CDK6: from discovery to therapy. *Cancer Discov.* **6**, 353–367 (2016).
2. Sánchez-Martínez, C., Lallena, M. J., Sanfeliciano, S. G. & de Dios, A. Cyclin dependent kinase (CDK) inhibitors as anticancer drugs: recent advances (2015–2019). *Bioorg. Med. Chem. Lett.* **29**, 126637 (2019).
3. Martin, C. A. et al. Palbociclib synergizes with BRAF and MEK inhibitors in treatment naïve melanoma but not after the development of BRAF inhibitor resistance. *Int. J. Cancer* **142**, 2139–2152 (2018).
4. Syn, N. L. et al. Pan-CDK inhibition augments cisplatin lethality in nasopharyngeal carcinoma cell lines and xenograft models. *Signal Transduct. Target Ther.* **3**, 9 (2018).
5. Schaer, D. A. et al. The CDK4/6 inhibitor abemaciclib induces a T cell inflamed tumor microenvironment and enhances the efficacy of PD-L1 checkpoint blockade. *Cell Rep.* **22**, 2809–2817 (2018).
6. Parry, D. et al. Dinaciclib (SCH 727965), a novel and potent cyclin-dependent kinase inhibitor. *Mol. Cancer Ther.* **9**, 2344–2353 (2010).
7. Li, C., Qi, L., Bellail, A. C., Hao, C. & Liu, T. PD-0332991 induces G1 arrest of colorectal carcinoma cells through inhibition of the cyclin-dependent kinase-6 and retinoblastoma protein axis. *Oncol. Lett.* **7**, 1673–1678 (2014).
8. Hsu, C.-L. et al. Integrated genomic analyses in PDX model reveal a cyclin-dependent kinase inhibitor Palbociclib as a novel candidate drug for nasopharyngeal carcinoma. *J. Exp. Clin. Cancer Res.* **37**, 233 (2018).
9. Sobhani, N. et al. Updates on the CDK4/6 inhibitory strategy and combinations in breast cancer. *Cells* **8**, 321 (2019).
10. Schoninger, S. F. & Blain, S. W. The ongoing search for biomarkers of CDK4/6 inhibitor responsiveness in breast cancer. *Mol. Cancer Ther.* **19**, 3–12 (2020).
11. Canepa, E. T. et al. INK4 proteins, a family of mammalian CDK inhibitors with novel biological functions. *IUBMB Life.* **59**, 419–426 (2007).
12. Silantyev, A. S. et al. Current and future trends on diagnosis and prognosis of glioblastoma: from molecular biology to proteomics. *Cells* **8**, 863 (2019).
13. Solomon, D. A., Kim, J.-S., Jean, W. & Waldman, T. Conspirators in a capital crime: co-deletion of p18INK4c and p16INK4a/p14ARF/p15INK4b in glioblastoma multiforme. *Cancer Res.* **68**, 8657–8660 (2008).
14. Lah, T. T., Novak, M. & Breznik, B. Brain malignancies: glioblastoma and brain metastases. *Semin Cancer Biol.* **60**, 262–273 (2020).
15. Mandl, M. M. et al. Inhibition of Cdk5 induces cell death of tumor-initiating cells. *Br. J. Cancer* **116**, 912–922 (2017).
16. Raub, T. J. et al. Brain exposure of two selective dual CDK4 and CDK6 inhibitors and the antitumor activity of CDK4 and CDK6 inhibition in combination with temozolomide in an intracranial glioblastoma xenograft. *Drug Metab. Dispos.* **43**, 1360–1371 (2015).
17. Zhang, P. et al. Therapeutic targeting of tumor-associated myeloid cells synergizes with radiation therapy for glioblastoma. *Proc. Natl Acad. Sci. USA* **116**, 23714–23723 (2019).
18. Wu, T. et al. Effect of abemaciclib (LY2835219) on enhancement of chemotherapeutic agents in ABCB1 and ABCG2 overexpressing cells in vitro and in vivo. *Biochem Pharmacol.* **124**, 29–42 (2017).
19. Torres-Guzmán, R. et al. Preclinical characterization of abemaciclib in hormone receptor positive breast cancer. *Oncotarget* **8**, 69493–69507 (2017).
20. Zhao, H. et al. Study of the mechanism by which dinaciclib induces apoptosis and cell cycle arrest of lymphoma Raji cells through a CDK1-involved pathway. *Cancer Med.* **8**, 4348–4358 (2019).
21. Alsayegh, K., Matsuura, K., Sekine, H. & Shimizu, T. Dinaciclib potently suppresses MCL-1 and selectively induces the cell death in human iPS cells without affecting the viability of cardiac tissue. *Sci. Rep.* **7**, 1–13 (2017).
22. Jane, E. P. et al. Dinaciclib, a cyclin-dependent kinase inhibitor promotes proteasomal degradation of Mcl-1 and enhances ABT-737-mediated cell death in malignant human glioma cell liness. *J. Pharm. Exp. Ther.* **356**, 354–365 (2016).
23. Tanaka, Y. et al. Abemaciclib, a CDK4/6 inhibitor, exerts preclinical activity against aggressive germinal center-derived B-cell lymphomas. *Cancer Sci.* **111**, 749–759 (2020).
24. Hino, H. et al. Abemaciclib induces atypical cell death in cancer cells characterized by formation of cytoplasmic vacuoles derived from lysosomes. *Cancer Sci.* **111**, 2132–2145 (2020).
25. Jeong, E. H. et al. Anti-tumor effect of CDK inhibitors on CDKN2A-defective squamous cell lung cancer cells. *Cell Oncol.* **41**, 663–675 (2018).
26. Wang, S., Wang, K., Wang, H., Han, J. & Sun, H. Autophagy is essential for flavopiridol-induced cytotoxicity against MCF-7 breast cancer cells. *Mol. Med Rep.* **16**, 9715–9720 (2017).
27. Chou, A. et al. Tailored first-line and second-line CDK4-targeting treatment combinations in mouse models of pancreatic cancer. *Gut* **67**, 2142–2155 (2018).
28. Feldmann, G. et al. Cyclin-dependent kinase inhibitor Dinaciclib (SCH727965) inhibits pancreatic cancer growth and progression in murine xenograft models. *Cancer Biol. Ther.* **12**, 598–609 (2011).
29. Bisht, S. et al. Cyclin-dependent kinase 5 (CDK5) controls melanoma cell motility, invasiveness, and metastatic spread—identification of a promising novel therapeutic target. *Transl. Oncol.* **8**, 295–307 (2015).
30. Qin, G. et al. Palbociclib inhibits epithelial-mesenchymal transition and metastasis in breast cancer via c-Jun/COX-2 signaling pathway. *Oncotarget* **6**, 41794–41808 (2015).
31. Singh, M. K. et al. HEI10 negatively regulates cell invasion by inhibiting cyclin B/Cdk1 and other promotility proteins. *Oncogene* **26**, 4825–4832 (2007).
32. Fang, L., Du, W. W., Awan, F. M., Dong, J. & Yang, B. B. The circular RNA circ-Ccnb1 dissociates Ccnb1/Cdk1 complex suppressing cell invasion and tumorigenesis. *Cancer Lett.* **459**, 216–226 (2019).
33. Ma, H., Seebacher, N. A., Hornicek, F. J. & Duan, Z. Cyclin-dependent kinase 9 (CDK9) is a novel prognostic marker and therapeutic target in osteosarcoma. *EBioMedicine* **39**, 182–193 (2019).
34. Thomas, A. L. et al. Inhibition of CDK-mediated Smad3 phosphorylation reduces the Pin1-Smad3 interaction and aggressiveness of triple negative breast cancer cells. *Cell Cycle* **16**, 1453–1464 (2017).
35. Baracca, A., Sgarbi, G., Solaini, G. & Lenaz, G. Rhodamine 123 as a probe of mitochondrial membrane potential: evaluation of proton flux through F0 during ATP synthesis. *Biochim Biophys. Acta - Bioenerg.* **1606**, 137–146 (2003).
36. Solaini, G., Baracca, A., Lenaz, G. & Sgarbi, G. Hypoxia and mitochondrial oxidative metabolism. *Biochim. Biophys. Acta - Bioenerg.* **1797**, 1171–1177 (2010).
37. Cui, H., Kong, Y. & Zhang, H. Oxidative stress, mitochondrial dysfunction, and aging. *J. Signal Transduct.* **2012**, 1–13 (2012).
38. Zorova, L. D. et al. Functional significance of the mitochondrial membrane potential. *Biochem. Suppl. Ser. A Membr. Cell Biol.* **12**, 20–26 (2018).
39. Zorova, L. D. et al. Mitochondrial membrane potential. *Anal. Biochem.* **552**, 50–59 (2018).
40. Brand, M. D. Mitochondrial generation of superoxide and hydrogen peroxide as the source of mitochondrial redox signaling. *Free Radic. Biol. Med.* **100**, 14–31 (2016).
41. Venkatachalam, G., Surana, U. & Clément, M. V. Replication stress-induced endogenous DNA damage drives cellular senescence induced by a sub-lethal oxidative stress. *Nucleic Acids Res.* **45**, 10564–40582 (2017).
42. Coluzzi, E., Leone, S. & Sgura, A. Oxidative stress induces telomere dysfunction and senescence by replication fork arrest. *Cells* **8**, 19 (2019).
43. Maltese, W. A. & Overmeyer, J. H. Methuosis: nonapoptotic cell death associated with vacuolization of macropinosome and endosome compartments. *Am. J. Pathol.* **184**, 1630–1642 (2014).
44. Silva-Pavez, E. et al. CK2 inhibition with silmitasertib promotes methuosis-like cell death associated to catastrophic massive vacuolization of colorectal cancer cells. *Cell Death Dis.* **10**, 73 (2019).
45. Overmeyer, J. H., Young, A. M., Bhanot, H. & Maltese, W. A. A chalcone-related small molecule that induces methuosis, a novel form of non-apoptotic cell death, in glioblastoma cells. *Mol. Cancer* **10**, 69 (2011).
46. Liu, R. et al. CDK1-mediated SIRT3 activation enhances mitochondrial function and tumor radioresistance. *Mol. Cancer Ther.* **14**, 2090–2102 (2015).

47. Salvador, J. M., Brown-Clay, J. D. & Fornace, A. J. Gadd45 in stress signaling, cell cycle control, and apoptosis. *Adv. Exp. Med Biol.* **793**, 1–19 (2013).
48. Nikonova, A. S., Astsaturov, I., Serebriiskii, I. G., Dunbrack, R. L. & Golemis, E. A. Aurora A kinase (AURKA) in normal and pathological cell division. *Cell. Mol. Life Sci.* **70**, 661–687 (2013).
49. Liao, H. et al. CDK1 promotes nascent DNA synthesis and induces resistance of cancer cells to DNA-damaging therapeutic agents. *Oncotarget* **8**, 90662–90673 (2017).
50. Song, Z. et al. Escape of U251 glioma cells from temozolomide-induced senescence was modulated by CDK1/survivin signaling. *Am. J. Transl. Res.* **9**, 2163–2180 (2017).
51. Wang, Q. et al. CDK20 interacts with KEAP1 to activate NRF2 and promotes radiochemoresistance in lung cancer cells. *Oncogene* **36**, 5321–5330 (2017).
52. Johnson, S. F. et al. CDK12 inhibition reverses de novo and acquired PARP inhibitor resistance in BRCA wild-type and mutated models of triple-negative breast cancer. *Cell Rep.* **17**, 2367–2381 (2016).
53. Mullins, C. S. et al. Establishment and characterization of primary glioblastoma cell lines from fresh and frozen material: a detailed comparison. *PLoS ONE* **8**, e71070 (2013).
54. Maletzki, C. et al. Host defense peptides for treatment of colorectal carcinoma-a comparative in vitro and in vivo analysis. *Oncotarget* **5**, 4467–4479 (2014).
55. Maletzki, C. et al. Deciphering molecular mechanisms of arginine deiminase-based therapy—comparative response analysis in paired human primary and recurrent glioblastomas. *Chem. Biol. Interact.* **278**, 179–188 (2017).
56. Oehmcke-Hecht, S. et al. Streptococcus gallolyticus abrogates anti-carcinogenic properties of tannic acid on low-passage colorectal carcinomas. *Sci. Rep.* **10**, 1–10 (2020).
57. Ramer, R., Rohde, A., Merkord, J., Rohde, H. & Hinz, B. Decrease of plasminogen activator inhibitor-1 may contribute to the anti-invasive action of cannabidiol on human lung cancer cells. *Pharm. Res.* **27**, 2162–2174 (2010).
58. Koczan, D., Fitzner, B., Zettl, U. K. & Hecker, M. Microarray data of transcriptome shifts in blood cell subsets during S1P receptor modulator therapy. *Sci. Data* **5**, 180145 (2018).

8.5.3 The Individual Effects of Cyclin-Dependent Kinase Inhibitors on Head and Neck Cancer Cells - A Systematic Analysis. Cancers.

cancers

MDPI

Article

The Individual Effects of Cyclin-Dependent Kinase Inhibitors on Head and Neck Cancer Cells—A Systematic Analysis

Nina Schoenwaelder [1,*], Inken Salewski [1], Nadja Engel [2], Mareike Krause [1], Björn Schneider [3], Michael Müller [4], Christin Riess [1,5], Heiko Lemcke [6,7,8], Anna Skorska [6,7,8], Christina Grosse-Thie [1], Christian Junghanss [1] and Claudia Maletzki [1]

[1] Department of Internal Medicine, Medical Clinic III—Hematology, Oncology, Palliative Medicine, University Medical Center Rostock, 18057 Rostock, Germany; Inken.salewski@med.uni-rostock.de (I.S.); mareike.krause@uni-rostock.de (M.K.); Christin.riess@med.uni-rostock.de (C.R.); christina.grosse-thie@med.uni-rostock.de (C.G.-T.); christian.junghanss@med.uni-rostock.de (C.J.); claudia.maletzki@med.uni-rostock.de (C.M.)
[2] Department of Oral and Maxillofacial Surgery, Facial Plastic Surgery, University Medical Center Rostock, 18057 Rostock, Germany; Nadja.Engel@med.uni-rostock.de
[3] Institute of Pathology, University Medical Center Rostock, Strempelstr.14, 18057 Rostock, Germany; bjoern.schneider@med.uni-rostock.de
[4] Core Facility for Cell Sorting & Cell Analysis, Laboratory for Clinical Immunology, University Medical Center Rostock, 18057 Rostock, Germany; Michael.Mueller2@med.uni-rostock.de
[5] University Children's Hospital, Rostock University Medical Centre, 18057 Rostock, Germany
[6] Department of Cardiac Surgery, Reference and Translation Center for Cardiac Stem Cell Therapy (RTC), University Medical Center Rostock, 18057 Rostock, Germany; Heiko.Lemcke@med.uni-rostock.de (H.L.); anna.skorska@med.uni-rostock.de (A.S.)
[7] Department of Cardiology, University Medical Center Rostock, 18059 Rostock, Germany
[8] Department Life, Light & Matter, Faculty of Interdisciplinary Research, University Rostock, 18059 Rostock, Germany
* Correspondence: nina.schoenwaelder@med.uni-rostock.de; Tel.: +49-381-494-5764

Simple Summary: This study examined the therapeutic potential of a combined therapy approach, based on clinical approved drugs (5-FU, Cisplatin, cetuximab) and cyclin-dependent kinase inhibitors (CDKi, dinaciclib, palbociclib, THZ1). We identified individual effects on head and neck squamous cell carcinoma cells, including induction of apoptosis/necrosis, and senescence as well as reduced invasiveness. Besides, we describe the relevance of the sequential timing of each combination partner to achieve synergistic effects. Another interesting finding of our study is the upregulation of immunologically relevant molecules on the tumor cell surface under certain CDKi-drug combinations. Here, dinaciclib and palboclicb had highest impact on immunogenicity, which even exceeded effects of the standard drugs. Finally, a therapeutic in vivo approach partially confirmed cell line-based results. Here, effective tumor growth control was seen when cisplatin was combined with dinaciclib. However, antitumoral effects were highly individual and nicely confirm the heterogeneity of this tumor entity.

Abstract: Cyclin-dependent kinase inhibitors (CDKi´s) display cytotoxic activity against different malignancies, including head and neck squamous cell carcinomas (HNSCC). By coordinating the DNA damage response, these substances may be combined with cytostatics to enhance cytotoxicity. Here, we investigated the influence of different CDKi´s (palbociclib, dinaciclib, THZ1) on two HNSCC cell lines in monotherapy and combination therapy with clinically-approved drugs (5-FU, Cisplatin, cetuximab). Apoptosis/necrosis, cell cycle, invasiveness, senescence, radiation-induced γ-H2AX DNA double-strand breaks, and effects on the actin filament were studied. Furthermore, the potential to increase tumor immunogenicity was assessed by analyzing Calreticulin translocation and immune relevant surface markers. Finally, an in vivo mouse model was used to analyze the effect of dinaciclib and Cisplatin combination therapy. Dinaciclib, palbociclib, and THZ1 displayed anti-neoplastic activity after low-dose treatment, while the two latter substances slightly enhanced radiosensitivity. Dinaciclib decelerated wound healing, decreased invasiveness, and induced MHC-I, accompanied by high amounts of surface-bound Calreticulin. Numbers of early and late apoptotic

check for updates

Citation: Schoenwaelder, N.; Salewski, I.; Engel, N.; Krause, M.; Schneider, B.; Müller, M.; Riess, C.; Lemcke, H.; Skorska, A.; Grosse-Thie, C.; et al. The Individual Effects of Cyclin-Dependent Kinase Inhibitors on Head and Neck Cancer Cells—A Systematic Analysis. *Cancers* **2021**, *13*, 2396. https://doi.org/10.3390/cancers13102396

Academic Editor: Samuel C. Mok

Received: 1 March 2021
Accepted: 11 May 2021
Published: 15 May 2021

Publisher's Note: MDPI stays neutral with regard to jurisdictional claims in published maps and institutional affiliations.

cells increased initially (24 h), while necrosis dominated afterward. Antitumoral effects of the selective CDKi palbociclib were weaker, but combinations with 5-FU potentiated effects of the monotherapy. Additionally, CDKi and CDKi/chemotherapy combinations induced MHC I, indicative of enhanced immunogenicity. The in vivo studies revealed a cell line-specific response with best tumor growth control in the combination approach. Global acting CDKi's should be further investigated as targeting agents for HNSCC, either individually or in combination with selected drugs. The ability of dinaciclib to increase the immunogenicity of tumor cells renders this substance a particularly interesting candidate for immune-based oncological treatment regimens.

Keywords: targeted therapy; combination strategies; immunogenic cell death; xenograft model

1. Introduction

Mammalian cell cycle is controlled by cyclin dependent kinases (CDKs) [1]. In tumors, CDKs are dysregulated and CDK/cyclin complexes frequently overexpressed [2–4]. Tumor cells bypass the CDK4/6-Rb axis because it is critical for cell cycle entry and cell proliferation [5]. The knowledge about these mutations is a chance to identify molecular targets for pharmacological interventions [6]. Indeed, several CDK inhibitors (CDKi's) been developed for cancer treatment. Additionally to the highly selective and FDA-approved CDKi's palbociclib, ribociclib, and abemaciclib, multi- and pan-CDKi's are now entering clinical trials. These include, among others, dinaciclib that targets CDK1, CDK2, CDK5, and CDK9 [7,8], and THZ1, which is active against CDK7, CDK12, and CDK13 [9,10].

Advances in understanding of pathobiology and molecular characteristics have contributed to the introduction of novel therapy approaches. Still, the treatment of solid tumors remains challenging. Additionally to intrinsic resistance mechanisms, the development or outgrowth of single subclones after therapy promotes immune escape and complicates precision medicine.

Head and neck cancers are paradigmatic for tumor heterogeneity. They can be found in the oral cavity, pharynx, larynx, salivary glands, nasal cavity, and paranasal sinuses [11]. The predominant histological type of head and neck tumors is squamous cell carcinomas (HNSCC) [11]. HNSCC is the 7th most common cancer worldwide [11–13]. Risk factors include tobacco, alcohol, and human papillomavirus (HPV) infection. The latter drives tumor formation in the oropharynx with distinct clinical, histopathological, and molecular characteristics [14,15]. Around 58% of the patients present with loco-regionally advanced disease at diagnosis and this patient cohort has a poor prognosis [11]. Hence, the implementation of targeted therapies in standard treatment schedules constitutes a promising and urgently needed approach for improving treatment and outcome. In 2019, a multicenter, multigroup, phase 2 trial reported promising activity outcomes in patients with platinum-resistant or cetuximab-resistant HPV-unrelated HNSCC receiving palbociclib and cetuximab [16]. Though combination strategies are promising, the sequential timing of each combination partner remains debatable [17–19]. To move forward, we here employed simultaneous and sequential combination strategies of clinically approved therapeutics and CDKi's for treating HNSCC with the aim to identify the best strategy.

2. Results

2.1. CDKi Treatment Impairs Viability and Exerts Synergistic Effects in Combination Therapy

UT-SCC-14 and UT-SCC-15 were used as in vitro cell culture models, since these cells are representative for primary and recurrent HNSCC. Both cell lines were susceptible to standard drugs and CDKi's in clinically relevant doses (below 1 μM for CDKi's and ≤90 μg/mL for cytostatic drug), as determined in preliminary experiments. For combination experiments, standard drugs 5-Fluorouracil (5-FU), Cisplatin, and cetuximab as well as CDKi's (dinaciclib, palbociclib, THZ1) were applied in doses below the IC_{50} (Figure 1A,B; cetuximab is the only exceptions, here IC_{50} doses were used). The time course of treatment

considered each cell lines' doubling times and attempted to mimic the in vivo situation. Therefore, cells received two treatment cycles of 72 h.

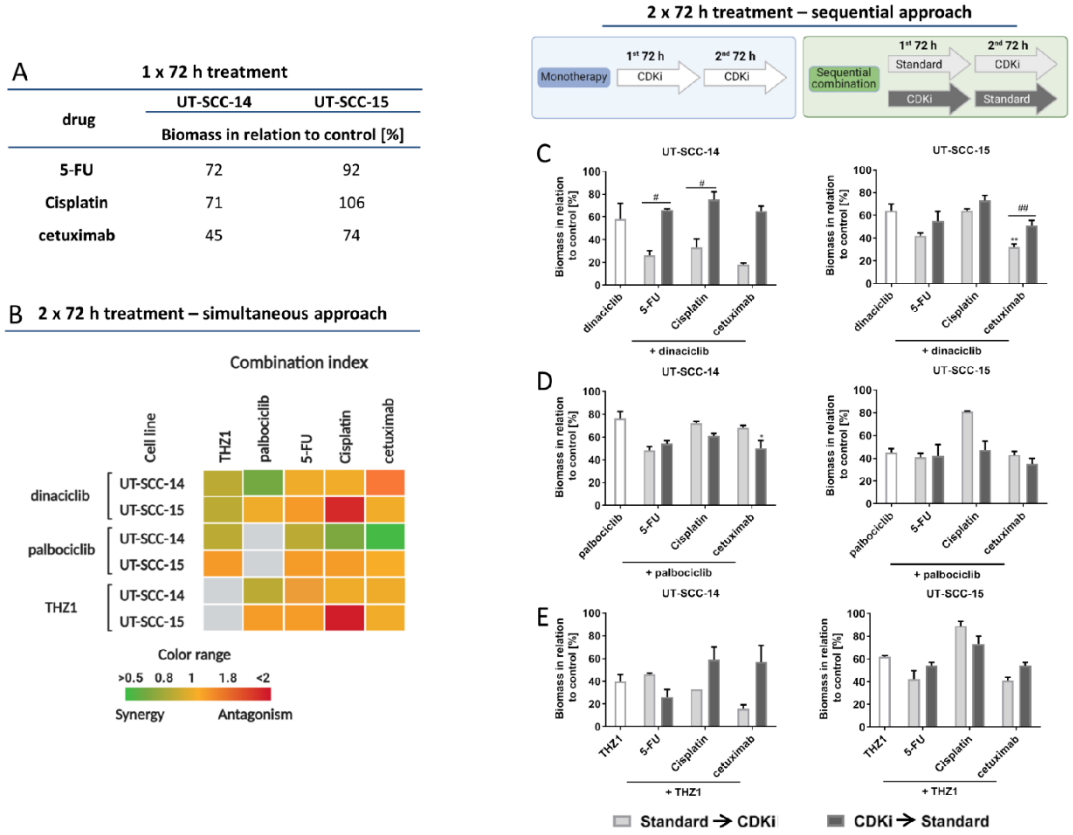

Figure 1. Simultaneous and sequential treatment schedules. (**A**) Biomass quantification after monotherapy with 5-FU, Cisplatin, and cetuximab (1 × 72 h). Doses used here were determined before using classical dose response curve analysis. Read out was done by crystal violet staining and biomass in relation to untreated controls quantified. In (**B**) the Bliss Independence model was used to calculate potential synergistic effects. The green color indicates a synergistic and red color an antagonistic effect of the simultaneous combinations. (**C**–**E**) Sequential treatment: (**C**) dinaciclib [0.005 µM], (**D**) palbociclib [1 µM], and (**E**) THZ1 [UT-SCC14: 0.02 µM; UT-SCC-15: 0.005 µM] in comparison to 2 × 72 h CDKi monotherapy (first bar of each graph). Drug doses were as follows: 5-FU [0.32 µg/mL]; Cisplatin [UT-SCC14: 0.5 µg/mL; UT-SCC-15: 0.05 µg/mL]; cetuximab [0.5 µg/mL]. Mann Whitney U-test (n = 3–4 independent experiments) # $p < 0.05$, ## $p < 0.01$ vs. 1st CDKi; Kruskal Wallis test (n = 3–4 independent experiments) * $p < 0.05$, ** $p < 0.01$ vs. monotherapy. The 1 × 72 h monotherapy with 5-FU, Cisplatin or Cetuximab confirms that the potential enhancing effect of sequential combination therapy is not due to the single administration of these substances but the effect of the 2 × 72 h CDKi monotherapy (in the left bar) is actually enhanced.

In a first series, simultaneous combinations were applied (Figure 1B). Notably, dual CDKi treatment was synergistic or additive in UT-SCC-14 and partially in UT-SCC-15 cells as determined by biomass quantification. Here, combinations of dinaciclib with palbociclib or THZ1 were synergistic (Figure 1B). CDKi/drug combinations were mainly antagonistic. The only exception was seen for Cisplatin in conjunction with dinaciclib (UT-SCC-14) and cetuximab with dinaciclib or THZ1 (UT-SCC-15).

To test if the effect of a 2 × 72 h CDKi monotherapy can be boosted, sequential combinations were performed (Figure 1C–E). The first bar of each graph shows CDKi monotherapy, followed by the sequential combination treatments. CDKi were either given before or after standard therapy. The sequential treatment with dinaciclib (Figure 1C) revealed higher biomass reduction in both cell lines when standard therapy was given first. There was a strong reduction for all three combinations in UT-SCC-14 and UT-SCC-15. The sequential treatment with palbociclib yielded opposite results (Figure 1D). Here, palbociclib pretreatment prior to Cisplatin or cetuximab was better than the other way around. The order of 5-FU application had no leverage. For the sequential combination with THZ1 (Figure 1E), cell line-specific responses were seen. UT-SCC-14 cells' viability was more affected when 5-FU was given first and second THZ1. Comparable effects were seen after THZ1/Cisplatin treatment in UT-SCC-15 cells. Still, the other combinations were only effective when the standard drug was given before.

The aforementioned findings nicely confirm the heterogeneous response pattern of HNSCC.

2.2. CDKi's Induce Apoptotic and Necrotic Cell Death and Mediate Calreticulin Translocation

To investigate the effects of different treatments on the two cell lines, an apoptosis-necrosis assay was performed on selected treatment schedules (Figure 2A,B). Cells were simultaneously treated with CDKi's and drugs (5-FU, Cisplatin) for 24 and 72 h (Figure 2A,B). Short-term dinaciclib monotherapy mainly induced early apoptotic and necrotic cell death. The other monotherapies had minor or no impact on cell viability. After 72 h, overall cell death was higher in treated cells, but with individual differences. Dinaciclib alone or in combination induced necrosis, THZ1 and its combinations triggered apoptosis or a mixed form of apoptosis and necrosis (Figure 2A,B). Additionally to the induced cell death, senescence was studied, since this is a common response to CDK inhibition (Figure S1). These experiments revealed senescence induction by specific CDKi's (e.g., dinaciclib) or its combination with standard drugs (e.g., 5-FU). However, senescence was not the dominating cellular response here, suggesting a minor role. UT-SCC-14 cells clumped together, especially under dinaciclib monotherapy and combination therapy, while UT-SCC-15 cell clusters were disrupted. The combination of THZ1 and 5-FU had similar effects to dinaciclib.

Then, the ability to induce immunogenic cell death was measured after 72 h by detecting calreticulin (CalR) on the tumor cells' surface (Figure 2C). The proportion of CalR positive cells and the mean fluorescence intensity signal (MFI) (Figure 2D) were recorded. Dinaciclib induced CalR translocation in monotherapy and combination therapy significantly. Notably, the combination of THZ1 and 5-FU likewise induced CalR translocation. While these findings already hint towards immune stimulating properties, we additionally checked for immunologically relevant markers (Figure 3A,B). The abundance of HLA-ABC (MHC class I) and PD-1 on tumor cells was examined. A significant increase in MHC class I was seen after dinaciclib monotherapy and combination therapy as well as upon palbociclib treatment of UT-SCC-14 cells (Figure 3A). The MHC class I abundance changed marginally in UT-SCC-15 cells irrespective of the treatment schedule used (Figure 3B). This was, however, likely because of the high basal MHC class I abundance, which was about 80%. Still, dinaciclib and their combinations tended to upregulate MHC class I, finally yielding ~100%. PD-1 was upregulated by certain treatments. This did, however, not reach statistical significance (Figure 3A,B).

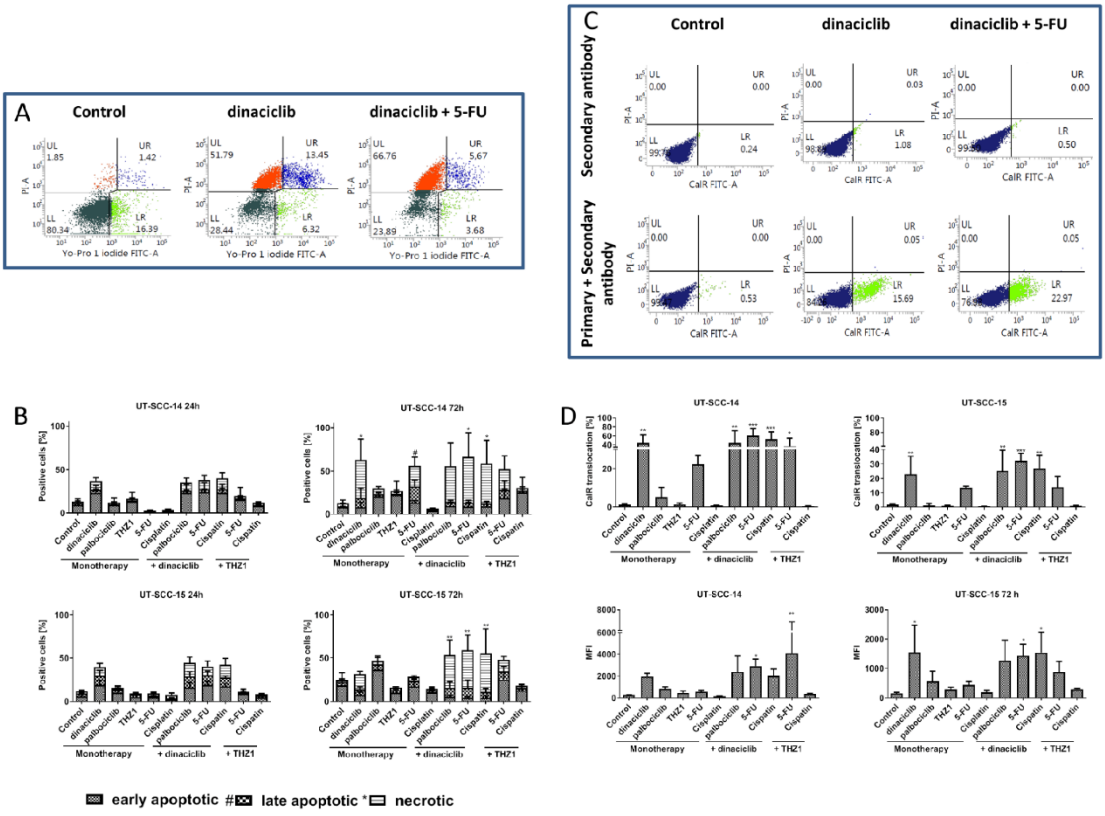

Figure 2. Apoptosis/necrosis assay and detection of immunogenic cell death (ICD). For (**A**,**B**) apoptosis/necrosis assay, cells were stained with Yo-Pro 1 iodide and PI. Cells that were positive for Yo-Pro 1 iodide were defined as early apoptotic, cells that were positive for PI were defined as necrotic, and double positive cells were defined as late apoptotic. Apoptosis/necrosis assay was done after 24 h and 72 h. (**A**) Representative dots plots showing distribution of viable and dead cells (either apoptotic or necrotic). (**B**) Quantitative analysis of apoptotic and necrotic cells subdivided into early apoptotic (Yo-Pro1$^+$/PI$^-$), late apoptotic (Yo-Pro1$^+$/PI$^+$) and necrotic ((Yo-Pro1$^-$/PI$^+$). (**C**,**D**)) ICD was detected after 72 h treatment by staining CalR on the cell surface. In both assays, 10,000 events were measured and the percentage of cells showing CalR translocation and the mean fluorescence intensity (MFI) of CalR$^+$ cells are provided. Drug doses were as follows: dinaciclib [0.02 µM]; palbociclib [1 µM]; THZ1 [UT-SCC14: 0.02 µM; UT-SCC-15: 0.005 µM]; 5-FU [90 µg/mL]; Cisplatin [0.1 µg/mL]. (**B**) Kruskal Wallis Test (n = 4–5 independent experiments); late apoptotic # $p < 0.05$ vs. control; necrotic * $p < 0.05$, ** $p < 0.01$ vs. control (**D**) 1way ANOVA (n = 3–4 independent experiments) * $p < 0.05$, ** $p < 0.01$, *** $p < 0.001$ vs. control.

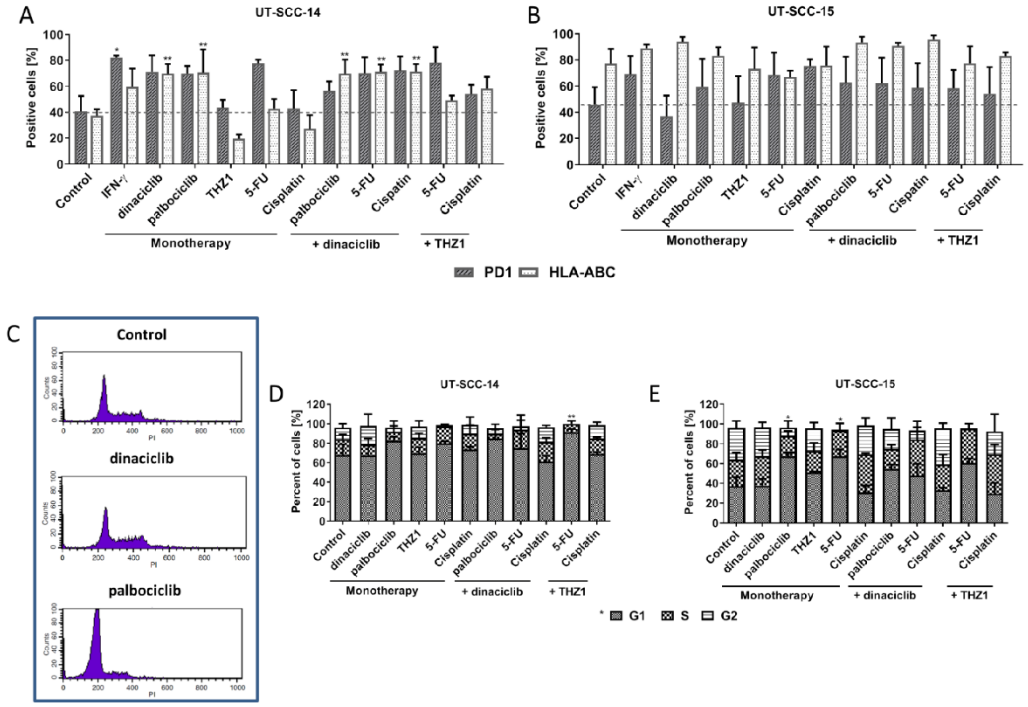

Figure 3. Phenotyping and cell cycle analysis. Phenotyping of (**A**) UT-SCC-14 and (**B**) UT-SCC-15 cells using multi-color flow cytometry. Therefore, cells were stained after 48 h treatment with test substances using the following antibodies: anti-HLA-ABC antibody (MHC I) and anti-CD279 (PD-1). Drug doses were as follows: IFN-γ [50 ng/mL]; dinaciclib [0.02 µM]; palbociclib [1 µM]; THZ1 [UT-SCC14: 0.02 µM; UT-SCC-15: 0.005 µM]; 5-FU [90 µg/mL]; Cisplatin [0.1 µg/mL]. 1 way ANOVA ($n \geq 3$ independent experiments) * $p < 0.05$, ** $p < 0.01$, vs. control. (**C–E**) Cell cycle analysis. Ethanol-fixed cells were stained with PI. (**C**) Representative histograms showing distribution of cell cycle phases in control cells and upon therapy. (**D**,**E**) Quantitative cell cycle analysis showing amounts of cells in G1, S, and G2 phase. Drug doses were as follows: dinaciclib [0.005 µM]; palbociclib [1 µM]; THZ1 [UT-SCC14: 0.02 µM; UT-SCC-15: 0.005 µM]; 5-FU [90 µg/mL]; Cisplatin [0.1 µg/mL]. 1way ANOVA ($n = 3$ independent experiments) * $p < 0.05$, ** $p < 0.01$ vs. control.

2.3. CDKi Induce Cell Cyclce Arrest

Due to the mode of action of CDKi's, cell cycle analysis was done on residual tumor cells (typically below 50%; Figure 3C–E). Representative histograms for all treatments are given in Figure S4. The number of residual cells after dinaciclib treatment was low. In these, tumor cells' cycle distribution was quite similar to controls. In UT-SCC-14 cells, a lucid G1 arrest was only seen after combined THZ1 and 5-FU therapy ($p < 0.05$ vs. control), while the remaining treatments had a minor impact on the cell cycle. UT-SCC-15 cells had significant changes after palbociclib and 5-FU monotherapy, but not in the combinations.

2.4. CDKi's Have Minor Impact on Double-Strand Breaks and Radiosensitivity

Treatment-induced double-strand breaks (DSBs) were determined by fluorescence microscopy using γ-H2AX (Figure 4). H2AX is phosphorylated by kinases after DNA double-strand breaks on serine 139. CDKi monotherapy or combination therapy itself had minor impacts on γ-H2AX foci, which were hardly detectable (Figure 4). To test if the applied regimens may enhance radiosensitivity, we then checked for irradiation-induced DSBs using 2 Gy (Figure 4B). Indeed, numbers of γ-H2AX-positive cells increased, with

highest amounts in cells treated with palbociclib. With regard to the combinations, γ-H2AX foci were primarily seen in palbociclib-or THZ1- based combinations with 5-FU. By contrast, such radiosensitizing effects were not seen in combinations with dinaciclib and may thus constitute a specific consequence of palbociclib or THZ1 treatment.

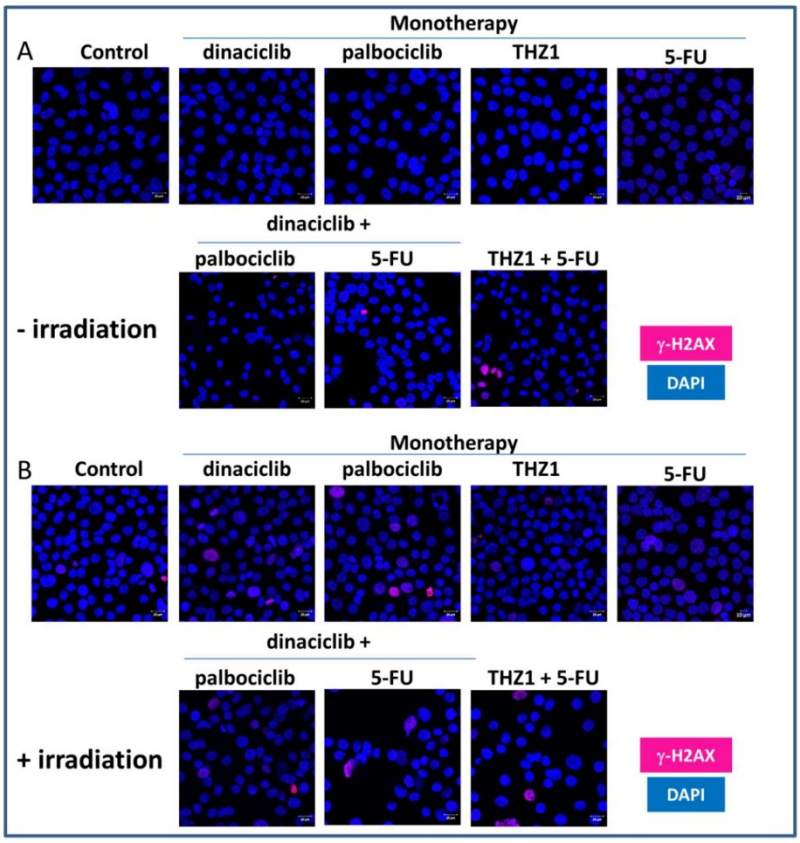

Figure 4. γ-H2AX staining of UT-SCC-14 cells. In order to detect a potential radiosensitizing effect of the test substances, cells were treated 24 h with selected monotherapy and combination therapies and then irradiated with 2 Gy using an IBL637. (**A**,**B**) We had three control groups. The first was completely untreated, the second was treated with the test substances but not irradiated, and the third was only irradiated but not treated with the test substances. Drug doses were as follows: dinaciclib [0.005 μM]; palbociclib [1 μM]; THZ1 [0.02 μM]; 5-FU [0.32 μg/mL]; γ-H2AX staining was performed 6 h after irradiation. Cell nuclei were stained with DAPI. Images were taken on a Zeiss LSM-780 Confocal Laser Microscope.

2.5. CDKi's Remodel the Actin Filament

Live cell monitoring via impedance measurements is particularly suitable for studying alterations in the cell monolayer, in the adhesion properties, and in the membrane integrity in real time. While the impedance increased over time in untreated control cells, dinaciclib treatment massively reduced impedance (Figure 5A,B). For palbociclib treated UT-SCC-14 cells, the measured impedance slightly decreased after 48 h, while THZ1 monotherapy slightly increased impedance (Figure 5A). Notably, the combination of THZ1 and 5-FU caused a delayed impedance breakdown in both cell lines. Here, impedance increased

within the first 20 h. Thereafter, the impedance stagnated for approximately 3 h, and then decreased for the next 48 h until no impedance was detectable. Dinaciclib in conjunction with cytostatics (Cisplatin, 5-FU) induced a complete and irreversible breakdown.

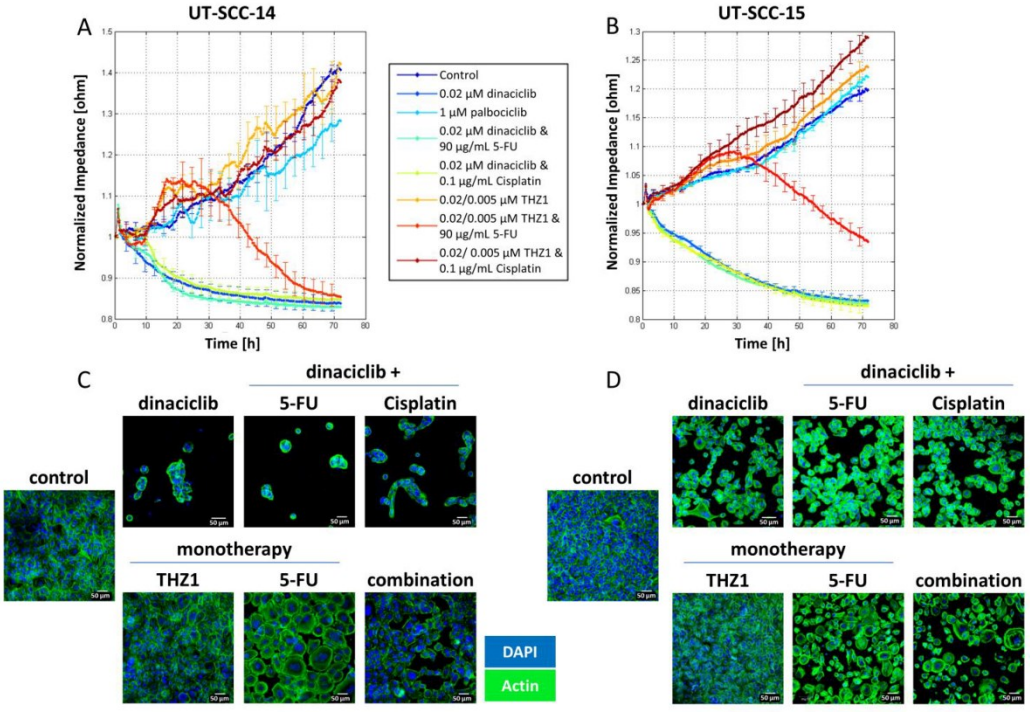

Figure 5. Impedance measurement and cytoskeletal staining. (**A**,**C**) UT-SCC-14 and (**B**,**D**) UT-SCC-15 cells. Cells were seeded in a 96-well ECIS array plate with 20 interdigitated electrodes/well and treated with selected test substances to investigate the impact of the treatment schedules. Drug doses were as follows: dinaciclib [0.02 µM]; palbociclib [1 µM]; THZ1 [UT-SCC14: 0.02 µM; UT-SCC-15: 0.005 µM]; 5-FU [90 µg/mL]; Cisplatin [0.1 µg/mL]. Impedance was monitored in real-time. The analysis of cell-cell contacts was performed by 4000 kHz using ECIS Software. Then, actin staining was performed with phalloidin green. Cell nuclei were stained with DAPI. Analysis was performed with a Zeiss LSM-780 Confocal Laser Microscope. Original magnification 200×.

To confirm the impedance data, actin fibers were stained 72 h after treatment (Figure 5C,D). Untreated UT-SCC-14 cells form a typical monolayer with a cortically formed cytoskeleton and less stress fibers within the cells. Dinaciclib itself caused massive cell detachment and consequently cell death. Nearly all UT-SCC-14 cells were detached after dinaciclib treatment, while some UT-SCC-15 cells remained attached and spread. Cytostatics (Cisplatin, 5-FU) intensified actin abundance in both cell lines.

THZ1 strengthened the formation of stress fibers in both cell lines that increases cellular stiffness and changes the motility properties [20]. This finding adds to the higher impedance under THZ1 treatment compared to the untreated control. THZ1 in combination with 5-FU caused higher cytotoxic effects, so most cells were detached.

2.6. Influence on Mitochondria, Lysosomes, the Endoplasmatic Reticulum and Vacuole Formation

CDKi-based treatments induced cytoplasmic vacuole formation. Hence, we checked the influence of the treatment schedules on mitochondria, lysosomes, and endoplasmatic reticulum (ER) (Figure 6). In both cell lines, mitochondrial activity increased after dinaciclib

monotherapy and combination therapy (Figure 6). Monotherapy with palbociclib, THZ1, or Cisplatin induced lysosome formation, but only in UT-SCC-14 cells. An effect of the treatments on the ER could not be demonstrated. After 5-FU treatment, the mitochondrial activity of UT-SCC-15 cells slightly increased that was reversed by THZ1. Cisplatin monotherapy had opposite effects that were neutralized by the combination partners (Figure 6B).

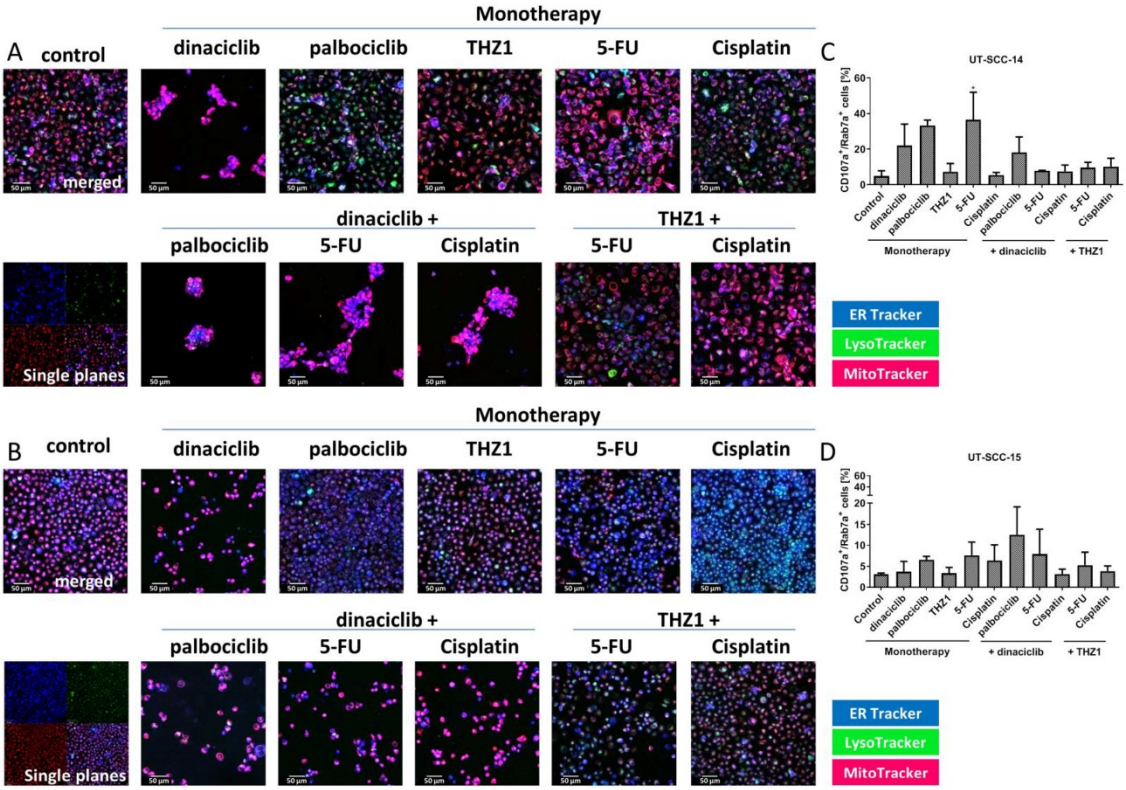

Figure 6. Influence on mitochondria, lysosomes, ER, and vacuole formation (**A**,**C**) UT-SCC-14 and (**B**,**D**) UT-SCC-15 cells. (**A**,**C**) To investigate the effect of the test substances on the mitochondrial activity, the lysosome formation, and the ER, cells were treated for 72 h with test substances and stained with MitoTracker (red), LysoTracker (green), and ER-Tracker (blue). Drug doses were as follows: dinaciclib [0.02 µM]; palbociclib [1 µM]; THZ1 [UT-SCC14: 0.02 µM; UT-SCC-15: 0.005 µM]; 5-FU [90 µg/mL]; Cisplatin [0.1 µg/mL]. Representative merged images are shown. For the control, a separated fluorescent image is shown. Analysis was performed with a ZEISS Elyra 7 Confocal Laser Microscope. (**C**,**D**) Cells were stained for CD107a and Rab7a as a hint for vacuole formation and measured via flow cytometry. The percentage numbers of double positive cells are shown. Drug doses were as follows: dinaciclib [0.02 µM]; palbociclib [1 µM]; THZ1 [UT-SCC14: 0.02 µM; UT-SCC-15: 0.005 µM]; 5-FU [90 µg/mL]; Cisplatin [0.1 µg/mL]. 1way ANOVA (n = 3 independent experiments) * $p < 0.05$ vs. control.

Cells were stained for specific late endo-lysosomal markers CD107a (LAMP1) and Rab7a to confirm above findings (Figure 6C,D). The GTPase Rab7a is primarily associated with late endosomes and LAMP1 is typically considered lysosomal [21]. Cell line specific responses were observed, with UT-SCC-14 cells showing higher numbers of these late endo-lysosomal markers after treatment. In detail, dinaciclib, palbociclib, and 5-FU monotherapy resulted in the highest increase of positive cells ($p < 0.05$ 5-FU vs. control)

(Figure 6C). The combinations could not boost effects. In UT-SCC-15 cells, highest numbers of $CD107a^+/Rab7a^+$ cells were detected after dual CDK inhibition (palbociclib + dinaciclib) (Figure 6D), implying that lysosomal formation plays a minor role here.

2.6.1. CDKi's Reduce Invasiveness and Migratory Potential

An assay was performed to explore the migration potential of cells to a cell free space under treatment. The cell line UT-SCC-14 filled the scratch within 24 h; the same was true for THZ1 and 5-FU monotherapy and combination therapy (Figure S2A). The toxic activity of dinaciclib induced cell death within 72 h and an accordingly incomplete scratch closure. Adding THZ1 to dinaciclib delayed migration, so the scratch was filled after 48 h. Using an invasion assay, the ability of cells to escape from the toxic environment was then investigated. For this experiment, selective treatments were included based on the obtained results shown before. The invasive cells from treatment medium were put in relation to invasive cells from control medium. CDKi treatment with dinaciclib significantly reduced invasiveness (Figure S2B). Effects were even stronger when two CDKi's were combined (dinaciclib + THZ1), but not by adding 5-FU. Still, these data confirm the potential of CDKi's to interfere with cellular invasion.

2.6.2. In Vivo Results

Finally, a xenograft mouse model was used to test if in vitro results can be transferred in vivo. For this proof-of-concept study, dinaciclib and Cisplatin were chosen as therapeutics and given alone or in combination (Figure 7A). We decided to use this combination, since dinaciclib had strong antitumoral effects in all previous analyses and Cisplatin is the accepted standard of care for HNSCC patients.

UT-SCC-14 xenografts showed a poor treatment response. Monotherapy had no influence on tumor growth and the combination was only able to decelerate growth (Figure 7B). In contrast, UT-SCC-15 xenograft growth was significantly reduced under therapy (Figure 7B). Dinaciclib and its combination with Cisplatin decreased the tumor volume to a minimum, the latter even stopped tumor growth until the experimental endpoint (two months follow-up). As a consequence of the better treatment response, mice challenged with UT-SCC-15 lived longer compared to those harboring UT-SCC-14 xenografts (Figure 7C). The outcome was best in the combination with a median survival of 63 days (vs. control 42 days, $p < 0.05$). As for dinaciclib monotherapy, mice had to be euthanized mostly because of tumor ulcerations. Hence, the poorer survival in both cases is not justified by the tumor volume as an endpoint but due to ethical aspects. Histology of residual tumors confirmed the different treatment responses. UT-SCC-14 xenografts presented with initial necrosis that increased after dinaciclib treatment (Figure 7D). After Cisplatin therapy, beginning necrosis with initial inflammatory reaction was visible, but also vital tumor tissue. In the combination, keratinized squamous cell carcinoma containing degenerated cells was found. In addition, neutrophilic infiltration was observed. The UT-SCC-15 xenograft sections of control mice showed characteristics of a keratinizing squamous cell carcinoma with developing necrosis. After dinaciclib treatment, degenerated and early apoptotic cells became prominent with surrounding necrosis. Cisplatin monotherapy primarily induced necrosis. The dark spot in the center of the image is degenerated keratinized squamous epithelium. Necrosis was dominating in the combination with some swollen cells, indicative of early cell damage in the initial stage.

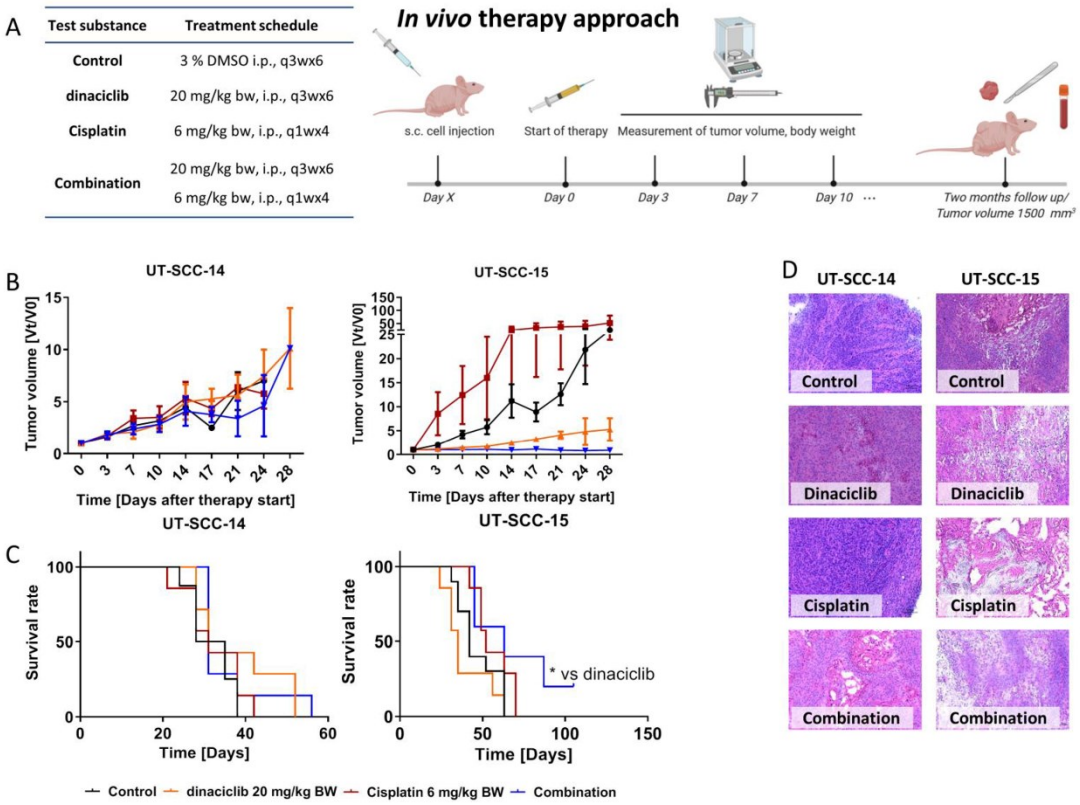

Figure 7. In vivo therapy approach. (**A**) Schematic overview over the treatment protocol with given doses of the test substances. (**B**) Tumor growth curve. Tumor volume was calculated as tumor volume at day × (Vt) divided through the tumor volume at the therapy start (V0). (**C**) Kaplan-Meier survival curve and Log-rank (Mantel-Cox) test. UT-SCC-14: control (n = 8 mice); Cisplatin/dinaciclib/combination (n = 7 mice/group); UT-SCC-15: control (n = 10 mice); Cisplatin/dinaciclib (n = 7 mice/group); combination (n = 5 mice); * $p < 0.05$ vs. dinaciclib. (**D**) Representative images of the HE stained tumors of each treatment group. Magnification 20×, Scale bar.

3. Discussion

CDKi's are being applied in clinical trials to treat solid and hematological malignancies (e.g., *NCT04169074*, *NCT04391595*, *NCT03981614*, and *NCT01627054*). For locally advanced or metastatic breast cancer, the CDK4/6 inhibitors palbociclib, ribociclib, and abemaciclib are FDA approved in combination with endocrine therapy [22,23]. Though approval for HNSCC is still pending, first preclinical and clinical reports are promising [16,24,25].

Our study adds another piece of evidence and identifies the CDK4/6 inhibitor palbociclib as well as the global acting CDKi's dinaciclib and THZ1 as promising candidates for HNSCC treatment. We additionally describe the strong dependency on (a) the combination partner and (b) the temporal order of applying each substance to reach therapeutic effects. Notably, simultaneous dual CDKi treatment, but not the combination with standard drugs, worked synergistically in our settings. The sequential application yielded heterogeneous results, depending on the CDKi used for combination. In theory, chemotherapeutic drugs should benefit from prior CDKi treatment by completing their effects [26,27]. However, this was only seen here when the CDK4/6 inhibitor palbociclib was used as first treatment, confirming findings from a recent study in which intrinsic resistance was reported when

Cisplatin was given before palbociclib because of drug-induced *c-Myc* and *Cyclin E* upregulation [19]. Though not analyzed in detail here, comparable molecular alterations can be anticipated. Besides direct antitumoral effects, another argument for applying specific CDKi's in the first-line is the protection of normal hematopoietic stem and progenitor cells via transient G1 cell cycle arrest induction and the maintenance of antitumor immunity to boost the patient's tolerability towards chemotherapy [28]. This "positive" side effect was recently observed in phase II trials on patients with small-cell lung cancer receiving the CDK4/6 inhibitor trilaciclib [28,29]. Hence, a favorable outcome can indeed be speculated if CDK4/6 inhibitors are applied in the first-line. For the more global acting CDKi's, such beneficial responses are very unlikely. Instead, leukopenia and neutropenia were reported as direct consequences of the complex mode of action, including interference with RNA polymerase II binding [30–32]. These systemic toxicities constitute a major limitation and clinicians will have to cope with this challenge. With regard to the sequential application applied here, first-line chemotherapy was superior to second-line chemotherapy. This regimen was comparable to or even better than two cycles of dinaciclib or THZ1 monotherapy. Mechanistically, effects were due to early apoptosis with a shift to necrosis afterward. Quite in line with this, Hossain et al. also observed apoptosis induction by short-term dinaciclib treatment [33]. Notably, THZ1, had a minor impact on apoptosis, though this was described in literature in an nM range and thus was comparable to doses used here [34]. This might be best explained by some kind of delayed apoptosis induction but not intrinsic apoptosis resistance of our HNSCC cells. In support of this, the specific CDK4/6 inhibitor palbociclib triggered apoptosis in both cell lines, confirming recent observations [35]. Senescence, another CDKi-induced cellular stress response, was also seen here; however, it was not as profound as described in the literature [36]. Hence, senescence may either play a minor role in HNSCC or it was an early event and thus undetectable after two rounds of treatment. The strong cytotoxicity of dinaciclib and certain CDKi/drug combinations argue in favor of the latter.

Quite in line with this, impedance reduced massively under dinaciclib monotherapy and combination therapy that was accompanied by remarkable changes in cell shape and cytoskeletal organization. This, in turn, may impair cell-cell contacts via adhesion molecules, electrical coupling, and passage through gap junctions [37]. A comparable, but delayed impedance breakdown was achieved when THZ1 was combined with 5-FU, likely because of the 5-FU's mechanism of action [38]. Such a delayed effect under 5-FU treatment was also seen in the wound healing assay. Conversely, THZ1 monotherapy slightly increased impedance, accompanied by re-organization of cortical actin into stress fibers. These stress fibers increase the cellular stiffness and reduce the motility [20,39,40]. We therefore propose the identified shift in actin organization as main response towards drugs applied in this study that has to be addressed in more detail prospectively. By performing a direct comparison of the two cell culture models used here, it is obvious that the cell line UT-SCC-15, established from a nodal recurrence of a primary tongue carcinoma [41], shows more cortical actin than intracellular stress fibers. In the UT-SCC-14 cells, it is exactly the other way around. The cortical actin filaments are important to create tension, leading to gradients that generate changes in the shape which are important during cell migration, cell division, and tissue morphogenesis [42]. Also, we hypothesize that the remodeling of the actin filament makes the cells more vulnerable to immune cells. A prerequisite—among others—for this is the induction of immunogenic cell death (ICD) in tumor cells to activate phagocytes [33,43,44]. Actually, we observed increased Calreticulin (CalR) translocation upon combined THZ1/5-FU treatment. While this effect was not visible under monotherapy, we suggest this treatment regimen as a promising strategy for immunotherapeutic approaches. Notably, dinaciclib was similarly able to induce CalR translocation and upregulation of the immunologically relevant marker MHC class I to an extent comparable to THZ1/5-FU combination therapy. This makes dinaciclib particularly interesting in the context of immunotherapy, as hypothesized before [33,45]. Hossain et al. treated murine CT26 colon cancer cells for 24 h with different dinaciclib

concentrations (0.05 μM–25 μM) and identified a linear increase in CalR translocation. The readout in this study was the mean fluorescence intensity, which was around 1200 after treatment with 0.05 μM dinaciclib [33]. In our work, a concentration of 0.02 μM dinaciclib yielded an MFI around 2000 for UT-SCC-14 and an MFI of around 1500 for UT-SCC-15 cells. Though the MFI is not directly comparable among different studies, it still confirms previous findings. Additionally to this, the observed upregulation of MHC class I enhances antigen presentation and ultimately stimulates $CD8^+$-T-cells to finally promote antitumor immunity [46].

Radiotherapy is the mainstay of therapy for HNSCC patients and can be combined with immunotherapy. While radiotherapy itself has the potential to reprogram the tumor microenvironment, several drugs including CDKi's have been identified as radiosensitizers [24,47,48]. However, the CDKi´s used here had a minor impact on double-strand breaks and radiosensitivity. Radiosensitization, if any, was seen after combining palbociclib or THZ1 with 5-FU. Wang et al. reported palbociclib-induced DNA damage in an p53-independent manner and repressed DNA damage repair ability via RAD51 downregulation [35]. THZ1 inhibits CDK7, CDK12, and CDK13 [49] and was described as radiosensitizer in a study on medulloblastomas [50]. Genes involved in homologous recombination such as Brca2, Rad51, and Rad50 were downregulated, accompanied by increased γH2AX-foci post irradiation [50]. Another study likewise confirmed increased amounts of γ-H2AX foci upon THZ1 treatment [51]. Hence, THZ1 has the potential to sensitize to radiation and impair recovery from radiation-induced DNA damage. The fact that another target of THZ1, CDK12, selectively controls the expression of genes involved in the DNA damage response, supports this theory [52]. The question remains why such effects were undetectable in our study. Apart from the radiation dose (2Gy), the time is a critical factor for detecting or missing a clear radiation response. Hence, it is conceivable that we have simply missed certain effects.

Another common response towards CDKi treatment is cell cycle alteration. Palbociclib induced a G1 phase arrest that complies with its mode of action and has been described in the literature [53–55]. Combined THZ1 and 5-FU therapy yielded comparable results in both cell lines that can be explained as follows: 5-FU limits the availability of thymidylate and inhibits the DNA synthesis [56,57]. THZ1 impairs CDK2 activity via inhibition of CDK7 [58,59]. CDK2 is required for the transition from G1 to S phase, blocking this CDK thus holds the cell cycle [49]. This has profound biological effects. In a very recent study on patient-derived glioblastoma models, we described the CDKi-induced loss of mitochondrial function in pioneering work, characterized by a multivacuolar phenotype and signs of early-methuosis [60]. Methuosis, a non-apoptotic cell death phenotype, is defined by the accumulation of large fluid-filled cytoplasmic vacuoles that originate from macropinosomes [61]. With regard to the HNSCC cells used here, dinaciclib monotherapy and combination therapy strengthened the mitochondrial activity. However, methuosis did not seem to play a major role, as late endosomes and vacuoles markers CD107a and Rab7a exclusively increased under CDKi or 5-FU monotherapy. Hence, CDKi's have indeed different effects on individual tumor cells.

In a final in vivo proof-of-concept experiment, dinaciclib and Cisplatin were chosen based on the following criteria: Dinaciclib has complex effects on HNSCC tumor cells, including growth inhibition, prevention of migration/invasion, and cytotoxicity. Besides, dinaciclib is a potent ICD inducer and a promising candidate for combined immunotherapies. Cisplatin is a well-known cytostatic drug approved as 1st line HNSCC treatment and widely applied in the clinic [11,62,63]. Additionally, preclinical reports on combined dinaciclib-Cisplatin application are promising, as recently shown for a subcutaneous ovarian cancer xenograft model in nude mice [64]. Here, the combination approach was likewise superior to either single treatment and most effective in suppressing UT-SCC-15 growth. While this cell line was established from a nodal recurrence, it is tempting to speculate that advanced tumors may even benefit more from this regimen than lower-stage tumors. However, this has to be tested on a larger series of (matched) tumor samples. However, the

accelerated growth of UT-SCC-15 xenografts under Cisplatin monotherapy is worth mentioning. Intrinsic resistance is unlikely, since these cells showed good sensitivity in vitro. Also, acquired resistance can be excluded because tumors grew constantly under treatment. Comparable effects were not reported in the literature. We can therefore only assume that outcomes may be improved by changing the treatment schedule (i.e., dose, application route, and the number of injections). Still, the complex interaction of tumor, normal stromal, and immune cells influences outcomes—a major contributing factor that can only partially be considered in vitro [65].

To sum up these findings, we provide another piece of evidence for the therapeutic activity of CDKi's, their complex mode of action, and the rationale to combine targeted agents with "conventional" drugs or even immune-restoring approaches to succeed in the long run.

4. Materials and Methods

4.1. Tumor Cell Lines and Culture Conditions

Two patient-derived cell lines: UT-SCC-14 and UT-SCC-15, were used. The UT-SCC-14 was established from a primary tumor of the tongue and the UT-SCC-15 derived from a nodal recurrence of the same origin. Both cell lines are HPV negative. Cells were maintained in full medium: DMEM/HamsF12 supplemented with 10% fetal calf serum (FCS), glutamine (2 mmol/L) and antibiotics (medium and antibiotics were purchased from Pan Biotech, Aidenbach, Germany, FCS from Sigma-Aldrich, Darmstadt, Germany and glutamine from Biochrom, Berlin, Germany) and kept in low passages.

4.2. Cytostatic Drugs and Targeted Substances

The approved cytostatic drugs 5-FU (50 mg/mL) and Cisplatin (1 mg/mL), the approved therapeutic antibody cetuximab (5 mg/mL) and the targeted substances dinaciclib, palbociclib, and THZ1 (all 10 mM) were used. 5-FU, Cisplatin and cetuximab were purchased from the pharmacy of the University Hospital Rostock, dinaciclib and palbociclib from Selleckchem, Munich, Germany, and THZ1 from Hycultec, Beutelsbach, Germany.

4.3. Dose Response Curves and Combination Therapy

For dose response curves, cells were seeded in 96 well plates in three technical replicates per cell line and incubated for 24 h at 37 °C and 5% CO_2. Afterwards, cells were treated for 2 × 72 h in monotherapy with the different test substances in concentrations ranging between 0.05 µg/mL and 1 mg/mL for approved drugs and 1 nM and 1 µM for CDKi's. Thereafter, various combinations were tested in simultaneous and sequential settings. Doses used for combinations were as follows: 5-FU [0.32 µg/mL or 90 µg/mL], Cisplatin [0.05 µg/mL, 0.5 µg/mL, or 0.1 µg/mL], cetuximab [0.5 µg/mL], dinaciclib [0.005 µM or 0.02 µM], palbociclib [1 µM], and THZ1 [0.02 µM or 0.005 µM] depending on the treatment duration of each substance (1 × 72 h or 2 × 72 h). Readout was done by crystal violet staining. In sequential combination therapy, two different approaches were applied. Firstly, the cells were treated with the standard therapy for 72 h and the CDKi's afterwards, and secondly, the administration was done in reverse order. To rule out the possibility that the single 72-h administration of the approved therapeutics is responsible for the potentially stronger effect, they were tested in monotherapy for 72 h. Potential synergistic or additive effects between the substances in a 2 × 72 h simultaneous combination approach were analyzed with the Bliss Independence model.

4.4. γ-H2AX Staining

Tumor cells were treated for 24 h in Chamber Slides with selected concentrations and combinations of the test substances and then irradiated with 2 Gy (Cs-137 γ-irradiation; IBL 637, CIS Bio-International, Codolet, France). γ-H2AX staining was performed 6 h after irradiation. Cells were washed with phosphate-buffered saline (PBS), fixed in 4% paraformaldehyde w/o methanol (Thermo Scientific, Darmstadt, Germany) for 30 min,

washed again, followed by cell permeabilization in 0.5% Triton X−100 (Sigma-Aldrich, Darmstadt, Germany) for 15 min. After blocking the unspecific binding sites with 1% bovine serum albumin (Serva, Heidelberg, Germany), cells were incubated with the monoclonal γ-H2AX antibody (1:100; BioLegend, San Diego, CA, USA) over night at 4 °C. Cells were washed and nuclei stained with 4′,6-diamidino-2-phenylindole (DAPI) (AAT Bioquest, Sunnyvale, CA, USA). Analysis was performed with a ZEISS Elyra 7 Confocal Laser Microscope (Zeiss, Jena, Germany).

4.5. Apoptosis-Necrosis Assay, Phenotyping, and Immunogenic Cell Death

Apoptosis-necrosis was determined after 24 and 72 h treatment, phenotyping was done after 48 h, and determination of immunogenic cell death (ICD) was recorded after 72 h treatment. Cells were analyzed on a Flow Cytometer (BD FACSVerse™, BD Pharmingen, San Jose, CA, USA). Data analysis was done using the BD FACSuite software (BD Pharmingen).

For Apoptosis-necrosis, cells were stained for 20 min at room temperature with 0.2 µM Yo-Pro 1 iodide (Thermo Scientific, Ex/Em 491/509 nm; blue laser 488 nm) and 20 µg/mL Propidiumiodide (PI) (Sigma-Aldrich, Darmstadt, Germany; Ex/Em: 535⁄617 nm; blue laser 488 nm). PI was added shortly before flow cytometry. For phenotyping, cells were stained for 30 min at 4 °C with FITC anti-HLA-ABC antibody (MHC I) (1:50; ImmunoTools, Friesoythe, Germany) and APC anti-CD279 (PD-1) (1:50; both from BioLegend, blue (488 nm) and red (633 nm) laser). ICD was detected by staining translocated CalR on the cell surface. Cells were incubated for 30 min at 4 °C with the polyclonal rabbit CalR primary antibody (1:50; Abgent, San Diego, CA, USA). Cells were washed and labeled with FITC-conjugated secondary antibody (donkey anti rabbit, 1:50; BioLegend), and incubated again for 30 min at 4 °C. In order to exclude non-specific binding of the FITC-labeled secondary antibody, control cells were additionally stained with the secondary antibody without using the primary antibody. For CalR quantification, the number of cells that were positive for the secondary antibody was subtracted from the CalR+ secondary antibody stained cells.

4.6. Cell Cycle Assay

Cell cycle was determined after 48 h of treatment. Cells were harvested, counted, and resuspended with 1 mL ice cold 70% ethanol. Cells were incubated overnight at −20 °C, washed again, and incubated with 0.5 mL 0.25% TritonX-100 for 15 min on ice. Cells were washed and resuspended in RNAse A (100 µg/mL), supplemented with PI (20 µg/mL). After 30 min incubation on ice, cells were analyzed on a Flow Cytometer (FACSCalibur, BD, San Jose, CA, USA). Data analysis was done using BD FlowJo software (BD Pharmingen, San Diego, CA, USA).

4.7. Influence on Mitochondria, Lysosomes, ER, and Vacuole Formation

The influence on mitochondria, lysosomes, and the ER was examined with immunofluorescence staining. Cells were seeded in Chamber Slides and stained after 72 h treatment. Then, cells were washed and the staining with MitoTracker Red CMXRos (20 nM, CellSignaling Technology, Danvers, MA, USA) and ER-Tracker Blue-White DPX (1 µM, Invitrogen) was done simultaneously for 35 min at 37 °C. Cells were washed and stained with LysoTracker DND-26 (50 nM, CellSignaling Technology) for 2 min at room temperature. Analysis was performed on a ZEISS Elyra 7 Confocal Laser Microscope (Zeiss).

Additionally, vacuole formation was analyzed after 72 h treatment using specific antibodies. Cells were harvested and incubated with Alexa488 anti-CD107a antibody (Biolegend, 1:50 in 0.1% BSA) for 30 min at 4 °C. Then, cells were washed and resuspended in 0.5 mL FluorFix™ Buffer (Biolegend) for 20 min at room temperature. Afterwards, cells were washed twice with 1× intracellular staining perm wash buffer and incubated with Alexa594 anti-Rab7a antibody (Biolegend, 1:50 in 0.1% BSA) for 30 min at room temperature. The reaction was stopped with PBS and washed before cells were resuspended

in 200 µL PBS (+2 mM EDTA). Cells were analyzed by flow cytometry on a Flow Cytometer (FACSAriaII, BD, blue (488nm) and yellow-green (561 nm) laser). Data analysis was performed using BD FACSDiva software (BD).

4.8. Senescence

Senescence-associated β-galactosidase (SA-β-gal, Cell Signaling Technology, Cambridge, UK) was analyzed after 72 h of treatment. Cells were washed and fixed. After a second washing step, cells were stained with a Galactosidase Staining Solution. Therefore, cells were incubated at 37 °C overnight in a dry incubator and checked for senescence the following day under a microscope. To analyze the number of senescent cells, ImageJ was used.

4.9. Impedance Measurement and Actin Staining

Impedance was measured with a commercial Electric Cell-Substrate Impedance Sensing system (ECIS Zθ; Applied Biophysics, New York, NY, USA) equipped with a 96-well array station (Applied Biophysics) to monitor time and frequency dependent complex impedance, Z (t, f). Cells were grown on a 96-well ECIS array plate with 20 interdigitated electrodes/well (96W20idf PET; ibidi GmbH, Gräfelfing, Germany). Prior to cell seeding, electrodes were stabilized with serum-free media overnight in the incubator with high humidity at 37 °C and 5% CO_2. Impedance measurements were performed directly in the treatment medium in the incubator, allowing real-time monitoring of all impedance alterations at 11 frequencies (0.0625, 0.125, 0.25, 0.5, 1, 2, 4, 8, 16, 32, and 64 kHz) in a 180-s interval. 24 h after cell seeding, treatment was added for 72 h. Analysis of cell-cell contacts was performed by 4000 kHz using ECIS Software (Applied Biophysics).

To confirm the results of the impedance measurement, the actin filament was stained with phalloidin (1:300; Invitrogen, Darmstadt, Germany). Therefore, cells were treated for 72 h in Chamber Slides, fixed, permeabilized, stained, and analyzed as described for γ-H2AX.

4.10. Wound Healing and Invasion Assay

A wound healing assay was done in 12-well plates. After formation of a confluent cell layer, a defined scratch was set. Medium was removed, cells were washed with cell culture media, and the corresponding treatment based on the most promising simultaneous combinations was added. Scratch closure was documented by light microscopy routinely during the following 72 h.

For the invasion assay, inserts (8.0 µm translucent; Greiner bio-one, Frickenhausen, Germany) were coated with 70 µL Matrigel (1:25 in serum free media; Corning, NY, USA) and cells seeded in serum free, treatment containing media. The inserts were placed in a 24-well plate containing 750 µL media with 10% FCS and incubated for 72 h. Invasiveness was analyzed by WST-1 assay. The inserts were placed into a new 24-well plate containing WST-1 in serum free media. WST-1 containing medium without cells served as a blank. After 2.5 h of incubation, absorption was measured at a wavelength of 450 nm.

4.11. In Vivo Study

4.11.1. Ethical Statement

The German local authority approved all animal experiments: Landesamt für Landwirtschaft, Lebensmittelsicherheit und Fischerei Mecklenburg-Vorpommern (7221.3-1-066/18), under the German animal protection law and the EU Guideline 2010/63/EU. Mice were bred in the animal facility of the University Medical Center in Rostock under specific pathogen-free conditions. All animals received enrichment in the form of mouse-igloos (ANT Tierhaltungsbedarf, Buxtehude, Germany), nesting material (shredded tissue paper, Verbandmittel GmbH, Frankenberg, Deutschland), paper roles (75 × 38 mm, H 0528–151, ssniff-Spezialdiäten GmbH), and wooden sticks (40 × 16 × 10 mm, Abedd, Vienna, Austria). During the experiment, mice were kept in type III cages (Zoonlab GmbH, Castrop-Rauxel,

Germany) at 12-h dark:light cycle, the temperature of 21 ± 2 °C, and relative humidity of 60 ± 20% with food (pellets, 10 mm, ssniff-Spezialdiäten GmbH, Soest, Germany) and tap water ad libitum.

4.11.2. Experimental Protocol

Xenografts were generated by injecting 5×10^6 cells of UT-SCC-14 or UT_SCC-15 (in 50 µL PBS) subcutaneously in the right flank of 6–8 weeks old female NMRI Foxn1^{nu} mice. Two weeks later, mice bearing tumors of ~50 mm^3 were allocated to treatment groups (Figure 7). Tumor diameters were measured with caliper every three to four days. Tumor volumes were calculated as (length × width^2)/2. Mice were euthanized before tumors reached 1500 mm^3. Tumors were embedded in Cryomatrix (Thermo Scientific, Darmstadt, Germany) and used for HE staining.

4.12. Statistics

All values are expressed as mean ± SD (in vitro analysis) or mean ± SEM (in vivo therapy approach). Differences between controls and treated cells were determined by using one-way *ANOVA* (Bonferroni's Multiple Comparison Test) after proving the assumption of normality (Shapiro-Wilk test). If normality failed, the Kruskal Wallis test was applied. This information is given in the figure captions. Kaplan-Meier survival analysis was done by applying the log rank (Mantel Cox) test. Statistical evaluation was performed using GraphPad PRISM software, version 8.0.2 (GraphPad Software, San Diego, CA, USA). The criterion for significance was set to $p < 0.05$.

5. Conclusions

Cyclin-dependent kinase inhibitors (CDKi) have broad therapeutic potential. Here, we show that CDKi's can be combined with standard cytostatic drugs and that dual CDK inhibition is at least as successful as CDKi/drug combinations. These findings contribute to our understanding of how the treatment of HNSCC can be improved prospectively. The complex effects exerted by specific CDKi-combinations include apoptotic and necrotic cell death as well as methuosis, an uncommon form of cell death, associated with vacuolization of macropinosome and endosome compartments. Dinaciclib and THZ1 were most effective and even better in combination with 5-FU. Another novel finding is the impact on actin fibers and motility properties of tumor cells by specific CDKi's. Prospective studies should focus on the effects on immune cells—especially because of the CDKi's potential to increase tumor immunogenicity.

Supplementary Materials: The following are available online at https://www.mdpi.com/article/10.3390/cancers13102396/s1. Figure S1: Senescence, Figure S2: Scratch-Assay and Invasiveness UT-SCC-14., Figure S3: Influence on mitochondria, lysosomes, ER, and vacuole formation. Figure S4: Cell cycle analysis.

Author Contributions: Conceptualization, N.S. and C.M.; methodology, N.S., I.S., N.E., M.K., M.M., B.S., and C.R.; validation, N.S., C.M.; formal analysis, N.S.; investigation, N.S., I.S.; resources, C.M., C.J., N.E., and H.L.; data curation, N.S., N.E., M.K.; writing—original draft preparation, N.S., I.S.; writing—review and editing, C.M., C.G.-T., A.S.; visualization, N.S., C.M.; supervision, C.M.; project administration, C.M. All authors have read and agreed to the published version of the manuscript.

Funding: This research received no external funding.

Institutional Review Board Statement: The study was conducted according to the guidelines of the Declaration of Helsinki, and approved by the German local authority Ethics Committee) Landesamt für Landwirtschaft, Lebensmittelsicherheit und Fischerei Mecklenburg-Vorpommern, under the German animal protection law and the EU Guideline 2010/63/EU (protocol code: 7221.3-1-066/18 and date of approval: 15 January 2019).

Informed Consent Statement: Not applicable.

Data Availability Statement: The data presented in this study are available in this article (and supplementary material).

Acknowledgments: The patient-derived cell lines UT-SCC-14 and UT-SCC15 were kindly provided by Reidar Grénman (Turku University Hospital, Turku, Finland).

Conflicts of Interest: The authors declare no conflict of interest.

References

1. Schafer, K.A. The Cell Cycle: A review. *Vet. Pathol.* **1998**, *35*, 461–478. [CrossRef]
2. Jingwen, B.; Yaochen, L.; Guojun, Z. Cell cycle regulation and anticancer drug discovery. *Cancer Biol. Med.* **2017**, *14*, 348. [CrossRef] [PubMed]
3. Roskoski, R. Cyclin-dependent protein serine/threonine kinase inhibitors as anticancer drugs. *Pharmacol. Res.* **2019**, *139*, 471–488. [CrossRef] [PubMed]
4. Sánchez-Martínez, C.; Lallena, M.J.; Sanfeliciano, S.G.; de Dios, A. Cyclin dependent kinase (CDK) inhibitors as anticancer drugs: Recent advances (2015–2019). *Bioorgan. Med. Chem. Lett.* **2019**, *29*, 126637. [CrossRef] [PubMed]
5. Asghar, U.; Witkiewicz, A.K.; Turner, N.C.; Knudsen, E.S. The history and future of targeting cyclin-dependent kinases in cancer therapy. *Nat. Rev. Drug Discov.* **2015**, *14*, 130–146. [CrossRef]
6. Patel, V.; Jakus, J.; Harris, C.M.; Ensley, J.F.; Robbins, K.C.; Yeudall, W.A. Altered expression and activity of G1/S cyclins and cyclin-dependent kinases characterize squamous cell carcinomas of the head and neck. *Int. J. Cancer* **1997**, *73*, 551–555. [CrossRef]
7. Parry, D.; Guzi, T.; Shanahan, F.; Davis, N.; Prabhavalkar, D.; Wiswell, D.; Seghezzi, W.; Paruch, K.; Dwyer, M.P.; Doll, R.; et al. Dinaciclib (SCH 727965), a novel and potent cyclin-dependent kinase inhibitor. *Mol. Cancer Ther.* **2010**, *9*, 2344–2353. [CrossRef] [PubMed]
8. Paruch, K.; Dwyer, M.P.; Alvarez, C.; Brown, C.; Chan, T.Y.; Doll, R.J.; Keertikar, K.; Knutson, C.; McKittrick, B.; Rivera, J.; et al. Discovery of dinaciclib (SCH 727965): A potent and selective inhibitor of cyclin-dependent kinases. *ACS Med. Chem. Lett.* **2010**, *1*, 204–208. [CrossRef]
9. Schoninger, S.F.; Blain, S.W. The Ongoing Search for Biomarkers of CDK4/6 Inhibitor Responsiveness in Breast Cancer. *Mol. Cancer Ther.* **2020**, *19*, 3–12. [CrossRef] [PubMed]
10. Greber, B.J.; Perez-Bertoldi, J.M.; Lim, K.; Iavarone, A.T.; Toso, D.B.; Nogales, E. The cryoelectron microscopy structure of the human CDK-activating kinase. *Proc. Natl. Acad. Sci. USA* **2020**, *117*, 22849–22857. [CrossRef] [PubMed]
11. Grünwald, V.; Chirovsky, D.; Cheung, W.Y.; Bertolini, F.; Ahn, M.J.; Yang, M.H.; Castro, G.; Berrocal, A.; Sjoquist, K.; Kuyas, H.; et al. Global treatment patterns and outcomes among patients with recurrent and/or metastatic head and neck squamous cell carcinoma: Results of the GLANCE H&N study. *Oral Oncol.* **2020**, *102*, 104526. [PubMed]
12. Bray, F.; Ferlay, J.; Soerjomataram, I.; Siegel, R.L.; Torre, L.A.; Jemal, A. Global cancer statistics 2018: GLOBOCAN estimates of incidence and mortality worldwide for 36 cancers in 185 countries. *CA. Cancer J. Clin.* **2018**, *68*, 394–424. [CrossRef]
13. Gebre-Medhin, M.; Brun, E.; Engström, P.; Haugen Cange, H.; Hammarstedt-Nordenvall, L.; Reizenstein, J.; Nyman, J.; Abel, E.; Friesland, S.; Sjödin, H.; et al. ARTSCAN III: A Randomized Phase III Study Comparing Chemoradiotherapy With Cisplatin Versus Cetuximab in Patients With Locoregionally Advanced Head and Neck Squamous Cell Cancer. *J. Clin. Oncol.* **2021**, *39*, 38–47. [CrossRef] [PubMed]
14. McDermott, J.D.; Bowles, D.W. Epidemiology of Head and Neck Squamous Cell Carcinomas: Impact on Staging and Prevention Strategies. *Curr. Treat. Options Oncol.* **2019**, *20*, 1–13. [CrossRef] [PubMed]
15. Salakova, M.; Koslabova, E.; Grega, M.; Smahelova, J.; Klozar, J.; Vencalek, O.; Tachezy, R. Mucosal and skin HPV types in tumour-free tonsils and tonsillar tumours. *Neoplasma* **2018**, *65*, 278–286. [CrossRef]
16. Adkins, D.; Ley, J.; Neupane, P.; Worden, F.; Sacco, A.G.; Palka, K.; Grilley-Olson, J.E.; Maggiore, R.; Salama, N.N.; Trinkaus, K.; et al. Palbociclib and cetuximab in platinum-resistant and in cetuximab-resistant human papillomavirus-unrelated head and neck cancer: A multicentre, multigroup, phase 2 trial. *Lancet Oncol.* **2019**, *20*, 1295–1305. [CrossRef]
17. Yoon, N.; Vander Velde, R.; Marusyk, A.; Scott, J.G. Optimal Therapy Scheduling Based on a Pair of Collaterally Sensitive Drugs. *Bull. Math. Biol.* **2018**, *80*, 1776–1809. [CrossRef] [PubMed]
18. Li, Y.F.; Chang, L.; Li, W.H.; Xiao, M.Y.; Wang, Y.; He, W.J.; Xia, Y.X.; Wang, L.; Chen, Y. Radiotherapy concurrent versus sequential with endocrine therapy in breast cancer: A meta-analysis. *Breast* **2016**, *27*, 93–98. [CrossRef]
19. Robinson, A.M.; Rathore, R.; Redlich, N.J.; Adkins, D.R.; VanArsdale, T.; Van Tine, B.A.; Michel, L.S. Cisplatin exposure causes c-Myc-dependent resistance to CDK4/6 inhibition in HPV-negative head and neck squamous cell carcinoma. *Cell Death Dis.* **2019**, *10*, 867. [CrossRef]
20. Northcott, J.M.; Dean, I.S.; Mouw, J.K.; Weaver, V.M. Feeling stress: The mechanics of cancer progression and aggression. *Front. Cell Dev. Biol.* **2018**, *6*, 1–12. [CrossRef]
21. Humphries, W.H.; Szymanski, C.J.; Payne, C.K. Endo-lysosomal vesicles positive for rab7 and lamp1 are terminal vesicles for the transport of dextran. *PLoS ONE* **2011**, *6*, e26626. [CrossRef]
22. Shah, A.; Bloomquist, E.; Tang, S.; Fu, W.; Bi, Y.; Liu, Q.; Yu, J.; Zhao, P.; Palmby, T.R.; Goldberg, K.B.; et al. FDA approval: Ribociclib for the treatment of postmenopausal women with hormone receptor-positive, HER2-negative advanced or metastatic breast cancer. *Clin. Cancer Res.* **2018**, *24*, 2999–3004. [CrossRef]

23. Groenland, S.L.; Martínez-Chávez, A.; van Dongen, M.G.J.; Beijnen, J.H.; Schinkel, A.H.; Huitema, A.D.R.; Steeghs, N. Clinical Pharmacokinetics and Pharmacodynamics of the Cyclin-Dependent Kinase 4 and 6 Inhibitors Palbociclib, Ribociclib, and Abemaciclib. *Clin. Pharmacokinet.* **2020**, *59*, 1501–1520. [CrossRef] [PubMed]
24. Göttgens, E.L.; Bussink, J.; Leszczynska, K.B.; Peters, H.; Span, P.N.; Hammond, E.M. Inhibition of CDK4/CDK6 Enhances Radiosensitivity of HPV Negative Head and Neck Squamous Cell Carcinomas. *Int. J. Radiat. Oncol. Biol. Phys.* **2019**, *105*, 548–558. [CrossRef]
25. Billard-Sandu, C.; Tao, Y.G.; Sablin, M.P.; Dumitrescu, G.; Billard, D.; Deutsch, E. CDK4/6 inhibitors in P16/HPV16-negative squamous cell carcinoma of the head and neck. *Eur. Arch. Oto-Rhino-Laryngol.* **2020**, *277*, 1273–1280. [CrossRef] [PubMed]
26. Deep, G.; Agarwal, R. New combination therapies with cell-cycle agents. *Curr. Opin. Investig. Drugs* **2008**, *9*, 591–604.
27. Shah, M.A.; Schwartz, G.K. Cell cycle-mediated drug resistance: An emerging concept in cancer therapy. *Clin. Cancer Res.* **2001**, *7*, 2168–2181. [PubMed]
28. Weiss, J.M.; Csoszi, T.; Maglakelidze, M.; Hoyer, R.J.; Beck, J.T.; Domine Gomez, M.; Lowczak, A.; Aljumaily, R.; Rocha Lima, C.M.; Boccia, R.V.; et al. Myelopreservation with the CDK4/6 inhibitor trilaciclib in patients with small-cell lung cancer receiving first-line chemotherapy: A phase Ib/randomized phase II trial. *Ann. Oncol.* **2019**, *30*, 1613–1621. [CrossRef] [PubMed]
29. Hart, L.L.; Ferrarotto, R.; Andric, Z.G.; Beck, J.T.; Subramanian, J.; Radosavljevic, D.Z.; Zaric, B.; Hanna, W.T.; Aljumaily, R.; Owonikoko, T.K.; et al. Myelopreservation with Trilaciclib in Patients Receiving Topotecan for Small Cell Lung Cancer: Results from a Randomized, Double-Blind, Placebo-Controlled Phase II Study. *Adv. Ther.* **2021**, *38*, 350–365. [CrossRef]
30. Mitri, Z.; Karakas, C.; Wei, C.; Briones, B.; Simmons, H.; Ibrahim, N.; Alvarez, R.; Murray, J.L.; Keyomarsi, K.; Moulder, S. A phase 1 study with dose expansion of the CDK inhibitor dinaciclib (SCH 727965) in combination with epirubicin in patients with metastatic triple negative breast cancer. *Invest. New Drugs* **2015**, *33*, 890–894. [CrossRef] [PubMed]
31. Kumar, S.K.; LaPlant, B.; Chng, W.J.; Zonder, J.; Callander, N.; Fonseca, R.; Fruth, B.; Roy, V.; Erlichman, C.; Stewart, A.K.; et al. Dinaciclib, a novel CDK inhibitor, demonstrates encouraging single-agent activity in patients with relapsed multiple myeloma. *Blood* **2015**, *125*, 443–448. [CrossRef]
32. Riess, C.; Irmscher, N.; Salewski, I.; Strüder, D.; Classen, C.F.; Große-Thie, C.; Junghanss, C.; Maletzki, C. Cyclin-dependent kinase inhibitors in head and neck cancer and glioblastoma—backbone or add-on in immune-oncology? *Cancer Metastasis Rev.* **2020**, *40*, 153–171. [CrossRef] [PubMed]
33. Md Sakib Hossain, D.; Javaid, S.; Cai, M.; Zhang, C.; Sawant, A.; Hinton, M.; Sathe, M.; Grein, J.; Blumenschein, W.; Pinheiro, E.M.; et al. Dinaciclib induces immunogenic cell death and enhances anti- PD1–mediated tumor suppression. *J. Clin. Investig.* **2018**, *128*, 644–654. [CrossRef] [PubMed]
34. Zhang, Y.; Zhou, L.; Bandyopadhyay, D.; Sharma, K.; Allen, A.J.; Kmieciak, M.; Grant, S. The covalent CDK7 inhibitor THz1 potently induces apoptosis in multiple myeloma cells in vitro and in vivo. *Clin. Cancer Res.* **2019**, *25*, 6195–6205. [CrossRef]
35. Wang, T.H.; Chen, C.C.; Leu, Y.L.; Lee, Y.S.; Lian, J.H.; Hsieh, H.L.; Chen, C.Y. Palbociclib induces DNA damage and inhibits DNA repair to induce cellular senescence and apoptosis in oral squamous cell carcinoma. *J. Formos. Med. Assoc.* **2020**. [CrossRef]
36. Wagner, V.; Gil, J. Senescence as a therapeutically relevant response to CDK4/6 inhibitors. *Oncogene* **2020**, *39*, 5165–5176. [CrossRef] [PubMed]
37. Dominiak, A.; Chełstowska, B.; Olejarz, W.; Nowicka, G. Communication in the cancer microenvironment as a target for therapeutic interventions. *Cancers* **2020**, *12*, 1232. [CrossRef]
38. Zhang, N.; Yin, Y.; Xu, S.J.; Chen, W.S. 5-Fluorouracil: Mechanisms of resistance and reversal strategies. *Molecules* **2008**, *13*, 1551–1569. [CrossRef]
39. Brückner, B.R.; Nöding, H.; Skamrahl, M.; Janshoff, A. Mechanical and morphological response of confluent epithelial cell layers to reinforcement and dissolution of the F-actin cytoskeleton. *Prog. Biophys. Mol. Biol.* **2019**, *144*, 77–90. [CrossRef]
40. Shannon, S.; Jia, D.; Entersz, I.; Beelen, P.; Yu, M.; Carcione, C.; Carcione, J.; Mahtabfar, A.; Vaca, C.; Weaver, M.; et al. Inhibition of glioblastoma dispersal by the MEK inhibitor PD0325901. *BMC Cancer* **2017**, *17*, 121. [CrossRef]
41. Yaromina, A.; Zips, D.; Thames, H.D.; Eicheler, W.; Krause, M.; Rosner, A.; Haase, M.; Petersen, C.; Raleigh, J.A.; Quennet, V.; et al. Pimonidazole labelling and response to fractionated irradiation of five human squamous cell carcinoma (hSCC) lines in nude mice: The need for a multivariate approach in biomarker studies. *Radiother. Oncol.* **2006**, *81*, 122–129. [CrossRef] [PubMed]
42. Chugh, P.; Paluch, E.K. The actin cortex at a glance. *J. Cell Sci.* **2018**, *131*, 1–9. [CrossRef]
43. Gardai, S.J.; McPhillips, K.A.; Frasch, S.C.; Janssen, W.J.; Starefeldt, A.; Murphy-Ullrich, J.E.; Bratton, D.L.; Oldenborg, P.A.; Michalak, M.; Henson, P.M. Cell-surface calreticulin initiates clearance of viable or apoptotic cells through trans-activation of LRP on the phagocyte. *Cell* **2005**, *123*, 321–334. [CrossRef]
44. Kroemer, G.; Galluzzi, L.; Kepp, O.; Zitvogel, L. Immunogenic Cell Death in Cancer Therapy. *Ann. Rev. Immunol.* **2013**, *31*, 51–72. [CrossRef]
45. Riess, C.; Schneider, B.; Kehnscherper, H.; Gesche, J.; Irmscher, N.; Shokraie, F.; Classen, C.F.; Wirthgen, E.; Domanska, G.; Zimpfer, A.; et al. Activation of the Kynurenine Pathway in Human Malignancies Can Be Suppressed by the Cyclin-Dependent Kinase Inhibitor Dinaciclib. *Front. Immunol.* **2020**, *11*, 55. [CrossRef]
46. Li, B.B.; Khan, N.; Ubellacker, J.M.; Xie, S.; Metzger-filho, O.; Roberts, T.M.; Kim, H.; Mcallister, S.S.; Jean, J. CDK4/6 inhibition triggers anti-tumor immunity. *Nature* **2017**, *548*, 471–475.
47. Wang, J.; Yang, T.; Xu, G.; Liu, H.; Ren, C.; Xie, W.; Wang, M. Cyclin-dependent kinase 2 promotes tumor proliferation and induces radio resistance in glioblastoma. *Transl. Oncol.* **2016**, *9*, 548–556. [CrossRef] [PubMed]

48. Xie, X.; Zheng, W.; Chen, T.; Lin, W.; Liao, Z.; Liu, J.; Ding, Y. CDK4/6 inhibitor palbociclib amplifies the radiosensitivity to nasopharyngeal carcinoma cells via mediating apoptosis and suppressing DNA damage repair. *Onco. Targets. Ther.* **2019**, *12*, 11107–11117. [CrossRef] [PubMed]
49. Olson, C.M.; Liang, Y.; Leggett, A.; Park, W.D.; Li, L.; Mills, C.E.; Elsarrag, S.Z.; Ficarro, S.B.; Zhang, T.; Düster, R.; et al. Development of a Selective CDK7 Covalent Inhibitor Reveals Predominant Cell-Cycle Phenotype. *Cell Chem. Biol.* **2019**, *26*, 792–803.e10. [CrossRef]
50. Veo, B.; Danis, E.; Pierce, A.; Wang, D.; Fosmire, S.; Sullivan, K.D.; Joshi, M.; Khanal, S.; Dahl, N.; Karam, S.; et al. Transcriptional control of DNA repair networks by CDK7 regulates sensitivity to radiation in Myc-driven medulloblastoma. *Cell Rep.* **2021**, *35*, 109013. [CrossRef]
51. Pessina, F.; Giavazzi, F.; Yin, Y.; Gioia, U.; Vitelli, V.; Galbiati, A.; Barozzi, S.; Garre, M.; Oldani, A.; Flaus, A.; et al. Functional transcription promoters at DNA double-strand breaks mediate RNA-driven phase separation of damage-response factors. *Nat. Cell Biol.* **2019**, *21*, 1286–1299. [CrossRef] [PubMed]
52. Krajewska, M.; Dries, R.; Grassetti, A.V.; Dust, S.; Gao, Y.; Huang, H.; Sharma, B.; Day, D.S.; Kwiatkowski, N.; Pomaville, M.; et al. CDK12 loss in cancer cells affects DNA damage response genes through premature cleavage and polyadenylation. *Nat. Commun.* **2019**, *10*, 1757. [CrossRef]
53. Maskey, R.S.; Wang, F.; Lehman, E.; Wang, Y.; Emmanuel, N.; Zhong, W.; Jin, G.; Abraham, R.T.; Arndt, K.T.; Myers, J.S.; et al. Sustained mTORC1 activity during palbociclib-induced growth arrest triggers senescence in ER+ breast cancer cells. *Cell Cycle* **2020**, *20*, 65–80. [CrossRef]
54. Yu, Y.; Liao, H.; Xie, R.; Zhang, Y.; Zheng, R.; Chen, J.; Zhang, B. Overexpression of miRNA-3613-3p Enhances the Sensitivity of Triple Negative Breast Cancer to CDK4/6 Inhibitor Palbociclib. *Front. Oncol.* **2020**, *10*, 2541. [CrossRef] [PubMed]
55. Vijayaraghavan, S.; Karakas, C.; Doostan, I.; Chen, X.; Bui, T.; Yi, M.; Raghavendra, A.S.; Zhao, Y.; Bashour, S.I.; Ibrahim, N.K.; et al. CDK4/6 and autophagy inhibitors synergistically induce senescence in Rb positive cytoplasmic cyclin e negative cancers. *Nat. Commun.* **2017**, *8*, 15916. [CrossRef]
56. Focaccetti, C.; Bruno, A.; Magnani, E.; Bartolini, D.; Principi, E.; Dallaglio, K.; Bucci, E.O.; Finzi, G.; Sessa, F.; Noonan, D.M.; et al. Effects of 5-Fluorouracil on Morphology, Cell Cycle, Proliferation, Apoptosis, Autophagy and ROS Production in Endothelial Cells and Cardiomyocytes. *PLoS ONE* **2015**, *10*, e0115686. [CrossRef]
57. Tokunaga, E.; Oda, S.; Fukushima, M.; Maehara, Y.; Sugimachi, K. Differential growth inhibition by 5-fluorouracil in human colorectal carcinoma cell lines. *Eur. J. Cancer* **2000**, *36*, 1998–2006. [CrossRef]
58. Schachter, M.M.; Fisher, R.P. The CDK-activating kinase Cdk7. *Cell Cycle* **2013**, *12*, 3239–3240. [CrossRef] [PubMed]
59. Higashi, H.; Suzuki-Takahashi, I.; Saitoh, S.; Segawa, K.; Taya, Y.; Okuyama, A.; Nishimura, S.; Kitagawa, M. Cyclin-dependent kinase-2 (Cdk2) forms an inactive complex with cyclin D1 since Cdk2 associated with cyclin D1 is not phosphorylated by Cdk7-cyclin-H. *Eur. J. Biochem.* **1996**, *237*, 460–467. [CrossRef]
60. Riess, C.; Koczan, D.; Schneider, B.; Linke, C.; del Moral, K.; Classen, C.F.; Maletzki, C. Cyclin-dependent kinase inhibitors exert distinct effects on patient-derived 2D and 3D glioblastoma cell culture models. *Cell Death Discov.* **2021**, *7*, 54. [CrossRef]
61. Maltese, W.A.; Overmeyer, J.H. Methuosis: Nonapoptotic cell death associated with vacuolization of macropinosome and endosome compartments. *Am. J. Pathol.* **2014**, *184*, 1630–1642. [CrossRef]
62. Ghosh, S. Cisplatin: The first metal based anticancer drug. *Bioorg. Chem.* **2019**, *88*, 102925. [CrossRef] [PubMed]
63. Dasari, S.; Bernard Tchounwou, P. Cisplatin in cancer therapy: Molecular mechanisms of action. *Eur. J. Pharmacol.* **2014**, *740*, 364–378. [CrossRef] [PubMed]
64. Chen, X.X.; Xie, F.F.; Zhu, X.J.; Lin, F.; Pan, S.S.; Gong, L.H.; Qiu, J.G.; Zhang, W.J.; Jiang, Q.W.; Mei, X.L.; et al. Cyclin-dependent kinase inhibitor dinaciclib potently synergizes with cisplatin in preclinical models of ovarian cancer. *Oncotarget* **2015**, *6*, 14926–14939. [CrossRef] [PubMed]
65. Egeblad, M.; Nakasone, E.S.; Werb, Z. Tumors as organs: Complex tissues that interface with the entire organism. *Dev. Cell* **2010**, *18*, 884–901. [CrossRef] [PubMed]

9. Danksagung

Ich möchte mich sehr gern bei allen bedanken, die dazu beigetragen haben, dass diese Arbeit realisiert werden konnte.

Zunächst bedanke ich mich sehr bei Herrn Prof. Dr. med. Carl-Friedrich Classen für die Bereitstellung des Themas, die langjährige Unterstützung und motivierenden Worte, insbesondere aber für den wissenschaftlichen Freiraum, den er mir gewährt und das Vertrauen, das er mir dabei entgegengebracht hat, um die Fertigstellung dieser Arbeit zu ermöglichen. Die Wertschätzung, die mir zu Teil wurde, möchte ich für meine Zukunft stets als Ermutigung und Zuspruch in Erinnerung behalten. Ganz herzlichen Dank, Kalle!

Mein besonderer Dank gilt Frau PD Dr. rer. nat. Claudia Maletzki für ihre Geduld und allumfassende Betreuung, nicht nur bei der Laborarbeit, sondern ebenso beim Korrekturlesen der Manuskripte. Dank der ausgezeichneten Einarbeitung und herausragenden Zusammenarbeit, sowie dem offenen Ohr bei Problemstellungen unterschiedlicher Natur war es mir erst möglich, diese Arbeit anzufertigen. Ihre wissenschaftlichen Kenntnisse und die kritische Auseinandersetzung mit meiner Arbeit haben diese maßgeblich bereichert. Vielen Dank auch für die vielen zwischenmenschlichen Gespräche und seelische Unterstützung, liebe Claudia.

Mein großer Dank gebührt „meinen“ drei Medizinerinnen, Katharina del Moral, Charlotte Linke und Anna Sophie Schulz, die ich für das Gelingen ihrer Doktorarbeiten mit anleiten durfte. Es hat mir sehr viel Freude bereitet mit euch zusammenarbeiten. Katharina, ich danke dir herzlichst für deine tatkräftige Unterstützung. Du hast einen essentiellen Beitrag für diese Arbeit geleistet. Vielen lieben Dank auch meinen ehemaligen Bürokolleginnen Birthe Herziger und Ruth Melinda Müller. Durch Ihre positive und humorvolle Art sowie offenen Diskussionen konnte so manch stressiger Tag Erheiterung erfahren und für neuen Elan sorgen. Ihr seid großartig!

Ich bedanke mich darüber hinaus bei allen Kooperationspartnern und Mitarbeitenden der Core Facilitys der Universitätsmedizin Rostock für die hilfsbereiten und wissenschaftlichen Diskurse und vielseitigen Unterstützungen. Hierbei möchte ich insbesondere Herrn PD Dr. rer. nat. Tomas Fiedler, Herrn Dr. phil. nat. Björn Schneider und Herrn Dr. Dirk Koczan erwähnen. Ausdrücklich möchte ich mich auch bei allen anderen bedanken, die an den hier zusammengefassten Publikationen mitgewirkt haben. Vielen Dank für die konstruktiven

Ideen und Ratschläge zu diversen Fachgebieten. Weiterhin gilt mein Dank Frau PD Dr. rer. nat. Dagmar-Christiane Fischer für das Bereitstellen Ihrer Räumlichkeiten. Ein besonderer Dank gilt hier auch Anja Rahn, die mir bei den vielen kleinen und größeren Fragestellungen, insbesondere bei der Bestelllogistik, hilfreich zur Seite stand.

Den Korrekturlesern bin ich sehr dankbar, dass sie sich die Zeit genommen haben, einen gewissenhaften Blick auf meine Arbeit zu werfen.

Meiner Familie und meinen Freunden danke ich sehr, dass sie immer für mich da sind, insbesondere in dieser herausfordernden Zeit. Bei meinen Eltern möchte ich mich hierbei besonders von ganzem Herzen bedanken, da sie mich immer und in jeglicher Hinsicht bedingungslos unterstützt, gefördert und aufgemuntert haben.

Zu guter Letzt geht ein außerordentlich großer und liebevoller Dank an meinen Mann und unsere wundervollen Kinder, die mein Fels in der Brandung sind, mich in allen wichtigen Lebenslagen unterstützen und mir stets den Rücken stärken.